FLEX/Sentinel-3 Tandem Mission

FLEX Bridge Study

FINAL REPORT

January 2016

ESA ESTEC Contract No. 4000112341/14/NL/FF/gp

FLEX Bridge Study – Final Report – January 2016

ESA ESTEC Contract No. 4000112341/14/NL/FF/gp

Gina H. Mohammed (P & M Technologies, Canada) (Chapters 1, 3, 4, 6-9)
Roberto Colombo (University of Milano-Bicocca, Italy) (Ch. 2)
Jose Moreno (University of Valencia, Spain) (Ch. 2, 5)
Christiaan van der Tol (University of Twente, The Netherlands) (Ch. 4)
Uwe Rascher (Institute of Bio- and Geosciences, Forschungszentrum Jülich GmbH, Germany) (Ch. 3)
Alexander Ač (Global Change Research Centre AS CR, Czech Republic) (Ch. 3)
Luis Alonso (University of Valencia, Spain; and IBIMET-CNR, Italy) (Ch. 5)
Marco Celesti (University of Milano-Bicocca, Italy) (Ch. 2)
Sergio Cogliati (University of Milano-Bicocca, Italy) (Ch. 2)
Alexander Damm (University of Zurich, Switzerland) (Ch. 2, 3)
Dominic Fawcett (University of Zurich, Switzerland) (Ch. 2, 3)
Jose Gomez-Dans (University College London and NERC/NCEO, United Kingdom) (Ch. 4)
Claudio Henry (University of Zurich, Switzerland) (Ch. 3)
Philip Lewis (University College London and NERC/NCEO, United Kingdom) (Ch. 4)
Natasha MacBean (LSCE – Laboratoire des Sciences du Climat et de l'Environment, France) (Ch. 4)
Federico Magnani (University of Bologna, Italy) (Ch. 4)
Jacques Malaprade (University College London and NERC/NCEO, United Kingdom) (Ch. 4)
Maria Matveeva (Institute of Bio- and Geosciences, Forschungszentrum Jülich GmbH, Germany) (Ch. 3)
Julie Olejníčková (Global Change Research Centre AS CR, Czech Republic) (Ch. 3)
Dan Pernokis (P & M Technologies, Canada) (Ch. 4)
Francisco Pinto (Institute of Bio- and Geosciences, Forschungszentrum Jülich GmbH, Germany) (Ch. 3)
Sabrina Raddi (University of Florence, Italy) (Ch. 4)
Nastassia Rajh Vilfan (University of Twente, The Netherlands) (Ch. 4)
Juan Pablo Rivera (University of Valencia, Spain) (Ch. 2, 4)
Micol Rossini (University of Milano-Bicocca, Italy) (Ch. 2, 4, 5)
Neus Sabater (University of Valencia, Spain) (Ch. 2)
Anke Schickling (Institute of Bio- and Geosciences, Forschungszentrum Jülich GmbH, Germany) (Ch. 3)
Carolina Tenjo (University of Valencia, Spain) (Ch. 2)
Wout Verhoef (University of Twente, The Netherlands) (Ch. 2, 4)
Jochem Verrelst (University of Valencia, Spain) (Ch. 2)
Jorge Vicent Servera (University of Valencia, Spain) (Ch. 5)
Matthias Drusch (ESTEC, The Netherlands)

Study Manager:
Dr. Gina H. Mohammed
Research Director
P & M Technologies
66 Millwood Street
Sault Ste. Marie, Ontario P6A 6S7
Canada

ESA/ESTEC Technical Officer:
Dr. Matthias Drusch
Land Surfaces Principal Scientist
Mission Science Division (EOP-SME)
European Space Agency, ESTEC
Earth Observation Programmes
Postbus 299, 2200 AG Noordwijk
The Netherlands

FLEX Bridge Study

ESA Contract No: 4000112341/14/NL/FF/gp	**Subject:** Final report	**Contractor:** P & M Technologies
***ESA CR( ) No:**	**No. of volumes:** 1	**Contractor's reference:** 39451

ABSTRACT: The FLEX Bridge Study advanced approaches for retrieval and applications of solar-induced fluorescence (SIF) for assessment of photosynthesis and stress status in terrestrial vegetation, including development of a calibration/validation strategy for FLEX products. Specific advances included: (i) optimisation of SIF retrieval algorithms, formalisation of fluorescence-derived indices, and development of biophysical products; (ii) SIF-photosynthesis model improvements and evaluation of data assimilation techniques; (iii) testing of stress indices, extension of the range of potential applications, and evaluation of non-photochemical protection mechanisms; and (iv) development of calibration/validation strategies, including metrics for validation error and product accuracies, definition of FLEX Level-2/3 products and their validation plan, and definition of a common protocol and state-of-the-art instruments to be used for estimation of fluorescence in the context of cal/val activities. This activity forms the foundation for subsequent science and applications development during FLEX mission development and deployment.

The work described in this report was done under ESA Contract. Responsibility for the contents resides in the author(s) and organisation(s) that prepared it.

Names of authors:

Gina H. Mohammed (P & M Technologies, Canada)
Roberto Colombo (University of Milano-Bicocca, Italy)
Jose Moreno (University of Valencia, Spain)
Christiaan van der Tol (University of Twente, The Netherlands)
Uwe Rascher (Institute of Bio- and Geosciences, Forschungszentrum Jülich GmbH, Germany)
Alexander Ač (Global Change Research Centre AS CR, Czech Republic)
Luis Alonso (University of Valencia, Spain)
Marco Celesti (University of Milano-Bicocca, Italy)
Sergio Cogliati (University of Milano-Bicocca, Italy)
Alexander Damm (University of Zurich, Switzerland)
Dominic Fawcett (University of Zurich, Switzerland)
Jose Gomez-Dans (University College London, United Kingdom)
Claudio Henry (University of Zurich, Switzerland)
Philip Lewis (University College London, United Kingdom)
Natasha MacBean (LSCE – Laboratoire des Sciences du Climat et de l'Environment, France)
Federico Magnani (University of Bologna, Italy)
Jacques Malaprade (University College London, United Kingdom)
Maria Matveeva (Institute of Bio- and Geosciences, Forschungszentrum Jülich GmbH, Germany)
Julie Olejníčková (Global Change Research Centre AS CR, Czech Republic)
Dan Pernokis (P & M Technologies, Canada)
Francisco Pinto (Institute of Bio- and Geosciences, Forschungszentrum Jülich GmbH, Germany)
Sabrina Raddi (University of Florence, Italy)
Nastassia Rajh Vilfan (University of Twente, The Netherlands)
Juan Pablo Rivera (University of Valencia, Spain)
Micol Rossini (University of Milano-Bicocca, Italy)
Neus Sabater (University of Valencia, Spain)
Anke Schickling (Institute of Bio- and Geosciences, Forschungszentrum Jülich GmbH, Germany)
Carolina Tenjo (University of Valencia, Spain)
Wout Verhoef (University of Twente, The Netherlands)
Jochem Verrelst (University of Valencia, Spain)
Jorge Vicent Servera (University of Valencia, Spain)
Matthias Drusch (ESTEC, The Netherlands)

ESA Study Manager: Matthias Drusch **Division: SM **Directorate: EOP	****ESA Budget Heading:**

* To be completed by ESA ** Information to be provided by ESA Study Manager

Table of Contents

Acknowledgements

The FLEX Bridge Study benefited greatly from the contributions of many individuals and organisations. We especially thank those who provided key datasets and collaborated on the workpackage reports and other activities: Gustau Camps-Valls, Daniel Kováč, MaPilar Cendrero Mateo, Silvia Garbari, Luis Guanter, Ari Kornfeld, Jordi Muñoz-Marí, Caroline Nichol, Cinzia Panigada, Patrick Rademske, Fabian Schneider, Giulia Tagliabue, Sebastian Wieneke, and Mat Williams.

Helpful inputs and feedback were provided by various members of the FLEX Mission Advisory Group, including Yves Goulas, Andreas Huth, Elizabeth Middleton, Franco Miglietta, and Ladislav Nedbal. We also thank ESA's Stefan Kraft, Umberto Del Bello, and Dirk Schüttemeyer for their insights on FLEX/FLORIS technical aspects and related campaigns.

Funding for the FLEX Bridge Study was provided by the European Space Agency through ESTEC Contract No. 4000112341/14/NL/FF/gp.

Additional funding support for activities in Section 4.3.1 was provided by a personal grant (to C. van der Tol) from the Transregional Collaborative Research Centre 32, and for activities of Section 4.4.1 from the Netherlands Organization for Scientific Research, Grant ALW-GO/13-32.

Abstract

Within the context of ESA's Earth Explorer 8 Phase A/B1 assessments of the FLuorescence EXplorer (FLEX), the FLEX Bridge Study was conducted to (i) optimise approaches for SIF retrievals and applications in assessment of photosynthesis and stress status in terrestrial vegetation, and (ii) develop a calibration/validation strategy for FLEX mission products.

Capabilities were enhanced for the retrieval and analysis of sun-induced fluorescence from FLEX. These included provision of new simulation datasets, consolidation of algorithms for atmospheric correction of FLEX signals, improvements for SIF retrieval, formalisation of fluorescence-derived indices, and development of biophysical products.

Opportunities and protocols for stress detection were expanded and refined using published and new datasets, testing of stress indicators/indices, and evaluation of strategies to assess non-photochemical quenching and minimise sources of variability and error.

The SCOPE model and A-SCOPE graphic user interface (version 1.61) were improved with new functionality for accommodating plant functional types, and SCOPE now has improved computation speed and greater accuracy of the fluorescence output. A new leaf RT model was introduced to incorporate xanthophyll effects. Several types of applications were investigated.

The FB Study also formulated a comprehensive calibration/validation strategy for FLEX mission products. The strategy covers methods to determine validation error metrics and product accuracies, cal/val for basic fluorescence products, validation of FLEX Level-2/3 products, and definition of common protocols and state-of-the-art instruments for use in the strategy.

This work supports the development of best practices for the retrieval, interpretation, and application of fluorescence measurements from space. These aspects are crucial in order to realise the full potential of space-based SIF technology in helping to meet the land challenges identified in ESA's Living Planet Programme.

Recommendations for future research activities have been made in several areas, including improvements in signal retrieval and analysis, data assimilation, modelling, calibration/validation, and applications.

Executive Summary

Background

The European Space Agency (ESA) has been investigating remote sensing methods for detection of chlorophyll fluorescence in terrestrial plants through its research activities over the past decade and more (e.g., Miller *et al.* 2005; Magnani *et al.* 2009; Mohammed *et al.* 2014; Moreno *et al.* 2014; Rascher *et al.* 2015). Current activities have focused on the Fluorescence Explorer (FLEX), one of two candidates included in Phase A/B1 assessments for ESA's Earth Explorer 8 mission (ESA 2015b). FLEX is oriented to bridging the land challenges identified in ESA's Living Planet Programme: Scientific Achievements and Future Challenges (ESA 2015a) through an advanced scientific Earth observation capacity that will support management of the world's vegetation resources (ESA 2015b).

As part of the FLEX Phase A/B1 activities, several initiatives were completed previously, including (i) the FLEX/Sentinel-3 Tandem Mission Photosynthesis (PS) Study, which developed a process-based model and simplified algorithms linking solar-induced fluorescence and photosynthesis, as well as fluorescence-based stress indicators (Mohammed *et al.* 2014); (ii) the Performance Analysis and Requirements Consolidation Study (PARCS), which developed approaches for retrieval of solar-induced chlorophyll fluorescence (SIF) from FLEX (Moreno *et al.* 2014); and (iii) the *HyFLEX* initiative, consisting of dedicated field campaigns executed with the airborne demonstrator *HyPlant*, to investigate fluorescence characteristics over a range of vegetation types and to explore the effects of stresses on SIF (Rascher *et al.* 2015). The current FLEX Bridge (FB) Study builds upon the foundation of those activities by focusing on optimisation of signal retrieval methodologies, extension of stress indicators, strengthening of the process-based modelling capabilities of the SCOPE model, and development of calibration/validation strategies for FLEX products.

Goals of the FLEX Bridge Study

The overall goals of the FLEX Bridge Study were to:

1. optimise approaches for SIF retrievals and applications in assessment of photosynthesis and stress status in terrestrial vegetation; and
2. develop a calibration/validation strategy for FLEX products.

Specific objectives were to:

- optimise the fluorescence retrieval algorithm developed under the PARCS activity;
- optimise the SCOPE photosynthesis model (v1.53) and related algorithms developed under the Photosynthesis Study;
- consolidate and develop retrievals for additional Level-2 data products;
- advance further applications based on Level-2 data products.

Science tasks

The FLEX Bridge Study was divided into four major science tasks:

1. **Solar induced fluorescence retrieval optimisation and analysis.** This task built upon the PARCS activities (Moreno *et al.* 2014) by: consolidating algorithms for atmospheric correction in FLEX configuration; optimising and improving algorithms for SIF retrieval; formalising fluorescence-derived indices; and developing biophysical products.

2. **Development of vegetation stress indicators and applications.** This activity advanced the range of applications and protocols for stress detection using SIF by: utilising datasets from campaigns with the airborne demonstrator *HyPlant* to extend stress-based applications of SIF; evaluating strategies to assess non-photochemical quenching (NPQ) using optical measurements; testing and reviewing stress indicators developed in the PS Study; and reviewing sources of variability and error in stress detection.

3. **Photosynthesis model optimisation, updates, and applications.** The SCOPE model version (1.53) that was developed in the PS Study was updated with new functionality, and foundations were laid for future developments by: considering effects of xanthophylls (known to contain additional information about stress); defining model parameters for specific plant functional types that can be linked to operational global dynamic vegetation models; further quantifying vegetation structural effects on the measured SIF signal; and investigating data assimilation techniques for a broader range of applications, including global ecology, climate- and carbon modelling.

4. **Development of a calibration/validation strategy.** The need for a comprehensive cal/val strategy was identified in the PS Study and at the 5th International Workshop on Remote Sensing of Vegetation Fluorescence (in 2014). This priority was addressed here by: determining validation error metrics and product accuracies; defining a cal/val strategy for basic fluorescence products; defining FLEX Level-2/3 products and their validation plan; and defining common protocols and state-of-the-art instruments to be used in estimation of fluorescence in the context of calibration/validation activities.

Results

Solar induced fluorescence retrieval optimisation and analysis

Capabilities were enhanced for the retrieval and analysis of sun-induced fluorescence from FLEX. These included provision of new simulation datasets, consolidation of algorithms for atmospheric correction of FLEX signals, improvements for SIF retrieval, formalisation of fluorescence-derived indices, and development of biophysical products.

In **data generation**, the existing FLEX/S3 spectral radiance databases were expanded with new simulations that allow for generation of either single pixels or synthetic composite imagery. Some of the new datasets were generated with the FLEX End-to-End Mission Performance Simulator (FLEX-E). The new databases afford versatility in simulating ideal or realistic scenarios and are valuable inputs for algorithm development.

The **atmospheric correction algorithm** was developed to a Level-2 processing chain, while also improving the coupling of atmospheric correction and fluorescence retrieval.

Fluorescence retrievals were improved for retrieval of the full SIF spectrum, and analyses conducted here demonstrated the feasibility of decoupling the Photosystem I and II (PSI and PSII) spectra from total canopy fluorescence.

Strategies were evaluated for better **estimates of absorbed photosynthetically active radiation (APAR)**, important for the calculation of yields. Further, insights were gained into potential causes of retrieval issues. **Normalisation strategies** of the SIF signal were evaluated for their capacity to minimise the impact of environmental conditions and vegetation structural parameters, and the importance of APAR and fAPAR for normalisation was substantiated.

Progress was made toward development of higher-level products for retrieval of **biophysical parameters** (or canopy state variables). For complex imagery, a retrieval strategy was developed to extract LAI estimates. A complementary approach for cases of relatively homogenous pixels showed that a simplified version of SCOPE was able to simultaneously retrieve surface reflectance, fluorescence, and most biophysical paramaters of the model.

Development of vegetation stress indicators and applications

Opportunities and protocols for stress detection were expanded and refined using published and new datasets, testing of indicator prototypes, and evaluation of strategies to assess non-photochemical quenching and minimise sources of variability and error.

SIF can be used to study a wide variety of **abiotic and biotic stresses** across many species. In addition to water stress, temperature stresses, and nitrogen deficit studied during the PS Study, the influence of air pollution, insecticides, senescence, biotic stress, combined stresses, heavy metals, herbicide, ozone, UV radiation, salt and micro- and macronutrients deficiency were evaluated. Stress indices introduced in the PS Study were tested, and the results reiterated the importance of having ancillary measures for interpretation of SIF and to distinguish among stresses. Application of SIF for stress detection requires a good understanding of vegetation ecophysiology, suitable sampling methods, techniques for merging of data from various domains, and sound mechanistic models. The spectral and spatial resolution of FLORIS and the complementarity of the tandem mission position FLEX advantageously for applications.

The value of the **photochemical reflectance index** (PRI) for interpretation of fluorescence is well known. Here, we have considered how best to incorporate PRI for canopy-level assessments and have proposed avenues by which PRI could be strengthened as a measure of non-photochemical quenching through compensating for the impacts of confounding factors, especially structural effects, illumination effects, and pigment pool sizes.

Finally, field datasets were utilised from stress experiments with the ***HyPlant*** airborne sensor which helped to quantitatively link vegetation stress and SIF. The far-red fluorescence was used here, for which the potential interplay of canopy characteristics with stress responses and fluorescence emission was indicated. An informative point was the apparent strong correlation

of F_{760} to EVI (hence leaf area index, LAI), at least under heat stress. In the near future, as the extraction of the red fluorescence data from *HyPlant* campaigns is completed, this will more fully advance our understanding of stress responses in the field.

Photosynthesis model optimisation, updates, and applications

The SCOPE model and A-SCOPE graphic user interface were improved with new functionality for accommodating plant functional types, and SCOPE now has improved computation speed and greater accuracy of the fluorescence output. Further improvements will be facilitated with the creation here of a new leaf RT model that incorporates xanthophyll effects. Several types of applications were investigated.

Several modelling developments were relevant to applications of SIF for photosynthetic and stress evaluation. First, a new model, Fluspect_B_CX, was introduced to represent **xanthophyll pigment changes** related to NPQ and PRI. Second, a new model of **energy partitioning** between the two photosystems was proposed to provide preliminary estimation of PSI and PSII fluorescence radiance. Third, the possibility was investigated to estimate **sustained NPQ** from changes in leaf PRI, thereby strongly reducing model uncertainty.

Testing and evaluation of recent versions of the models were done. The **Fluspect model** provided realistic chlorophyll fluorescence simulations, with most of the fluorescence variability explicable from the PROSPECT parameters. However, the spectral distribution of the excitation light affected the shape of the chlorophyll fluorescence spectrum in a way that the Fluspect model could not fully reproduce. Ideally, measurements carried out under natural light conditions should be used to complete a full validation of the Fluspect model. The **SCOPE model** was compared to field data of far-red fluorescence from *HyPlant*. The model reproduced the magnitude and seasonal cycle of fluorescence. In unstressed conditions, the effects of canopy structure and leaf composition dominated fluorescence variations in the far-red band, with a smaller contribution of photosynthetic regulation due to photochemical and non-photochemical quenching.

To facilitate applications and user convenience, a **simple model** for red and far-red fluorescence and photosynthesis has been formulated based on SCOPE. The simple model runs approximately six orders of magnitude faster than the full SCOPE model. Also, an **Emulator toolbox**, developed as a complementary activity to the FB Study, is useful to evaluate various model emulators.

Data assimilation of fluorescence products will be key to applications. As a first attempt, data assimilation has been applied to a *HyPlant* scene, producing a map of canopy photosynthesis from the reflectance and retrieved fluorescence of *HyPlant*. Additional activity explored SIF datasets of coarse spatial resolution that could inform FLEX activities at the more detailed scale. Data assimilation using SIF to constrain the DVGM ORCHIDEE yielded promising results. Considering that canopy 3D geometry influences SIF values, there is merit to having 'structure-corrected' data for future use.

A further product was the '**Automated Scene Generator Module' (A-SGM)** for the generation of simulated scenes according to plant functional types. This module is available in a user-friendly GUI format in the ARTMO framework, and it can rapidly generate simulated scenes for any optical sensor specified within ARTMO. The A-SGM accommodates data from either a radiative transfer model (RTM) or an RTM emulator.

Development of a calibration/validation strategy

The FB Study has formulated a comprehensive cal/val strategy for FLEX mission products. The strategy covers methods to determine validation error metrics and product accuracies, cal/val for basic fluorescence products, validation of FLEX Level-2/3 products, and definition of common protocols and state-of-the-art instruments for use in the strategy.

A **"bottom-up" validation** strategy was proposed, with validation based on trusted top-of-canopy (TOC) SIF measurements over large relatively homogeneous sites from towers or masts, upscaled to moderate resolution via a combination of high resolution mapping with RT models.

The possibility exists to extend to several vegetation types (or even for inhomogeneous canopies of a single type) using *in-situ* imaging spectrometers and/or unmanned aerial vehicles (UAV)-based miniature spectrometers, along with RTMs and/or high-resolution mapping. Dedicated field campaigns with airborne FLEX simulators and extensive field measurements deployed at selected sites will provide high accuracy validation of upscaling processes, radiative transfer fluorescence models and TOC SIF measurements. Validation should extend globally over relevant biomes and latitudes, and continuously over seasonal changes, with data from the different validation sites compiled in a homogenised database. We have further proposed procedures for evaluation of instrument performances under natural illumination so as to identify the most suitable, cost-effective and precise instruments for deployment.

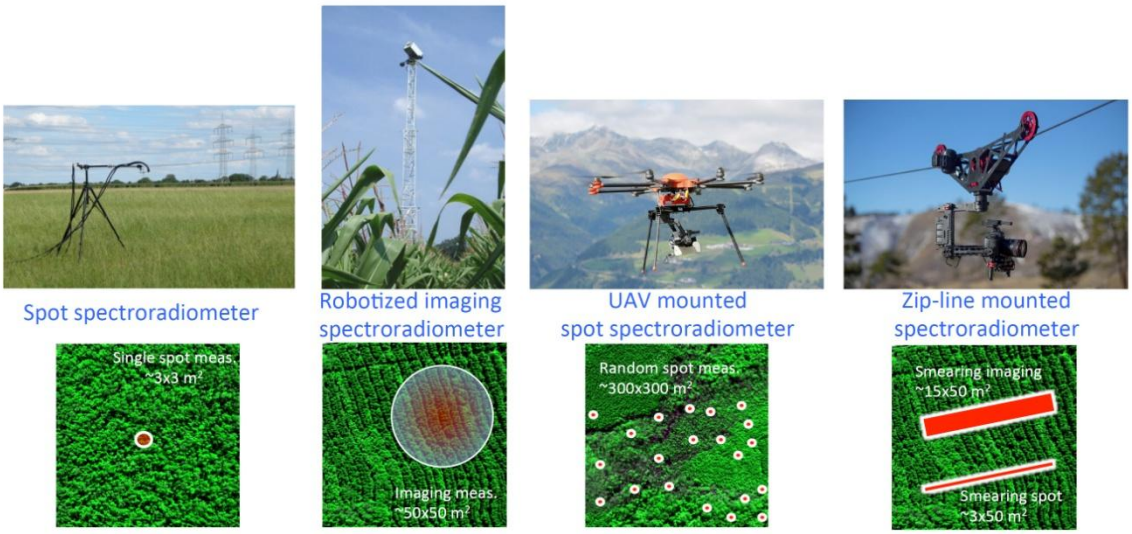

Instrumental setups to achieve field and landscape characterisation using various sampling strategies

Significance for the FLEX mission

The FB Study supports the development of best practices for the retrieval, interpretation, and application of fluorescence measurements from space. These aspects are crucial in order to realise the full potential of space-based SIF technology in helping to meet the land challenges identified in ESA's Living Planet Programme (ESA 2015a). The completion of the FB Study also coincides with the conclusion of ESA's selection process for Earth Explorer 8 and the Agency's official announcement in mid-November 2015 that FLEX has been selected. Thus, the Study serves as a 'bridge' to future science activities.

Outputs of FLEX Bridge that are of key relevance to the FLEX/Sentinel-3 mission:

1. **fluorescence retrieval & quantification** – extension of FLEX/S3 spectral radiance databases to support algorithm development; improvement in atmospheric correction and development to a Level-2 processing chain; improvement in retrieval of the full SIF spectrum; decoupling of PSI and PSII spectra; normalisation strategies for estimation of APAR; progress in retrieval of biophysical parameters; definition of calibration/validation approaches.
2. **fluorescence interpretation** – strategies to incorporate PRI through compensating for confounding factors; evaluation of *HyPlant* campaign data on stress responses; strategies for quantifying and modelling NPQ and its components; formulation of a new leaf RT model incorporating xanthophylls; prototype model for energy partitioning between PSI and PSII; preliminary strategies to incorporate canopy 3D geometry effects; calibration/validation approaches.
3. **fluorescence applications** – identification of SIF indicators to study a wide variety of abiotic and biotic stresses; development of a prototype simplified model based on SCOPE; development of an Automated Scene Generator Module to incorporate plant functional types; creation of an emulator toolbox; testing of updated versions of SCOPE and Fluspect with simulated and field data.

Recommendations

To build upon the findings of this study, we offer several recommendations.

First, additional developments are needed on optimisation of **signal retrieval and analysis**. Algorithms for decoupling PSI/PSII contributions should be tested under realistic scenarios. Similarly, estimation of biophysical parameters should be studied in more detail under such scenarios. Further work is required on quantification and incorporation of canopy structural effects on the SIF signal and for the individual PAR terms (especially APAR), notably in complex vegetation canopies; and a strategy for normalisation of SIF in the red region to compensate for vegetation structure must be formulated, especially considering reabsorption of the red band fluorescence. In general, methodologies need to be tested with more 'real world' datasets.

Second, a concerted effort is required on **data assimilation** techniques amenable to a broad range of applications, including global ecology, climate- and carbon modelling. Preliminary activity here utilised GOME-2 data to inform the more detailed acquisitions that will be possible with FLEX, but future activity will need to focus on finer-resolution captures and on both red and far-red fluorescence, for which the *HyPlant* airborne sensor will be a valuable platform.

Third, the new and enhanced **models** developed here require fuller validation and testing with more datasets on a wider variety of vegetation types. The new leaf-level models of physiology or RT will need to be implemented into SCOPE once final testing and validation are completed. It should also be noted that a few very challenging areas of science were tackled here related to estimation of non-photochemical quenching. That story is not yet complete and further refinement or correction of these analytical models likely will be needed. Efforts should also continue on formulation and testing of simplified models or emulators for use at canopy level, and usage of the new emulator toolbox will expedite such investigation.

Fourth, pre-implementation of the **cal/val** strategy that was pioneered here needs to start soon so that the necessary infrastructure can be put in place. Developments on SIF proximal and remote sensing systems are needed to improve performances, accommodate heterogeneous landscapes, handle automatic sampling, and conduct automatic processing & archiving. Additionally, there would be benefits to establishing or engaging a common calibration facility and having portable cal/val standards. A helpful step will be to identify institutions, groups, and companies capable of such developments and manufacturing. To keep abreast of new developments, future activities will benefit from interaction with other initiatives (e.g., COST action OPTIMISE ES1309) involving diverse teams of scientists sharing a common interest in fluorescence spectroscopy under natural conditions.

Finally, a priority should be placed on advancement of SIF **applications** and supporting the **users** of FLEX. There is a need for studies on stress applications of SIF in a wide variety of vegetation systems, along with investigation into PSI/PSII behaviour and implications for SIF retrievals and quantification. The user network will need to be consolidated and supported with necessary expertise and other resources. A communications plan should be developed and implemented to keep the FLEX user community informed and ready to adopt new developments. This activity should occur contemporaneously with work on the cal/val pre-implementation, as these users will also be involved in refinement of site selection and methodologies for the different application areas.

1. Introduction

Chlorophyll fluorescence is the red and far-red light emitted from vegetation upon absorption of photosynthetically active radiation. The emission is subtle in amplitude yet measurable with sufficiently sensitive spectrometers. Importantly, the signal is responsive to photosynthetic activity in the plant tissues, making it an indicator of photosynthetic and stress status. Extensive application of chlorophyll fluorescence over the last several decades has encompassed agriculture, horticulture, forestry, and aquatics science. Techniques have utilised both active and passive approaches, and they have been used increasingly in recent years at the remote scale, especially passive methodologies. Thousands of papers have been published that have utilised chlorophyll fluorescence as a physiological tool to study photosynthetic performance, and many reviews have addressed the topics of fluorescence theory, instrumentation, and applications (e.g., Ač *et al.* 2012; Fernandez-Jaramillo *et al.* 2012; Tremblay *et al.* 2012; Rodriguez *et al.* 2011; Rohacek *et al.* 2008; Theisen 2002; Schreiber *et al.* 1994; Krause & Weis 1991; Lichtenthaler & Rinderle 1988).

The capacity to observe solar-induced chlorophyll fluorescence (SIF) from terrestrial vegetation presents a totally novel option for space-based remote sensing. Attention to this subject has intensified in recent years as a result of reports of early retrievals of fluorescence from atmospheric satellite sensors of the far-red emission (Joiner *et al.* 2013, 2012, 2011; Frankenberg *et al.* 2011a,b). The capacity of SIF to provide information about actual – rather than just potential – photosynthetic function signifies a critical advance over current satellite sensors that tend to measure vegetation "greenness" or other static attributes. Because the fluorescence emission is related to the function of the two photosystems active during photosynthetic initiation in green plants, it provides a glimpse into the actual dynamics of the light reactions of photosynthesis.

The European Space Agency (ESA) has been investigating remote sensing methods for detection of chlorophyll fluorescence in terrestrial plants through its research activities over the past decade and more (e.g., Miller *et al.* 2005; Magnani *et al.* 2009; Mohammed *et al.* 2014; Moreno *et al.* 2014; Rascher *et al.* 2015). Current activities have focused on the Fluorescence Explorer (FLEX), one of two candidates included in Phase A/B1 assessments for ESA's Earth Explorer 8 mission (ESA 2015b). FLEX is oriented to bridging the land challenges identified in ESA's Living Planet Programme: Scientific Achievements and Future Challenges (ESA 2015a) through an advanced scientific Earth observation capacity that will support management of the world's vegetation resources (ESA 2015b).

As part of the FLEX Phase A/B1 activities, four main initiatives were completed previously: (i) the Photosynthesis (PS) Study, which developed a process-based model and simplified algorithms linking solar-induced fluorescence and photosynthesis, as well as fluorescence-based stress indicators (Mohammed *et al.* 2014); (ii) the Performance Analysis and Requirements Consolidation Study (PARCS), which developed approaches for retrieval of SIF from FLEX (Moreno *et al.* 2014); (iii) the *HyFLEX* initiative, consisting of dedicated field campaigns executed with the airborne demonstrator *HyPlant*, to investigate fluorescence characteristics over a broad range of vegetation types and species, and to explore the effects of

stresses on SIF (Rascher *et al.* 2015); and (iv) the Atmospheric Corrections for Fluorescence Signal Retrieval (FLUSS) project, which investigated atmospheric corrections for the fluorescence signal and surface pressure retrieval over land (Lindstrot *et al.* 2013). The current FLEX Bridge (FB) Study builds upon the foundation of those activities by focusing on optimisation of signal retrieval methodologies, extension of stress indicators, strengthening of the process-based modelling capabilities of the SCOPE model, and development of calibration/validation strategies for FLEX products.

Goals & objectives of the FLEX Bridge Study

The overall goals of the FLEX Bridge Study were to:

1. optimise approaches for SIF retrievals and applications in assessment of photosynthesis and stress status in terrestrial vegetation; and
2. develop a calibration/validation strategy for FLEX products.

Specific objectives were to:

- optimise the fluorescence retrieval algorithm developed under the PARCS activity;
- optimise the SCOPE photosynthesis model (v1.53) and related algorithms developed under the Photosynthesis Study;
- consolidate and develop retrievals for additional Level-2 data products;
- advance further applications based on Level-2 data products.

Science tasks

The study goals and objectives were addressed through four science tasks:

1. **Solar induced fluorescence retrieval optimisation and analysis.** This task built upon the PARCS activities (Moreno *et al.* 2014) by: consolidating algorithms for the atmospheric correction in FLEX configuration; optimising and improving algorithms for SIF retrieval; formalising fluorescence-derived indices; and developing biophysical products.

2. **Development of vegetation stress indicators and applications.** This activity advanced the range of applications and protocols for stress detection using SIF by: utilising datasets from campaigns with the airborne demonstrator *HyPlant* to extend stress-based applications of SIF; evaluating strategies to assess non-photochemical quenching using optical measurements; testing and reviewing stress indicators developed in the PS Study; and reviewing sources of variability and error in stress detection.

3. **Photosynthesis model optimisation, updates, and applications.** The SCOPE model version (1.53) that was developed in the PS Study was updated with new functionality, and foundations were laid for future developments by: considering effects of xanthophylls (known to contain additional information about stress); defining model parameters for specific plant functional types that can be linked to

operational global dynamic vegetation models; further quantifying vegetation structural effects on the measured SIF signal; and investigating data assimilation techniques amenable to usage in a broader range of applications, including global ecology, climate- and carbon modelling.

4. **Development of a calibration/validation strategy.** The need for a comprehensive cal/val strategy was identified in the PS Study and at the 5th International Workshop on Remote Sensing of Vegetation Fluorescence (22-24 April 2014, Paris, France). This priority was addressed here by: determining validation error metrics and product accuracies; defining a cal/val strategy for basic fluorescence products; defining FLEX Level-2/3 products and their validation plan; and defining common protocols and state-of-the-art instruments to be used in estimation of fluorescence in the context of calibration/validation activities.

Benefits: Progress for bridging the land challenges

The FLEX Bridge Study supports the development of best practices for the retrieval, quantification, and application of fluorescence measurements from space. These aspects are crucial in order to realise the full potential of space-based SIF technology in helping to meet the land challenges identified in ESA's Living Planet Programme. The completion of the FB Study also coincides with the official announcement by ESA (mid-November 2015) that FLEX is the successful candidate for the Earth Explorer 8 mission, making this study a timely transitional platform to future science activities, if so indicated.

2. Solar-induced fluorescence (SIF) retrieval optimisation and analysis

2.1 Introduction

This activity builds upon the PARCS results (Moreno *et al.* 2014) by addressing key aspects emerging from that study and the recent published literature, within the context of FLEX requirements. It targets the development of simulation datasets, as well as the processing chain for deriving fluorescence in FLEX configuration. In addition, two activities regarding fluorescence-derived indices and biophysical parameters useful for fluorescence interpretation are developed.

The main objectives were to:

- consolidate algorithms for atmospheric correction in FLEX configuration;
- set up algorithms for retrieval of sun-induced chlorophyll fluorescence;
- identify fluorescence-derived indices for multi-temporal composites; and
- advance retrieval of biophysical parameters.

There were four main areas of activity:

- data generation—to develop a new database of spectral radiance datasets to be used as input for subsequent algorithm development;
- advances toward Level-2a products—to generate a primary chain for producing accurate fluorescence retrieval;
- advances toward Level-2b products—to formalise primary indices computed directly from fluorescence data for evaluation and implementation in the FLEX mission; and
- advances toward Level-2c products—to support higher-level products by development of biophysical parameter retrieval algorithms, and simultaneous retrieval of canopy state variables.

2.2 Data generation

2.2.1 Extension of SCOPE-generated FLEX/S3 spectral database

The spectral database created by the University of Twente during the PARCS work was extended here. SCOPE (version 1.60) was used in the present activity, in which the Fluspect model (Fluspect_bcar; see Section 4.2) includes carotenoid absorption, and in which canopy fluorescence was modelled more realistically by including the contributions due to canopy-scattered and soil-reflected fluorescence. The number of cases in the database was increased from 31 to 40, and new outputs were added, e.g., fluorescence contributions from PSI and PSII (at least for both FLORIS WBS and NBS spectrometers), atmospherically corrected data (methodology as per University of Valencia), and spectral data (directional fluorescence and reflectance) in the direction of the backward-looking SLSTR sensor. The additional cases of the database comprise two more leaf angle distributions, two more chlorophyll contents, three more LAIs, and two more atmospheric visibilities. In the thermal domain, TOC radiance at 10 microns, brightness temperature, emissivity and TOC kinetic temperature were added as

outputs, as well as all relevant energy fluxes (net radiation, evapotranspiration, sensible heat and ground flux) have been added as outputs. Access to data in the database is facilitated by a Matlab script. This data is representative of single spectra and ideal scenarios of S3/FLEX, and were used in Section 2.5.2 for derivation of canopy state variables by inversion of SCOPE-simulated tandem mission data.

2.2.2 Generation of a synthetic Level-1b products dataset using FLEX End-to-End Mission Performance Simulator (FLEX-E)

Several simulated images (from simple to more realistic scenes) were generated in this component and used as inputs in Section 2.5.1. Below is a summary of the image simulated atmospheric characteristics, the surface reflectance, and fluorescence spectra used:

- three vegetated surface reflectance spectra and 1 bare soil spectrum;
- two different topographic heights : 0 km and 2 km above sea level;
- atmospheric conditions for aerosol optical properties (constant for all the images) and vapour content (depends on topographic height and cloud presence);
- a binning process performed for the forward modelling;
- Level-1b TOA radiance obtained after applying the PSF and the ISRF in the Level-1b module of the FLEX End-to-End Mission Performance Simulator (FLEX-E).

The scenes generated were used in retrievals of biophysical parameters (Section 2.5.1).

2.3 Towards Level-2a products

2.3.1 Optimisation of the atmospheric correction algorithm using S3/FLEX

The previous PARCS project extensively evaluated the retrieval of the atmospheric parameters. Nevertheless, the PARCS database created to evaluate the atmospheric correction performance was on a pixel basis and it did not focus on geometrically and radiometrically merging images from different sensors (i.e., FLORIS, OLCI and SLSTR) before atmospheric characterisation. In the present FB activity, this pre-processing step has now been tested thanks to the images provided by the FLEX-E in the preceding section.

As to the computational time, the Matlab code to perform the atmospheric correction implemented in the FLEX-E has been optimised and was at first parallelised. However, because parallelisation did not always save time, and sometimes presented Matlab code conflicts, in the end parallelisation was not applied.

Regarding the lookup table (LUT) design, every image used here had a set of LUTs expressly created to process that image. LUTs used in the forward modelling contained only grid points needed for the simulation. However, in order to perform the Level-2 retrieval it is necessary to define a LUT that covers a wide range of values, i.e., lower and higher values than the value used in the scene simulation. The grid points selection, especially for the retrieval LUT, balances the time computational cost and range needed to test the atmospheric correction algorithm performance.

2.3.1.1 Level-2 processing chain: Atmospheric correction algorithm

From Level-1b data (i.e., TOA radiance acquired by the sensor), the Level-2 processing algorithm must be able to retrieve surface apparent reflectance (i.e., surface real reflectance modified by the fluorescence emission). For the FLEX mission, the Level-2 processing chain could be divided by three main blocks or processes: (i) data pre-processing; (ii) atmospheric characterisation; and (iii) application of the fluorescence retrieval method using as inputs the apparent reflectance and the irradiance at surface level obtained from the atmospheric correction.

The fluorescence retrieval method identified in Section 2.3.2 was utilised here to analyse the coupling process with the atmospheric correction. Figure 2.1 shows the three main steps performed to obtain fluorescence.

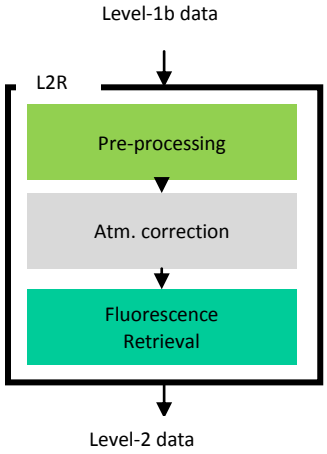

Figure 2.1. Level-2 processing scheme

Images acquired by Sentinel-3 and FLEX instruments must be pre-processed before starting with the atmospheric characterisation and the fluorescence retrieval process. This pre-processing step must guarantee several key aspects such as:

- geometric co-registration between images from the different sensors;
- consistency between radiometric levels from S3 and FLEX images (achieved by using a cross-calibration process); and
- spectral calibration

a) Geometric co-registration between images

Acquisition geometry from OLCI, SLSTR and FLORIS is different. Initially, images must be geolocated independently. This process is performed using geometry information provided by the sensor (in this case provided by the Level-1b module of the FLEX-E): line of sight (LOS) vectors which indicate where the sensor is pointing; orbit state (OS) vectors that indicate sensor position; image acquisition time; and the digital elevation model (DEM). The co-registration

between images is performed by means of a 2-dimensional cubic splines interpolation. Data from FLORIS, OLCI and SLSTR nadir and oblique viewing from the test scene are projected in a common latitude/longitude grid.

b) Cross-calibration

Consistency between the radiometric levels from the S3 and FLEX instruments is guaranteed by performing a cross-calibration process after co-registration. By calculating the ratio between the OLCI real and OLCI simulated (using FLORIS) bands, it is possible to obtain a scalar factor per band. Finally, these per-band scalar factors are interpolated for the entire FLORIS range and then applied to the FLORIS image.

c) Spectral calibration

Spectral calibration is performed before FLORIS atmospheric correction. A good characterisation of band central wavelength shifts and the instrument spectral response function (ISRF) shape for the FLORIS sensor has a tremendous impact on the fluorescence retrieval. Spectral characterisation is performed on a per column basis, in which several equidistant columns are selected to apply the spectral calibration process. Once the spectral calibration is performed for the selected columns, parameters obtained to define the ISRF shape and the band central wavelengths are interpolated to cover all image columns.

The spectral calibration process is based on (i) the characterisation of the band central wavelength shift and (ii) the characterisation of the ISRF shape. In Figure 2.2, the scheme followed to detect the central wavelength shift is shown. The main idea is to use the atmospheric parameters retrieved from the S3 atmospheric correction to perform an initial FLORIS atmospheric correction. We look for similar surface reflectance pixels in a column, giving priority to bare soil pixels to be considered as non-fluorescence pixels. If there are no bare soil pixels available in the column, vegetated pixels are selected, prioritising those which are expected to emit less fluorescence (i.e., selection by any greenness index such as the Normalised Difference Vegetation Index, NDVI). Mean surface reflectance spectra is then calculated and subsequently smoothed (only with no-vegetation pixels). In comparison, atmospheric correction is done over the mean TOA radiance from pixels selected before testing different spectral shift values and assuming the ISRF shape is known. Minimising the cost function makes it possible to find the resultant band central wavelength shift from each column. Minimising the cost function makes it possible to find a good estimation of the slope and the bandwidth values.

After detecting each FLORIS band central wavelength, a similar process is applied to characterise the ISRF shape, assumed here as a double sigmoid function where the bandwidth and the slope values can vary.

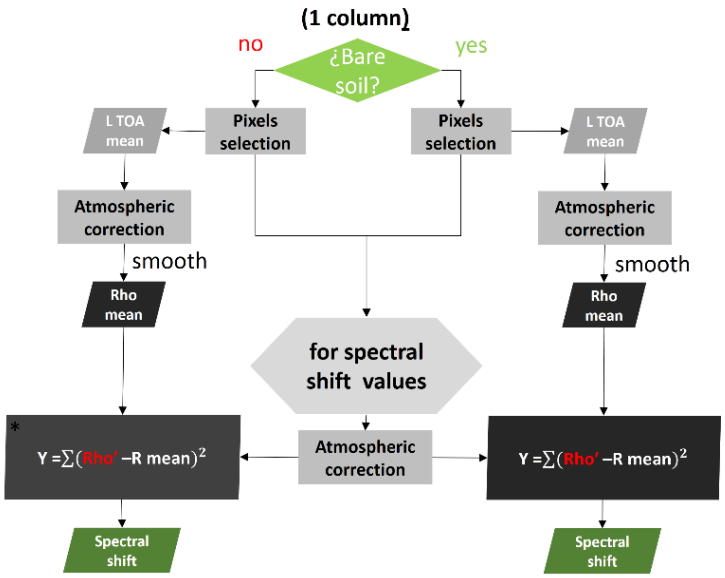

Figure 2.2. Spectral calibration process performed to detect the central wavelength spectral shift.

2.3.1.2 Atmospheric characterisation and correction

Although FLORIS has exceptional capabilities to measure the fluorescence signal, its spectral range (from 500 nm to 780 nm) is insufficient to extract information about the atmospheric state, in particular aerosol optical thickness and columnar water vapour. In this sense, the use of Sentinel-3 data from OLCI and SLSTR are essential to perform the atmospheric correction algorithm proposed here.

The atmospheric correction consists of the retrieval of apparent reflectance (i.e., surface reflectance modified by fluorescence radiance emission) by inversion of the radiative transfer expression (Equation 2.1). This process first retrieves the atmospheric properties (e.g., columnar water vapour, aerosol optical properties, temperature, atmospheric pressure) and then simulates the atmospheric transfer functions for these atmospheric properties using an atmospheric RTM (i.e., MODTRAN5).

$$\rho_{app} = \rho + \frac{\pi F}{E_{TOC}} \qquad (2.1)$$

where ρ_{app} and ρ are apparent and true reflectance (respectively), F is fluorescence radiance, and E_{TOC} is total irradiance at TOC.

The atmospheric characterisation and correction algorithm proposed here is divided into different phases: (1) masking out clouds, (2) retrieval of the columnar water vapour content and the aerosol optical properties, and (3) use of retrieved atmospheric parameters as inputs in the atmospheric radiative transfer inversion of FLORIS data to obtain surface apparent reflectance, surface irradiance (with and without oxygen), and surface radiance. All of these atmospheric correction products are needed to determine the sun-induced fluorescence

emission and correct the apparent reflectance spectra from FLORIS to obtain real surface reflectance as an atmospheric correction product.

a) Retrieval of aerosol optical properties

Determination of aerosol properties is performed on cloud-free pixels by using a MODTRAN LUT inversion algorithm that uses the spectral information from OLCI and SLSTR (dual view). The aerosol retrieval algorithm determines the aerosol content and type through parameterisation of the aerosol optical properties: aerosol optical thickness (AOT), Angstrom parameter which takes into account wavelength dependency of AOT, and Henyey-Greenstein scattering phase function asymmetry parameter. Because aerosol concentration varies with topography, the inversion will not be performed pixel-wise but instead over wider areas considered to be topographically uniform. (A 30 km^2 size is chosen here as a trade-off between the largest area in which the atmosphere can be considered constant and the smallest one providing enough variability in the surface (Guanter 2006).)

The aerosol optical properties retrieval is subsequently based on an iterative process that minimises the cost function:

$$\delta_\lambda = \sum_{pix} \left[\frac{1}{N} \sum_\Omega \sum_\lambda^N \varphi (L_{sen}^{SLSTR} - L_{sim}^{SLSTR})^2 + \frac{1}{M} \sum_\lambda^M \omega \, (L_{sen}^{OLCI} - L_{sim}^{OLCI})^2 \right] \qquad (2.2)$$

where N and M are the number of bands in SLSTR (not including thermal bands) and OLCI sensors respectively, Ω refers to the dual viewing angle of SLSTR, φ and ω are weighting functions defined as $\sim 1/\lambda^2$ according to each sensor configuration bands, L_{sen} are OLCI and SLSTR nadir and oblique viewing angle TOA radiances, and L_{sim} are the corresponding simulated TOA radiances for each sensor.

Whereas atmospheric properties remain nearly constant for wide areas, surface properties tend to present a more heterogeneous spatial pattern. This natural contrast is introduced mathematically as a boundary condition. Thus, pixels included in the minimisation cost function must be selected to be representative of the diversity in surface reflectance while atmospheric conditions are fixed.

The aerosol characterisation algorithm was applied over a synthetic scene created using the FLEX-E. Figure 2.3 shows the aerosol optical properties retrieved, i.e., AOT, Angstrom coefficient and Henyey-Greenstein phase function asymmetry parameter. It can be observed that there is constant value for all the images. In addition cloud presence has been masked out. Values retrieved were exactly the same used as input. In this case the simulation was performed selecting the optical properties typical from rural aerosol type and medium load.

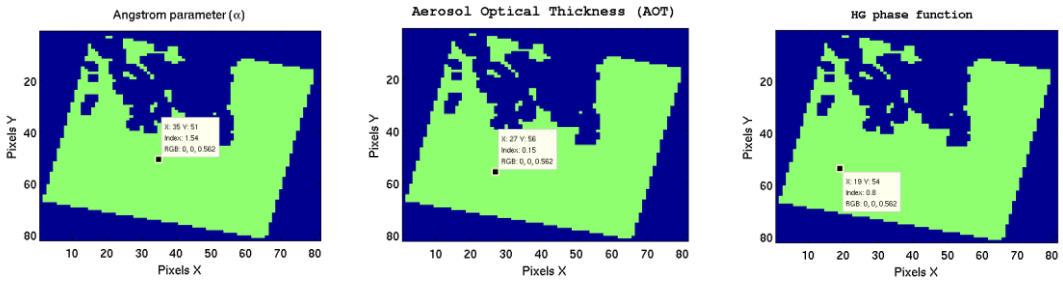

Figure 2.3. Aerosol optical properties retrieved, e.g., AOT, Angstrom coefficient, and Henyey-Greenstein isotropy parameter of the scattering phase function.

b) Columnar water vapour retrieval

Water vapour content is derived through a differential absorption technique using OLCI water absorption channels. In essence, differential absorption techniques calculates the ratio $R = {L_{out}}/{L_{in}}$ between radiances inside (L_{in}) and outside (L_{out}) the water vapour absorption band. Particularly, in OLCI this ratio is calculated at 940 nm. While L_{in} is directly TOA radiance acquired inside the absorption band, L_{out} is obtained by linear regression from the reference channels, i.e., channels close to the absorption band but not affected by it.

The CWV is retrieved by a LUT inversion, using Brent's method to minimise the cost-function between the sensed and simulated ratios $\chi = R_{sim} - R_{sen}$. The simulated ratio uses the previously derived aerosol properties and approximates the surface reflectance in the measurement spectral channel as a linear interpolation between the reference channels. The retrieval is done on a pixel-wise basis due to the high spatial variability of this parameter.

c) FLORIS apparent reflectance retrieval

The final step is the inversion of the TOA radiance expression (Equation 2.1). The apparent and at-ground solar irradiance for FLORIS are needed to determine vegetation fluorescence emission. In addition, OLCI and SLSTR (nadir) apparent reflectance are also obtained to subsequently derive vegetated biophysical parameters.

2.3.1.3 Improving the coupling of atmospheric correction and fluorescence retrieval

Once the FLORIS apparent reflectance signal and the solar irradiance at the surface level are obtained, it is possible to start the fluorescence retrieval process. It is a two-step procedure, i.e., doing first the atmospheric correction and then the fluorescence retrieval.

The fluorescence retrieval algorithm is based on a spectral fitting technique to provide the full fluorescence spectrum. The spectral fitting method is an iterative process that needs initial fluorescence estimation at O_2 absorption bands to initialise the process. The methodology followed to initialise the spectral fitting was discussed and developed in the PARCS project. However, this algorithm in PARCS was tested over a number of pixel based simulations where only radiometric noises were added and no other errors were applied over the images.

In this case, the spectral fitting algorithm was applied over the atmospherically corrected test image, where errors derived from an imperfect spectral calibration process or water vapour retrieval can drive errors in the spectral fitting method.

To improve the coupling of atmospheric correction and fluorescence retrieval, we have added an extra step before applying the fluorescence spectral fitting method. This extra step corrects errors arising with respect to the water vapour estimation and during spectral calibration of the FLORIS wide band spectrometer (WBS). Spectral calibration at the WBS is more difficult than at the narrow band spectrometer (NBS). The FLORIS NBS provides a higher number of spectral channels (which characterise the O_2 absorption bands). These narrow channels make it easier to detect possible central wavelength shifts and to estimate the ISRF shape. So, assuming a non-ideal water vapour retrieval and a non-ideal spectral calibration correction, the surface apparent reflectance spectrum can be corrected to avoid water vapour residual, especially at the red-edge region. In this way, the spectral fitting method, which takes into account the entire spectrum from 670 to 770 nm, will produce lower errors.

2.3.2 Optimisation of retrievals of the full SIF spectrum and contributions from Photosystem I & II

This workpackage aimed at consolidating and optimising the *Spectrum Fitting* (SpecFit) algorithm to retrieve the full SIF spectrum. The SpecFit algorithm allows decoupling SIF and surface reflected radiances spectra from the upward radiance in the 670-780 nm spectral window. The consolidation of the retrieval algorithm will contribute to providing an accurate, computationally efficient, operational algorithm to be used for the FLEX mission.

The specific objectives of this workpackage were to optimise the full SIF spectrum retrieval algorithm, and to test the possibility of deriving the specific PSI and PSII emission spectra. Three different approaches were evaluated which differ in their assumptions on the fluorescence spectral function: (i) the empirical approach of Cogliati *et al*. (2015b), which uses two pseudo-Voigt asymmetric functions (hereafter P-Voigt); (ii) the statistical method of Zhao *et al.* (2014) and Liu *et al*. (2015), which relies on the singular vector decomposition (SVD) technique (hereafter SVD); and (iii) a novel approach based on the PSI and PSII source spectral functions (hereafter PSIII-EM). These different retrieval models were evaluated exploiting the novel radiative transfer (RT) datasets developed in Section 2.2.

Accuracy of the SpecFit retrieval algorithm was tested using the dataset of radiative transfer simulations based on the coupled SCOPE and MODTRAN models. The dataset (Section 2.2.1) provides PSI and PSII spectra at the top of the canopy, an essential requirement here for evaluating the possibility of deriving the two contributions separately. The evaluation was conducted exploiting the RT dataset at the following levels: (i) top-of-canopy fluorescence spectra; (ii) top-of-canopy radiance without noise and atmospheric correction; and (iii) top-of-canopy radiance with noise and after atmospheric correction. Analysis at the three different levels is helpful for understanding the different sources of error (e.g., errors in the proposed retrieval models, atmospheric corrections, etc.).

The retrieval algorithm performances were assessed comparing the SIF and ρ from SCOPE (inputs of the RT calculations) and the retrieved values at the different λ. The main statistical index considered was the Root Mean Square Error (RMSE), which represents a way of quantifying the amount by which an estimation differs from the true value of the quantity.

2.3.2.1 Results

2.3.2.1.1 Retrieval of the fluorescence spectrum

The different fluorescence spectrum models were first tested directly on the TOC fluorescence by SCOPE (i.e., layer 8 of the RT database). This step verifies that the spectral models considered were capable of fitting diverse fluorescence spectra. All three methods were able to fit with a good level of accuracy the different TOC fluorescence spectra. The quantitative comparison between the three methods proposed in terms of RMSE is shown in Figure 2.4. The SVD performed best (RMSE 0.019 mW $m^{-2}sr^{-1}nm^{-1}$), the P-Voigt method provided similar results (RMSE 0.022 mW $m^{-2}sr^{-1}nm^{-1}$), and the method based on the PSI and PSII spectral functions showed a slightly larger error (RMSE 0.042 mW $m^{-2}sr^{-1}nm^{-1}$). Although the SVD method had the highest average accuracy, it also had larger errors for 4-5 different cases.

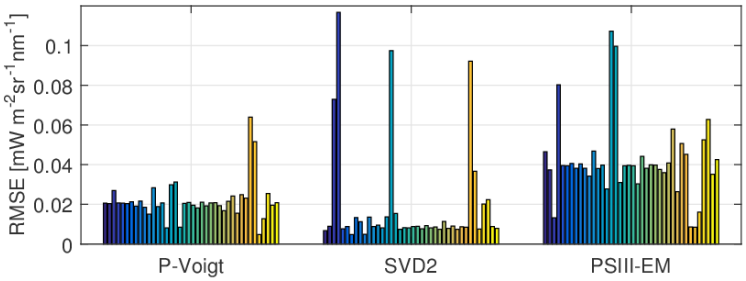

Figure 2.4. RMSE values calculated for the 40 different RT simulations for top-of-canopy (layer 8). Results are clustered for the three different SIF retrieval models.

Testing was then conducted on TOC radiance spectra without noise (layer 3). The top-of-canopy radiance (i.e., reflected and fluorescence contributions) was used to assess the capability of the different retrieval algorithms in decoupling surface reflectance and SIF spectra. The P-Voigt and SVD methods performed well for most of the simulated cases, while the PSIII-EM method underestimated the red SIF up to about 730 nm (RMSE 0.40 mW $m^{-2}sr^{-1}nm^{-1}$). The reason for this bias is not yet clear and will be investigated further. The SVD and P-Voigt had the best accuracies with average RMSE of 0.048 and 0.091 mW $m^{-2}sr^{-1}nm^{-1}$ respectively (Figure 2.5).

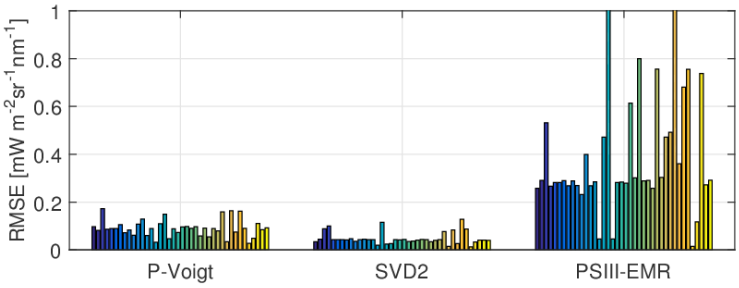

Figure 2.5. RMSE values for the three different SIF retrieval models obtained from top-of-canopy radiance spectra without noise (layer 3).

The retrieval algorithms were also tested on TOC radiance with a realistic inclusion of the sensor noise and atmospheric correction (layer 5 of the database) in order to evaluate the accuracy level in realistic scenarios representative for the FLORIS sensor. The P-Voigt and SVD methods had accurate retrieval of the red fluorescence (i.e., 687 nm), but the far-red peak was systematically underestimated by both methods. This finding can be linked to a bias in the atmospheric correction method applied in the database – in fact the apparent reflectance at the top of the canopy appeared to be overestimated (compared to the pure reflectance) in the NIR region. The PSIII-EM method underestimated both the red and far-red fluorescence. Accuracies (Figure 2.6) were relatively similar between P-Voigt and SVD methods, but with a slightly larger sensitivity of the SVD method to instrumental noise.

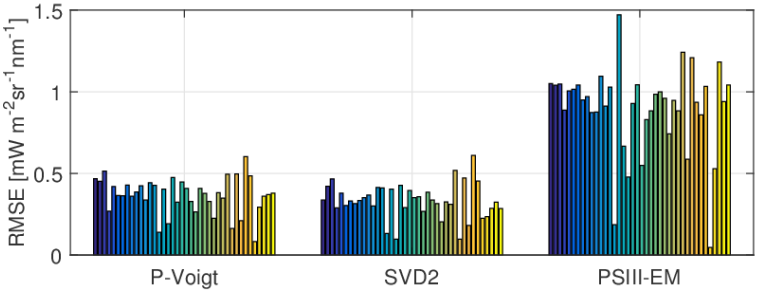

Figure 2.6. RMSE values for the three different SIF retrieval models obtained from top-of-canopy radiance with noise after atmospheric correction (layer 5).

In summary, all three methods were able to accurately fit the TOC fluorescence spectra. The PSIII-EM model, in particular, was able to correct the PSI/PSII source spectra after the inclusion of the reabsorption term in the model. The shape of the spectrum was consistent with the TOC fluorescence from SCOPE. Results obtained in decoupling the TOC radiance into its reflected and fluorescence contributions were almost similar for the P-Voigt and SVD approaches. The SVD seemed to provide slightly better accuracy, but it was more sensitive to instrumental noise. The advantage of the SVD method is a faster computational time, however it depends on the training set used in deriving the singular vectors in the retrieval. The PSIII-EM method did not provide the most accurate results in the estimation of the red fluorescence peak for most of the radiative transfer cases simulated. However, it is currently the only method available for decoupling the PSI/PSII spectra.

2.3.2.1.2 Retrieval of PSI & PSII spectra

The initial test to retrieve PSI and PSII spectra was applied on TOC fluorescence spectra. Only the PSI/PSII approach (PSIII-EM) could be used in this case for decoupling the total fluorescence emission into the distinct PSI and PSII contributions. Figure 2.7 shows the total top-of-canopy fluorescence, the PSI, and PSII spectra retrieved together with the reference values (SCOPE simulations). There was good agreement between the retrieved and reference spectra in most cases, except for a few simulations in which the algorithm confused the PSI and PSII contributions in the spectral region in which they overlapped.

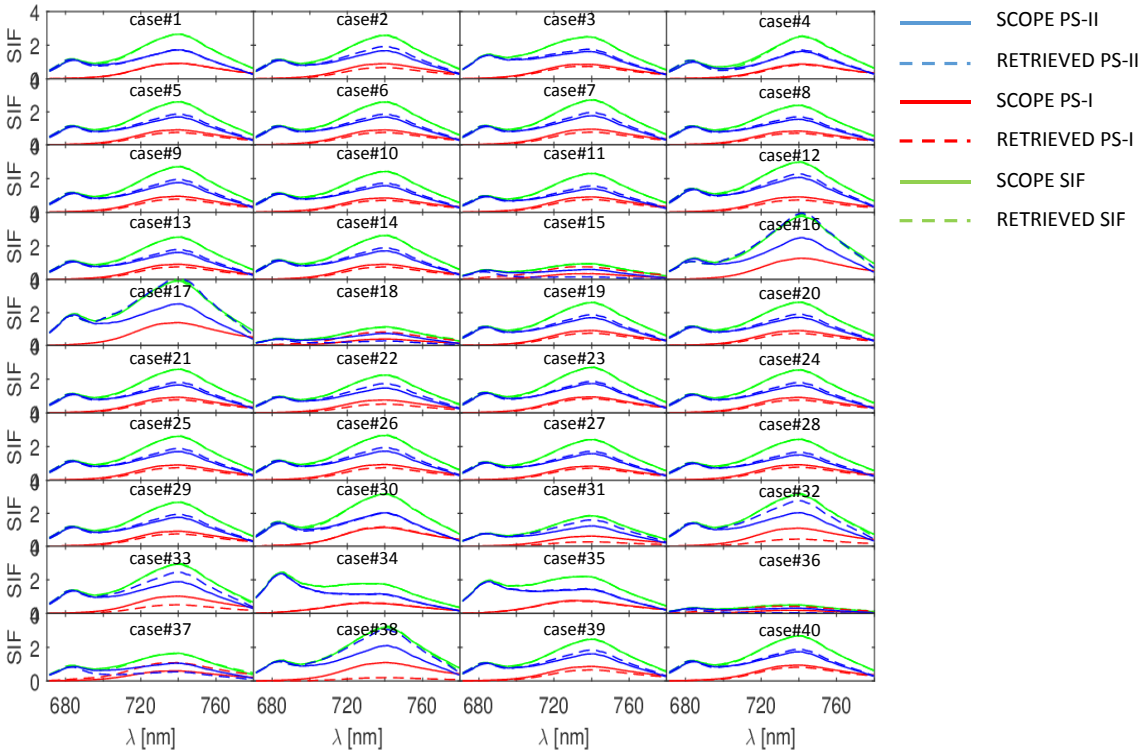

Figure 2.7. Retrieval of total fluorescence, PSI, and PSII spectra from top-of-canopy fluorescence spectra.

The results show that the PSI and PSII spectra can be obtained from total TOC fluorescence with an RMSE lower than 0.1 mW $m^{-2}sr^{-1}nm^{-1}$ in most of the simulated cases (Figure 2.8).

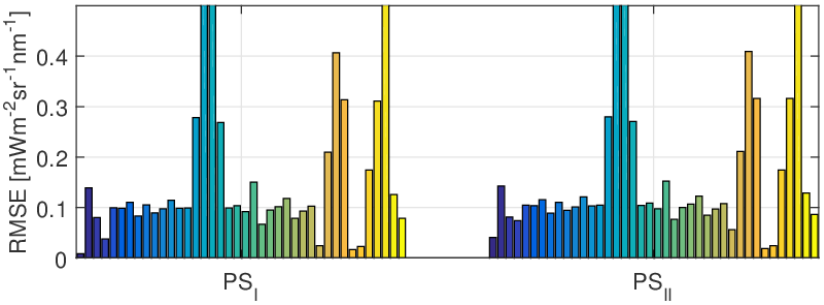

Figure 2.8. RMSE values for PSI and PSII spectra obtained by employing PSIII-EM method on TOC fluorescence spectra.

All the three methods could then be used to estimate the total fluorescence, PSI, and PSII spectra from the top-of-canopy radiance measurements. In fact, the methods can be used in series in order to retrieve the total fluorescence in the first step, followed by the decoupling of the PSI/PSII spectra. Figure 2.9 shows the results achieved by using the P-Voigt method obtained with the initial retrieval of the total SIF spectrum, and the successive use of the PSIII-EM method. Similar results have been found by combining SVD and PSIII-EM methods (data not shown). Both approaches proved the possibility of deriving PSI and PSII spectra from TOC radiance spectra with RMSE values about of 0.2 mW $m^{-2}sr^{-1}nm^{-1}$ for PSI and 0.1 mW $m^{-2}sr^{-1}nm^{-1}$ for PSII in most of the analysed cases (Figure 2.10).

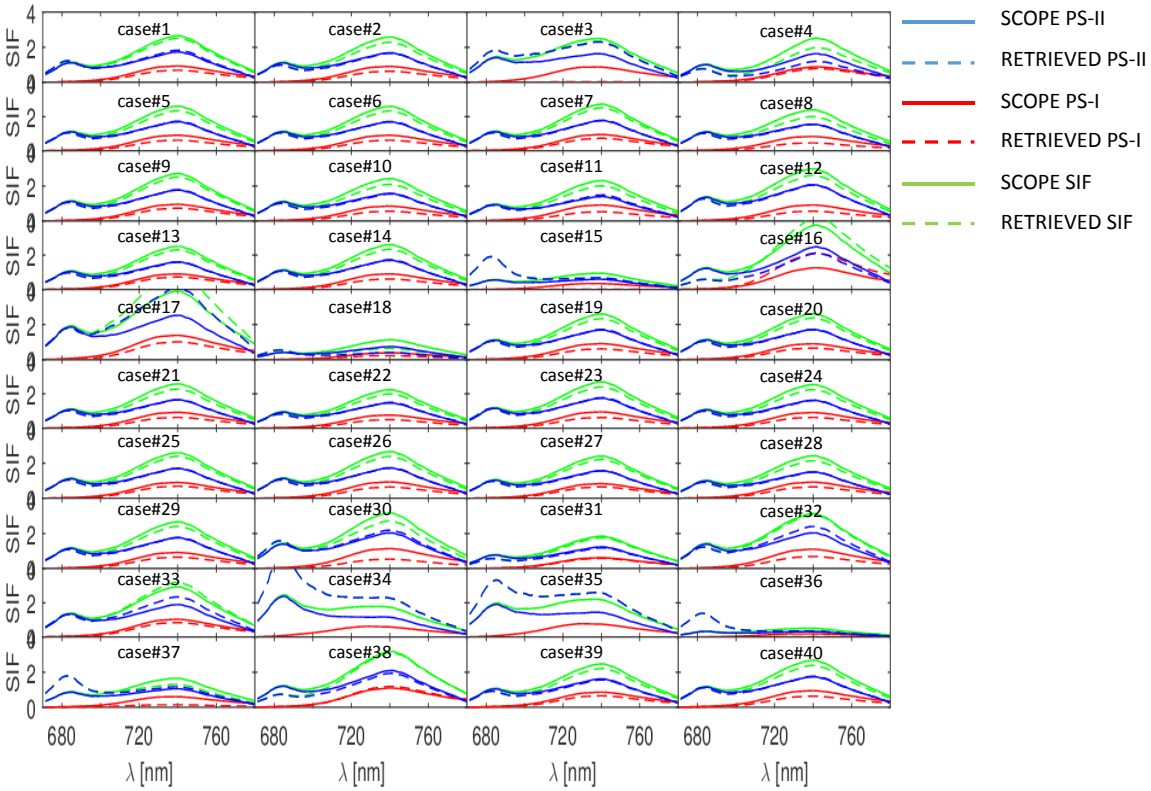

Figure 2.9. Retrieval of total fluorescence, PSI, and PSII spectra from top-of-canopy radiance spectra (without noise), by combining the P-Voigt and PSIII-EM methods for total SIF retrieval and PSI/PSII decoupling respectively.

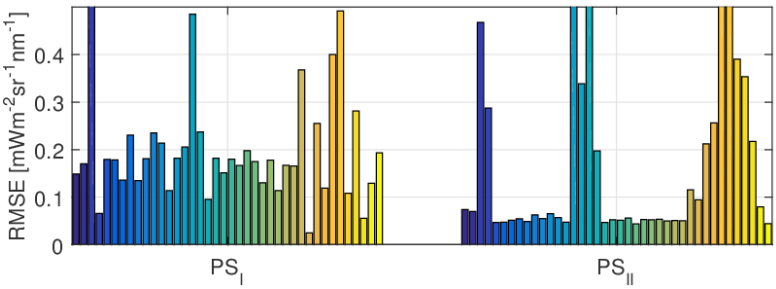

Figure 2.10. RMSE values for PSI and PSII spectra retrieved by combining P-Voigt and PSIII-EM methods on TOC radiance spectra without noise (layer 3).

A more realistic evaluation tested the methods using TOC radiance with noise/atmospheric correction (i.e., layer 5 of the database). The P-Voigt and SVD methods may be used to derive the top-of-canopy fluorescence, then the PSIII-EM to decouple PSI and PSII spectra (Figure 2.11). As already observed, results achieved from this layer were affected by a bias in the atmospheric correction for the far-red region, causing an underestimation of total far-red fluorescence, and the complete loss of PSI contribution. On the other hand, the red-peak of fluorescence is well represented by both the approaches. Figure 2.12 shows the RMSE values obtained, the PSII spectra were successfully retrieved with RMSEs about of 0.1 mW $m^{-2}sr^{-1}nm^{-1}$ while the PSI spectra were not detected in most of the cases (RMSEs 0.5 mW $m^{-2}sr^{-1}nm^{-1}$).

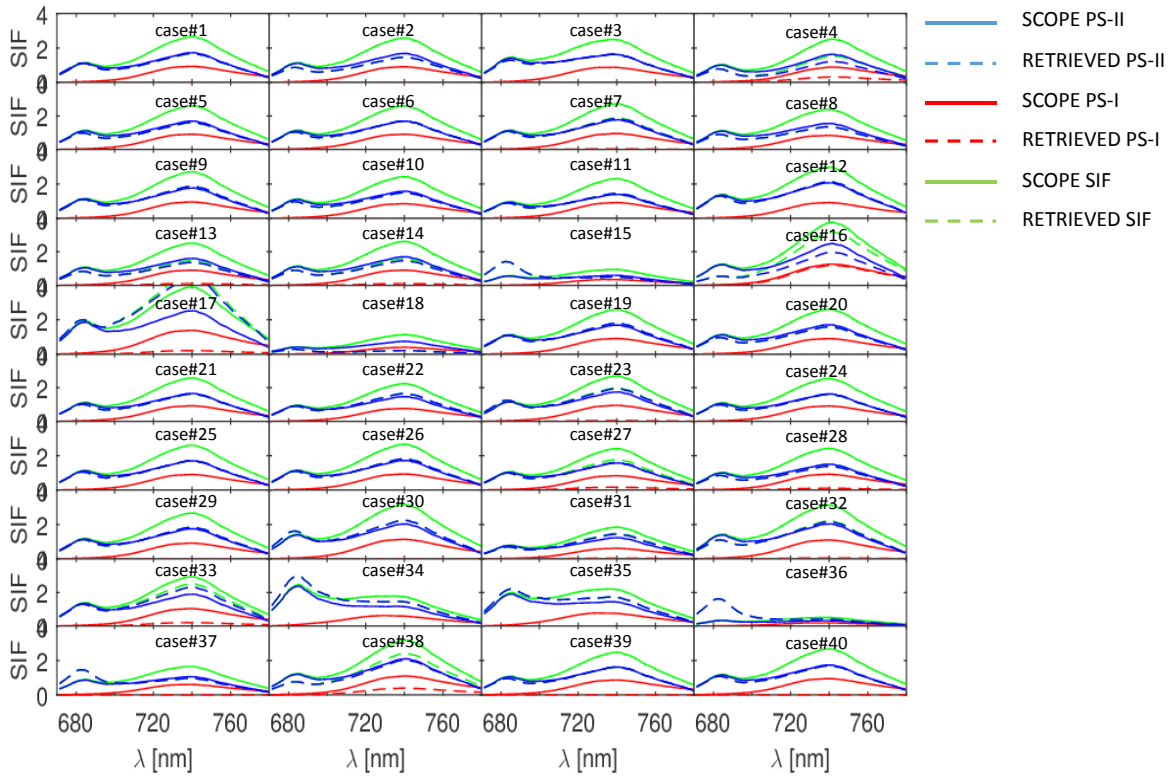

Figure 2.11. Retrieval of total fluorescence, PSI, and PSII spectra from top-of-canopy radiance spectra with noise and after atmospheric correction, by combining the P-Voigt and PSIII-EM methods for total SIF retrieval and PSI/PSII decoupling respectively.

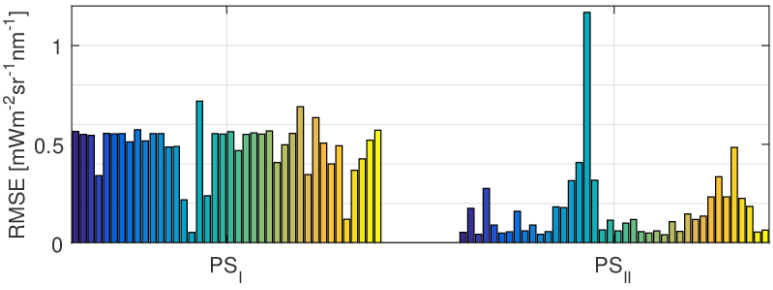

Figure 2.12. RMSE values for PSI and PSII spectra obtained from top-of-canopy radiance spectra with noise and after atmospheric correction (layer 5) by combining P-Voigt and PSIII-EM methods.

In summary, three different fluorescence retrieval methods for total fluorescence, the PSI, and PSII spectra have been carried out in this workpackage. The methods differ in their assumptions on the fluorescence spectral function. The P-Voigt method is the most empirical because it relies only on basic/common mathematical functions (i.e., Voigt profiles) in representing the SIF spectrum, the advantage of this approach being that it does not rely on the forward model used in producing the testing RT dataset. The SVD method relies on a statistical analysis of the forward simulations, therefore it is more dependent on the RT forward model with the possibility that the model cannot accurately represent the different real scenarios. Moreover, the results here were based on singular vectors obtained by applying the SVD technique on the same TOC fluorescence later used for the evaluation of accuracy. Thus, accuracies here could be overestimated compared to the performances of the algorithm with actual observations. This situation could be addressed in the future by considering a wider set of RT simulations, and sub-dividing the large database into training and testing subsets. The PSIII-EM approach is more based on physical modelling of the radiative transfer within the canopy, using a linear combination of PSI and PSII source spectra with an additional term for reabsorption effects at leaf and canopy levels. All the three methods are able to accurately fit the top-of-canopy fluorescence spectrum.

The analysis has shown the further possibility to separate the PSI and PSII spectra from the total canopy fluorescence. The current solution relies on the coupling of the P-Voigt/SVD methods to retrieve the total fluorescence, followed by decoupling of the PSI and PSII spectra by using the PSIII-EM. This approach can allow an accurate decoupling of the spectra from the different photosystems.

2.4 Towards Level-2b products

2.4.1 Assessment of strategies to improve APAR estimates for calculation of yields

The interpretation of fluorescence measurements and the calculation of fluorescence yield require accurate information about APAR (absorbed photosynthetic active radiation) and NPQ, putting high demands on their retrieval precision. The retrieval of APAR, however, is challenging because it relies on several assumptions about incident photosynthetic active radiation (PAR) and the vertical distribution of PAR within vegetation canopies. Because of this complexity, available approaches often require *a priori* knowledge of land cover or plant distribution functions and rely on the inversion of physical-based models or simple band ratios.

Here, we evaluate published APAR retrieval methods to judge their robustness and flexibility with respect to application for FLEX. Conceptual suggestions for potential improvements or alternative strategies will be discussed. The specific objectives are to:

- summarise published methods to estimate APAR from optical remote sensing data;
- identify and summarise limitations of existing approaches, complemented with simplified experiments; and
- suggest alternative strategies to overcome identified limitations.

2.4.1.1 Results

2.4.1.1.1 APAR definitions, retrieval approaches and uncertainties

The accurate determination of photosynthesis requires an estimation of PAR absorbed by green leaves ($APAR_{green}$) (Gamon 2015; Gitelson & Gamon 2015; Gitelson *et al*. 2015). But in practice $APAR_{green}$ is difficult to measure. A detailed description of $APAR_{green}$ neglecting any horizontal fluxes is given by Gitelson & Gamon (2015) and Widlowski (2010) as:

$$APAR_{green} = (PAR_{inc} - PAR_{out} - PAR_{trans} + PAR_{soi}) \cdot \frac{LAI_{green}}{LAI_{tot}} \quad (2.3)$$

where PAR_{inc} is the incoming PAR radiation, PAR_{out} is the reflected PAR radiation measurable with a remote sensing instrument, PAR_{trans} is PAR radiation transmitted through the canopy, and PAR_{soi} is PAR_{trans} reflected by the soil background in direction of the sensor.

Direct measurements of $APAR_{green}$ are not possible and its retrieval is particularly challenging. Only one component (PAR_{out}) of the radiative transfer (RT) is measurable. The remaining RT components must be approximated using assumptions or models. The literature revealed a list of issues determining the reliability of available APAR products. Main results are listed hereafter. It must be noted that the normalisation of fluorescence requires absorbed light energy in absolute units. However, most published approaches provide information about the relative fraction of APAR (fAPAR). Because APAR can be obtained by multiplying fAPAR with PAR incident on the Earth surface, we consider below reported findings and retrieval issues for fAPAR as representative for APAR retrievals as well.

The various fAPAR retrieval strategies proposed to date differ in their underlying methodology and are either physical-based or empirical using vegetation indices. Since only a limited number of components of the underlying RT can be directly measured and APAR is a complex wavelength-dependent function not resolvable with available satellite instrumentation, calculations of fAPAR (and eventually APAR) rely on different assumptions and definitions (considering diffuse and direct irradiance fluxes), as well *a priori* knowledge of underlying biome types (D'Odorico *et al*. 2014; Pickett-Heaps *et al*. 2014).

D'Odorico *et al*., (2014) and Pickett-Heaps *et al*. (2014) provided a recent overview of available approaches that range from simple empirical methods employing spectral vegetation indices, to complex physical-based model inversion schemes. The AVHRR product, for example, is based on the NDVI (Donohue *et al*. 2008). The MERIS and SeaWiFS products are derived from generic vegetation indices in combination with correction coefficients derived from RT modelling (Gobron *et al*. 2006). Yet other fAPAR products such as for MODIS are based on the inversion of complex 3D models (Myneni *et al*. 2002).

The diversity of available fAPAR approaches results in large differences between available fAPAR products across time and space. D'Odorico *et al*. (2014) particularly associated these differences to insufficiently considered structural effects and various assumptions on the optical properties of underlying vegetation surfaces. Considering three fAPAR products over Europe, they found uncertainties of up to 50% between fAPAR products, with average

uncertainties of 12%. Similar findings were reported in Pickett-Heaps *et al*. (2014) for a study focussing on Australia only and in Tao *et al*. (2015) for a global study. These uncertainties can be considered as systematic biases and it was argued that canopy structural effects and model assumptions are responsible for them.

Besides the spatial variability between fAPAR products, D'Odorico *et al*. (2014) also investigated the temporal agreement of fAPAR products for different sites. In general, the seasonal behaviour of fAPAR was well captured by all three products, with some disturbances in the broadleaved forest "Soroe". However, there was a substantial divergence between all fAPAR products compared to a reference signal obtained from EC-flux tower data (Figure 2.13). Largest uncertainties were found for the more empirical approaches (up to 60%). Further, the agreement between the individual fAPAR products varied markedly across ecosystems and showed differences of up to 40%. These uncertainties can be considered as systematic biases and it was argued that canopy structural effects and model assumptions were responsible.

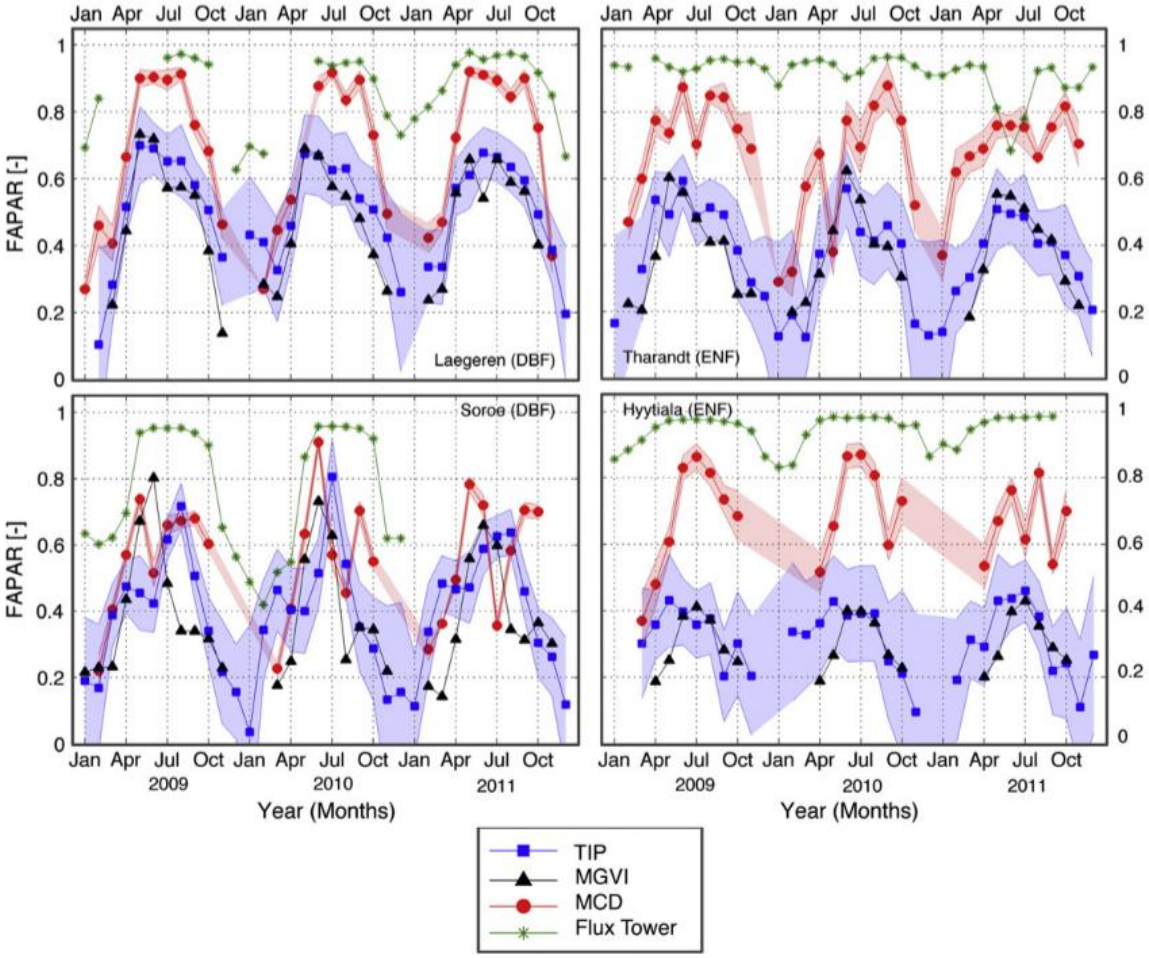

Figure 2.13. Temporal consistency of three different fAPAR products (JRC-TIP, ESA/JRC MGVI, and Boston University MCD, for details cf., D'Odorico *et al*. (2014)) in comparison to in-situ measured flux tower fAPAR (D'Odorico *et al*. 2014).

Lack of agreement across fAPAR products, and potentially APAR, indicates a need for new paradigms to overcome limitations of available approaches, e.g., the approximation of non-measurable fluxes (PAR_{trans}, PAR_{soil}, PAR_{inc}), or the dependency on *a priori* knowledge about underlying land cover types. Furthermore, retrievals of $APAR_{green}$ theoretically require knowledge of green biomass to compensate for light absorption by non-photosynthetic active canopy elements. Several experimental strategies using vegetation greenness as correction factor have been suggested (Gitelson & Gamon 2015; Gitelson *et al*. 2015; Haboudane *et al*. 2004) for this purpose but no operational solution exists yet.

2.4.1.1.2 Impact of uncertain irradiance fluxes for calculation of APAR

We used a 3D virtual scene of a mixed temperate forest in Switzerland (Laegeren) (Schneider *et al*. 2014) derived from extensive ground observations and 3D modelling with the radiative transfer DART model (Gastellu-Etchegorry *et al*. 2004) to evaluate uncertainties in estimating $APAR_{green}$ related to assumptions of different RT components as stated in Equation 2.3. (For details on the modelling, see http://www.geo.uzh.ch/microsite/3dveglab/).

We found a substantial variability of PAR_{inc} over this complex structured forest, ranging between 26% for diffuse irradiance and 30% for direct irradiance. Bulk approximations of surface irradiance with coarse resolution digital elevation models consequently introduce uncertainties in APAR calculations. For high spatial resolution data (2m), we observed an average overestimation of 49% (standard deviation 150%), with largest uncertainties in cast shadows. This uncertainty can be considered as worst case since surfaces appear highly heterogeneous in high resolution data. However, in view of data validation purposes with airborne demonstrators, such potential uncertainties need to be taken into account. With increasing pixel size, averaging effects cause a decrease of APAR overestimations, although for FLEX-like observations (300m pixel size), the uncertainty is negligible, ranging around 1% (+/- 0.15%).

Varying understory (soil, herb layers) can cause uncertainties in estimated APAR of roughly 8.3% (+/- 7.6%), independent of the spatial sampling size. Further, if only top-of-canopy observations are used to estimate APAR, and the vertical variability is neglected, pixel-size-independent uncertainties of calculated APAR of roughly 17% (+/- 10%) can occur.

The simple sensitivity analysis conducted here allowed quantification of uncertainties in APAR calculation, associated with assumptions applied to various PAR terms of the underlying RT. The analysis was based on a limited dataset covering a complex structured mixed forest. However, the complexity of this forest – in combination with the underlying topography – was high, and uncertainty estimates can be considered as values at the upper level of the uncertainty range.

We did not investigate yet the impact of assumptions on LAI_{green}, eventually required to derive $APAR_{green}$. Focusing on the various PAR fluxes, however, still provided important insight into causes of uncertainties observed for operational fAPAR products that were mainly related to atmospheric effects and canopy structure.

2.4.1.1.3 Improved APAR retrievals using high resolution digital object models

One particular problem in the calculation of APAR is the accurate estimate of surface irradiance, including the direct and diffuse irradiance components, considering canopy topography. We tested the suitability of using high resolution digital object models (DOMs) and potential uncertainties attributed to the use of coarse digital elevation models (DEMs).

First, we used a fine (1m) resolution DOM to retrieve a reference APAR map. Such high resolution DOMs allow reliable retrievals of APAR and compensating for most of the cast shadow effects as present in the at-sensor radiance maps. Using a coarse DEM data set (25 m), basically following the surface topography rather than canopy height, caused substantial effects in the resulting APAR maps. Although coarse topography features can be corrected, fine structures such as mutual shadowing and cast shadow stemming from illumination effects persist in the resulting APAR map. Further, in case the slope and aspect information derived from the DEM does not match with the actual slope and aspect of the canopy, this is particularly a problem in steep areas – the resulting APAR basically follows patterns of the surface exposition rather than reflecting a valid APAR pattern. When compared to the reference APAR map, average differences of 0.5% can be obtained, with underestimations of up to 55.0% and overestimations of up to 64.8%. Largest differences occurred in steep areas, especially the north-facing slope and in shaded areas. Assuming a flat surface, illumination and topography pattern persisted in resulting APAR maps, and the average overestimation of APAR was found to be 7.8%, ranging between underestimations of up to 32.0% and overestimations of up to 12.8%. Largest differences occurred in the north-facing slope, particularly in shaded areas. Considering the FLEX pixel size of 300 m and using a coarse DEM, we observed an average difference of 0.1%, with underestimations up to 40.0% and overestimations up to 28%.

2.4.1.1.4 Identification and conceptual development of alternative strategies for estimating APAR

The vertical structure of vegetation canopies and understory information are typically unknown and are the less constrainable parameters for the retrieval of APAR. This causes intrinsic uncertainties in current APAR retrievals irrespective of algorithms used. The challenge is to compensate for this lack of knowledge to minimise respective uncertainties in APAR products. One possible strategy was recently proposed by Laurent *et al*. (2014; 2013; 2011a, b). The proposed approach refines the coupling between the surface and the atmosphere and moves the retrieval problem of surface information from the top-of-canopy level by exploiting reflectance data to the sensor level using radiance data.

TOC approaches basically compare reflectance signals that are on the one hand modelled and on the other hand obtained from remote sensing (RS) observations. The simulation of surface reflectance is based on RT models, while the resulting physical quantity corresponds to bi-hemispherical reflectances (BHR). Atmospheric compensation approaches are applied to remove the effects of atmospheric absorption and scattering, to eventually obtain surface reflectance information from measured radiance data, typically resulting in hemispheric-conical reflectance factors (HCRF).

According to Laurent *et al.* (2013) or Damm *et al.* (2015b), several problems are intrinsic to the TOC approach, limiting its reliability and applicability especially for complex surfaces. First, atmospheric, optical, directional, and topographic effects are corrected sequentially, although they are correlated and mutually influential. Further, the state of the atmosphere is often unknown and assumptions on individual atmospheric parameters introduce uncertainties in retrieved surface reflectances. In addition, there is a mismatch between reflectance quantities that are compared to obtain surface information, i.e., BHR and HCRF, which affect the accuracy of estimated surface properties as well.

At-sensor radiance approaches to advance estimates of surface variables

Alternative to the TOC approach is a strategy that moves the retrieval problem to the sensor level by directly exploiting at-sensor radiances. This alternative approach potentially allows compensating some of the above issues that are intrinsic to the TOC approach. The at-sensor radiance approach couples a canopy and an atmosphere RT model to simulate at-sensor radiance. In a second step, Bayesian statistics (or other inversion methods) are used to invert the coupled model to eventually retrieve surface information from measured at-sensor radiance signals. The inversion of the coupled model is more physically sound and, thus, accurate compared to the TOC approach that successively inverts an atmosphere and a canopy model. Another beneficial aspect is that several effects, e.g., optical, directional, and topographic effects, as well sensor properties can be included in the coupled canopy-atmosphere model to directly compare simulated and measured radiances. This avoids a mismatch between physical quantities as is the case for the TOC approach. The possibility to incorporate various constraints and *a priori* information provides further flexibility to increase the reliability of retrieved surface information. Last, the coupling of canopy and atmosphere models reduces the number of unknowns, limiting the under-determination of the inverse problem. Statistical parameters (certainty measures, probability functions) implicitly provided by Bayesian inversion provides quantitative measures to judge the retrieval quality.

The at-sensor radiance approach is novel. A few pioneering studies (Verhoef & Bach 2003a,b) outline the possibility to apply this approach in forward mode to obtain accurate simulations of radiances at satellite level. Laurent *et al*. (2013) demonstrated the possibility to accurately simulate at-sensor radiances for an airborne setup, and also the possibility to simultaneously retrieve eight surface variables, including vegetation class, vegetation cover, LAI, leaf chlorophyll content, leaf dry matter content, leaf water content, fraction of brown pigments, and leaf thickness (Laurent *et al*. 2014).

The increased quality and resolution of RS data (also envisaged for FLEX) requires a more precise modelling of the physical, optical, and biochemical processes determining light-atmosphere-surface interactions and asks for more sophisticated statistical tools. First encouraging results obtained with the at-sensor radiance data analysis scheme suggest it as a potential strategy to advance $APAR_{green}$ retrievals as well.

We have implemented and tested an inversion scheme using a Monte Carlo Markov Chain (MCMC) technique that is based on Bayesian statistics and efficiently explores unknown

parameter spaces spanned by the various factors influencing the RT of coupled atmosphere-surface systems. MCMC does not sample the parameter space uniformly (as for Bayesian methods) but according to the variables' probability distribution function. This means that the sampling is regulated by the probability of parameter values. The advantage of this strategy is that high dimension parameter spaces can be easily explored and the adaptive space sampling scheme allows dealing with the model degeneracies. Simultaneous retrievals of atmospheric and surface parameters are consequently possible. Further, the MCMC inversion scheme allows consideration of model constraints, e.g., corrections for adjacency effects, topographic effects, and adding temporal and spatial constraints. MCMC is, thus, particularly interesting for $APAR_{green}$ retrievals since it facilitates estimating the individual PAR fluxes from Equation 2.3 as well as the contributions from photosynthetically active plant materials.

Bayesian model inversion, especially for high dimensional retrieval problems, can easily become computationally expensive. A flexible strategy recently suggested by Rivera *et al*. (2015) and Verrelst *et al*. (2015a) involves calculating a LUT containing a critical set of simulations representative for all possible measurements. Later, the LUT is parameterised with machine learning (ML) approaches (i.e., neuronal networks). If the inversion routine requests a certain simulation, ML approaches can provide an approximated simulation. This strategy was found to be at the cost of accuracy but is a mandatory step for an operational implementation.

In summary, a sensitivity analysis was applied here to provide a first estimation of the impact of different model assumptions for the individual PAR terms required. Using a modelled 3D scene of a complex structured forest, we could quantify substantial uncertainties in APAR and relate them to assumptions of the various PAR terms. Uncertainties related to the individual PAR fluxes already provide important insight into potential causes of APAR retrieval issues, particularly for an operational implementation of an APAR product. Results allow setting priorities for potential refinements of algorithms.

In view of supporting potential FLEX data users with relevant auxiliary data for applications (e.g., in stress detection), it is suggested to put emphasis on the optimisation of APAR retrieval algorithms. The envisaged FLEX-fluorescence retrieval approach is based on the at-sensor radiance approach. This is a large advantage since a substantial contribution towards more accurate APAR products is easily possible.

2.4.2 Definition and derivation of additional SIF-derived indices

The maximum rate of carboxylation (V_{cmo}) is a key control parameter of photosynthetic capacity. However, according to the recent Global Sensitivity Analysis (GSA) of the SCOPE model (Verrelst *et al*. 2015b), it drives only a relatively small portion of the SIF signal. Broadband incoming shortwave radiation (R_{in}), leaf chlorophyll content (LCC), and leaf area index (LAI) are major drivers of fluorescence emission intensity. Therefore, if variations in the spatial and temporal domains of these drivers are not properly accounted for, it can lead to biased interpretation of remotely sensed SIF. Here, we evaluate various fluorescence-derived indices in order to identify those best suited to normalise variations in environmental conditions, vegetation characteristics and temporal composites.

Database generation, SIF-derived indices and evaluation criteria

The analysis was carried out using a simulated dataset generated with a recent version (1.60) of the SCOPE model (Van der Tol *et al*., 2009), using the A-SCOPE graphical interface (Verrelst *et al*., 2014). SCOPE input variables were left at default values, except for R_{in}, LAI and LCC, which were ranged stepwise as follows: R_{in} 400-1200 W m^{-2} (5 steps); LAI 0.5-6 m^2 m^{-2} (7 steps); LCC 10-70 µg cm^{-2} (7 steps). A dataset of 245 simulations was thus generated. A selection of SCOPE outputs was then extracted from A-SCOPE MySQL database and used to compute the fluorescence-derived indices.

Several well known metrics were tested, some of them sensible to the incident irradiance, others to the radiation absorbed by leaves and used for photosynthesis. Others are reflectance-based indices, used as proxies for physical quantities of interest that are not easily obtained from remote sensing data. A summary of the tested metrics is shown in Table 2.1.

Each SIF-derived normalisation index was computed dividing the array of simulated SIF spectra by the correspondent array of normalisation metric (e.g., PAR, APAR, NDVI, etc.). In order to make these results comparable one to each other, the original array of SIF spectra and the normalised ones were individually scaled linearly between zero and one. After that, the values at four different wavelengths (687nm, 690nm, 740nm and 760nm) were extracted. These wavelengths correspond to the SIF red and far-red emission peaks (SIF_{690} and SIF_{740}, respectively) and to the O_2-B and O_2-A oxygen absorption bands (SIF_{687} and SIF_{760}, respectively).

Table 2.1. SIF-derived indices and A-SCOPE outputs used for their calculation. SIF_x is the SIF value at wavelength "x", extracted from the modelled SIF full spectrum.

Index	A-SCOPE outputs used for calculation
SIF_x / Lin_{680}	Incident irradiance at 680 nm
SIF_x / Lin_{758}	Incident irradiance at 758 nm
SIF_x / PAR	Incident irradiance integrated between 400-700 nm
SIF_x / APAR	Absorbed PAR by Chlorophyll *a,b*
SIF_x / fAPAR	Fraction of absorbed PAR
SIF_x / NDVI	Reflectance $(\rho_{780:800}-\rho_{660:680})/(\rho_{780:800}+\rho_{660:680})$
SIF_x / SR	Reflectance $(\rho_{780:800}/\rho_{660:680})$
SIF_x / ρ_{NIR}	Reflectance $(\rho_{780:800})$

The evaluation of the performance of each index in reducing the influence of LCC, LAI and R_{in} on SIF intensity, was performed by computing iteratively the coefficient of variation (CV) of SIF values setting all model variables fixed but one. To calculate the dispersion of populations, the bare ratio was calculated for every group of simulations (i.e., for every varying input variable), and the resulting coefficients of variation summed. This was repeated for every SIF wavelength considered (i.e., SIF_{687}, SIF_{690}, SIF_{740} and SIF_{760}). In this way each normalisation method was characterised by just one value (one "CV"), for every investigated SIF wavelength.

2.4.2.1 Results

Figure 2.14 summarises the results. Each bar plot shows the coefficients of variation of all tested normalisation methods for a certain case. The first bar in each plot (red) is the CV corresponding to the non-normalised values (pre-normalisation), and should be read as a "zero" point for evaluating the other values.

In all cases, normalising for the metrics related only to the incident irradiance (L_{in} and PAR) did not change the values of the aggregated CV, nor those calculated using only LCC or LAI isolines. While this could be partly due to methodological constraints, it indicates that at least in this simplified scenario, different levels of incoming radiation did not affect the shapes of LAI and LCC isolines. The other possibility is that they are affecting the pre-normalised and the normalised values in the same way, and this was not selectively corrected by the normalisation.

APAR and fAPAR values were in general the best performing normalisation metrics. In particular, APAR displayed good to very good performance in normalising the effect of both LCC and LAI variation on SIF values in the far-red emission region (SIF_{740} and SIF_{760}), while for the red region (SIF_{687} and SIF_{690}) performance was lower. In fact, in this spectral region APAR was able to account for LCC variation well, but the high CV obtained (considering LAI variability only) increased the total CV. The fAPAR had similar performance to APAR, but was more effective in correcting in the red region than in the far-red.

The overall performance of APAR and fAPAR indicated that these normalisations could be extremely important and effective in normalising the far-red SIF values (e.g., SIF_{740} and SIF_{760}). The results highlight the importance of having APAR/fAPAR measurements or products associated with SIF measurements, if aiming to compare the photosynthetic capacity of plants differing in key drivers such as LAI, LCC and Rin using SIF signal. Nevertheless, using these normalisations, SIF in the red region still seemed to be influenced by vegetation structural parameters that are not properly accounted and which drive reabsorption and scattering of the emitted signal inside the canopy. Further developments are needed in that regard, testing more metrics and extending the simulated dataset. Moreover, developments in obtaining better estimates of APAR from remote sensing data have been achieved in the study, and hopefully will contribute to testing the present methodology on real world datasets.

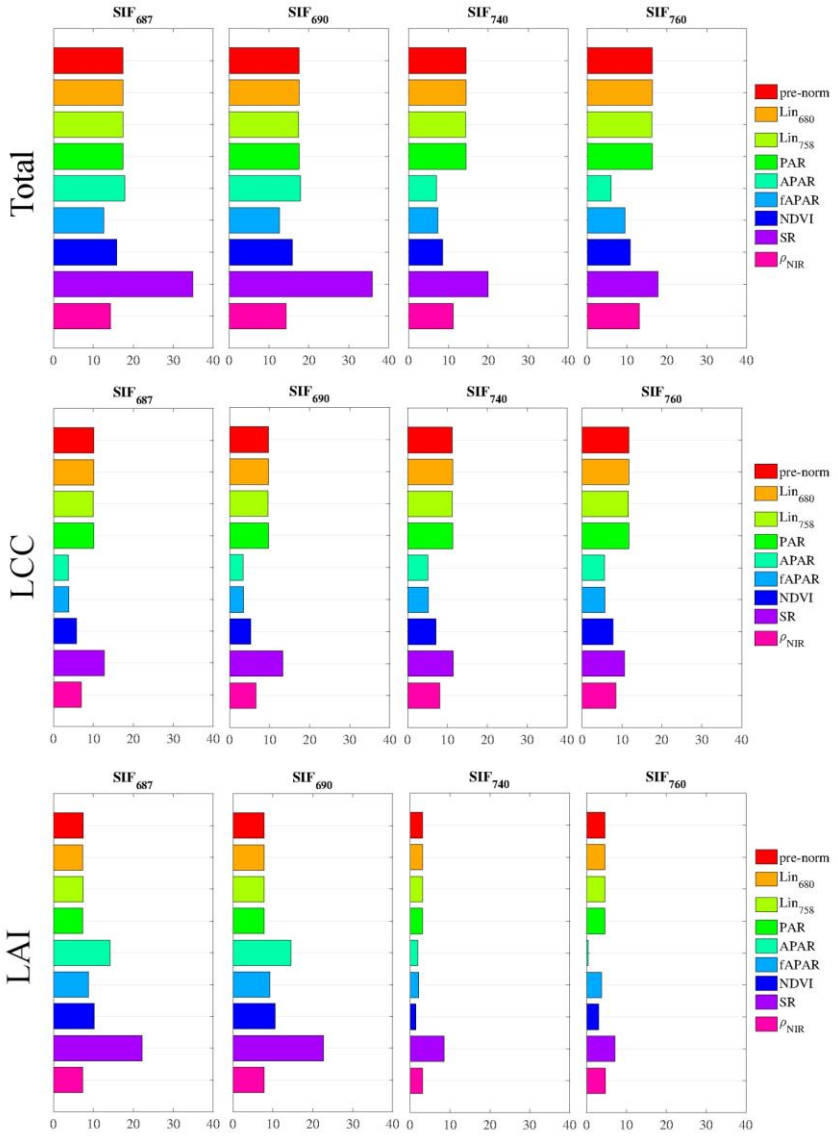

Figure 2.14. Comprehensive view of the CV for all tested normalisation metrics: from left to right in each row, the CV related to the four SIF wavelengths. The first row ("Total") shows the total aggregated CV, calculated by summing all values (calculated both along LAI and LCC isolines), the second row ("LCC") shows the CV aggregated summing values calculated along LAI isolines, and the third row ("LAI") shows the CV calculated along LCC isolines.

2.5 Towards Level-2c products

2.5.1 Development of biophysical parameter retrieval algorithms for advanced exploitation of FLEX data products

The objective of this workpackage was to investigate retrieval of biophysical parameters from FLORIS Level-2a data (TOC reflectance). Data generated by the FLEX-E (see also Section 2.2.2) was used here, which allows generation of TOA radiance with a 3D propagation through the

atmosphere and inclusion of a variety of radiometric and instrumental noises (Vicent *et al*. 2015b), with the proposed atmospheric correction algorithm of Sabater *et al*. (2015).

The biophysical parameters considered were LAI and LCC. These two variables not only are the most important biophysical variables when it comes to interpretation of fluorescence maps (they are key drivers of fluorescence (Verrelst *et al*. 2015b)), but also input maps of LAI and LCC have been generated with the FLEX-E in the development of TOA radiance data. These maps can now function as a reference.

To advance the development of a consolidated retrieval strategy, these steps were taken:

1. training and testing various Machine Learning Regression Algorithms (MLRAs) with a single dataset coming from the FLEX-E (e.g., a subset from the 'Mallorca' simulations);
2. applying the best validated strategy to a FLEX-E simulated image and then validating it against the FLEX-E input maps of LAI and LCC;
3. creating an external training dataset with SCOPE, validating it, applying it to a FLEX-E image, and then again validating it against the FLEX-E input maps of LAI and LCC; and
4. optimising the most promising retrieval strategy towards a robust retrieval strategy.

Recent advances in the field have demonstrated that novel hybrid approaches, i.e., making use of powerful, kernel-based machine learning regression algorithms (MLRAs) are promising. More often than not, kernel-based MLRAs outperform widely used neural networks in operational processing chains (Verrelst *et al.* 2012b; Camps-Valls *et al.* 2006). Particularly Gaussian processed regression (GPR), developed in a Bayesian framework and providing associated uncertainties, have shown promise (Verrelst *et al.* 2012a).

Apart from novel MLRAs, the powerful spectral dimensionality reduction method has been introduced. Such methods are mandatory in the case of FLORIS, which is characterised by over 450 bands and therefore deal with a large amount of band redundancy. A library of dimensionality reduction methods has been implemented into ARTMO's MLRA toolbox, enabling hyperspectral data to be processed efficiently and triggering higher accuracies in the retrieval scheme.

All MLRA methods were tested, but eventually GPR was chosen as the core retrieval algorithm and then further optimised. First, only data from the FLEX-E simulated 'Mallorca' image was used for training and validation. However, that dataset appeared to have a low variability, therefore a new SCOPE dataset for training was developed. Various optimisation strategies have been tested in order to achieve accurate retrievals when applied against an FLEX-E simulated image and validated against corresponding LAI FLEX-E input map. They include dimensionality reduction methods, varying training/validation distributions and adding noises. It was found that especially the introduction of some noise over the LAI training data caused an improvement in the retrievals. The final retrieval strategy was optimised with errors below 10% (NRMSE: 7.29%, R^2: 0.98). Figure 2.15 shows the final retrieved LAI map compared to the reference map. Mostly the same spatial patterns were obtained.

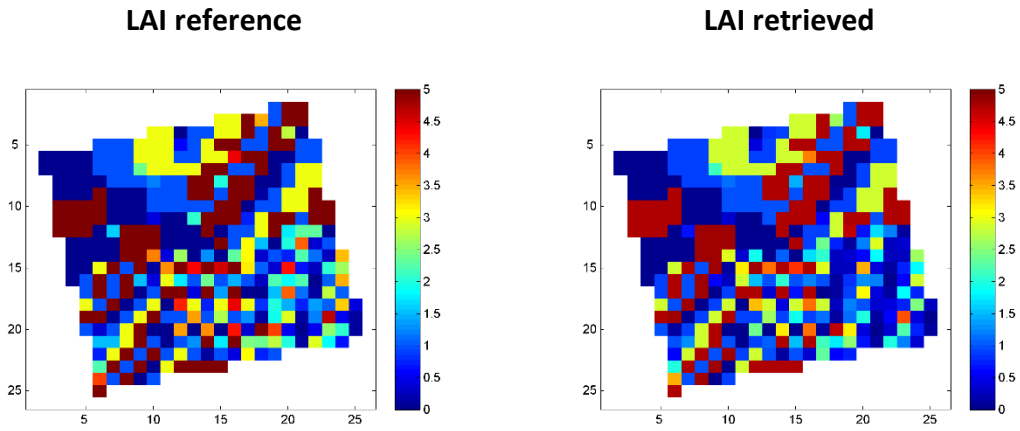

Figure 2.15. LAI reference map (left) and retrieved LAI map (right).

Both absolute uncertainty (standard deviation, SD, around the mean estimate) and relative uncertainty (SD divided by mean estimate x 100) are shown in Figure 2.16. These maps provide insight into the per-pixel retrieval performance relative to the training dataset. Because the magnitude of the SD typically depends on the magnitude of the LAI estimate, the relative uncertainties are easier to interpret. Typically a threshold is applied, e.g., retrievals with relative uncertainties below 20% are considered as reliable retrievals. (The map shows several pixels exceeding that threshold, but these mostly referred to pixels with LAI values approaching zero.)

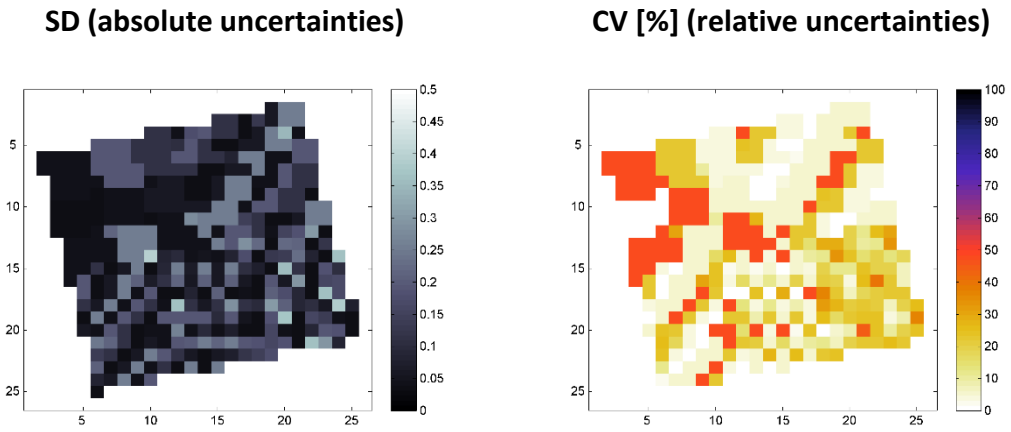

Figure 2.16. Associated absolute uncertainty (left) and relative uncertainty (right) maps of GPR-retrieved LAI map.

In summary, in this WP a retrieval strategy was developed for processing FLEX-FLORIS data towards Level-2c products (LAI, LCC). Emphasis was on LAI retrieval from FLEX-FLORIS data because it is technically more challenging – but precisely the same approach can be applied to S3-OLCI data. Although neither an operational processing line was developed nor a final ATBD, significant progress was made into the identification and elaboration of a successful retrieval approach. The strength of this work is that the retrieval algorithms have been applied against Level-2a FLORIS data, i.e., simulated FLORIS data with various kinds of instrumental noise and an atmospheric retrieval algorithm. Hence, this data can be considered as closely matching reality.

A more systematic analysis may be needed to further optimise and strengthen the retrieval strategy. Also, a similar retrieval strategy needs to be developed and optimised for the estimation of LCC.

2.5.2 Simultaneous retrieval of canopy state variables by model inversion of integrated tandem mission data

Using the database of simulated tandem mission data that was generated in Section 2.2.1, the retrieval of object biophysical properties and fluorescence from TOA radiance data by model inversion was tested.

A light version of the SCOPE model was used, which does not include the energy balance iterations and the calculation of canopy fluorescence. Since this light version of the SCOPE model does not provide fluorescence, the fluorescence contribution in the FLEX/S3 data was fitted by adding to the simulated top-of-canopy reflected radiance spectrum a fluorescence contribution using four fluorescence principal component spectra (PCs) obtained from independent SCOPE simulations. With four PCs the maximum residual error was less than 0.04 mW m^{-2} sr^{-1} nm^{-1}, which is five times smaller than the expected fluorescence retrieval error of 0.2 mW m^{-2} sr^{-1} nm^{-1}. The reconstruction error was usually less than 0.02 over the spectral range 640 – 770 nm, which is applicable to the FLORIS sensor.

The total number of variables allowed to vary during the model inversion is 17, of which four describe the soil's spectrum, five describe leaf characteristics, four the canopy structure, and four the fluorescence spectrum (with PCs). The dry soil's reflectance spectrum was modelled with an overall brightness parameter and two parameters describing its spectral shape. This was achieved by applying a Cartesian to Spherical co-ordinate transformation to the GSV spectra (Jiang & Fang 2012). Before applying the routine *RTMo*, the Fluspect_bcar model (see Section 4.2) was used to generate leaf reflectance and transmittance spectra from the five input leaf biochemical properties, and for retrieval of biophysical variables.

The prototype retrieval algorithm accomplishes the simultaneous retrieval of surface reflectance, fluorescence, and most biophysical parameters of SCOPE (i.e., LAI, leaf angle distribution, leaf chlorophyll, dry matter, water, brown pigment, dry soil reflectance spectrum, soil moisture) by using the combined TOA radiance data from all sensors of the FLEX/S3 tandem mission as inputs. Moreover, incoming PAR and the ratio of diffuse/direct incoming radiation may in principle be derived as important by-products. More advanced options could be considered in which also the atmosphere is allowed to vary, and those in which also canopy temperature is retrieved. APAR can easily be calculated as a by-product of the model's radiative transfer implementation. Also a two-stage approach can be envisioned in which, after the first retrieval, the complete SCOPE model is employed to fit all data and then GPP and light use efficiency could be estimated. These are however all considered to be options for the future.

Differences between the database spectra and the ones generated in the forward model ensured that successful model inversions could not be fully attributed to using identical models during both the data generation and the model inversion. Differences included different origins of soil spectra, inclusion of realistic levels of sensor noise in the TOA radiance spectra for the

database, and use of uniform Lambertian surface fluorescence (model) or directional fluorescence (database)).

An important difference with the approach applied in the FLEX PARCS study was the use here of a standard Matlab routine, namely the function *lsqnonlin*, rather than a specially written optimisation routine. The *lsqnonlin* function can optimise a vector of model outputs against "observations" instead of just minimising a scalar cost function, and it can work with upper and lower bounds to the input variables of the model. A summary of the applied model variables is given in Table 2.2. Mathematical transformations were applied because of model peculiarities or to improve linearity, and all input variables were normalised to their respective ranges.

Table 2.2. Model variables with lower and upper bounds.

Model variable	Lower bound	Upper bound
Soil brightness	0	0.9
Soil "latitude"	10	50
Soil "longitude"	40	70
Soil moisture %	5	55
Leaf chlorophyll	0	100
Leaf water	0	0.04
Leaf dry matter	0	0.05
Leaf brown pigment	0	0.3
Leaf mesophyll N	1	3
Canopy LAI[1])	0	6
Canopy LIDFa[2])	-1	+1
Canopy LIDFb[2])	-1	+1
Canopy hotspot par	0.001	0.5
Fluorescence weight pc1	0	40
Fluorescence weight pc2	-20.0	20.0
Fluorescence weight pc3	-10.0	10.0
Fluorescence weight pc4	-2.0	2.0

[1]Range of transformed LAI is 0 – 0.7.
[2]Actually these are the ranges of two transformed variables.

Retrieval errors of fluorescence were, on average, about 0.1 mW m^{-2} sr^{-1} nm^{-1}, which is only half the error level specified for FLEX.

With this approach, integrated data from all sensors of the FLEX/S3 mission were simulated to demonstrate simultaneous retrieval of biophysical canopy and soil variables along with TOC

fluorescence. A TOA radiance approach, in which the atmospheric effects were forward-modelled instead of corrected, appeared to be very successful. In this approach only a good atmospheric characterisation is required, but the atmospheric correction is not executed. An advantage of this method is that irreversible processes like surface BRDF effects, the adjacency effect and the convolution of TOA radiance spectra with sensor spectral response functions can all be taken fully into account, whereas in the atmospheric correction approach all these effects must be approximated by using highly simplified models, with an unpredictable impact on the quality of the atmospherically corrected data.

The fluorescence contribution to top-of-canopy radiance was modelled by four principal component spectra, and this appeared to give sufficient flexibility to accommodate all variations in leaf chlorophyll, canopy structure and directional effects.

Retrievals of biophysical variables were remarkably successful in the great majority of cases (Figure 2.17). This is believed to be caused by employing all tandem mission data together, so that sufficient spectral and directional information was available.

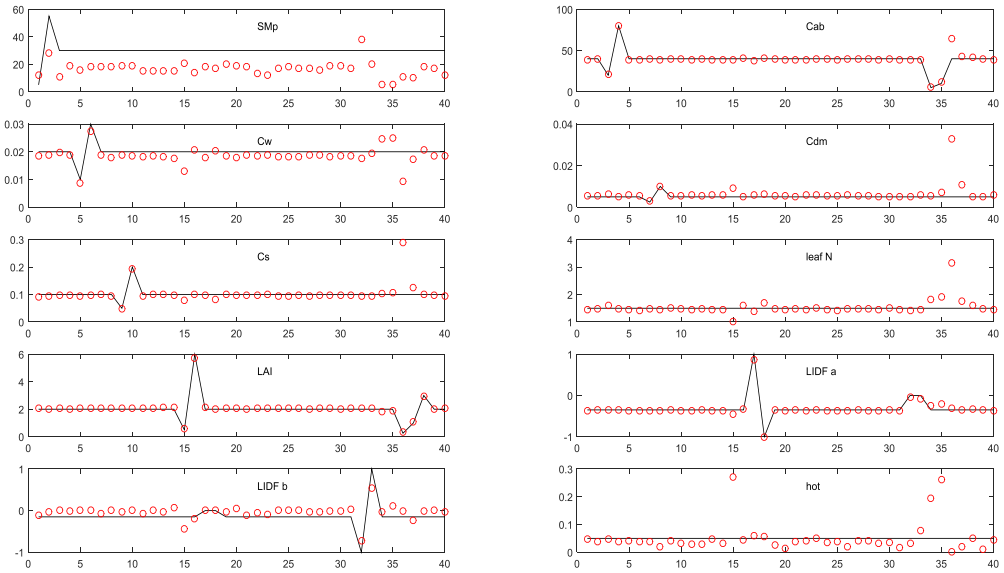

Figure 2.17. Retrieved biophysical variables for the 40 cases. The black solid line shows the input variables of the database, while the red circles indicate the retrieved values.

Canopy fluorescence was also successfully retrieved, with a peak RMS error of about 0.2 mW m^{-2} sr^{-1} nm^{-1} (which was found at a visibility of 5 km) and an average RMS error of 0.1 mW m^{-2} sr^{-1} nm^{-1}, which is twice better than the specification in the MRD requirement.

The optimisation was successful but execution is very slow, about 3-5 minutes per case. For operational applications, perhaps it could be accelerated by using look-up tables, a more efficient atmospheric propagation, parallel processing, etc.

2.6 Conclusions

Advances from this task enhance capabilities for the retrieval and analysis of sun-induced fluorescence from FLEX.

In the area of data generation, **new simulation dataset** were created that extend the FLEX/S3 spectral radiance databases developed under PARCS, and which are useful for generation of either single spectra and ideal scenarios, or synthetic composite imagery of more realistic scenarios, the latter created using the FLEX-E. The new database supplies valuable inputs for subsequent algorithm development.

The activity advanced the optimisation of the **atmospheric correction algorithm** and developed a Level-2 processing chain, also improving the coupling of atmospheric correction and fluorescence retrieval.

Fluorescence retrievals were improved for retrieval of the full SIF spectrum. In addition, analyses conducted here demonstrated the feasibility of decoupling the PSI and PSII spectra from total canopy fluorescence.

Strategies were assessed to obtain better **estimates of APAR** for the calculation of yields, and insights were gained into potential causes of retrieval issues. A method for comparison of different **normalisation strategies** of the SIF signal is proposed that is able to minimise the impact of environmental conditions and vegetation structural parameters. The importance of APAR and fAPAR was evident for normalisations, especially for the far-red SIF.

Activities also support development of higher-level products for retrieval of **biophysical parameters** and simultaneous retrieval of canopy state variables. A retrieval strategy was developed to process FLORIS data into LAI estimates, using the dataset of realistic scenarios generated by the FLEX-E. In the future, this can proceed to ATBD (i.e., for implementation into the official FLEX processing chain). A complementary approach using the dataset representing relatively homogenous pixels along with a simplified version of SCOPE was able to simultaneously retrieve surface reflectance, fluorescence, and most biophysical paramaters of the model.

3. Development of vegetation stress indicators and applications

3.1 Introduction

Chlorophyll fluorescence emission is a widely used signal reporting on plant photochemical function, and it has been especially useful under stress conditions (reviewed, e.g., Ač *et al.* 2015; Nedbal & Koblížek 2006). The early responsiveness of the CF signal to biotic and abiotic stresses makes it a potentially powerful indicator of vegetation health status and/or stress resilience – in addition to its utility for deriving actual photosynthetic rate or GPP.

The previous PS Study identified fluorescence indicators of water stress, temperature extremes, and nitrogen deficit (Ač *et al.* 2015; Mohammed *et al.* 2014). The present work advances the range of applications and protocols for stress detection and photosynthetic estimation.

The primary objectives were to:

- test and extend stress indicators developed in the PS Study;
- review sources of variability and error in stress detection;
- evaluate strategies to assess NPQ using optical measurements; and
- utilise datasets from campaigns using the airborne *HyPlant* sensor to analyse in more detail the link between SIF and stress, and to expand stress-based applications of SIF.

3.2 Stress indicators and applications

This activity updated the results of the literature review and meta-analysis conducted during the PS Study for water deficit stress, temperature extremes, and nitrogen deficiency (Ač *et al.* 2015; Mohammed *et al.* 2014). Second, the effects of additional abiotic and biotic stresses were evaluated from the literature. Lastly, we tested and re-calibrated the indices-based algorithms introduced in the PS Study, specifically the Temperature Stress Fluorescence Index (TSFI), the Water Stress Fluorescence Index (WSFI), and the Nitrogen Stress Fluorescence Index (NSFI), using existing datasets.

3.2.1 Results

3.2.1.2 Extension of stress responses information

References that were added to the database for water stress, temperature stress, and nitrogen deficit are listed in Table 3.1. (The full publications are contained in the Technical Data Package for deliverable D-5 submitted to ESA.)

Additional literature review investigated the effects of abiotic stresses such as heavy metals, salt, and air pollution, as well as biotic stresses such as viruses, fungi, or insects. Table 3.2 presents an overview of the topics and number of studies. References related to water and nitrogen stress represent the greatest number of studies, followed by studies dealing with heavy metal and biotic stress, temperature, combined stress and application of herbicides. “Other” stress factors encompassed mostly deficiency of macro- and micronutrients. Only one-fifth of the studies focused on passive fluorescence signal retrievals and an even smaller

proportion dealt with canopy-level studies. On the other hand, more than 75 different plant species are represented, providing a broad range of functional plant/growth types.

Table 3.1. Additional references for the literature database of water deficit, temperature stress, and nitrogen deficiency effects on chlorophyll fluorescence.

Additional database references		
Campbell *et al.* (2014)	Kuckenberg *et al.* (2009)	McMurtrey *et al.* (1994)
Cendrero-Mateo (2013)	Lang *et al.* (1995)	Mohammed *et al.* (2014)
Chappelle *et al.* (1984)	Leufen *et al.* (2013)	Suárez *et al.* (2008)
Chappelle & Williams (1987)	Leufen *et al.* (2014)	Tartachnyk *et al.* (2006)
Gouveia-Neto *et al.* (2011)	Lichtenthaler & Babani (2000)	Theisen (2002)
Konanz *et al.* (2014)	Lichtenthaler & Rinderle (1988)	

Comparing fluorescence responses to all stress factors (all measurements – both active and passive methods, at the leaf and canopy scales), there was a relatively high variability in responses (Figure 3.1). Since different fluorescence units and methodologies were reported among studies, we used here a relative change in the fluorescence signal expressed as a ratio between control and stress responses (S/C ratio), in order to permit comparisons.

For the red fluorescence bands, stresses such as air pollution, biotic stress, insecticides, herbicides and heavy metals tended to increase the signal; whereas water deficit, ozone and combined stresses led mostly to its decline. For the far-red band, most stresses led to either no significant change in intensity (e.g., heavy metals, herbicides, air pollution) or in some cases a statistically significant decline (water, nitrogen, ozone, senescence, biotic stress), while only insecticide stress led to an increase. It should be noted that results for the insecticides were significant and with relatively high repetition (n=15). However, they were based on only two scientific studies and two plant species, thus a high level of autocorrelation can be expected. Regarding the red to far-red fluorescence ratio, all stresses except air pollution showed increased values, although again with a considerable variability in some cases (lowest median values for water, and highest for herbicides). From the PS Study, the most consistent effect of temperature stress was a decline in the red to far-red ratio, while for nitrogen deficiency it was an increase in that ratio (Ač *et al.* 2015; Mohammed *et al.* 2014).

Table 3.2. Characteristics of reviewed papers dealing with effects of various environmental stresses on chlorophyll fluorescence. The factors assessed are water, temperature, nitrogen, air pollution, insecticides, senescence, biotic stress, combined stresses, heavy metals, herbicide, ozone, UV radiation, salt and micro- and macronutrients deficiency. Note: the number of cases exceeds the number of papers (indicated in brackets) because some papers dealt with more than one case.

Number of species +75				
Number of cases (papers) 311 (116)				
Stress factors				
Water	Temperature	Nutrients	Other (see below)	
79 (44)	19 (12)	51 (29)	162 (46)	
Scale				
Leaf			Canopy	
266			45	
Method used				
Passive			Active	
55			256	
Plant functional types				
Grass+herb+algae	Trees+shrub evergreen		Trees+shrub deciduous	
188	35		88	
Other: Number of species 43				
Number of cases (papers) 162 (46)				
Stress factors				
Air pollution	Insecticide	Senescence	Biotic stress	
9 (3)	15 (2)	15 (7)	27 (11)	
Combined stress	Heavy metals	Herbicide	Ozone	Other
17 (5)	31 (9)	16 (5)	4 (3)	28 (11)
Scale				
Leaf			Canopy	
149			13	
Method used				
Passive			Active	
20			142	
Plant functional types				
Grass+herb+algae	Trees+shrub evergreen		Trees+shrub deciduous	
97	11		54	

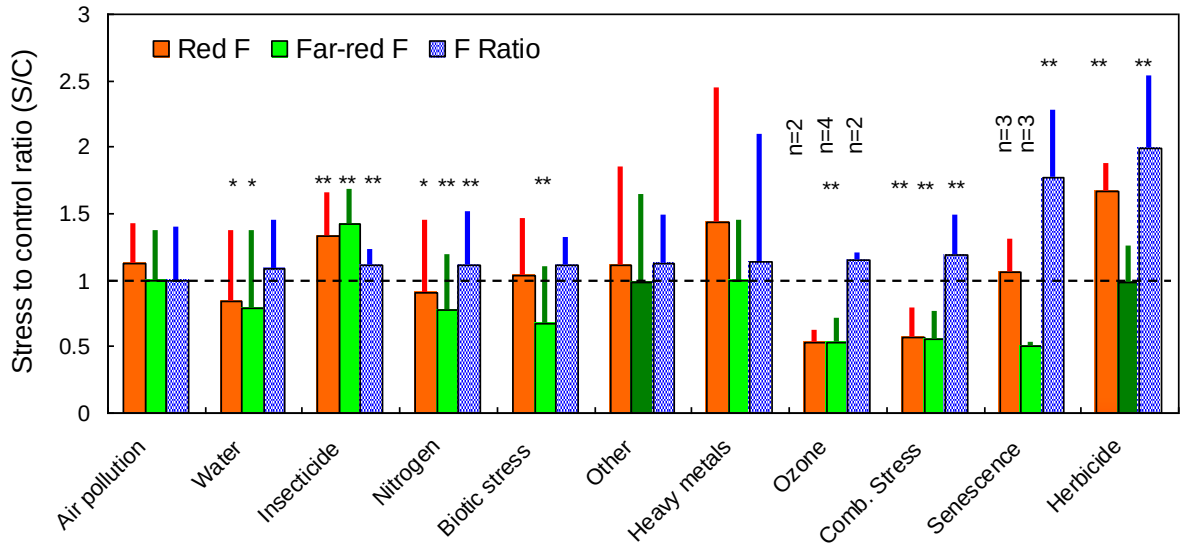

Figure 3.1. Changes in fluorescence signals (red, far-red, and red to far-red ratio) presented as the ratios of stress to corresponding control values (error bars show standard deviations). Data are ordered upwards according to fluorescence ratio median values. "Other" stress is mostly macro- and micro nutrients deficiency. Asterisks indicate significant difference from 1 (control) at * $p \leq 0.05$ and ** $p \leq 0.01$ (Mann-Whitney test). Cases where the number of repetitions was lower or equal to 4 are highlighted. Temperature effect is not shown, as the same data are available in the previous report for the Photosynthesis Study (Mohammed *et al.* 2014).

The variability in responses emphasises the need to interpret results with caution, taking into account other aspects such as pigment content, duration of stress exposure, and the influence of non-photochemical protection processes. Chlorophyll content, for example, can change in response to various stresses or during normal seasonal or developmental changes in vegetation tissues, and the changes in chlorophyll will influence photosystem responses and reabsorption especially of red fluorescence (Mohammed *et al.* 2014). To explore the effect of chlorophyll content on fluorescence, we plotted the stressed/control ratio (S/C ratio, how fluorescence changed in stressed plants compared to control ones) and S/C ratio of chlorophyll content (Figure 3.2). The highest (and statistically significant) dependency on chlorophyll content changes was observed for the fluorescence ratio, where increasing chlorophyll led to decreased values of the ratio. Likely this was driven in part by the reabsorption effect on the red fluorescence, but it was noted that only 12% of the variability in red fluorescence was explained by chlorophyll change, with a varying degree of correlation depending on the stress agents (not shown). In the case of the far-red fluorescence, declining chlorophyll content tended to decrease fluorescence emission but the effect was minimal.

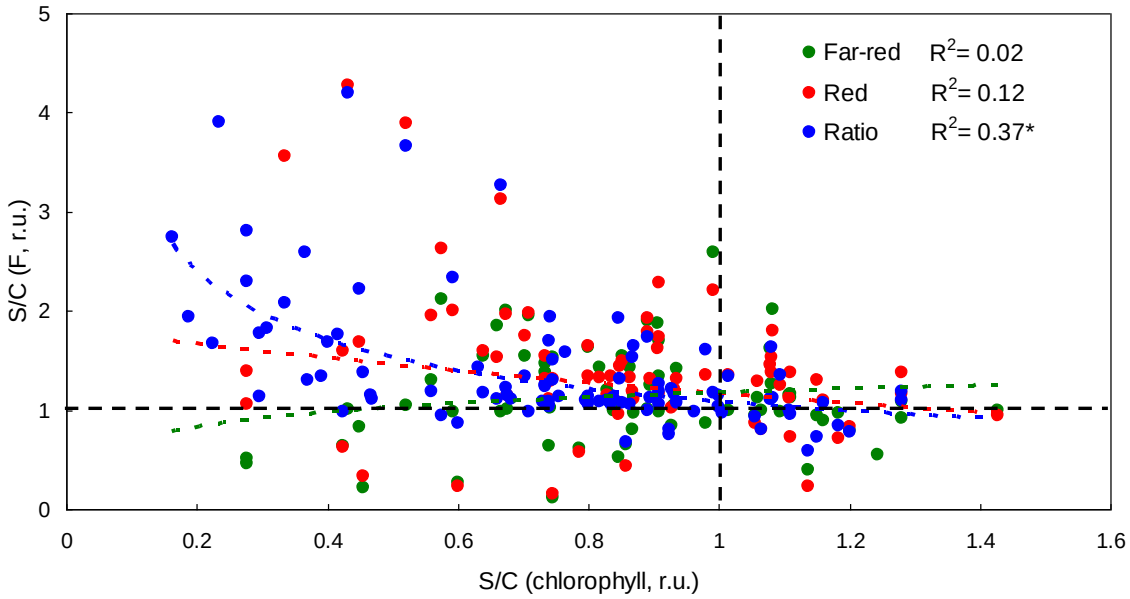

Figure 3.2. Stress to control (S/C) changes in fluorescence and changes in the total S/C chlorophyll contents. Red fluorescence (red circles), far-red fluorescence (green circles), red to far-red ratio (blue circles).

Another source of variability that we explored was the duration of stress exposure. The temporal evolution of fluorescence and chlorophyll effects arising from various abiotic and biotic stresses was studied, and an example is provided in (Figure 3.3). We distinguished three categories of stress duration: short-term (hours to 7 days), mid-term (1 week to 1 month), and long-term (+1 month). Chlorophyll content reacts relatively slowly, with the effects of decreased chlorophyll content evident after relatively longer exposure of plants to stress factors (Figure 3.4).

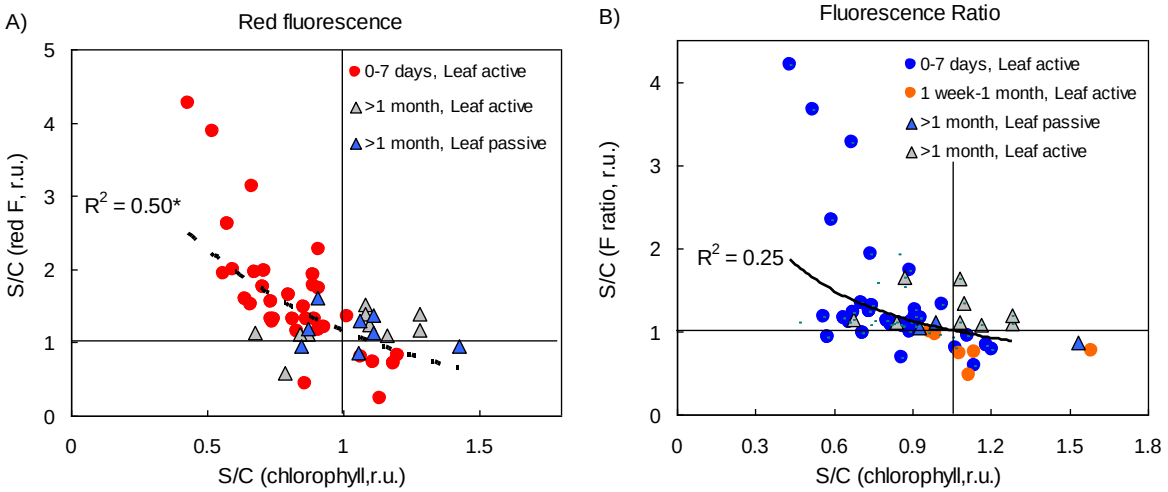

Figure 3.3. Stress to control (S/C) changes in fluorescence and chlorophyll content. Stresses included herbicide, insecticide and heavy metals, analysed by duration of exposure and measurement method. An exponential fit was applied to the data.

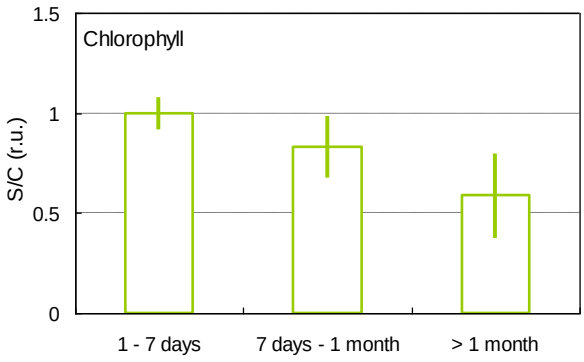

Figure 3.4. Chlorophyll content change in nitrogen stressed plants. Average of 17 studies.

Another aspect that can influence the fluorescence signal of stressed plants is the heterogeneity of the distribution of a stress effect. Typical examples are stress effects from biotic stressors such as viruses, fungal infection, herbivores, etc. These types of stresses do not affect the vegetation homogeneously but instead create "patches" on infected leaves or plants. Many studies deal with this kind of stress, but most of them use proximal chlorophyll imaging methodology with active excitation of fluorescence. This kind of localised patchiness would not necessarily be detected from remote sensing platforms with relatively large spatial footprints until effects were more widely manifested structurally and physiologically.

3.2.1.3 Validation of fluorescence stress indicators

We tested previously suggested SIF stress indices that were developed in the PS Study for water stress, temperature stress, and nitrogen deficit (Mohammed *et al.* 2014). A recalculation was done for water stress in order to reduce the area of uncertainty, since the long-term effects differ from that of short-term ones. Temperature and nitrogen components remained the same. There was a partial overlap between the effects of water and temperature stress, while the nitrogen deficiency effect remained separated (Figure 3.5). Other abiotic and biotic stresses were introduced into the figure. Other abiotic stresses almost completely overlapped with nitrogen deficiency, while large variability regarding the biotic stress means that biotic stress also partly overlapped with all other stress factors.

Several studies enabled partial validation of the previously proposed indexes: They were Rossini *et al.* 2015; Panigada *et al.* 2014; Calderon *et al.* 2013; Lee *et al.* 2013; Liu *et al.* 2013; Cendrero-Mateo 2012; and Meroni *et al.* 2008. Two studies investigating water stress effects (Lee *et al.* 2013; Panigada *et al.* 2014, blue triangles) confirmed a declining effect of water stress on far-red fluorescence. Unpublished data provided by Cendrero-Mateo (green triangles) on effects of nitrogen deficiency on canopy level responses were found to be outside previously identified ranges. (Unfortunately, only data on far-red fluorescence were available, thus precluding full validation.) However this decline was within the variability observed in the case of nitrogen deficiency for the active fluorescence methods. A study by Calderon *et al.* (2013) dealing with the spread of pathogens using airborne measurements found a relatively small effect in the far-red fluorescence. These results fell very closely within the defined space of biotic stress,

although those boundaries were based here on active fluorescence measurements only because of absence of passive studies in this field. The study of Meroni *et al.* (2008, grey triangle) investigating the effects of ozone fell well within range of abiotic stresses. Finally, results from experiments with the herbicide diuron (Rossini *et al.* 2015, trio of grey triangles) were outside the boundary but close to the boundaries of abiotic stress. No new studies investigating the effects of temperature stress were found, therefore, these results still must be considered as preliminary.

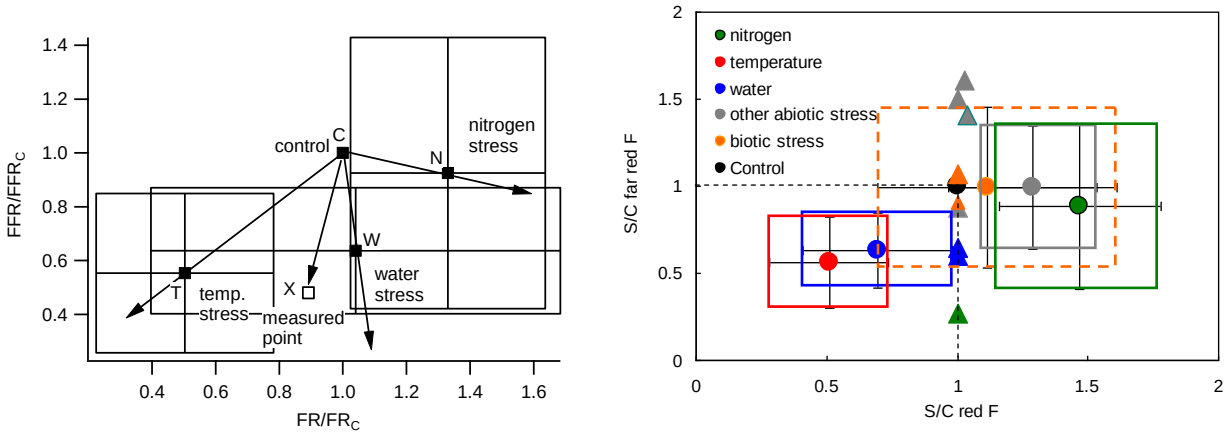

Figure 3.5. Stress to control ratios of far-red fluorescence. Left graph shows areas (the central point is the average and borders are SDs) of the stress to control ratios for different stresses as proposed in Mohammed *et al.* (2014). Right graph shows validation (triangles with colours corresponding to the stress) of recalibrated and additional stresses. Dashed orange square is calibrated based on active fluorescence measurements, since only these were available in the literature.

In summary, although there are challenges in comparing results from different studies, trends for red and far-red fluorescence behaviour under stressful conditions were evident, with the specifics depending on the particular stress factor, duration of exposure, and likely other circumstances.

Stress indices proposed in the PS Study (Mohammed *et al.* 2014) were promising for detection of plant stress from satellite-based platforms. However, distinguishing among individual stress factors and stress exposure duration would need ancillary measures – at a minimum of chlorophyll content (e.g., using reflectance measurements), which can account for some but not the majority of fluorescence changes. Chlorophyll content seems to affect the ratio of red to far-red fluorescence more dependably than the individual bands, and it tends to change slowly over time. Most of the studies to date evaluating chlorophyll content were carried out on annual crops and under different levels of nitrogen. Therefore, further studies are imperative to assess the relationship of the fluorescence signal with chlorophyll content or photosynthetic activity, especially taking into account effects on SIF reabsorption.

Future remote sensing studies should focus on resolving canopy chlorophyll fluorescence changes, by scaling structurally simpler experimental designs up to more complex multi-species canopies (e.g., natural forests) impacted by combined multi-agent stress events of varying

intensities and durations. Despite intensive recent development, special attention should be paid to passive remote sensing methods, which are still rather under-represented with respect to the spatio-temporal assessment of actual vegetation stress loads. (Fortunately, this situation is starting to change with the advent of newer passive methodologies for remote sensing of fluorescence.) Outcomes of such experiments will be crucial for timely detection of plant stress events.

3.3 Sources of variability and error in stress detection

Chlorophyll fluorescence as an indicator of photosynthetic functioning has the potential to be a highly useful tool for quantifying stress effects in vegetation. While much attention on space-based fluorescence retrievals to date has focused on relating solar-induced fluorescence to GPP, there is an equally important need to consider stress effects that may be manifested in space-based fluorescence data (Mohammed *et al.* 2014).

A key knowledge gap identified in the PS Study (Mohammed *et al.* 2014) was the need to better understand sources of variability, uncertainty and error in SIF data that might affect its application as a vegetation stress indicator. This need was also evident from the previous workpackage where stress effects on fluorescence were found to be variable depending on the specifics of the stress and circumstances. The present synthesis uses a literature review to focus on this information gap by providing an introduction to potential underliers of variation in chlorophyll fluorescence information and to ways by which uncertainties might be mitigated. Guidelines were distilled to support protocols for measurement, interpretation, and application of fluorescence, especially for remote sensing of SIF in terrestrial vegetation using space-based platforms.

It should be recognised that a positive aspect of variability is that it makes fluorescence applications possible — that is, if there were no discernible differences in fluorescence signals between stressed and unstressed vegetation, it would be pointless to try to use fluorescence as a stress reporter. On the other hand, it is essential to discriminate changes in fluorescence arising from stress effects versus those due to, for example, measurement protocols, normal changes in vegetation physiology & biochemistry, inherent canopy heterogeneity, or other factors.

Although sources of variability, uncertainty and error in fluorescence stress applications at the remote scale have not previously been the exclusive subject of review papers, the topic has received attention in reviews of fluorescence-GPP associations at the remote scale and of stress applications of fluorescence at the leaf level or near-remote scale (e.g., Porcar-Castell *et al.* 2014; Fernandez-Jaramillo *et al.* 2012; Suárez & Berni 2012; Tremblay *et al.* 2012; Bussotti *et al.* 2011; Meroni *et al.* 2009; Cifre *et al.* 2005). In addition, the subject has been considered within study-specific situations involving remote fluorescence and in sensitivity analyses of fluorescence drivers (Verrelst *et al.* 2015b).

3.3.1 Results

3.3.1.1 Contributors to variability or uncertainty in fluorescence data

Diverse factors were found to influence fluorescence emission, retrieval, and interpretation. These factors represent potential sources of variability in fluorescence results and thus are important to consider when designing studies and exploring applications. The factors may be organised into three main categories: Vegetation factors, Environmental factors, and Instrument/Data factors (Mohammed *et al.* 2014). This analysis focused on vegetation and environmental factors. Further details on SIF retrieval algorithms and methodologies, for example, may be found in Moreno *et al.* (2014).

Some factors may not be at play in a given situation, or their influence might be relatively non-significant for the particular purpose. For example, sensitivity analyses (Verrelst *et al.* 2015b) using the SCOPE model suggested that in heterogeneous vegetation situations, photosynthetic capacity accounted for far less of the observed fluorescence variability than did other leaf and canopy biochemical & structural properties, the latter properties accounting for over 80% of the variation. Therefore, it is essential to take attributes of the vegetation site into account.

Sources of variability operate at respective biological and temporal scales (Table 3.3). Most factors change over the medium and long term and thus need to be considered when interpreting fluorescence data. Even over the short term, a range of factors can affect fluorescence. The number of factors potentially affecting photosynthetic function (and thus fluorescence) increases with biological – hence spatial – scale, understandably necessitating consideration of more drivers when going to the large ecosystem or landscape level where heterogeneous assemblages of canopies are to be expected.[1]

Appreciation of scale effects can be helpful in gauging the relative suitability of a particular remote fluorescence technology for a given objective, or in designing future spaceborne fluorescence platforms, by taking into account their capacity to provide information at the relevant biological (spatial) and temporal scales. Consideration of scale also can be helpful in setting reasonable boundaries for how fluorescence data from existing platforms might be utilised.

[1] Terms used here: 'Canopy' refers to a homogeneous or heterogeneous community of individual plants or tree crowns. 'Ecosystem' and 'landscape' according to accepted definitions do not necessarily imply particular area sizes – for example, technically an ecosystem is a biological community that can be tiny (e.g., a few square metres in area) or large (in the order of square kilometres) – but in the context of this report, ecosystem is assumed to cover an assemblage of interacting canopies covering a sizable area. 'Landscape' is characterised by an interacting mosaic of elements (e.g., ecosystems) relevant to some phenomenon under consideration. Here, 'ecosystem-landscape' is used to encompass a continuum involving a mosaic of canopies and possibly plant functional types, beyond which are regional or global-scale scale biomes.

Table 3.3. Biological and temporal scales within which vegetation and environmental factors may vary and which can affect photosynthetic activity. Note: 'Canopy' refers to a homogeneous or heterogeneous community of individual plants or tree crowns. 'Ecosystem-Landscape' refers to a mosaic of canopies and plant functional types, beyond which are regional or global-scale scale biomes.

Factor	Biological scale				Temporal scale		
	Leaf	Individual	Canopy	Ecosystem-Landscape	Short (< day)	Medium (days-wks)	Long (mos-yrs)
Vegetation factors							
acclimation / adaptation	←	—	—	→	←	—	→
age / stage of development		←	—	→		←	→
heterogeneity & structure		←	—	→		←	→
leaf area index			←	→		←	→
leaf inclination		←	—	→	←	—	→
leaf structure & anatomy	←	—	—	→		←	→
non-foliar photosynthesis		←	—	→		←	→
photochemistry / biochemistry	←	—	—	→	←	—	→
pigments / fluorophores	←	—	—	→	←	—	→
species / genetics			←	→	←	—	→
diurnal rhythms		←	—	→	←		
annual rhythms		←	—	→		←	→
vegetation height			←	→		←	→
whole-plant physiology			←	→	←	—	→
Environmental factors							
abiotic / biotic stresses	←	—	—	→	←	—	→
air temperature	←	—	—	→	←	—	→
atmospheric effects	←	—	—	→	←	—	→
gas concentration (CO_2, O_2)	←	—	—	→	←	—	→
elevation & geography			←	→			
light intensity	←	—	—	→	←	—	→
light spectral quality	←	—	—	→	←	—	→
relative humidity / VPD	←	—	—	→	←	—	→
photoperiod				← →		←	→
soil moisture			←	→	←	—	→
nutrients		←	—	→		←	→
soil temperature			←	→	←	—	→
vegetation growing regime			←	→		←	→
windspeed		←	—	→	←	—	→

While there are many factors that introduce variability to fluorescence emission characteristics, a couple of important examples may be considered.

Pigments and fluorophores – which include chlorophylls, carotenoids (carotenes, xanthophylls), phycobilins, tannins, and anthocyanins – have important biological functions in vegetation tissues, including primary or accessory roles in light absorption, protection from photodamage, and other metabolic functions (Agati *et al.* 2013, 2012; Avital *et al.* 2006; Lichtenthaler & Babani 2004). Pigments influence the fluorescence signal by modulating the light energy

available to the photosystems, by contributing to non-photochemical quenching, by affecting fluorescence radiative transfer through plant tissues (reabsorption effects), and, in the case of chlorophyll-*a*, by emitting fluorescence. They can have overlapping spectral regions of action (Figure 3.6), so that the measured fluorescence emission is the product of various effects which can increase or decrease the fluorescence emission amplitude in one or both peaks.

Pigment composition and concentrations vary with species, geographic location, stress level, time of day, season, foliar or plant age, and location on the leaf. They can be highly responsive to stress, for example, increasing (e.g., carotenoids, anthocyanins, tannins) or decreasing (chlorophyll) with the onset of colder autumn temperatures in northern plants. Pigments can also change in ways that are not due to stress; for example, a significant amount of variation in the F685/F735 ratio can arise as a result of variation in chlorophyll content and corresponding changes in optical properties of leaves which may or may not be related to stress.

Fluorophores – substances that emit fluorescence upon absorption of excitation light (and which include chlorophyll) – include certain phenolic constituents that emit in the visible wavelengths. Phenolic substances such as flavonols are present in some species and conditions in the epidermal layer of foliage, and one of their functions appears to be the screening of ultraviolet light, thus indirectly reducing red and far-red fluorescence emission by making less incident light available to tissues for excitation of chlorophyll fluorescence (Cerovic *et al.* 1999). Phenolic fluorophores are common in the foliage of some monocots and also various conifers, and their levels can increase under stress. Emissions from such fluorophores occurs in the blue-green regions of the spectrum. Also yellow autofluorescent compounds can form in mesophyll cell walls in some species in the presence of e.g., ozone stress (Bussotti *et al.* 2005), fluorescing at ~568 nm, thus potentially affecting the accuracy of PRI calculation.

Considering stresses, these may act singly or in concert to influence fluorescence emissions (see Section 3.2 and Ač *et al.* 2015). Frequently it is the latter in field situations, with one stress predisposing vegetation tissues to another related stress (Levitt 1980). As an example, red fluorescence can decrease because of a reduction in electron transport with concomitant increase in NPQ, or due to heat stress or water deficit (the latter also producing a decrease in far-red fluorescence).

Often, the ratio of red to far-red fluorescence can be informative where simple consideration of one or the other peak do not yield consistent results. According to the meta-analysis by Ač *et al.* (2015), use of the ratio is advisable for nitrogen deficiency and cold/heat temperature stress. But the ratio can have inconsistent behaviour e.g., with water stress.

Because various mechanisms may be in play, it is not always clear from a mechanistic standpoint what is producing the final effect on fluorescence. Some responses may simply be due to acclimatory reactions in plant tissues that are not indicative of damaging strain. This latter point makes it necessary to perform repeated measurements in the field so that a pattern of response may be derived. It is also imperative that canopy structural aspects and the possible influence of measurement geometry and sun angle be taken into account (e.g., Verrelst *et al.* 2015b).

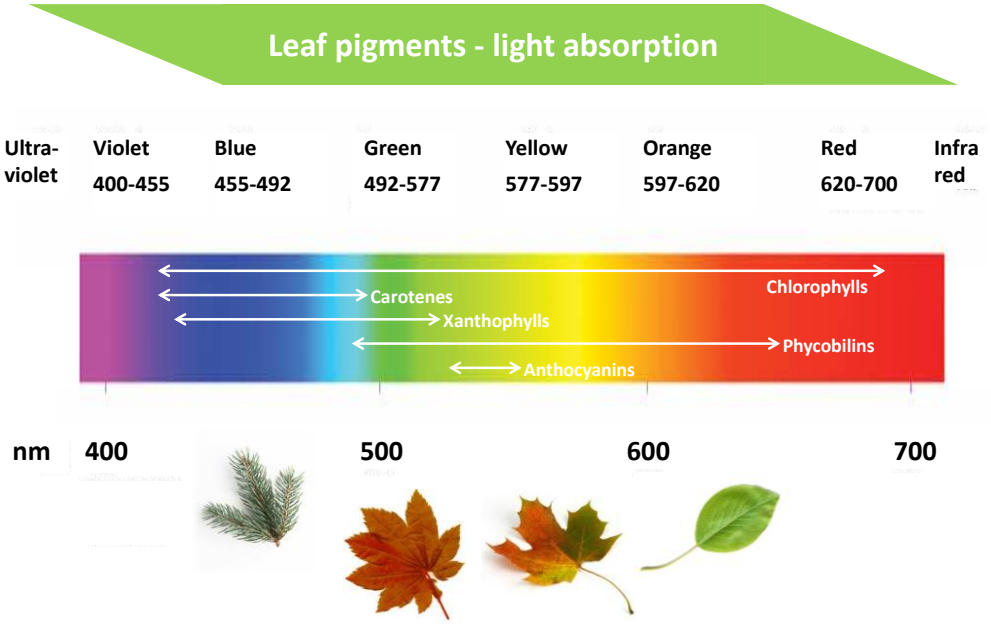

Figure 3.6. Absorption of light in the visible wavelengths by major plant pigments.

The duration of stress exposure is identified, not surprisingly, as an important source of variability, especially given that some changes such as chlorosis can develop rather slowly (Section 3.2). It is likely that the best use of fluorescence will not be in identifying stress-induced early chlorosis (chlorophyll content decline), but in other early responses related to photosynthetic rate decline or sustained non-photochemical quenching – such as might arise due to drought stress, temperature stress, air pollution, heavy metal stress, and ozone. The findings of Section 3.2 indicate that indices-based algorithms, while promising, can have overlapping effects so should be interpreted with the help of ancillary data.

Stresses – especially chronic levels – tend to increase variability in vegetation responses. It may be expected that even within a relatively homogeneous vegetation canopy there could be different levels of strain manifested that arise as a result of genetic/cultivar differences; relative amounts of succulent new leaf tissue vs. older hardened foliage; and microenvironmental conditions of the stress exposure, soil characteristics, light availability (e.g., shading from taller plants), and localised nutrient levels. In mixed canopies, some species may be more greatly affected, and there can be spatial gradients of stress delivery through the canopy. These types of realities emphasise the need for remote measurements to be amenable to validation and interpretation with auxiliary data, including ground- or airborne remote retrievals of fluorescence and other needed information. Importantly for FLEX, it will be valuable to have information from other remote sensors which are monitoring stress factors – e.g., aerosol pollutants, drought conditions, temperature patterns, hazardous events, etc. Data from these sensors will inform FLEX interpretations as to possible/likely pressures.

3.3.1.2 Accounting for variability and managing uncertainty in fluorescence data

Certain important themes emerge when considering how best to account for and understand variability, and to reduce uncertainties and error. (Each of these themes is significant and they are arranged alphabetically below only for convenience.)

Ancillary measurements: These measurements are useful, for example, for performing corrections within the fluorescence retrieval process, for interpretation of fluorescence data, and for calibration/validation activities. They are helpful for understanding the influences of all vegetation and environmental factors, and to help fill data gaps where observation frequency is not high. The types of measurements performed contemporaneously with space-based SIF retrievals will depend on study objectives and can include spectral indices (e.g., NDVI, PRI), surface temperature, LAI, and chlorophyll content. For ground-based or airborne cal/val activities, measurements would include chlorophyll fluorescence, photosynthesis, vegetation descriptions, site factors, and stress indicators. Active methods can be important for understanding mechanisms and reasons for patterns observed in passive data. Standardised, proven methods should be used. Studies should take into account the types of factors likely to change and affect fluorescence within the biological or temporal scale(s) of the investigation, and there should be sufficient ground-based infrastructure (including tower networks) to support spatial scaling from leaf to canopy levels and interpretation of remotely acquired fluorescence signals. Thorough availability of ancillary measurements is especially crucial during the tenure of an optimised research platform such as FLEX to deduce the essential measurements for different scenarios.

Biology/ecology/ecophysiology of the vegetation type: Understanding the nature of the target vegetation is necessary to postulate potential influences of acclimation/adaptation, leaf age, photochemistry & biochemistry, pigments & fluorophores, leaf structure & anatomy, non-foliar photosynthesis, plant age, species/genetics, annual rhythms, whole plant physiology, abiotic & biotic stresses, light spectral quality, soil moisture, relative humidity, air & soil temperature, and observation frequency. The concept of 'plant functional type' (PFT) is a useful one that may be applicable in many situations, but it is also important to understand qualities unique to each species because these can differ within a given PFT (e.g., shade tolerances, stress resistances).

Data merging from different sampling & temporal domains: Merging of diverse types of data is important for dealing with aspects of landscape heterogeneity and for addressing data gaps if observation frequency is not high. It is a vital component of cal/val initiatives, as these will involve data from various ground-based and airborne platforms and from information acquired at times which may differ somewhat from those of the space-based acquisitions.

Mechanistic models & data assimilation: Given the various interacting parameters and variables relevant to fluorescence emission, it is important to have process-based models which are able to capture the influences of e.g., canopy heterogeneity &

structure, leaf inclination (leaf angle distribution), photochemistry & biochemistry, pigments & fluorophores, leaf structure & anatomy, annual rhythms, vegetation height, whole plant physiology, light quality, soil moisture, observation frequency, and solar zenith angle. As an example, the SCOPE canopy model is an advanced formulation suitable for horizontally homogeneous canopies, but three-dimensional models that extend analysis to heterogeneous canopies and dynamic global vegetation models that use advanced data assimilation techniques also are needed. Research is progressing in that direction (see Chapter 4).

Multi-angular measurements: Data from multi-angle perspectives are relevant to correcting for effects of observation geometry and canopy heterogeneity & structure, and for facilitating fluorescence retrieval procedures.

Repeated measurements: Multiple observations of vegetation targets over the course of the year (especially during and proximal to the growing season) and across years are beneficial for capturing information related to acclimation/adaptation, photochemistry & biochemistry, pigments & fluorophores, annual rhythms, and abiotic & biotic stress effects. Observation frequency must be sufficient to capture major changes in fluorescence that arise from significant stress events that can unfold over the course of weeks, months, and years. At least monthly repeats are advisable, more frequently if the stress develops quickly or if certain sites are of very high priority for regular assessment.

Signal to noise ratio: Since fluorescence is a subtle signal (typically < 5% of reflected light), SNR must be adequate to capture potentially reduced fluorescence amplitudes that can be triggered by stress and which also occur during seasonal deactivation of photosynthetic activity.

Spatial resolution: A sufficiently high spatial resolution is needed to capture fluorescence features of heterogeneous landscapes consisting of vegetation of different species, ages, stress conditions, and growing regimes. The specific resolution needed will depend on the goals of the remote sensing program and the sizes of the land management units of interest. Relatively high resolutions of a few hundred square metres provide versatility for many land types.

Spectral range & resolution: The full benefit of fluorescence analysis rests in having access to the whole spectral emission, including both red and far-red peaks. That information is helpful in capturing influences of many vegetation and environmental factors, and in performing corrections necessary for accurate fluorescence signal retrievals. Whereas much of the space-based SIF detection to date has focused on the far-red fluorescence (owing to the fact that the sensors were not specialised for full fluorescence retrievals), the information is incomplete and limits the ability to derive important interpretive information for identifying and tracking stress effects, and also for quantification of photosynthetic rates. The visible and near-infrared spectrum is important for retrieval of both red and far-red fluorescence peaks, peak wavelength positions & shifts, and

ancillary indices such as PRI and NDVI (or EVI). SWIR bands provide information on e.g., water content & drought stress, and can be indirectly informative about nitrogen, protein, lignin, cellulose, sugar, and starch. Spectral resolution needs to be sufficiently high to capture fluorescence changes in both peaks. The red fluorescence emission in particular needs a suitably fine resolution (e.g., better than 0.5 nm).

In summary, it was shown that diverse factors influence variability, uncertainty, and error in fluorescence data. Sources of variability operate at respective biological and temporal scales which need to be considered in designing and interpreting studies. Additionally, the influence of pigments and fluorophores should be taken into account. In the case of stress effects, it is important to understand and quantify non-photochemical protection and to consider the temporal development of the stress. A valuable foundation for information is the provision of complementary information, including that from other EO missions, monitoring programs, and validation programs using ground-based and airborne instruments. Within this integrative framework, the FLEX mission can introduce a spatial dimension of stress effects assessment that is maximally informative and efficient. The data from the Sentinel-3 OLCI and SLSTR sensors fit into this picture by providing crucial vegetation canopy information and atmospheric/environmental parameters to provide full information to aid interpretation (as well as signal retrievals).

3.4 Linking *HyPlant* data to vegetation stress

In this work, *HyPlant* data and supporting ground data from previous campaigns were analysed with the aim to extract quantitative relationships between vegetation stress and sun-induced fluorescence. From a large pool of campaign data, stress-related datasets were extracted and a quantitative analysis of the relation of sun-induced fluorescence and selected vegetation stresses was performed.

After a careful review of available datasets, two key ones were selected for further analysis:

1. Measurements from 2014 in Latisana, Italy, which record controlled and experimentally induced stresses in a homogeneous grassland (*Festuca* spp.).

2. Two datasets from 2015 at Campus Klein-Altendorf, Germany, which describe the effects of a naturally occurring heat wave on various crops.

The first dataset is from an experiment generally referred to as the 'Experimental Field Laboratory' (http://blogs.esa.int/campaignearth/) which provides an excellent starting point to evaluate the links between *HyPlant* data and very specific vegetation stresses. The stresses are well defined and quantifiable.

The second pair of datasets took advantage of a heat wave that occurred in Summer 2015 in Germany, where canopy temperature increased dramatically within a 2-day period. This posed a unique chance to evaluate the effect of extremely high temperature on sun-induced fluorescence and other vegetation parameters. It is expected that such suddenly occurring heat events might trigger various physiological reactions in vegetation ranging from direct

biochemical effect on Rubisco, effects on membrane fluidity to increase evaporative demand, and other impacts. Thus, this dataset complements that of the single cause first experiment.

In the Latisana study, three different types of stresses were applied: (i) to simulate long-term acclimation of plants to persistent high light, a highly reflective white powder, **Caolin**, was applied to increase reflectance of the grass surface and thus reduce absorption of PAR; (ii) to reduce stomatal conductance and induce drought stress, an antitranspirant, **Vapor Gard®**, was applied; and (iii) to block photosynthetic electron flow at Photosystem I and II, respectively, the chemical herbicides **Paraquat** and **DCMU** were applied.

Detailed descriptions of the Latisana field site, treatments and the data acquisition are available in the data acquisition report of this campaign (Technical Assistance for the Deployment of an advanced hyperspectral imaging sensor during FLEX-EU, DAR, 29 March 2015, ESA Contract No. 000107143/12/NL/FF/If). A core dataset of flight lines (+/- 1 hour of solar noon) was selected to cover the changes of the different treatment on 15 consecutive days. Associated ground measurements such as top-of-canopy reflectance and fluorescence emission, as well as canopy gas-exchange measurements, were acquired for the time series.

3.4.1 Results

3.4.1.1 Latisana – controlled stresses

The Caolin treatment greatly changed the reflectance of the leaves, with higher reflectivity in the visible and NIR, illustrating the reduced APAR. NDVI of plots treated with Caolin showed ~20% lower values than the control plots and significantly higher PRI values. However, fluorescence (i.e., F_{760}) was comparable in control and treated plots, despite a reduced effective PAR.

Vapor Gard-treated plots did not differ from control plots for NDVI and F_{760} values. However, PRI in the Vapor Gard-treated plots was higher than in the control plots.

Paraquat treatment decreased the far-red fluorescence immediately after treatment and it dropped substantially two days later (Figure 3.7). This was accompanied by a decline in NDVI and a drastic reduction in PRI even within the first hours after treatment.

DCMU treatment triggered a rapid increase of F_{760} and PRI within a few hours after the treatment. NDVI in contrast remained almost constant throughout the first hours of the experiment (Figure 3.7). The rapid increase of F_{760} was expected and indicates the blockage of linear photosynthetic electron transport. Figure 3.8 shows the responses in ground-based TOC measurements (shown here as these were less affected by variable atmospheric conditions).

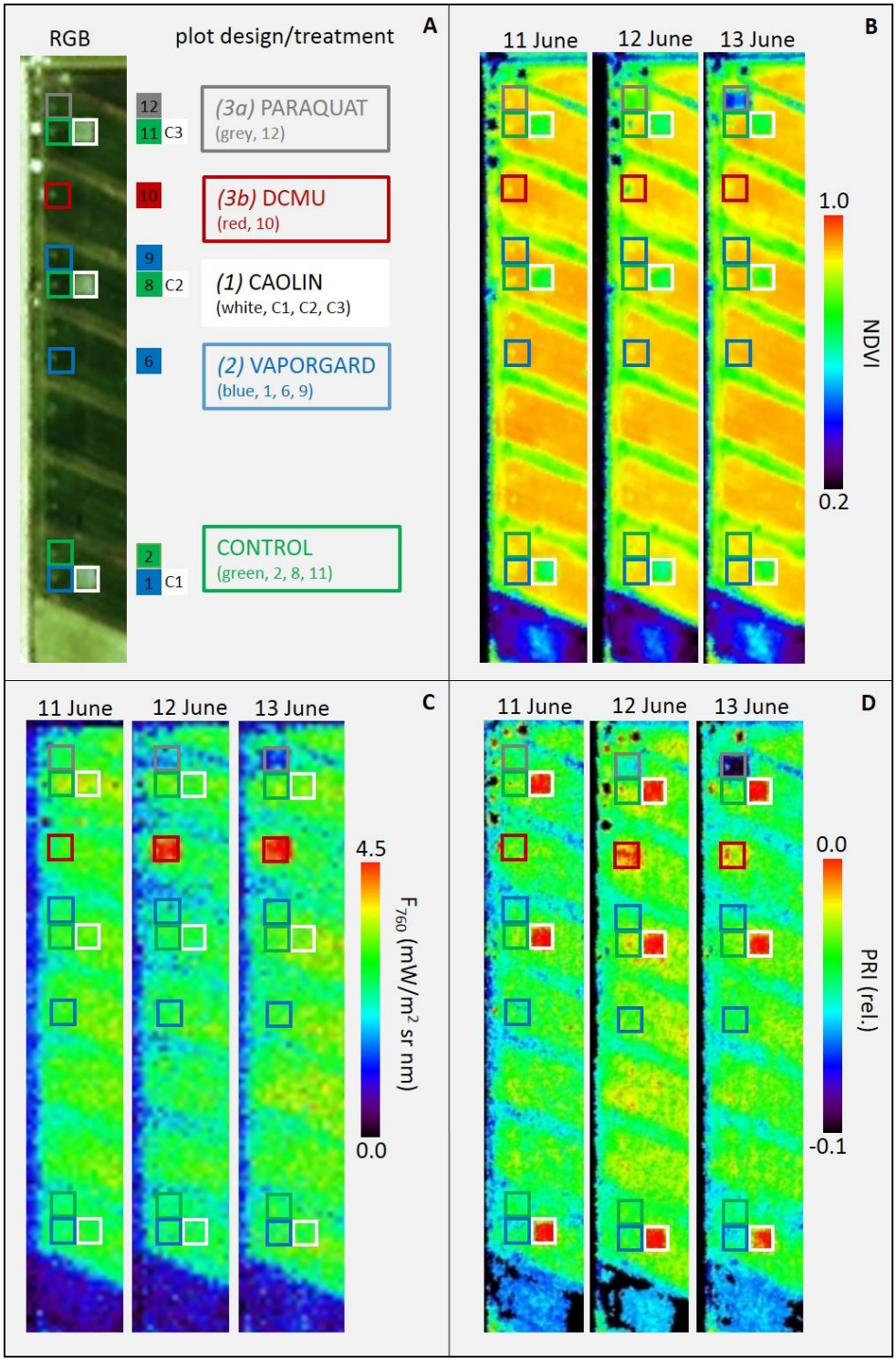

Figure 3.7. RGB images of an example flight line, including the plot design of the different treatments (A), plus maps on three consecutive days (11–13 June 2014) showing NDVI (B), sun-induced fluorescence at 760 nm (F_{760}) (C), and PRI (D). In each map, Paraquat treated plot (12) is marked grey, DCMU plot (10) is marked red, Vapor Gard treated plots (1, 6, 9) are marked as blue, and Caolin treated plots (C1, C2, C3) are marked in white.

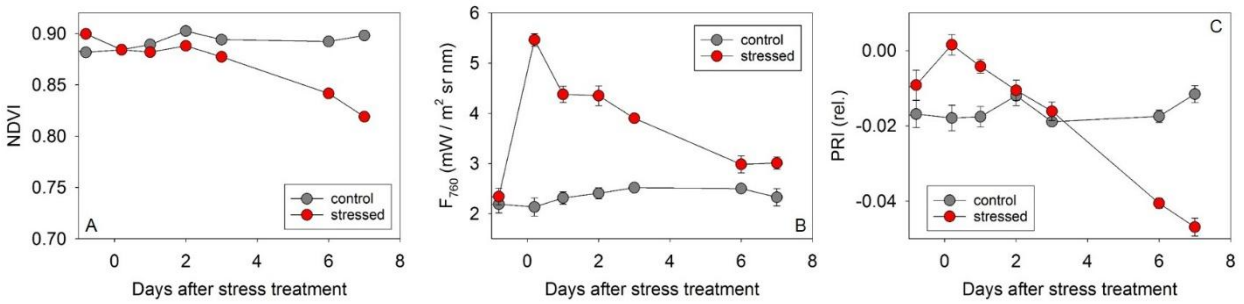

Figure 3.8. Time series of NDVI (A), fluorescence at 760 nm (F_{760}) (B), and PRI (C). Recorded by TOC measurements up to 7 days after the DCMU treatment in the same plots that were observed by *HyPlant*.

These time series showed a gradual decrease of NDVI starting 3 days after the treatment. An evaluation of atmospherically corrected hemispherical conical reflectance factor (HCRF) indicates that the decline in NDVI may have been related to chlorophyll degradation in the DCMU-treated vegetation a few days after application (i.e., increasing HCRF in the red, data not shown). The F_{760} in contrast peaked immediately after treatment and then gradually recovered to almost the base value in the subsequent days. PRI had a different temporal pattern, decreasing steadily after a slight initial increase. The initial rise in PRI might have been associated with a reduction in NPQ arising from blockage of electron transport and thus failure to establish the proton gradient essential for de-epoxidation of violaxanthin. Subsequent decreases in PRI appeared to be linked with reduction in carotenoid levels (based on HCRF, data not shown). Control plot measurements were stable throughout.

The results from our controlled stress experiment were not altogether expected. Reduced APAR (Caolin Experiment) did not result in a lower F_{760} as expected. This contradicts some results that were reported earlier in the literature that describe the intensity of F_{760} primarily as a function of absorbed PAR (Rossini *et al.* 2010). On the leaf level F_{760} should be clearly related to APAR as long as no changes occur in pigment composition or functional status of photosynthesis. Our results can be explained only by taking additional canopy effects into account. The application of Caolin changes both the distribution of light within the canopy and also the path of emitted leaf fluorescence within the canopy. Thus, the constant F_{760} after Caolin treatment could possibly be interpreted as a canopy effect. Such effects may be modelled by a canopy energy flux model such as SCOPE. Our dataset may be valuable for such a modelling exercise.

The treatment with Paraquat was likely too severe. A short term inhibition of electron transport at PSI could not be resolved and the subsequent destruction of the photosynthetic apparatus was evident from the different indices and also F_{760}. However, these results do provide an interesting basis for discussion in the context of linking fluorescence with vegetation stress.

In the Vapor Gard treatment, gas exchange measurements confirmed that Vapor Gard sealed the leaf stomata and carbon uptake rate was slightly reduced. However, no effect on F_{760} was detected, neither in *HyPlant* images nor in ground top-of-canopy measurements. This was in contradiction to results of the meta-analysis of Ač *et al*. (2015) and also what was hypothesised in Damm *et al*. (2010). Thus we could not confirm the reduction of F_{760} as a result of drought-

induced reduction in stomatal conductance. Possibly, the effects on photosynthesis were too slight to be discernible in F_{760} results. Also, in general, drought triggers a very complex cascade of functional reactions within plants. Thus, it is possible that such effects are too manifold to be easily captured by a single correlation with F_{760} only.

DCMU, as expected, greatly increased F_{760} immediately after the application. This was a clear indication of the blockage of photosynthetic electron transport at PSII. These results strongly confirm the results of Rossini *et al*. (2015). In addition to the short term reactions, a longer term effect can be resolved from this dataset. Starting at one day after treatment, continuous changes in NDVI, PRI and F_{760} were observed in the DCMU plots. The mechanisms for these changes likely involve both reduced capacity for NPQ and pigment changes. DCMU is known to cause pigment degradation that is more severe in dicot plants. Currently there is a further study underway to evaluate the dose response effects of DCMU on F_{760} and PRI, and that study may help to unravel the functional effects (blocking of electron transport) from pigment changes (Pinto *et al*., in preparation).

In the near future, as the extraction of the red (O_2-B) fluorescence data from *HyPlant* campaigns is completed, a full picture of stress responses in the field will be possible. We aim to adapt a modified version of the spectral fitting approach to retrieve a full set of FLEX-like data from *HyPlant* imagery, which will include the intensity and position of both fluorescence peaks and the integrated value of total fluorescence emission. This whole set of FLEX-like data is necessary to identify specific stresses and to develop quantitative vegetation stress products.

3.4.1.2 Campus Klein-Altendorf – summer heat wave

The agricultural experimental area Campus Klein-Altendorf was repeatedly covered by *HyPlant* overpasses on consecutive days (June 30th to July 2nd 2015) during morning, midday, and afternoon. Extremely high temperatures (up to 40°C air temperature) were present during all measurement days. Fields with wheat, corn, rapeseeds and barley were in general not irrigated.

For our analysis two flight lines from this extensive data set were selected, namely an afternoon (15:50 local time) overpass on June 30th, when surface temperatures were moderately high (around 30°C) but still in the range considered normal for midsummer in Germany. A second flight line was selected on July 2nd at approximately the same time of the day (15:16 local time); on that date, surface and canopy temperatures were very high (36-39°C), exceeding norms for crops in Germany. This sudden increase of temperature above 35°C can be considered an extraordinary temperature range, to which mid-European crops are not adapted. Thus, we expected a clear stress response from the crops.

This sudden temperature increase resulted in clear changes in all vegetation indices and also in F_{760}. NDVI and EVI increased in corn, but decreased in the other crops. PRI became less negative in rapeseed and corn, and more negative in barley and wheat. F_{760} decreased in rapeseed, barley and wheat, but increased in corn. In corn, however, a reverse behaviour was observed in the irrigated corn plot, where F_{760} decreased.

These changes were further analysed and showed that F_{760} was related to EVI. Across all crops a clear dependency between EVI and F_{760} could be described (Figure 3.9). Only slight deviations from this 1:1 line were observed e.g., in the irrigated corn plot. Thus it can be assumed that during the two-day period some crops grew and other crops decreased their LAI because of seed filling and senescence. This seemed to be the main effect that determined the intensity of F_{760}. Only slight deviations from the linear correlation line were observed, which could be interpreted as an additional functional response of the photosynthetic apparatus to the extreme high temperatures.

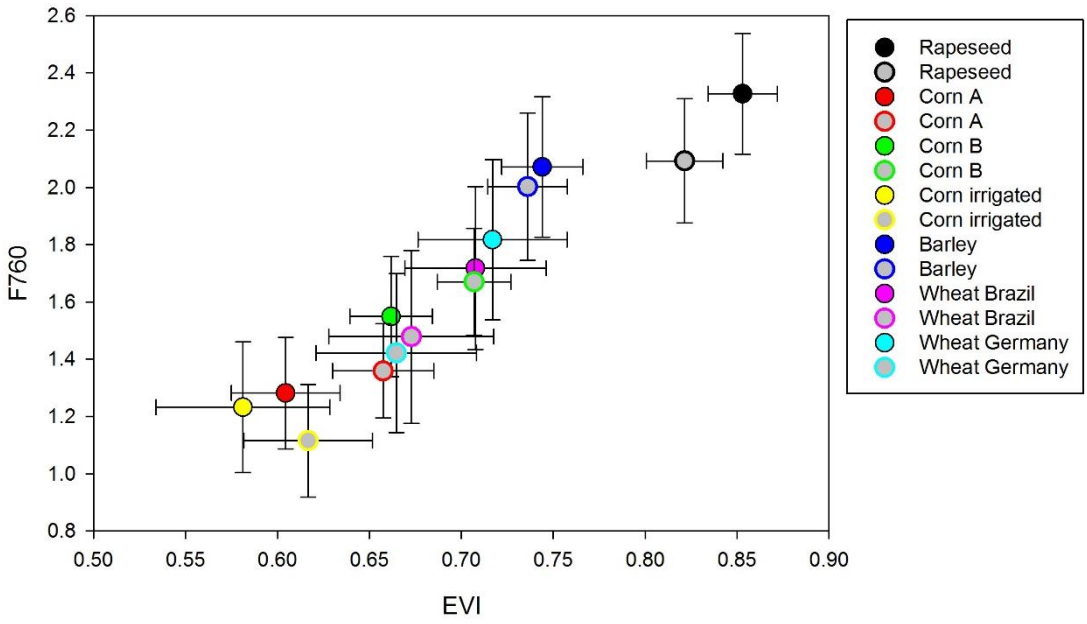

Figure 3.9. Correlation of EVI and F_{760}.

These results did not indicate a link of F_{760} with the physiological status of photosynthesis. The only exception was for corn, where the irrigated plot showed a trend opposite to the two crop fields, but the magnitude of this signal was small in comparison to the dominating effect of EVI and LAI.

In conclusion, the results for the heat wave effects indicated a small functional contribution of changing physiological status during the high temperature event. It remains an open question as to whether the temperatures were still in a range that did not cause a major temperature stress to the crops, or if high temperature simply does not affect the intensity of F_{760}. In the meta-analysis of Ač *et al*. (2015), albeit with a limited number of heat-stress studies, it was concluded that high temperature did not have a clear effect on far-red fluorescence, which seems to be in line with the results here. Furthermore, results here are consistent with the SCOPE modelling analysis of Verrelst *et al*. (2015b), which described the superior sensitivity of the red fluorescence peak to photosynthetic activity. A further reason for the reduced sensitivity here could be related to saturation of photosynthesis with high APAR such that slight changes in photosynthesis were not easily discriminated by F_{760}.

3.5 Evaluation of strategies to assess non-photochemical quenching using optical measurements

Approximating the actual state of NPQ is essential to establish a solid relationship between SIF and photosynthesis. NPQ, as a result of its high sensitivity to ambient stress levels, alters the sensitivity of SIF to track changes in photosynthesis and GPP in a straightforward way (Damm *et al.* 2015a), particularly at canopy scale where three-dimensional structure causes gradients in light interception and light quality (Nobel *et al.* 1993; Stewart *et al.* 2003). However, NPQ can be a challenge to measure using reflectance measurements only, because its impact on plant optical properties is small. Therefore indirect proxies are commonly used, most notably, the photochemical reflectance index (PRI), which is calculated using green wavebands between 500-600 nm and which is sensitive to reflectance changes arising from the operation of the carotenoid xanthophyll cycle. Nevertheless, there are additional superimposing factors that influence the optical properties of vegetation canopies in this wavelength region, thus potentially altering the rate of NPQ (Niinemets *et al.* 2003; Demmig-Adams 1998) and affecting the sensitivity of SIF for photosynthesis and GPP estimation.

Objectives of this workpackage were to:

- address open questions regarding the link between NPQ and optical proxies such as PRI;
- analyse experimental data to evaluate relationships between non-photochemical protection and PRI; and
- evaluate new concepts to estimate NPQ beyond the commonly used NPQ-PRI linkage.

Both literature review and analysis of experimental data from previous studies were included.

3.5.1 Results

3.5.1.1 Assessment of PRI retrieval uncertainties

The Photochemical Reflectance Index was designed to monitor pigment changes related to the xanthophyll cycle (Gamon *et al.* 1992), a biochemical process involved in NPQ. In addition, strong experimental evidence supports the capacity of PRI to provide information on photosynthetic light use efficiency (LUE_p) based on the light use efficiency concept of Monteith (1972) (i.e., $GPP = APAR \times LUE_p$) and assuming that LUE_p is affected by NPQ. PRI has been found to explain 42%, 59%, and 62% of the LUE_p variability at leaf, canopy, and ecosystem scale, respectively (Garbulsky *et al.* 2011). However, despite strong experimental evidence, there remains a question regarding the capability of PRI to consistently describe pigment changes related to the xanthophyll cycle and, thus, its suitability as proxy of NPQ.

An increasing number of studies report sensitivities of the PRI for effects other than xanthophyll cycle changes. These include changes in pigment pool sizes (i.e., chlorophyll and carotenoids). Gamon & Berry (2012) recently classified pigment impacts on PRI into facultative short term changes related to the xanthophyll cycle, and constitutive long term changes of pigment pool size acting at a seasonal time scale and driven by changes in carotenoid:chlorophyll ratio (Gamon & Berry 2012; Hmimina *et al.* 2015; Wong & Gamon 2015).

Here, a sensitivity analysis was conducted on the impact of changing pigments (here only chlorophyll) on the retrieval accuracy of PRI. Figure 3.10 shows that wavelengths used to calculate the PRI (i.e., 531 nm and 570 nm) are sensitive to changes of the chlorophyll content as well leaf structure. If not corrected, a slight change of the chlorophyll content causes a variation of PRI values obtained, irrespective of any change in xanthophylls or NPQ.

Structure is frequently indicated as an important confounding factor of PRI-NPQ relationships, particularly at canopy level (Barton & North 2001; Grace *et al.* 2007; Wu *et al.* 2015), where effects such as leaf orientation and leaf area in combination with illumination/observation geometry, and varying background contributions, substantially impact PRI. Structural effects on the PRI can be explained by the effect of surface anisotropy in combination with uncertainties stemming from data pre-processing. Atmospheric compensation, for example, relies on various assumptions (i.e., Lambertian surface reflectance, surface homogeneity) imposing wavelength-dependent retrieval errors on reflectances, and thus, on vegetation indices calculated from these data (Damm *et al.* 2015b).

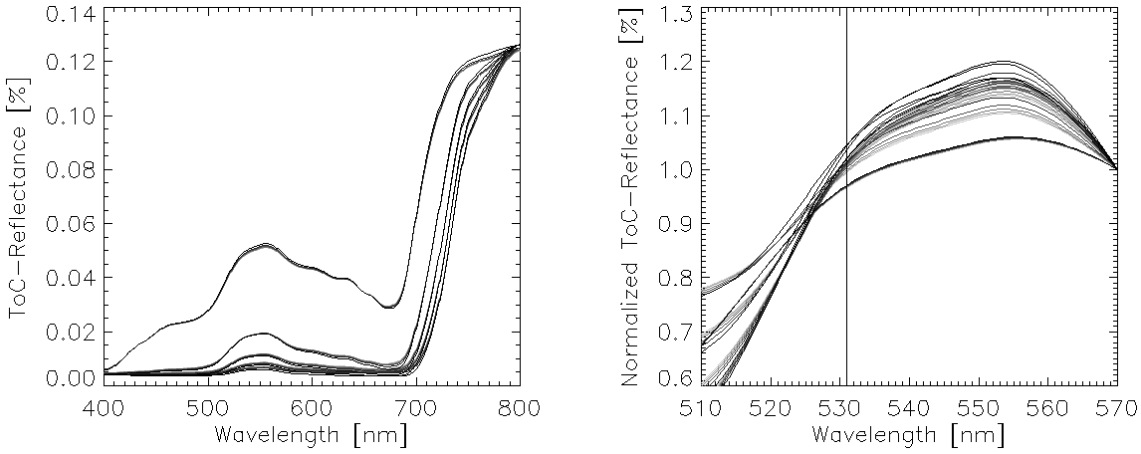

Figure 3.10. Change of leaf reflectance for varying chlorophyll contents and leaf thickness. Left: Leaf reflectance simulated with PROSPECT for chlorophyll contents between 40 and 80 µg cm^{-2} and leaf thickness between 1 and 2. Right: Normalised leaf reflectance considering the reflectance at 570 nm (one wavelength used to calculate the PRI). The vertical line indicates the second wavelength at 530 nm used to calculate the PRI.

Related to the impact of structure is an additional sensitivity of PRI for illumination effects (Damm *et al.* 2015b; Mottus *et al.* 2015) which introduce inaccuracies related to estimation of surface irradiance, particularly the correct fractions of direct and diffuse surface irradiance. For example, uncertainties in retrieved surface reflectance can result if the direct surface irradiances are wrongly estimated (e.g., due to an insufficient consideration of surface topography). The wavelength dependency of this error is critical, with strongest impacts in the visible wavelength range and around strong atmospheric absorption lines. These errors directly translate into subsequently derived vegetation indices.

Recent studies by Damm *et al.* (2015b) and Mottus *et al.* (2015) quantitatively estimate the sensitivity of the PRI for errors associated with the estimation of surface irradiance considering spatial high resolution. Depending on the vegetation type (canopy structure), uncertainties of the PRI for inaccurate estimates of surface irradiance of up to 20% are possible.

These various aspects influence the applicability of the PRI, particularly at canopy level, and suggests that the PRI can be reliably used as proxy for NPQ only if the confounding factors do not vary, i.e., under ideal controlled conditions. It is possible that in more realistic scenarios, observed linkages between PRI and NPQ may, in fact, be dominated by spurious relationships. Wong & Gamon (2015), for example, established that the PRI is sensitive to xanthophyll pigment changes but also to seasonally changing carotenoid:chlorophyll ratios, and to a yet unreported shifting of leaf albedo. Strong seasonal relationships between PRI and NPQ thus are driven by the covariance between both measures with one or a few of these confounding factors. Importantly, the PRI had relatively low sensitivity to xanthophyll changes when considering all aspects discussed above. Depending on the impact of the individual factors, different relationships across species, spatial scales, and time scales (diurnal vs. seasonal) may be expected.

3.5.1.2 Experimental assessment of PRI-NPQ relationships at leaf level

Experimental data obtained during the CEFLES-2 field campaign in 2007 (Rascher *et al.* 2009), and diurnal courses of PRI and NPQ data measured at leaf level in a winter wheat field were used here. A hyperbolic relationship existed between electron transport rate (ETR) and PRI normalised for chlorophyll content (Figure 3.11). The relationship between PRI and NPQ was less consistent and no clear conclusions could be drawn. When qualitatively assigning underlying environmental conditions to the individual data points, it becomes obvious that the PRI was not only sensitive for NPQ but also to other effects at leaf level, i.e., pigment pool sizes. More concise and relatively strong relationships between PRI and NPQ have been reported for forests over a seasonal time scale (ESA 2015b), which were measured under controlled conditions (i.e., same species, leaf level, etc.).

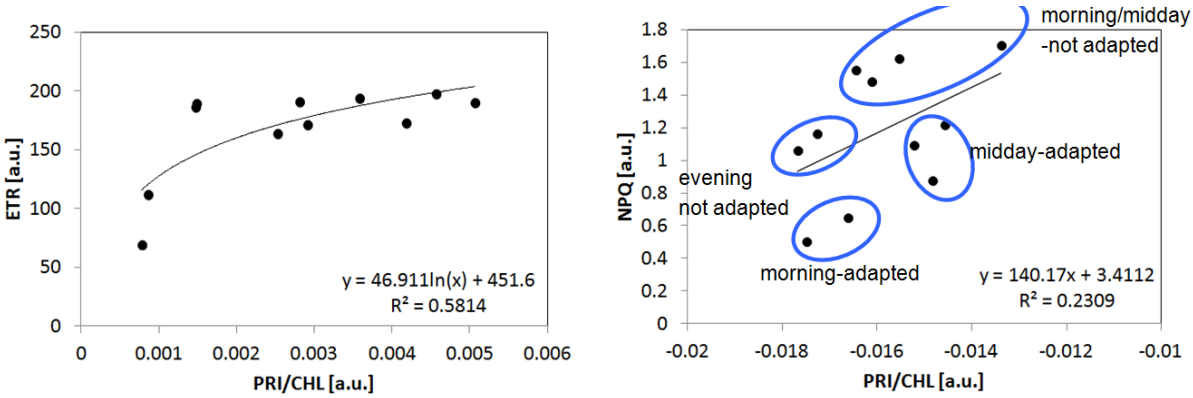

Figure 3.11. Relationship between PRI and ETR (left) and NPQ (right) of winter wheat. Measurements were acquired at leaf level for a time period of five days. PRI and chlorophyll content were acquired from reflectance data measured with an ASD spectrometer equipped with a LiCOR-1800 integrating sphere. NPQ and ETR were obtained from a hand-held PAM-2000 chlorophyll fluorometer.

Comparison of experimental results obtained at diurnal and seasonal time scales indicated weaker relationships at the leaf scale but stronger relationships at canopy or ecosystem scale, as was also reported by Garbulsky *et al.* (2011). The decreasing relationship for data obtained at shorter time scales likely can be explained by the strong impact of confounding factors on PRI which could mask any PRI-NPQ relationship, whereas at seasonal time scales the variability of confounding effects likely coincided with strong physiological effects, resulting in a tighter agreement between PRI and NPQ. It must be acknowledged that the database is limited, so that conclusions must be drawn carefully.

3.5.1.3 New definitions of PRI for application at canopy scale

Theoretical and experimental evidence support the usage of the wavelength region around the green spectral peak (500-600 nm) to derive information on the de-epoxidation state of xanthophylls and to estimate NPQ. Nonetheless, the considerations discussed above indicate a need to adjust the PRI calculation to more effectively quantify NPQ. Different approaches have been suggested in the literature including (i) strategies to normalise the PRI, as well as (ii) compensation for structural effects and (iii) for illumination effects in surface reflectance data.

(i) Normalisation strategies

Various strategies have been suggested to normalise the PRI and make it more applicable at canopy scale. Typically, these suggest compensating individual confounding factors such as the PRI sensitivity for pigment pool sizes, canopy structure, and illumination effects.

(a) Canopy structure

Hernandez-Clemente *et al.* (2011), for example, suggested using different wavelengths less affected by canopy structure (i.e., LAI) and reported improvements if 512 nm is used as reference band instead of 570 nm. They reformulated the PRI to obtain a canopy PRI (cPRI) as:

$$cPRI = \frac{(R_{531} - R_{512})}{(R_{531} + R_{512})} \quad (3.1)$$

Wu *et al.* (2015) empirically corrected the PRI for sensitivity to LAI, using experimental data to obtain a saturating relationship between PRI and LAI and employing the resulting fitting coefficients to compensate the PRI sensitivity for LAI as follows:

$$rPRI = PRI - 0.15\big(1 - exp(-0.5LAI)\big) - 0.2 \quad (3.2)$$

(b) Pigment pool sizes

Kovac *et al.* (2013) proposed an alternative approach employing the continuum removal concept, particularly for coniferous forests ecosystems. They suggested using the "area under the curve normalised to maximal band depth between 511 nm and 557 nm" ($ANMB_{511\text{-}557}$) as an optical proxy equivalent to the PRI, but which is less sensitive to pigment changes:

$$ANMB_{511-557} = \frac{AUC_{511-557}}{MBD_{511-557}}, \quad (3.3)$$

$$AUC_{511-557} = \frac{1}{2}\sum_{i=1}^{n-1}(\lambda_{i+1} - \lambda_i)\left(R_{CR(\lambda_{i+1})} + R_{CR(\lambda_i)}\right), \quad (3.4)$$

where R_{CR} is the continuum removed reflectance and MBD is the maximum band depth between 511 nm and 557 nm.

Hmimina *et al.* (2015) proposed a compensation of the PRI's pigment sensitivity using a deconvolution approach.

Wu *et al.* (2010) suggested another formulation of the PRI to minimise its sensitivity for chlorophyll pool sizes:

$$cPRI = \frac{(R_{531} - R_{570})}{(2R_{550} - R_{531} - R_{570})} \quad (3.5)$$

(c) Illumination effects

Damm *et al.* (2015b) observed a sensitivity of PRI to a combination of reflectance anisotropy and artefacts related to the estimation of surface irradiance. In a yet unpublished work (Damm *et al.* in preparation), a normalisation of the PRI was suggested to compensate its sensitivity for illumination effects (i.e., cast shadows) persisting in HCRF data after atmospheric correction. The PRI normalised for illumination effects (iPRI) is formalised as:

$$iPRI = \frac{((R_{531} - m_{corr}) - R_{570})}{((R_{531} - m_{corr}) + R_{570})} \quad (3.6)$$

where

$$m_{corr} = (R_{550} - R_{570})/\Delta\lambda_{570-550} \cdot \Delta\lambda_{570-531} \quad (3.7)$$

This approach assumes that a constant intercept between the PRI reference band (570 nm) and a correction band (550 nm) (m_{corr}) minimises impact of varying illumination conditions and, to a certain extent, structural effects and pigment pool sizes. Sensitivity of the iPRI for illumination effects could be substantially reduced with the new formulation (Figure 3.12).

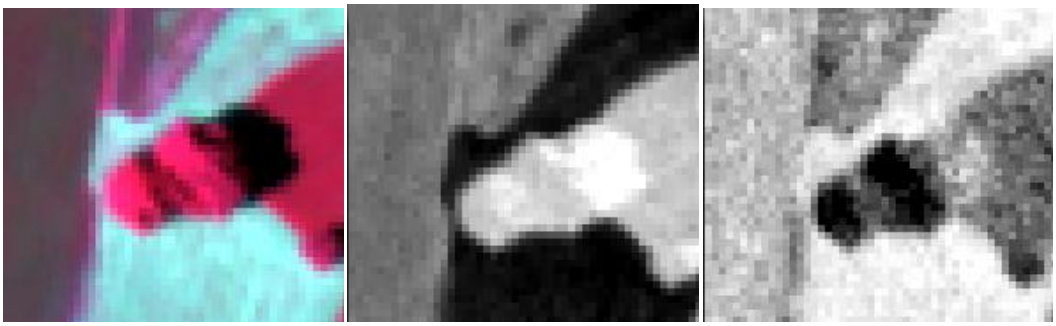

Figure 3.12. Colour-infrared image and PRI obtained from Airborne Prism Experiment (APEX) imaging spectroscopy data acquired on the 26 June, 5pm local time. Left: CIR data. Middle: uncorrected PRI. Right: corrected iPRI.

Proposed normalisation approaches must also take into account that confounding factors often are combined and the isolated compensation for one factor will not necessarily decrease the impact of another.

An approach that may be more flexible and reliable compared to the proposed approach of adjusting PRI values or reformulating PRI calculations would be an improvement of the data pre-processing to first to obtain more accurate HCRF values corrected for illumination and structural effects, followed by a more accurate retrieval of PRI values and other plant traits (i.e., pigments). Strategies to compensate structural and illumination effects were thus evaluated.

(ii) Compensation of structural effects using DASF

The probability that photons interact within the canopy is determined by canopy structure, resulting in a wavelength-independent impact of canopy structure (Knyazikhin *et al.* 2011). The theory of spectral invariants uses this idea and demonstrates that the simple algebraic combination of single-scattering albedo with canopy spectral transmittance and reflectance is not wavelength dependent. Based on this finding, three specific canopy structural variables have been determined – the canopy interceptance, the recollision probability, and the escape probability (Huang *et al.* 2007; Panferov *et al.* 2001). Recently, it was proposed to combine these three spectral invariants to formulate the directional area scattering factor (DASF), a correction factor for compensating structural effects as present in surface reflectance data (Knyazikhin *et al.* 2013b), and potentially allowing compensation of structural effects in the PRI.

The DASF is a new approach to compensate for structural effects, but its calculation depends on several assumptions, including that (i) the vegetation cover must be dense and (ii) a typical leaf albedo is known and representative for various vegetation types. We evaluated whether these assumptions limit the applicability of the DASF for improved PRI calculations. The model PROSAIL-5 was used to test the impact of different canopy parameters of a perfectly homogeneous canopy on the calculation of DASF. One parameter was varied at a time while the others were kept fixed to specified values (Henry 2015).

As expected, it was found that the DASF was sensitive to canopy structure (here LAI and average leaf angle). However, we also found a sensitivity of the DASF for varying leaf optical properties, particularly as affected by chlorophyll content, dry matter content, and leaf structure. This sensitivity can be explained by an impact of these variables on the optical properties of leaves, particularly for wavelengths used to calculate the DASF (i.e., 710-790 nm). Both a reduced representativeness of the DASF for dense vegetation canopies and its sensitivity for leaf biochemical properties limited the applicability of the DASF to correct the PRI for structural effects. Further investigation of this topic is needed, and we did not continue with our analysis to combining DASF for improved PRI calculations.

(iii) Compensation of illumination effects using digital object models in atmosphere correction

A recent study by Damm *et al.*, (2015b) indicated a strong sensitivity of retrieved surface reflectances (i.e., HCRF) to illumination effects, which eventually translates in uncertainties of retrieved vegetation indices. This effect is related to an inaccurate description of the radiative transfer underlying the radiance measurement used, resulting in uncertain estimates of surface

irradiance — particularly the lack of adequate auxiliary data (i.e., accurate DOMs in high resolution) or atmospheric parameters (i.e., actual aerosol phase functions) cause uncertain estimates of pixel-wise fractions of direct (E_{dir}) and diffuse (E_{dif}) irradiance, since they are only approximated using the sun-observer geometry or topography information based on coarse DEMs. Further, assumptions made during data processing are not representative for such surfaces, i.e., surface homogeneity (scattering elements are infinitesimally small compared to the sensor's field of view) and absence of shadowing effects caused by complex surface topography.

We tested the applicability of high resolution DOMs to better characterise surface irradiance including the fractional amounts of E_{dir} and E_{dif} in heterogeneous canopies. We incorporated Hay's model (Hay & McKay 1985), parameterised with the illumination angle derived from DOMs. It was found that if the pixel size of the DEM was larger than the area represented in the radiance measurement, the illumination angle obtained over complex surfaces was not representative for the actual illumination angle. Even if DOMs with a comparable spatial sampling were used, the fine structure of surface orientations within the heterogeneous vegetation canopy was only roughly approximated. Nevertheless, the use of a DOM resulted in a substantial improvement for the retrieval of surface reflectance and, eventually, PRI.

Sensitivity of reflectances and vegetation indices for illumination effects is intrinsic to all optical measurements. Results here were based on spatial high resolution data and represented an extreme case. With lower spatial resolution (i.e., 300 m as envisaged for FLEX) the illumination effect will be partly compensated but will still be present and need to be taken into account.

3.5.1.4 Application & comparison of canopy PRI indices to HyPlant experimental data

Discussed and experimentally demonstrated sensitivities of the originally formulated PRI – for pigment pool sizes, structural and illumination effects – imply the need for alternative strategies less sensitive to these effects but still capable of tracking changes of NPQ rates. Such strategies include several canopy PRI (cPRI) indices that can be easily implemented. More advanced solutions were found to still require substantial developmental efforts and dedicated analysis to make them applicable for real data. Consequently, we evaluated if suggested cPRI indices do indeed show a reduced sensitivity for pigment pool sizes, vegetation structure, and illumination effects, as well an increased capability to track changing NPQ rates.

The five cPRI indices summarised under normalisation strategies (Section 3.5.1.3; Wu *et al.* 2015, 2010; Kovac *et al.* 2013; Hernandez-Clemente *et al.* 2011; Damm *et al.* in preparation) were assessed here with respect to their sensitivities in comparison to the original formulation of Gamon *et al.* (1992). Using the *HyPlant* Latisana dataset of herbicide treatments of homogeneous grass carpets (Section 3.4), the various canopy PRI derivatives were assessed for their sensitivities to (i) structural and atmospheric effects (using the Paraquat dataset), and (ii) functional changes of plant photosynthesis (i.e., rates of NPQ) (using the DCMU dataset).

Table 3.4 summarises the results of the sensitivities to pigment pool sizes, canopy structure, and atmospheric disturbances. Most of the cPRIs allowed compensating the sensitivity for pigment pool sizes (differences between the averaged control signals and the Paraquat signals).

Only the cPRI of Damm *et al*. (in preparation) and Wu *et al*. (2010) had greater sensitivity than the original PRI. Considering canopy structure (i.e., divergence of the three control plots), the alternative derivations had decreased sensitivity, except for that of Wu *et al*. (2010). Atmospheric disturbances (indicated as variation of the averaged control signal in time) were lower in all cPRI derivatives compared to the original PRI. From these results, the derivations using Kovac *et al*. 2013 and Wu *et al*. 2015 appeared most promising.

Figure 3.13 shows the responsiveness of the cPRI indices to changing functional status. The original PRI, the cPRI of Wu *et al.* 2015, and to a lesser degree the cPRI of Wu *et al.* (2010), produced results consistent with a reduction in plant function that could have involved (at least initially) a reduced capacity for NPQ due to the blockage of PSII electron transport (Goss & Lepetit 2015). The cPRI index of Wu *et al*. (2015) showed a similar pattern of response to the original PRI.

Table 3.4. Sensitivity of the original PRI and five alternative cPRI formulations for pigment pool sizes, canopy structure, and atmospheric disturbances.

Index	Optimisation purpose	Pigment pool size sensitivity [%]	Structural sensitivity [%]	Atmospheric sensitivity [%]
PRI		71.3	64.0	57.4
cPRI (Hernandez *et al*. 2011	Pigments	60.4	8.1	14.9
cPRI Wu *et al*. 2015	Pigments	10.7	12.3	13.1
ANMB Kovac *et al*. 2013	Pigments/ structure	1.12	3.6	23.4
cPRI Wu *et al*. 2010	Structure	1148.1	73.6	48.1
cPRI Damm *et al*. in prep	Illumination	85.3	12.0	13.3

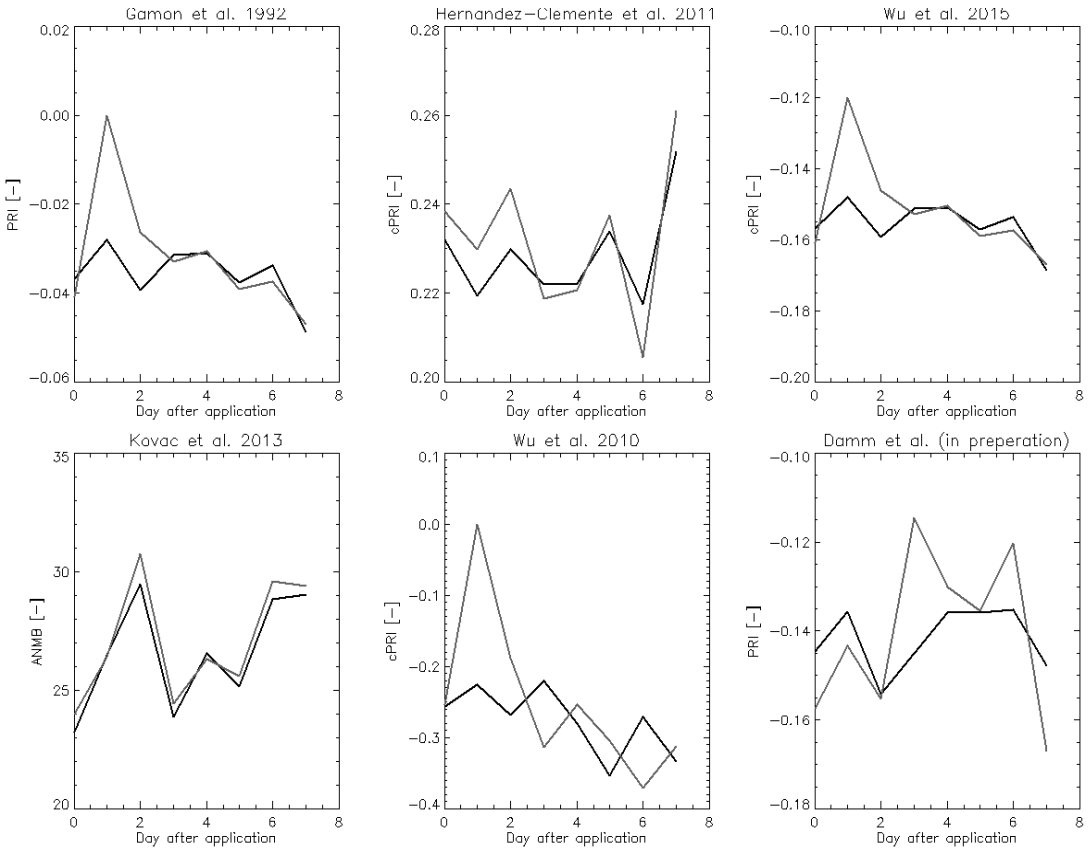

Figure 3.13. Temporal behaviour of PRI and five cPRI formulations for the average of three control plots (black line) and a herbicide treated plot (grey line) over a two-week period. DCMU was applied after the first measurement, and a change of the PRI was expected for the 1st day after application.

From these results, it appears that new formulations of the PRI and certain other normalisation strategies (e.g., Wu *et al*. 2015, Kovac *et al.* 2013) have significant potential to compensate sensitivities of the original PRI for various disturbing effects, whilst retaining sensitivity for functional changes of the photosynthetic apparatus. Such cPRI derivations warrant further study across a wider variety of treatments and species.

In summary, theoretical and experimental evidence from this workpackage indicates that the wavelength region around the green peak (500-600 nm) contains information related to the de-epoxidation state of xanthophylls as part of the Calvin cycle and can be used to approximate NPQ. However, the PRI, which is commonly used to assess NPQ in leaves and canopies, can be a challenge to interpret accurately, particularly at the canopy level, since it is affected by a complex set of confounding factors (i.e., structural and illumination effects, pigment pool sizes).

In view of that consideration, a helpful approach could include reformulation or development of an alternative PRI retrieval approach to provide a more sensitive and less affected measure of the NPQ. Illumination effects for example are most critical for high spatial resolution data and will be substantially compensated at the spatial scale envisaged for FLEX (300 m). However, species variability and the seasonal dependency of PRI-NPQ relationships caused by a possible

covariance between PRI and NPQ – with confounding factors – requires attention also for PRI retrievals at a spatial scale of 300 m.

Various strategies were identified to compensate the sensitivity of the original PRI for confounding factors. Most of the canopy PRI formulations showed a substantially reduced sensitivity for individual disturbing effects and thus theoretically provide better access to changes in canopy NPQ rates. However, a more general approach is required to account for potential combinations of effects. Further, even if structural or illumination effects are compensated, PRI seems to remain sensitive for pigment pool sizes. Nevertheless, a quantitative analysis based on experimental *HyPlant* data demonstrated the potential to improve optical indices potentially sensitive to NPQ using reformulations of the PRI. Further research is needed to link these optical proxies to NPQ using both modelling studies and experiments.

A potential strategy to accommodate all of the various sensitivities should include the following components: (i) improved retrievals of canopy reflectance using the theory of spectral invariants or at-sensor radiance approaches to compensate structural and illumination effects in retrieved HCRF data; (ii) retrieval of additional plant functional traits (pigment composition) in high accuracy to (iii) finally compensate the PRI sensitivity for pigment pool sizes.

The FLEX configuration with its high spectral resolution and coverage of a critical wavelength region in the visible provides an optimal setup to facilitate development of such a sophisticated retrieval scheme and provides flexibility for any strategy that might be implemented eventually.

3.6 Conclusions

For the development of vegetation stress indicators and applications, we sought to advance the results already achieved from earlier work in the PS Study and utilise new datasets proceeding from field campaigns and other research, including the *HyPlant* airborne system.

Reviews of the literature developed an understanding of how SIF might be used for a wide variety of **abiotic and biotic stresses** across many species. In addition to water stress, temperature stresses, and nitrogen deficit (which were initially studied during the PS Study), the influence of air pollution, insecticides, senescence, biotic stress, combined stresses, heavy metals, herbicide, ozone, UV radiation, salt and micro- and macro-nutrient deficiencies were considered, and trends were identified for red and far-red fluorescence responses. Stress indices introduced in the PS Study were tested here and reveal the importance of having ancillary measures (e.g., chlorophyll content) to help interpret fluorescence changes and distinguish among stresses. The value of having both red and far-red fluorescence information was again evident.

A synthesis here was completed on the factors that influence **variability, uncertainty, and error** in fluorescence data, and recommendations were made to strengthen certainty in interpretation of fluorescence data. To help account for variability and to manage sources of uncertainty, key requirements must include ancillary measurements, understanding of the biological & ecophysiological attributes of the vegetation, effective methods for merging of

data from various domains, improvements in mechanistic models & data assimilation, suitable sampling & measurement strategies, and sufficient spectral & spatial resolution of sensors. FLEX – in combination with Sentinel-3's OLCI and SLSTR sensors – will be well suited to meeting these needs.

The importance of the **PRI** for interpretation of fluorescence is well known. Here, we have considered how best to incorporate PRI for canopy-level assessments. We have suggested routes by which PRI could provide a more sensitive measure of non-photochemical quenching by compensating for the impacts of confounding factors – notably structural and illumination effects, and pigment pool sizes – on estimation of canopy photosynthesis or stress status.

Finally, stress experiments conducted with the ***HyPlant*** sensor have been utilised here to quantitatively link vegetation stress and SIF (only far-red fluorescence was considered here). Both controlled stress applications and a naturally occurring heat stress event were the focus. The potential interplay of canopy characteristics with stress responses and fluorescence emission was indicated. Furthermore, it appeared from the heat stress that F_{760} displays a clear relation to EVI (hence LAI).

4. Photosynthesis model optimisation, updates, and applications

4.1 Introduction

During the FLEX-Photosynthesis study, pieces of model code were assembled into a consolidated model for photosynthesis and fluorescence, SCOPE v1.53 (based on Van der Tol *et al.* 2009), that can be used to analyse the fluorescence-photosynthesis relationship. The model was able to produce realistic shapes of fluorescence spectra that can be used as a forward simulator for the sensors on FLEX and Sentinel-3. In the current activity, SCOPE v1.53 was updated with new content, and foundations were laid for future developments.

Key objectives were to:

- evaluate effects of xanthophylls, long-term non-photochemical quenching, and PSI-PSII energy partitioning, all of which are informative about stress;
- define model parameters for specific plant functional types that can be linked to operational dynamic global vegetation models (DGVMs);
- further quantify vegetation structural effects on the measured SIF signal; and
- investigate data assimilation techniques amenable to usage in a broader range of applications, including global ecology, climate- and carbon modelling.

These objectives were addressed under four themes: code management, model additions, model performance assessment, and model applications.

4.2 Model code management

Three versions of SCOPE were released during the FB Study: versions 1.54, 1.60 and 1.61. Version 1.54 added the leaf radiative transfer model Fluspect_bcar, which is an updated version of the original Fluspect model included in SCOPE v1.53 (PS Study, Mohammed *et al.* 2014). Fluspect_bcar includes absorption by carotenoids, but not xanthophyll dynamics. Major changes made in version 1.60 included revision of the radiative transfer code to include addition of the scattered fluorescence flux and the reflected fluorescence by the soil; improved computation and calculation speed; calculation of soil heat flux and correction of two bugs in reading input data for the soil heat flux time series; updates to 'SCOPE' input spreadsheets; and modification of default value of parameter 'fqe' in input spectrum to match FluoWat measurements. Version 1.61, which fixed a few bugs and resolved a long-running issue with saving total evaporation data, had a negligible effect on the simulation of fluorescence and photosynthesis (the fluorescence and photosynthesis output of v1.60 and v1.61 are almost equal).

Changes to the code can now also be tracked on https://github.com/christiaanvandertol/scope. A GNU General Public Licence has been added.

A new Fluspect model, Fluspect_B_CX, was developed here (Section 4.3.1) to include the effect of de-epoxidation state of xanthophylls on reflectance. The model has been empirically linked to the biochemical routine. Fluspect_B_CX cannot yet be used directly in SCOPE version 1.61, as

implementation requires substantial revision to several parts of the code which could not be achieved within the time frame of the FB Study. Therefore, Fluspect_B_CX is currently provided as a separate model.

All three SCOPE versions (1.54, 1.60, and 1.61) were made available in the ARTMO toolbox (A-SCOPE). In addition, an emulator toolbox (Section 4.5) was produced for SCOPE.

4.3 Model additions

4.3.1 Dynamic xanthophyll reflectance

A quantitative model was developed for the effect of de-epoxidation (as quantified by comparative concentrations of violaxanthin (*V*) and zeaxanthin (*Z*)) on the reflectance and transmittance. Conversion of violaxanthin into zeaxanthin is one of the mechanisms for NPQ. Linking NPQ with the concentrations of *V* and *Z* connects the radiative transfer of the leaf (Fluspect) and the leaf biochemical process routines, such that PRI and fluorescence quenching can be simulated concurrently.

As a starting point, the specific absorption spectra of chlorophyll *a* and *b*, and carotenoids from the PROSPECT-5 model (Féret *et al*. 2008), were compared. Below 480 nm the absorption by chlorophyll dominates, so that possible effects of changes in the xanthophyll composition will only become visible in the region 480 – 570 nm. Therefore it was postulated that in this spectral range a shift in the absorption spectrum of the carotenoids can be held responsible for the changes in leaf spectral properties associated with the conversion of *V* into *Z*.

In the new Fluspect_B_CX model – in which B stands for inclusion of leaf border effects, C for inclusion of carotenoid absorption, and X for the description of PRI effects via the xanthophyll transition – a new input parameter called V2Z was introduced to represent the xanthophyll de-epoxidation status of carotenoids in the leaf. A value of V2Z equal to zero corresponds to the case where no NPQ is active, whereas a value of one indicates maximum NPQ activity (i.e., all violaxanthin has been converted into zeaxanthin. In the latter case, PRI declines.

A test of these theoretical effects was conducted empirically using leaves of barley (*Hordeum vulgare*) that had been dark-adapted and then exposed to excitation light in the PAR range (~400-700 nm). Reflectance and fluorescence responses were measured in the laboratory over a 68-second period to capture the transition from the dark-adapted to the light-adapted state, during which time there are physiological adjustments in the relative amount of photochemical and non-photochemical quenching (PQ and NPQ).

4.3.1.1 Results

Figure 4.1 (top left) shows fluorescence spectra collected from the start of the experiment (black) until the end after 68 seconds (gray). Fluorescence over the duration of the experiment declined due to PQ and NPQ. The decline was similar (about a factor of 4) for the red and far-red peaks (top right). This indicates that at the start of the measurement sequence,

fluorescence was near the maximal level, which is usually about 5 times the dark-adapted value (Maxwell & Johnson 2000).

The reflectance between 500 and 580 nm first increased for a number of seconds, and then decreased (Figure 4.1 bottom right). To analyse the shape of the reflectance changes, we first normalised each reflectance spectrum to the average reflectance between 400-480 nm, then subtracted the reflectance of the first spectrum that was collected from each of the subsequently collected reflectance spectra. Figure 4.1 (bottom left) shows the resulting normalised spectra. Spectral changes related to NPQ occurred between 500 and 600 nm and extended somewhat beyond 570 nm.

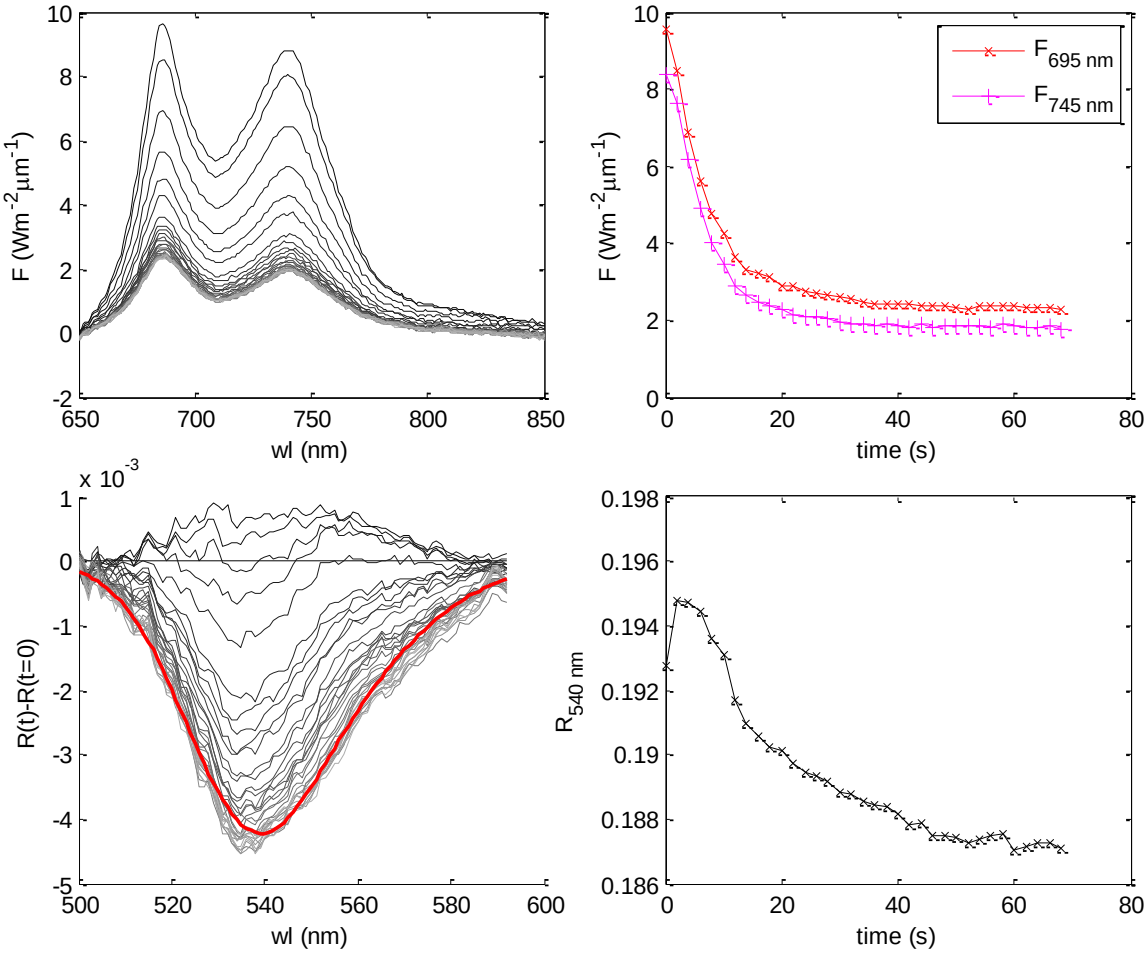

Figure 4.1. Fluorescence and reflectance spectra in barley leaf. Top left: Fluorescence measured at 2 s intervals for 68 seconds after exposing a dark adapted leaf to light. Top right: Fluorescence at two wavelengths plotted versus time. Bottom left: reflectance changes versus wavelength. The red line is a fitted Fourier curve through the last measurement (after 68 seconds). Bottom right: reflectance at 540 nm versus time.

The linear scaling coefficient termed f_{V2Z} quantifies the magnitude of the PRI effect by scaling the spectrum linearly from zero at the first measurement to 1 at the last measurement. The

objective of the measurements was to link f_{V2Z} to NPQ. The next step was to estimate NPQ from the fluorescence measurements. The problem is that it is not possible to objectively distinguish the effects of NPQ and PQ. This can be seen when considering the rate coefficients (K_p and K_n for PQ and NPQ, and K_d and K_f for heat dissipation and fluorescence, respectively, as in Van der Tol *et al.* 2014):

$$F \propto Q \frac{K_f}{K_f + K_d + K_p + K_n} \qquad \textbf{(4.1)}$$

where Q is the incident photon flux (µmoles m^{-2} s^{-1}). The rate coefficients K_f and K_d can be considered as constants (we set K_f+K_d = 1), but K_p and K_n are variable. To separate PQ from NPQ we used complementary measurements with the Pulse Amplitude Modulation (PAM) method.

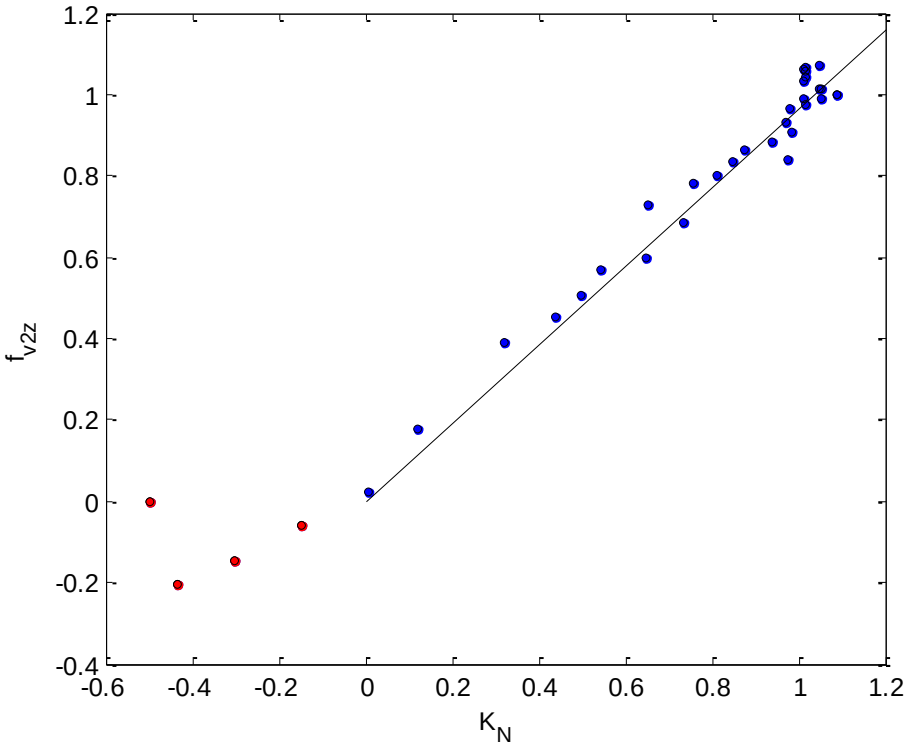

Figure 4.2. Reflectance change parameter f_{v2z} estimated from reflectance measurements versus K_n estimated from fluorescence measurements. The line is a linear regression through the origin using the blue-filled points (>8 seconds after the start of the experiment). The four red points correspond to the first 8 seconds of the measurement sequence, where neither PSII quantum yield nor the measurement light intensity may have been constant.

It appeared that f_{v2z} was linearly related to K_n (Figure 4.2). The four red points in the figure corresponded to the first 8 seconds of the measurement sequence, where neither PSII quantum yield nor the measurement light intensity may have been constant.

The maximum value for K_n, reached after 68 seconds, was 1.09. This value was low compared to other studies where values in the range between 0 and 2.5 for unstressed and 0-6 for water stressed plants were observed (Van der Tol *et al.* 2014). This was likely due to the fact that the barley plant was grown under relatively low light in a greenhouse with no water stress.

We finally compared the observed spectral changes due to NPQ to model simulations with the Fluspect_B_CX model (Figure 4.3), in order to relate the experimentally established changes in the spectra back to the underlying radiative transfer parameters, in particular the V2Z parameter of Fluspect. The magnitude of the observed PRI effect corresponded to a Fluspect V2Z parameter value of about 0.6, i.e., 60% of the maximum effect if zeaxanthin reaches its maximum concentration. This implies that we have explored only a part of the NPQ-PRI relationship, as we already expected from the low values of K_n. Furthermore, there were spectral differences between the measured and the simulated PRI effect: the maximum effect occurred at 538 nm in the measurements and at 528 nm in the simulations. The shortest and longest affected wavelength was also different: 500 and 600 nm in the measurements and 480 and 570 nm in the simulations.

Although the measurements provided a good starting point for modelling the relationship between PRI and NPQ, the fitted relationships did not cover the whole K_n range such that the link between PRI and NPQ still requires additional experimental data. Another point for investigation is the spectral differences between the simulations and the observations. It is difficult to explain spectral changes beyond 570 nm theoretically, because the zeaxanthin spectrum does not include this area.

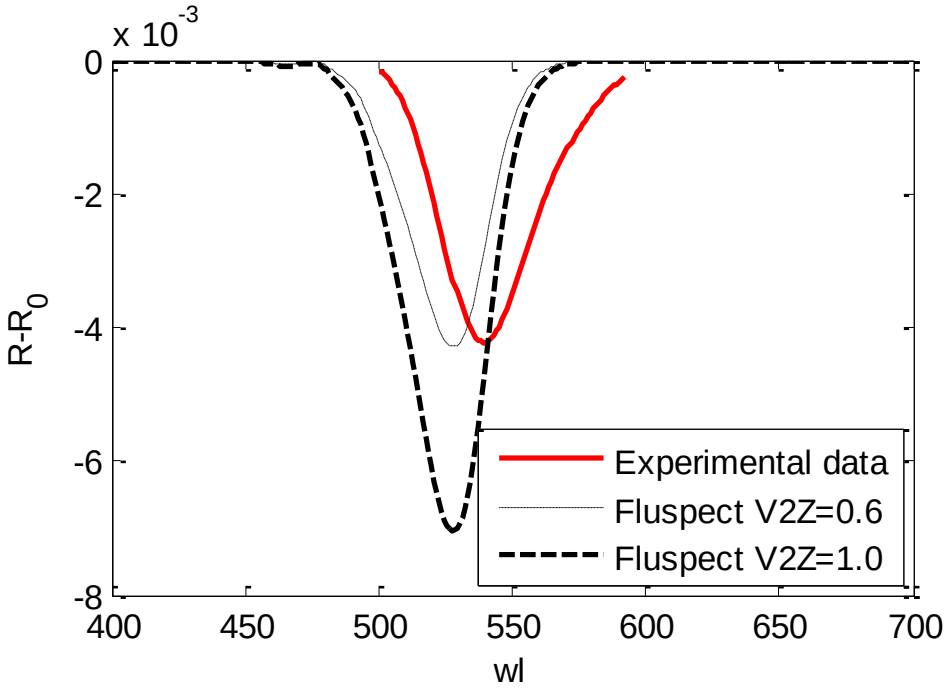

Figure 4.3. Reflectance changes due to NPQ in the experimental data (fitted Gaussian curve, and modelled with the Fluspect_B_CX model for two values of the V2Z parameter.

4.3.2 Spectral changes from variable energy partitioning between photosystems

At the leaf level, and under conditions of excess illumination and physiological stress, changes in the partitioning of absorbed light between PSI and PSII can occur (energy spillover or state transitions) (Tikkanen *et al.* 2011; Mullineaux & Emlyn-Jones 2005). The ratio of fluorescence at different wavelengths can be exploited (after correction for fluorescence reabsorption by chlorophyll) in order to disentangle the contribution coming from PSI and PSII, each having a specific fluorescence emission spectrum.

The occurrence of energy spillover and state transitions is one of the least investigated processes in photosynthetic electron transport and photosynthesis, yet it is highly relevant to analysis of fluorescence emissions. The quantification of changes in energy partitioning would have important implications both for the estimation of electron transport from photochemical yields and as a powerful probe of underlying mechanisms.

Whilst an equal partitioning of excitons between photosystems has been commonly assumed in the past, changes in partitioning could be involved whenever PSI and PSII photochemical efficiencies are unevenly affected by leaf conditions, in order to meet the energy requirements of linear electron transport. A greater partitioning to PSII, for example, could be required under conditions leading to xanthophyll de-epoxidation and non-photochemical energy quenching in PSII (Müller *et al.* 2001), so as to down-regulate PSI activity in parallel also. A greater partitioning to PSI, on the other hand, would be required in the occurrence of cyclic electron transport (Munekage *et al.* 2004); although the occurrence of cyclic electron transport under field conditions has been the subject of intense debate (Johnson 2005; Kramer *et al.* 2004; Munekage *et al.* 2004), its role in the regulation of energy transduction is now widely accepted (Kou *et al.* 2013; Joliot & Johnson 2011).

In the present analysis, variable energy partitioning between PSI and PSII has been assessed through the analysis of experimental data, consisting of a leaf-level dataset of fluorescence (spectral radiance and modulated fluorescence yield) and photosynthesis in *Nicotiana tabacum* under different temperatures and irradiances, acquired in previous ESA studies. This has resulted in a simple algorithm for the estimation of PSI-PSII energy partitioning from fluorescence radiance measurements at (at least) two wavelengths, which could prove useful for future data assimilation. The algorithm provides an unbiased computation of PSII fluorescence and photochemical yield; the relevance of the problem and the effectiveness of the algorithm have been demonstrated for the aforementioned dataset.

In addition, a novel model has been developed for the prediction of changes in energy partitioning (as a result of spillover or state transition) in response to internal and external factors. The model is based on an *a posteriori* approach, i.e., estimating the partitioning required to meet the ATP and NADPH consumption in photosynthetic dark reactions, but could be inverted to estimate the latter. The algorithms could prove useful for process simulation through the SCOPE model, despite the uncertainties discussed at the end of the section.

4.3.2.1 Reconstruction of energy partitioning from spectral fluorescence database

A methodology is outlined here for the estimation of changes in energy partitioning (as induced by either spillover or state transition) under variable environmental conditions, from an analysis of changes in spectral fluorescence at two wavelengths (680 and 730 nm), as could be obtained by the Fraunhofer Line Discrimination (FLD) method from measurements of apparent leaf reflectance in the O_2-A and O_2-B oxygen absorption bands (Meroni *et al.* 2010; Plascyk 1975). Alternatively, a more detailed analysis could be based on measurements over the entire fluorescence spectrum (Palombi *et al.* 2011).

Three alternative hypotheses were explored, namely that spectral fluorescence changes under variable environmental conditions are induced by a shift in energy partitioning (Hypothesis 1), by changes in PSI fluorescence yield (Hypothesis 2), or by changes in leaf absorbance (Hypothesis 3), all other factors being constant.

4.3.2.1.1 Results

Key results obtained under the assumptions of Hypothesis 1 (constant PSI fluorescence yield, variable energy partitioning among photosystems) were consistent with expectations, i.e., the fraction of photons partitioned to photosystem II was predicted to decline under increasing light conditions, and to settle to a value below 0.5 under high irradiance. High or low temperatures are predicted to slow down the process.

Both Hypothesis 2 and Hypothesis 3 were discarded as possible explanations, based on the observed pattern in spectral fluorescence radiance in *Nicotiana tabacum* leaves and the incompatibility of those hypotheses with current knowledge of fluorescence measurements and their interpretation.

Results obtained under the assumptions of Hypothesis 2 (variable PSI fluorescence yield, constant energy partitioning among photosystems) could only be explained by a more than 50% increase in PSI fluorescence yield in response to light, with a sharper rise under warmer temperatures. Such a large increase would come as unexpected, given that PSI fluorescence is generally understood to remain virtually constant (Pfundel 1998; Barber *et al.* 1989). Moreover, the implications of Hypothesis 2 seemed to conflict with our current understanding of fluorescence measurements and their interpretation: in particular, it would run contrary to the assumption that the steady-state fluorescence signal measured by modulated fluorometers (F_t) is proportional to PSII fluorescence yield. In the present experiment, the PSII fluorescence yield estimated under the assumptions of Hypothesis 2 was found to be very poorly correlated with F_t, as measured independently on the same leaves by modulated fluorescence techniques.

Under the assumptions of Hypothesis 3 (variable leaf optical density; constant energy partitioning and PSI fluorescence yield), the observed pattern in spectral fluorescence radiance would imply an increase in leaf absorbance with increasing light. This is in contrast with what was reported by Cazzaniga *et al.* (2013), who observed a reduction in leaf optical density in *Arabidopsis thaliana* in response to light, as a result of the re-arrangement of chloroplasts along the outer border of the cell as a photoprotective response. Similar responses have often been

reported in the literature, triggered in particular by blue light (Inoue & Shibata 1973; Brugnoli & Bjorkman 1992), but are not consistent with the observed pattern of chlorophyll fluorescence.

Dynamic changes in energy partitioning between the two photosystems (Hypothesis 1) would therefore appear to be the only mechanism that can fully explain the experimental data collected in the current experiment.

The novel technique proposed appears therefore as a viable methodology for the quantitative assessment of energy partitioning among photosystems; once combined with pulse-saturated modulated fluorescence (or with pulse-saturated measurements of spectral fluorescence radiance), the technique could result in more precise measurements of electron transport rates, so overcoming one of the key limitations of current methods.

4.3.2.2 Computation of energy partitioning from cyclic vs linear electron transport

A newly proposed model of energy partitioning between the two photosystems was developed here which provides preliminary estimation of PSI and PSII fluorescence radiance. The proposed approach for the representation of changes in energy partitioning is based on a stoichiometric analysis of the ATP and NADPH requirements of dark reactions (Rubisco carboxylation and oxygenation) for both C_3 and C_4 photosynthesis, and the associated rates of linear and cyclic electron transport (Kramer & Evans 2011). An example of model predictions is presented in Figure 4.4.

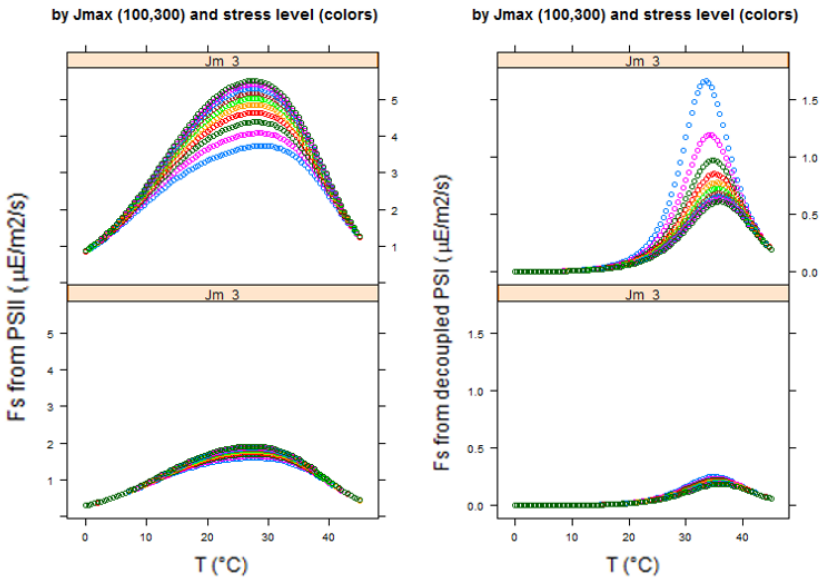

Figure 4.4. Simulated response to temperature of fluorescence radiance originating from (left) PSII units or (right) decoupled PSI supercomplexes. Top and bottom panels refer to high (300 µmol m^{-2} s^{-1}) and low (100 µmol m^{-2} s^{-1}) values of s. Colours correspond to different levels of partial pressure of CO_2 at the site of carboxylation.

Although based on our best understanding of photosynthetic processes, the model is however affected by substantial uncertainties that should be narrowed down before it can be operationally applied. In particular, three issues were highlighted in the study:

- there is a general uncertainty in the modulation of PSI fluorescence by quenchers; in particular, it is not clear if observed changes in PSI fluorescence are the result just of variable energy partitioning (as affected by PSII quenchers) or also by a direct quenching (e.g., by zeaxanthin) of the PSI itself. The PSI photochemical yield could also be directly affected by quenchers, on top of the back-regulation exerted by PSII (Hihara & Sonoike 2001). Such a possibility – which has been excluded in the current study – would have profound effects on model predictions;
- the exact stoichiometry of ATP/NADPH production and consumption is still the subject of debate, resulting in additional uncertainty in model quantitative (albeit not qualitative) predictions; and
- the exact mechanisms responsible for changes in energy partitioning are still the subject of intense debate, with both state transition and energy spillover potentially involved. An understanding of the contribution of the two mechanisms, which will be the subject of an additional analysis, is however not crucial for the application of the algorithm developed here.

4.3.3 Sustained non-photochemical quenching

The aim in this component was to produce a dataset of sustained (long-term) quenching parameters for different species under drought conditions. The first dataset was of seasonal changes in predawn and midday modulated fluorescence and hyperspectral reflectance in leaves of *Quercus ilex* (an evergreen broadleaf) and *Pinus pinaster* (an evergreen conifer), growing in San Rossore, Italy (Magnani *et al.* 2008; Porcar-Castell *et al.* 2008). The second was a high-resolution dataset of seasonal dynamics in leaf reflectance and fluorescence measured continuously on *Arbutus unedo*, an evergreen broadleaf (Florence, Italy).

The study assessed the seasonal dynamics under field conditions of fluorescence and photochemical parameters, including sustained (i.e., slowly reversible) non-photochemical quenching (NPQ_S), which is a measure of photoprotection; and the fraction of functional PSII reaction centres (qL_s), an indicator of photodamage. Focusing on the more detailed *A. unedo* high-resolution dataset, the study provided a statistical validation of the MD12 model (Magnani *et al.* 2009; implemented in SCOPE v1.53) for the prediction of photochemical yield from fluorescence yield (F_t), either with or without ancillary information on k_{NPQs} and qL_s. Finally, remote-sensing indices – the Red-Edge Index Position (REIP; Curran *et al*. 1995), the modified NDVI index ($NDVI_m$; Gitelson & Merzlyak 1997), and the PRI (estimated at 531 and 570 nm, as a measure of xanthophyll de-epoxidation; Gamon *et al.* 1997) – were estimated from parallel measurements of seasonal changes in leaf hyperspectral reflectance, and their potential to capture the estimated dynamics of maximum electron transport rate (J_{max})(Bernacchi *et al*. 2003), k_{NPQs} (Porcar-Castell 2011), qL_s (Porcar-Castell 2011) – and of MD12 model parameters – was tested.

4.3.3.1 Results

P. pinaster and Q. ilex

With respect to seasonal dynamics, pine had a marked increase in sustained NPQ over the summer, with a partial relaxation corresponding to the temporary increase in soil water content. This was accompanied by a marked decline in the fraction of active PSII reaction centres in summer.

Oak had a much stronger increase in sustained NPQ in winter, with smaller oscillations and a full mid-summer recovery that could be attributed to a shallower water table (data not shown). Its fraction of active PSII reaction centres remained quite constant.

The lack of any photodamage in oak was consistent with the pattern in leaf chlorophyll content, as captured by the $NDVI_m$ reflectance index, which increased slightly over the summer. In contrast, pine had a slight decline followed by a partial recovery during the autumn. No significant differences were observed between needle cohorts in either reflectance or fluorescence parameters. A wide change in leaf PRI, on the contrary, was observed in oak during the spring, possibly associated with phenological changes in leaf biochemical content.

Regarding the relationship between fluorescence parameters, there was a consistent relationship between PSII yield and NPQ. The relationship between leaf PRI and NPQ was quite good and consistent in pine, but not in oak, possibly also a result of phenological changes.

A. unedo

From the high-resolution dataset of *A. unedo*, predawn fluorescence displayed a clear seasonal pattern. Dark-acclimated fluorescence (F_o) declined over the winter and only partly recovered in the following spring, peaking at a temperature of about 16 °C. A similar pattern was observed in maximum fluorescence (F_m), but with a substantial short-term variability largely associated with air temperature. The rate constant of sustained non-photochemical quenching (NPQ_s) peaked during the winter, with short-term oscillations mirroring those in PSII maximum yield (F_v/F_m). A sharp increase in the fraction of damaged PSII reaction centres (= 1-qLs) was observed during both summers (2014, 2015), with a recovery during the winter coincident with an increase in photoprotection. Maximum electron transport rates (J_{max}) displayed a typical seasonal pattern, increasing with temperature (maximal temperatures were ~30°C). A clear response to temperature was also apparent in PSII maximum quantum yields, which was apparently more pronounced than observed in agricultural crops (e.g., Bernacchi *et al.* 2003). This appeared to be largely associated with the sharp increase in NPQ_S at temperatures below 15 °C, and at higher temperatures to a lesser extent. The NPQ_S response to temperature was consistent with other findings for *P. sylvestris* under boreal conditions (Porcar-Castell 2011), although the extent of photoprotection was clearly smaller under the milder Mediterranean winter. Both seasonal and short-term changes in NPQ_S appeared to be largely driven by temperature.

According to the MD12 model, the relationship between fluorescence radiance and electron transport rates is controlled by three parameters strongly related to qL_s, J_{max} and NPQ_S, and therefore should be modulated by the seasonal dynamics of these key traits. In order to verify such a functional association, the MD12 model was fitted onto daily fluorescence data for each leaf, resulting in a total of over 1500 values for each parameter; on average, the model explained 89.9% of the overall diurnal variability in the data. A comparison of estimated parameters with photosynthetic characteristics did indeed confirm the functional link hypothesised in the model (Figure 4.5). In particular, the parameter a4 (which controls the relationship under light-limiting conditions) was linearly related to NPQ_S, with a strong consistency among leaves. The two parameters controlling the light-saturated part of the relationship (a1 and a2) are expected to be inversely related to qL_s and J_{max}, respectively, as clearly demonstrated for the *A. unedo* dataset; the relationship was particularly strong and consistent among leaves for the a2 parameter.

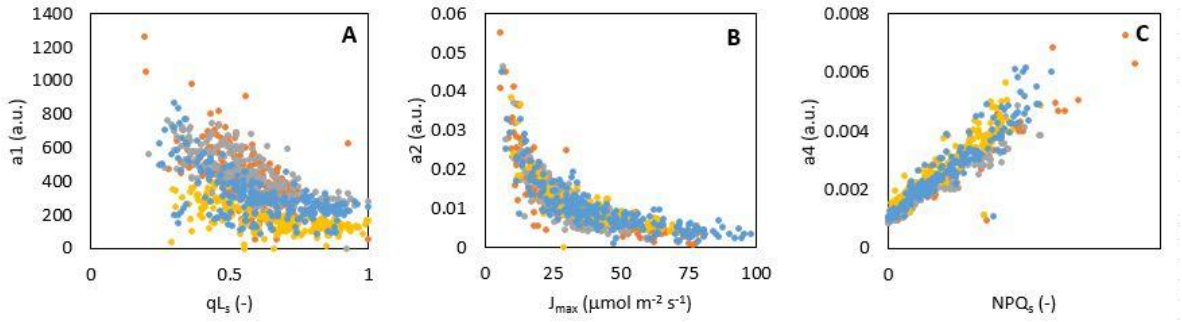

Figure 4.5. Relationship between MD model parameters and photochemical traits, as determined from fluorescence measurements over the course of the year in *A. unedo*. A, relationship between MD12 parameter a1 and the fraction of active reaction centres (qL_s); B, relationship between MD12 parameter a2 and maximum electron transport rate (J_{max}); C, relationship between MD12 parameter a4 and sustained non-photochemical quenching (NPQ_s). Colours refer to different leaves.

Of special interest is the association between NPQ_S and the a4 parameter, also in consideration of the expected overpass time of the planned FLEX satellite. A comparison with the PRI data acquired in the experiment points to a possible strategy for its remote estimation and a robust parameterisation of the MD12 model.

The seasonal dynamics of leaf PRI appeared to mirror the pattern of F_m (and hence NPQ), with a sharp decline during the winter in both the maximum (dark-acclimated) and the minimum (midday) values (Figure 4.6). A slightly different but even stronger relationship appears to hold for dark-acclimated conditions (left edge of the scatter in Figure 4.6B and Figure 4.7A) than for the rest of the data. Apart from further demonstrating the role of zeaxanthin retention in the overnight maintenance of NPQ under winter conditions (Adams III *et al*. 2004; Öquist & Huner 2003; Adams *et al*. 1995), this opens the way for the estimation of the MD12 a4 parameter from reflectance measurements (Figure 4.7B).

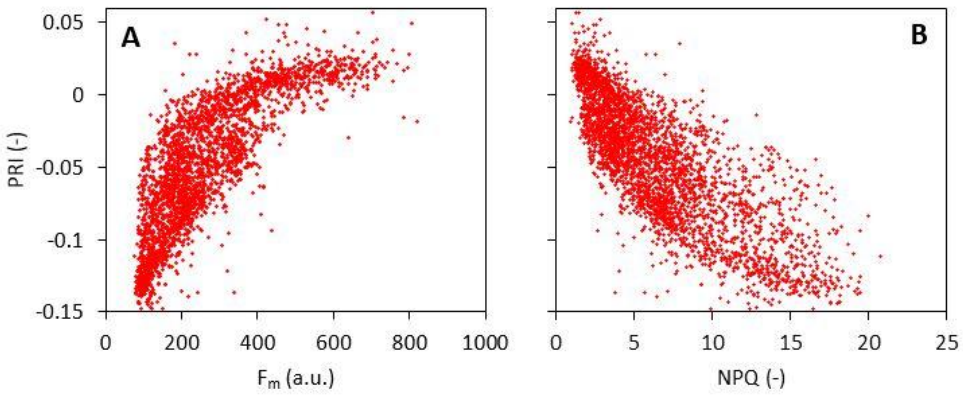

Figure 4.6. Relationship between the Photochemical Reflectance Index and (A) maximum modulated fluorescence (F_m) or (B) non-photochemical quenching in one *A. unedo* leaf over the course of the year.

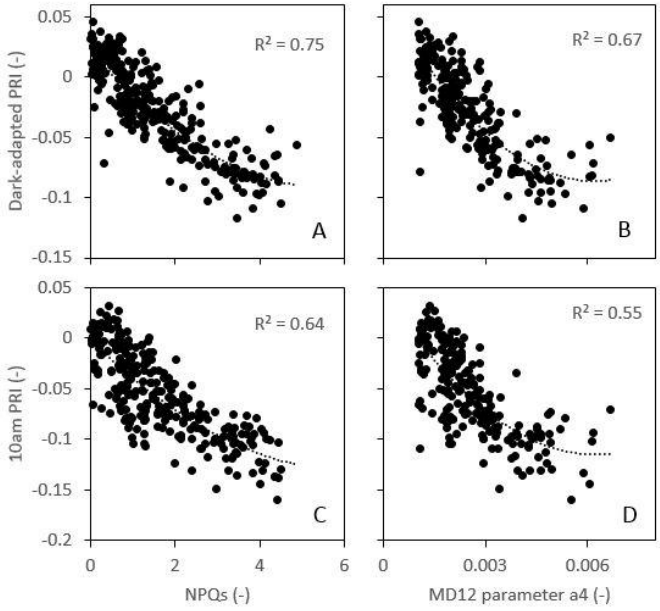

Figure 4.7. Relationship between (A, C) sustained (dark-adapted) non-photochemical quenching (NPQ_s) or the a4 parameter in the MD12 functional model and dark-adapted Photochemical Reflectance Index (PRI; from extrapolation of low-light measurements; panels A, B) or PRI measurements at 10am (panels C, D) in an *A. unedo* leaf over the course of the year.

Under natural irradiance, dark-adapted PRI had to be estimated here from a linear extrapolation of measurements under low light; this would of course be impractical in remote sensing applications, where typically a single acquisition is available each day. A close approximation, however, appears to be a measurement of leaf PRI taken between 9-11am (i.e., close to the planned FLEX overpass time), as a consequence of the strong seasonal pattern and the generally coherent effect of irradiance. The potential to estimate both NPQ_S (R^2 = 0.64) and the MD12 a4 parameter (R^2 = 0.55) from a single mid-morning measurement of PRI is demonstrated in Figure 4.7C and Figure D, respectively. In contrast, other model parameters

(qL_s, J_{max}, MD12 parameters a1 and a2) could not be estimated from remote sensing indices (R^2 = 0.34, 0.01, 0.04, and 0.01 respectively).

In conclusion, the investigation demonstrated:

(i) the relevance of seasonal changes in leaf photoprotection (NPQ_S) and photodamage (qL_s) in three Mediterranean species under field conditions, and their role in modulating the relationship between fluorescence yield, photochemical yield, and photosynthesis; and

(ii) the possibility to estimate NPQ_S from changes in leaf PRI, and hence to derive a critical parameter in the MD12 fluorescence model from parallel measurements of leaf reflectance, thereby strongly reducing model uncertainty.

4.4 Model performance assessment

4.4.1 Validation of the Fluspect model against measurements

Here, the Fluspect_bcar model was compared to experimental data of reflectance, transmittance, and chlorophyll fluorescence spectra. Fluspect_bcar was used instead of Fluspect_B_CX, which is equivalent to using Fluspect_B_CX with $f_{V2Z} = 0$ (i.e., no NPQ). The focus here was on evaluating how the fluorescence spectra depend on leaf properties. Wherever Fluspect is mentioned in the current paper, we refer to Fluspect_bcar. The PRI effect is a very small contribution to reflectance and transmittance and can be neglected in this section. We investigated the ability of the model to reproduce variations in fluorescence spectra as caused by variations in leaf composition.

Fluspect was first calibrated to leaf reflectance and transmittance data, resulting in parameter values which were then compared to destructively measured values. Next, fluorescence was simulated, and finally, we compared the simulated fluorescence to measurements.

Experimental data were obtained from greenhouse-grown plants of barley (*Hordeum vulgare L.*) and sugar beet (*Beta vulgaris L.*). Plants were grown under different light intensities to stimulate differences in leaf chlorophyll content and other acclimation to the different light levels. Some plants were also subject to water deficit. Leaf-based measurements of reflectance, transmittance, and fluorescence were taken. Leaves were also analysed morphologically (specific leaf area, leaf water content, dry matter content) and biochemically using extraction methods for chlorophyll *a*+*b* and carotenoid content (Lichtenthaler & Buschmann 2001).

Retrieved parameters were chlorophyll *a*+*b*, carotenoid content, leaf water content, dry matter content, senescent material content, leaf mesophyll structure parameter, and fluorescence quantum efficiency for PS-I and PS-II). These were obtained after fitting the modelled reflectance and transmittance spectra to measurements at one light intensity (iPAR = 300 µmol photons $m^{-2}s^{-1}$) over the range of 400 to 1800 nm.

Error propagation in the retrieval of parameters and the upward simulation of fluorescence was analysed using the local Jacobian (*J*) of the model. The uncertainty in the parameters was calculated from the standard deviation of the measured spectra.

4.4.1.1 Results

Reflectance and transmittance spectra were accurately reproduced. The root mean square error (RMSE) of repeated measured spectra of the same leaves (at different light intensities) were – with only few exceptions – less than 0.01 for the visible to the near-infrared, which indicates good reproducibility. RMSE values of modelled compared to measured spectra were several-fold higher than between measurements (Table 4.1). This can be attributed to the inability of the model to reproduce the spectral shape exactly, due to the fixed shape of the absorption spectra of the different constituents of the leaf on the input side of the model. Nevertheless, the RSME values normalised by the reflectance and transmittance, i.e., coefficient of variation, indicated that the spectra were well reproduced.

Table 4.1. Average root mean square error (RMSE) of measured reflectance (*R*) and transmittance (*T*) spectra for one representative leaf of barley and sugar beet. Spectra, measured at 5 different light intensities were compared to the spectrum measured at the second (2) light intensity. Also shown: RMSE of measured *R* and *T* spectra. Spectra were compared at 3 bands: VIS (400 - 700 nm), NIR1 (700 - 1000 nm, which is where the range of the second detector of the ASD ends) and NIR2 (1000 - 1800 nm).

		RMSE repeated measured spectra		RMSE measured-simulated spectra	
Spectral region		**Barley**	**Sugar beet**	**Barley**	**Sugar beet**
VIS(400 - 700 nm)	**R**	0.0024	0.0073	0.1313	0.1479
	T	0.0056	0.0150	0.0610	0.0801
NIR1(700 - 1000 nm	**R**	0.0061	0.0204	0.0459	0.0985
	T	0.0035	0.0025	0.1685	0.1240
NIR2(1000 - 1800 nm)	**R**	0.0037	0.0042	0.0705	0.0644
	T	0.0129	0.0066	0.0564	0.069

Parameters obtained by destructive analysis were compared to the retrieved PROSPECT parameters (Figure 4.8). Retrieved PROSPECT C_{ab} parameter for barley was in strong agreement with destructive measurements for barley (correlation coefficient ranges from 0.72 to 0.84 with RMSE of 2 to 3 [µg cm^{-2}] for the three tuning options), whereas sugar beet had much lower agreement, possibly due to lower sample number and higher variability.

The relationship between measured and simulated fluorescence at the two peaks (690 nm and 740 nm) at 3 light intensities for all samples is shown in Figure 4.9.

Generally, chlorophyll fluorescence was better reproduced for the red peak in both species. Moreover, model predictions were generally better for downward fluorescence. This was

expected, as the light passing through the leaf interacts more with inner leaf structure than reflected light (Van Wittenberghe *et al.* 2015). Reflected light and upward fluorescence emission are mostly affected by the upper layers where leaf physiology might play a more significant role in light propagation.

The agreement between measured and simulated upward fluorescence varied: for sugar beet they were in strong agreement notably for the red peak (R^2 ranged from 0.3 for 740 nm peak to 0.93 for 690 nm peak), in contrast to barley where the agreement was significantly lower, especially for the far-red peak. The magnitude of simulated upward fluorescence of barley was significantly lower than from the measurements, and simulations showed less variability. Generally, we could explain most of the variability of fluorescence emission at the top and bottom of the leaf from leaf composition alone (keeping emission efficiency at photosystem level constant) (Van Wittenberghe *et al.* 2015; Gitelson *et al*. 1998; Jacquemoud *et al.* 1996).

Figure 4.10 shows the relation of fluorescence to increasing chlorophyll concentration. Downward red fluorescence showed a typical decline with chlorophyll content (Pedrós *et al.* 2010; Gitelson *et al*. 1998), an effect due to increasing chlorophyll reabsorption with higher C_{ab} concentrations (Van Wittenberghe *et al*. 2014; Gitelson *et al*. 1998; Agati *et al.* 1993). Reproduced fluorescence was generally better for the red than the far-red peak, and for the downward than for the upward flux. Barley samples again showed much higher variations than sugar beet. Concurrent photosynthesis measurements indicated that sugar beet (in contrast to barley) was unstressed and had high photosynthesis rates, which could explain the higher agreement between measured and simulated fluorescence.

We investigated a possible error due to use of an artificial light source instead of natural sunlight, given that plant ontogenesis and spectral response are known to be affected by properties of the light source (Hogewoning *et al.* 2010; Gitelson *et al*. 1998). Although *R* and *T* spectra were similar (the same leaf was measured), there was a relatively high far-red fluorescence peak induced by sunlight as compared to artificial light. Another aspect is that the spectral distribution of the artificial light was such that the filter used in the measurement apparatus blocked about 30% of incoming artificial radiation but only 6% of the sunlight. The sudden drop in light intensity by 30% when sliding in the filter likely was a significant factor affecting the peak ratio.

Also, we explored the magnitude of the relative change in fluorescence due to the excitation spectrum. For this purpose, the model was tuned to fluorescence observations for the laboratory and outdoor measurements separately, by tuning the emission efficiencies ε_I and ε_{II}. Comparing optimised ε values for the two settings, it was found that the ratio $\varepsilon_{II} : \varepsilon_I$ was lower for the outdoor (ratio = 3) than laboratory (ratio = 5) measurements, mostly because ε_{II} was lower outdoors. Hence, there appear to be spectral effects unaccounted for by the model.

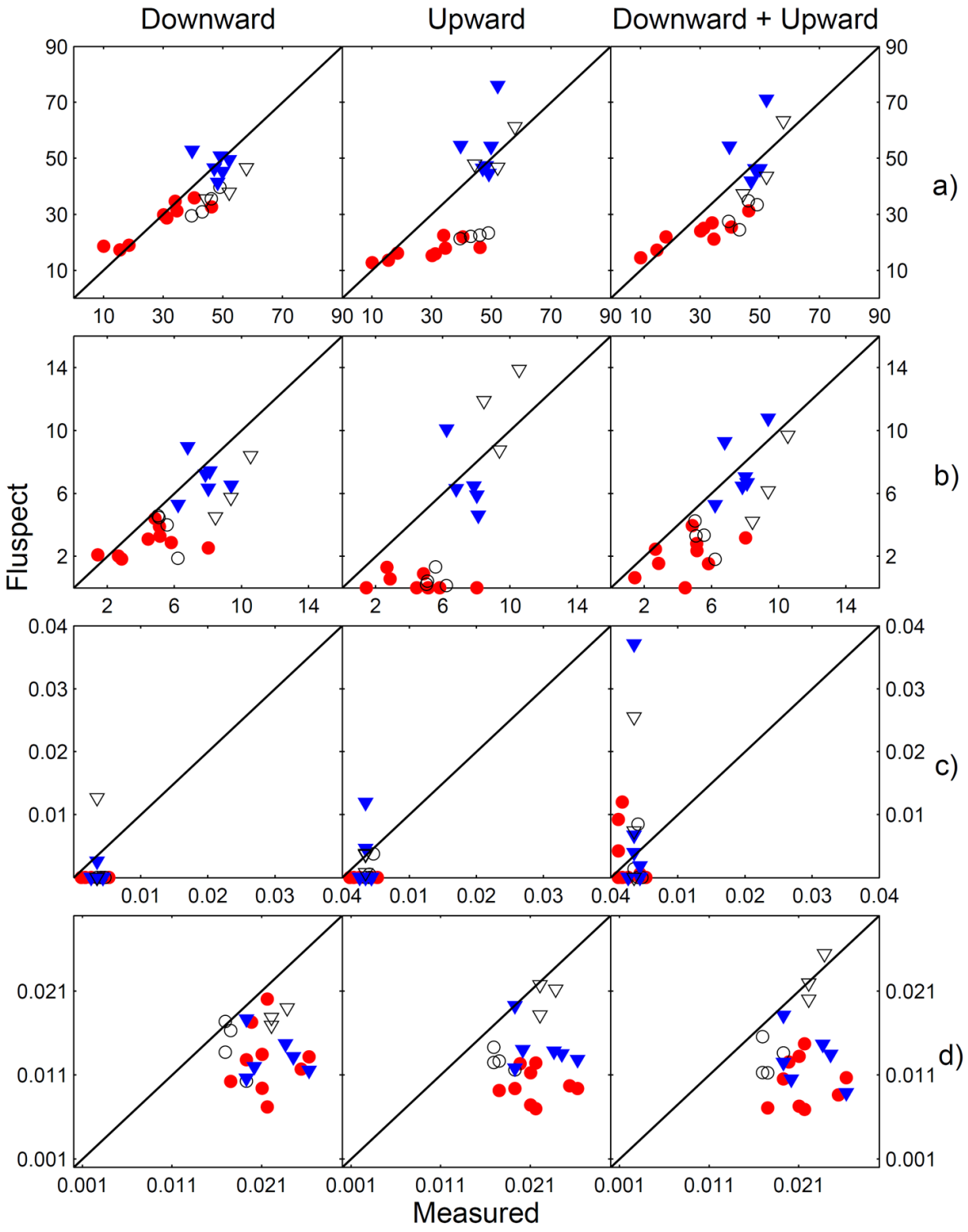

Figure 4.8. Optimised Fluspect parameters versus the measured (from destructive sampling) equivalents: a) chlorophyll (C_{ab} [µg cm^{-2}]) and b) carotenoid (C_{car} [µg cm^{-2}]) concentrations, c) leaf water (C_w [g cm^{-2}]) and d) dry matter (C_{dm} [g cm^{-2}]) content for the two species, barley (circles) and sugar beet (triangles). Open symbols represent reduced soil moisture samples. Parameters were optimised to best reproduce measured transmittance ('downward'), reflectance ('upward'), or both simultaneously.

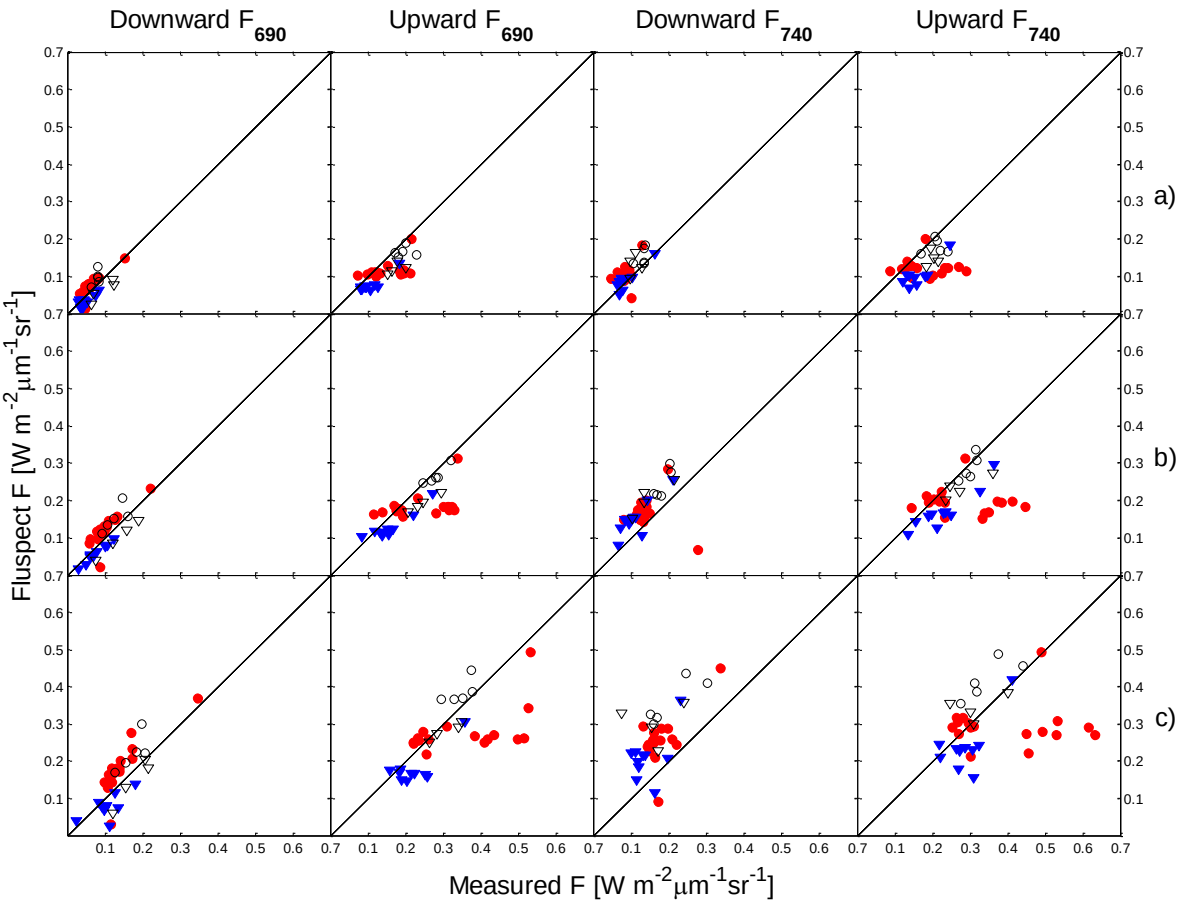

Figure 4.9. Fluspect modelled versus measured downward and upward fluorescence at 690 and 740 nm for 3 light intensities: a) 200, b) 300 and c) 500 µmol photons $m^{-2}s^{-1}$, for the two species, barley (circles) and sugar beet (triangles), without drought stress (closed symbols) and with drought stress (open symbols). All model parameters were fixed at the optimised values for one light intensity for each sample and the emission efficiency parameters for both photosystems were kept constant.

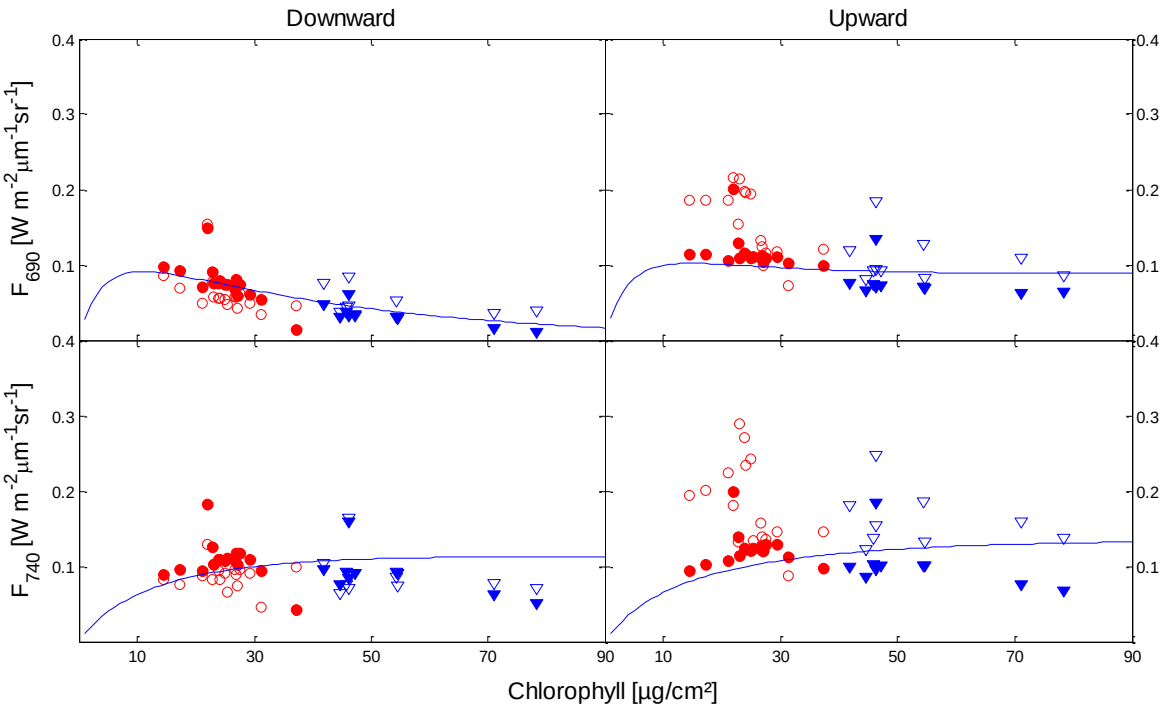

Figure 4.10. Modelled (closed symbols) and measured (open symbols) downward and upward fluorescence at 690nm and at 740nm *versus* the optimised Fluspect parameter C_{ab} for light intensity at 200 µmol photons $m^{-2}s^{-1}$ for the two species, barley (circles) and sugar beet (triangles), without drought stress. The blue curve represents modelled fluorescence versus chlorophyll concentrations, keeping all other model parameters fixed at the values of one representative barley leaf grown in high light.

4.4.2 Validation of the SCOPE model against field measurements

Here, a comparison was made between SCOPE-simulated and measured TOC SIF. The focus was on diurnal and seasonal cycles in order to capture the variability in canopy composition and illumination. Progress was also achieved towards development of a simplified model.

Canopy data were collected in field crops of rice (*Oryza sativa)* (Rossini *et al.* 2010) and alfalfa (*Medicago sativa)* (Cogliati *et al.* 2015a). Fields were equipped with meteorological and eddy covariance towers, and a portable automatic dual spectrometer system (Multiplexer Radiometer Irradiometer, MRI) operating in the visible and near-infrared region. A third dataset was collected over grass carpets treated with the herbicide DCMU (Rossini *et al*. 2015).

Numerical Optimisation (NO) was used for retrieval of parameters from reflectance for each of the measurement days. The model was iteratively executed to minimise a cost function, which was the sum of the squared differences between simulated and measured reflectance of all bands of the sensor, weighted by the wavelength-dependent measurement accuracy.

Diurnal cycles of SIF were simulated with the retrieved parameter values using flux tower weather station data as input. Two types of simulations of SIF were carried out for the crops:

1. Reference simulation: fluorescence emission efficiencies were kept constant over time, thereby 'switching off' physiological regulation of SIF and enabling quantification of effects of leaf and canopy composition on SIF. The SIF of this reference simulation is only a function of *R*.
2. Dynamic simulation (rice and alfalfa): fluorescence efficiency was calculated with the standard SCOPE model, i.e., using the drought parameterisation of Van der Tol *et al.* (2014), and using arbitrary but realistic values of V_{cmo} = 80 µmol $m^{-2}s^{-1}$ and *m*=6 and locally measured weather conditions (for illumination, temperature and humidity).

The reference simulation provides a theoretical optimum SIF for a healthy canopy with a given composition and structure. The differences between the two simulations, and between measured and simulated SIF, provide insight in the magnitude of the effect of PQ and NPQ on SIF, as compared to the effects of canopy composition and structure.

A final estimation was the propagation of uncertainty in the measured reflectance spectra into the model simulations using a Jacobian analysis.

4.4.2.1 Results

Figure 4.11 and Figure 4.12 show the simulated reflectance on seven and four dates during the growing season of rice and alfalfa, respectively, and Figure 4.13 the reflectance of the control and treated grass carpet on two days. Alfalfa was harvested (mowed without replanting) on DOY 180, and the first spectrum corresponds to the mid-season phase, whereas the other three spectra to the crop development phase. Generally, the model reproduced the reflectance well (RMSE between 0.006 and 0.011). The four reflectance spectra of the grass carpets were similar, with only small differences between the two dates and between the two plots.

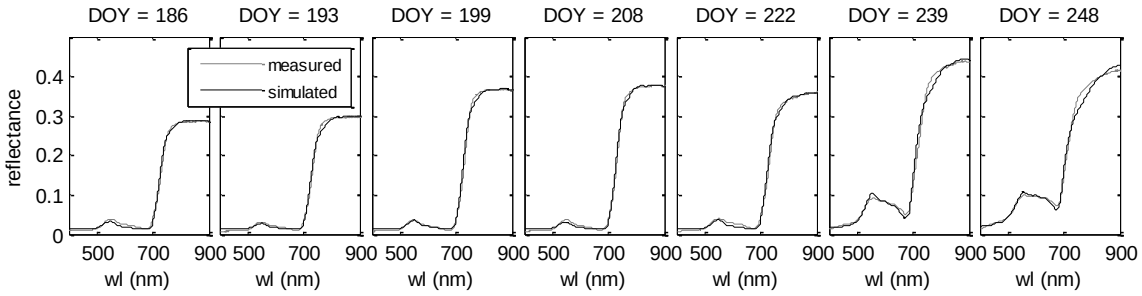

Figure 4.11. Measured and simulated reflectance spectra on seven Julian days for a rice growing season. Apparent reflectance (uncorrected for SIF) was used.

With the parameter values of SCOPE retrieved from the hyperspectral reflectance measurements, the diurnal cycles of SIF normalised by irradiance were calculated with SCOPE. Figure 4.14 and Figure 4.15 reveal how these simulations compared to observations.

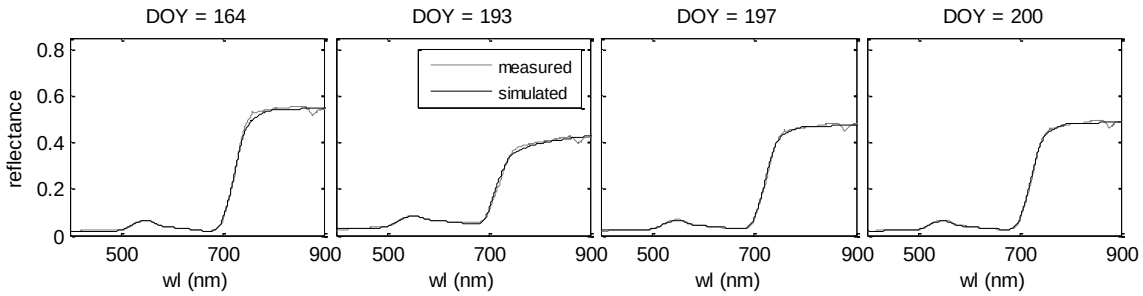

Figure 4.12. Measured and simulated reflectance spectra on four Julian days for alfalfa. Note that the crop was harvested (mowed without replanting) on DOY 180.

Clear differences between days were seen in measured normalised SIF for both rice and alfalfa. These differences were reproduced by both simulations. The reference simulation (with a constant fluorescence emission efficiency) also reproduced this cycle, implying that most of the seasonal cycle of normalised SIF could be explained from the parameters retrieved from *R*, i.e., information contained in SIF largely overlapped with the information contained in reflectance in these unstressed crops.

There was no clear diurnal signal in the measured normalised SIF. Any variations were small, indicating that SIF at 760 nm was almost proportional to irradiance during each day. The reference simulation in which physiological relation was 'switched off' also showed a weak diurnal cycle of SIF even after normalisation by irradiance. The diurnal cycle of the reference simulation was not due to the physiological response of the vegetation, but to the sun-observer geometry. The variations in SIF due to solar angle were nearly of the same magnitude as variations induced by physiological response. This implies satellite products of SIF, such as those of GOME-2 (Joiner *et al*. 2013), require correction for the bi-directional fluorescence distribution function (BFDF).

The dynamic simulation also showed a weak diurnal cycle. The shape of the diurnal cycle agreed with measurements for alfalfa, but not for rice. The small difference between the reference and dynamic simulation combined with the scatter in the SIF observations suggests that the scope for retrieving physiological regulation from SIF in these unstressed crops was limited. Moreover, the absolute level of simulated SIF had other uncertainties. Simulated SIF was linearly proportional to the default parameter values for the fluorescence emission efficiency. Here, values were estimated from leaf fluorescence spectra but the empirical support for these default values is still limited. Nevertheless, in a recent study SCOPE has been used to retrieve the photosynthetic capacity parameter V_{cmo} from a GOME-2 satellite product of SIF over large agricultural fields in the USA, resulting in improved estimates of gross primary productivity compared to using default values of V_{cmo} (Zhang *et al.* 2014). In the present study, we used only a small number of diurnal cycles, but Zhang *et al*. (2014) used the entire growing season. It is possible that, during an entire growing season including drought and senescence, the effects of PQ and NPQ (and thus V_{cmo}) become more apparent. Another explanation for the success of Zhang *et al*. (2014) could be that the retrieved V_{cmo} values compensated for other parameters. Atmospherically corrected multi-spectral reflectance from MODIS products were

used in that study rather than TOC hyperspectral reflectance. Possibly the leaf composition and leaf area index obtained from MODIS products had uncertainties, which were corrected for when calibrating SCOPE to SIF. The retrieved V_{cmo} may then compensate possible errors in leaf composition and leaf area index. This, in turn, may also lead to improvements in GPP.

The two crops, rice and alfalfa, were unstressed, and the unexplained part of SIF was small and noisy. However, the experiment in which DCMU was applied to grass shows that SIF can be used to reveal more extreme types of stress. After applying DCMU, SIF changed in a way that agreed with our expectation and with modelling results.

Since we did not have experimental data of a naturally stressed crop, the DCMU treated grass carpet was used to evaluate the effects of changing PQ and NPQ. The herbicide DCMU blocks the photochemical dissipation pathway, therefore a lower total (PQ+NPQ) quenching rate and thus a higher SIF would be expected versus in untreated vegetation. Indeed, measured SIF from the control plot followed the reference simulation on 5 September, whereas SIF of the treated carpet rose quickly to exceed that of the reference simulation after application of DCMU in the morning, and it remained at a level above the reference simulation throughout the day (Figure 4.16). However, actual SIF of the treated carpet was still substantially lower than the simulation of the theoretical maximum effect of DCMU. On 9 September, when a tenfold higher concentration of DCMU was applied, SIF of the treated carpet approached the simulation of the theoretical maximum effect of DCMU, while in the control carpet it was only slightly higher than the reference simulation.

In summary, a methodology was presented here to retrieve parameters from hyperspectral *R*, and to further use these parameters to simulate SIF.

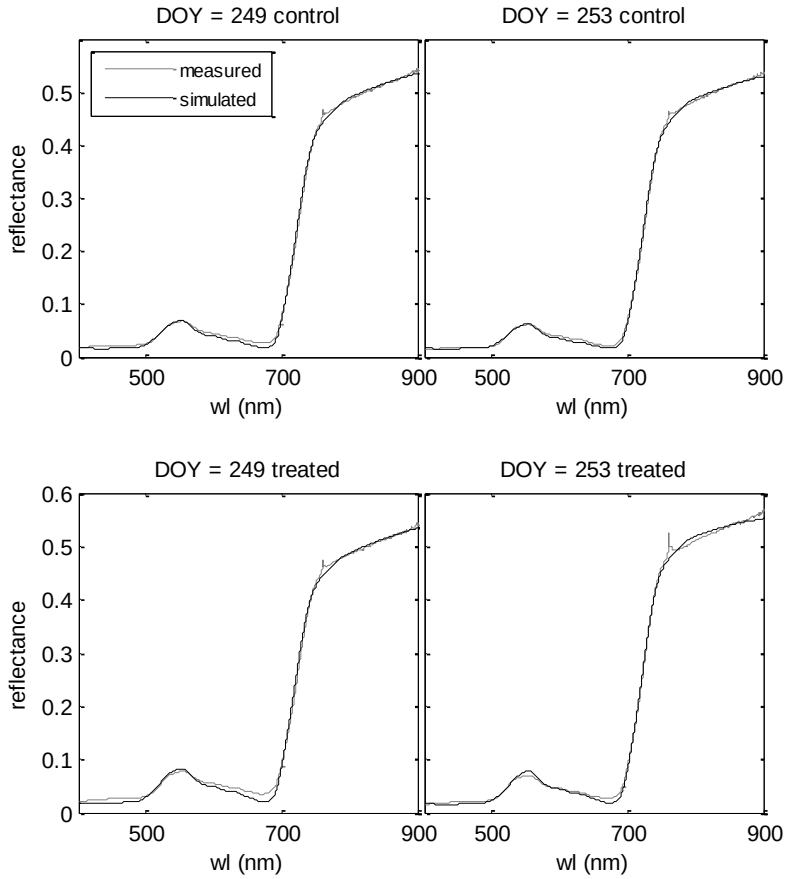

Figure 4.13. Measured and simulated reflectance spectra of a control and a DCMU-treated grass carpet for two days.

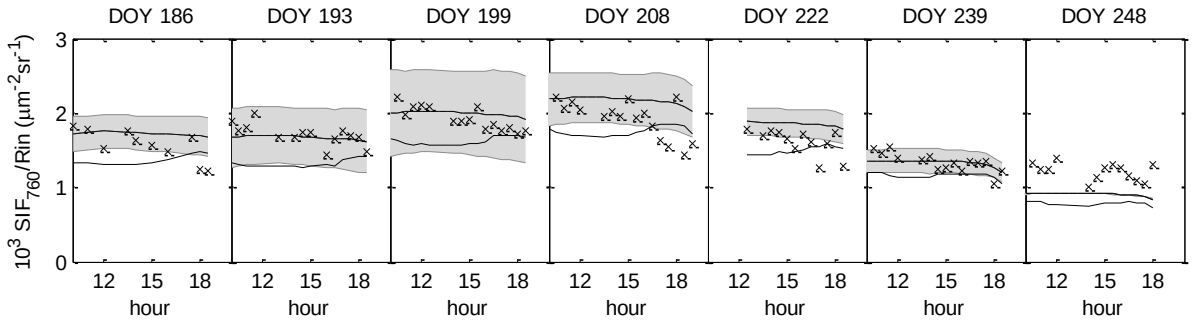

Figure 4.14. Diurnal cycles of simulated (lines) and measured (symbols) SIF normalised by irradiance for selected dates in the growing season of rice. The dashed line represents a model simulation with maximum fluorescence emission efficiency and the shaded area two times the standard deviation, whereas the solid line represents a simulation in which fluorescence emission efficiency was calculated from weather conditions and the parameters V_{cmo} and m.

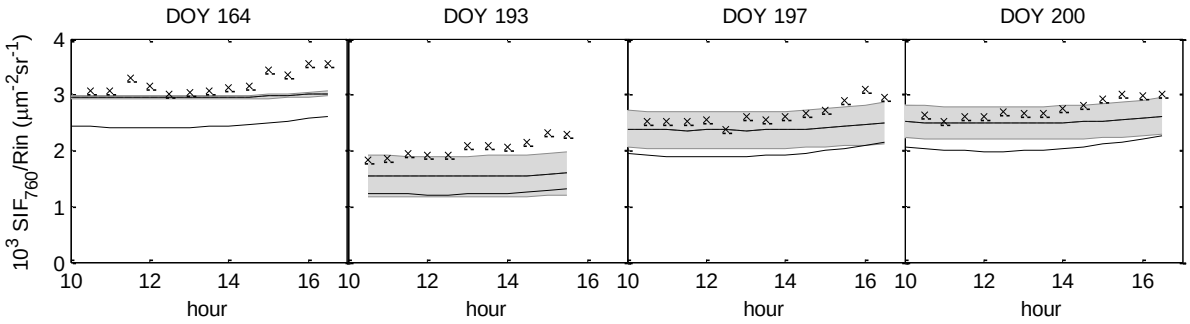

Figure 4.15. Similar to Figure 4.14, but for alfalfa. Note that the crop was harvested (mowed without replanting) on DOY 180.

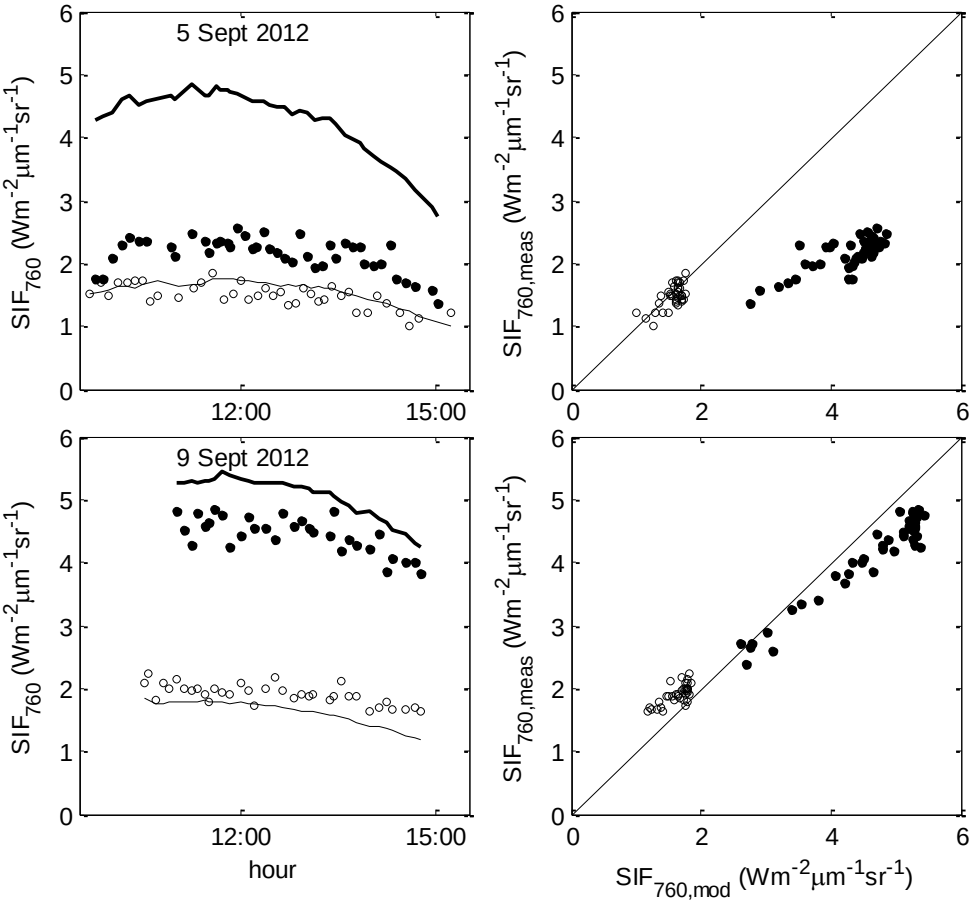

Figure 4.16. Modelled and measured fluorescence responses in control and DCMU-treated grass carpets. Left: Measured (symbols) and modelled (lines) diurnal cycles of SIF of two grass carpets: a control carpet (open symbols/fine line), and a DCMU-treated carpet (filled symbols/bold line). On 5 September (top) the applied concentration was 10^{-5} M in 1% ethanol/water, whereas on 9 September (bottom), the concentration was 10^{-4} M in 1% ethanol/water. Data have been published by Rossini *et al*. (2015). The simulation of the treated carpet assumed the maximum possible effect of DCMU. Right: The same data, plotted as modelled versus measured SIF. (The solid line is the 1:1 relationship.)

4.4.3 Effective relationships between fluorescence and photosynthesis – development of a simplified model

During the PS Study (Mohammed *et al.* 2014), initial investigation was conducted on simplified algorithms to relate SIF to net canopy photosynthesis or assimilation (*A*), including approaches incorporating key drivers of fluorescence and photosynthesis in SCOPE. It was recommended to pursue further the prospects for a simplified model. Here, we focus on this objective by analysing the effects of driving variables on simulated SIF and *A*. Different factors that affect SIF and *A* are discriminated here, specifically canopy density, leaf composition, solar illumination angle and energy quenching in the pigment bed. Equations describing the relationships are simple but nevertheless can account for most of the variability in SCOPE outputs. The simple model introduced here has obvious computational advantages: a computation time of three to four orders of magnitude, and suitability for routine application in mapping or data assimilation. Also, the simplified model enhances our overall understanding of the SIF signal and the possibility to estimate *A* directly from SIF. Performance of the simple model was also compared to that of the full SCOPE model.

4.4.3.1 Results

The simple model for photosynthesis *A* (µmol m^{-2} s^{-2}) and SIF (W $m^{-2}m^{-1}$ sr^{-1}) developed here has the following parameters: chlorophyll content C_{ab} (µg cm^{-2}), senescent material C_s and dry matter C_{dm}, spectrally integrated shortwave irradiance R_{si} (W m^{-2}), and four dimensionless parameters: leaf area index *L*, the sine of the solar zenith angle q_s, the carboxylation capacity V_{cmo} (µmol m^{-2} s^{-1}) normalised by the incident photosynthetically active radiation (*Q*), and the relative humidity *h* multiplied by the Ball-Berry parameter *m*. The equations for SIF and *A* are of the form:

$$SIF = \varepsilon_F \cdot R_{in} \tag{4.2}$$

$$A = \varepsilon_A \cdot R_{in} \tag{4.3}$$

where ε_F is a fluorescence efficiency (µ$m^{-2}s^{-1}$) and ε_A a photosynthesis efficiency (µm^{-1} sr^{-1}). SIF and ε_F are wavelength dependent. Here, SIF and ε_F always refer to SIF(λ_F) and $\varepsilon(\lambda_F)$. The efficiencies are modelled as:

$$\varepsilon = \varepsilon_0(C_{ab}) \cdot f_1(L, C_{ab}) \cdot f_2(C_{dm}) \cdot f_3(C_s) \cdot f_2(\sin(\theta_s) \cdot f_3\left(\frac{V_{cmo}}{Q}\right) \cdot f_4(m \cdot h) \tag{4.4}$$

In this equation, ε_0 is a chlorophyll concentration-dependent efficiency, and f_i are functions accounting for canopy and leaf composition (leaf area index *L* and C_{ab}), solar zenith angle q_s,

leaf physiology and weather (V_{cmo}/Q and mh). The functions f_i are dimensionless. ε_0 and all f_i are wavelength dependent for SIF.

Performance of the parameterised simplified model was tested against the full SCOPE model by means of two numerical experiments. In the first experiment, 100 SCOPE simulations were carried out with random input of C_{ab}, L, R_{in}, θ_s, m and h drawn from uniform distributions between zero and the maximum possible value for each of these variables. The SIF and A of SCOPE were then reproduced with Equation 4.2 and Equation 4.3. Figure 4.17 shows that there was good correspondence between the simple model and SCOPE. The simple model was more accurate for SIF than for A due to a sensitivity of A to stomatal effects (mh) that could not be fully quantified. In the second experiment, 40 simulations were carried out, but now all variables and parameters of SCOPE – including those that not incorporated in the simple model – were varied one at a time. The simple model can obviously only reproduce the effects of the six variables that are incorporated, thus it is insensitive to all other variables. A variation in any of these other variables may cause a difference between SIF from SCOPE and SIF from the simple model, this difference being due to a representation error of the simple model (compared to SCOPE). This was not a problem in most cases: SIF could be reproduced by the model with only few exceptions. This implies that the simple model contains most of the variables relevant for SIF. Only in the case of an extreme leaf inclination distribution (erectophile, planophile, plagiophile or extemophile) did SIF from the simple model deviate from SCOPE. It would be possible to develop another function that corrects for leaf inclination, but in practice leaf inclinations that deviate strongly from a spherical leaf inclination distribution are rare.

With the simple model, SIF and A may be simulated, provided that the six input variables are known. Alternatively, one can adjust prior estimates of the six parameters from a measured SIF. Inversion of the simple model is straightforward. For example, we tested how well A can be estimated from SIF by treating V_{cmo} as the only unknown and SIF from SCOPE as the true value of SIF. Other parameters of the simple model were considered to be precisely and accurately known. It was then possible to retrieve V_{cmo} from SIF for the 40 SCOPE runs discussed earlier, by resolving V_{cmo} from Equation 4.2 and Equation 4.3. Because we assumed that all other variables are known, we should be able to retrieve V_{cmo}. However, as anticipated, there were small differences between the simple model and SCOPE due to representation errors of the simple model (compared to SCOPE). These representation errors accumulate in the estimate of V_{cmo}, and the model sensitivity to V_{cmo} determines how large these errors will become. Figure 4.18 shows that in most cases, V_{cmo} (middle panel) could be retrieved accurately from SIF. Again, the exceptions were cases of extreme leaf inclination distribution. In those cases, the errors in V_{cmo} were large, because SIF was relatively insensitive to V_{cmo} and thus retrieved V_{cmo} was relatively sensitive to SIF. These relatively large errors in retrieved V_{cmo} then propagated into A (bottom panel).

Considering representation errors of the simple model compared to SCOPE, it is reasonable to assume that representation errors occur when comparing SCOPE to real measurements as well. Real measurements also have errors due to instrumentation and retrieval techniques, and

furthermore, not all input variables values may be known. In that case, treating V_{cmo} as the only unknown may not be appropriate. A better strategy in that case would be to include uncertainties in all parameters in a Bayesian approach. The simple model is suitable for such an approach because of its computational efficiency.

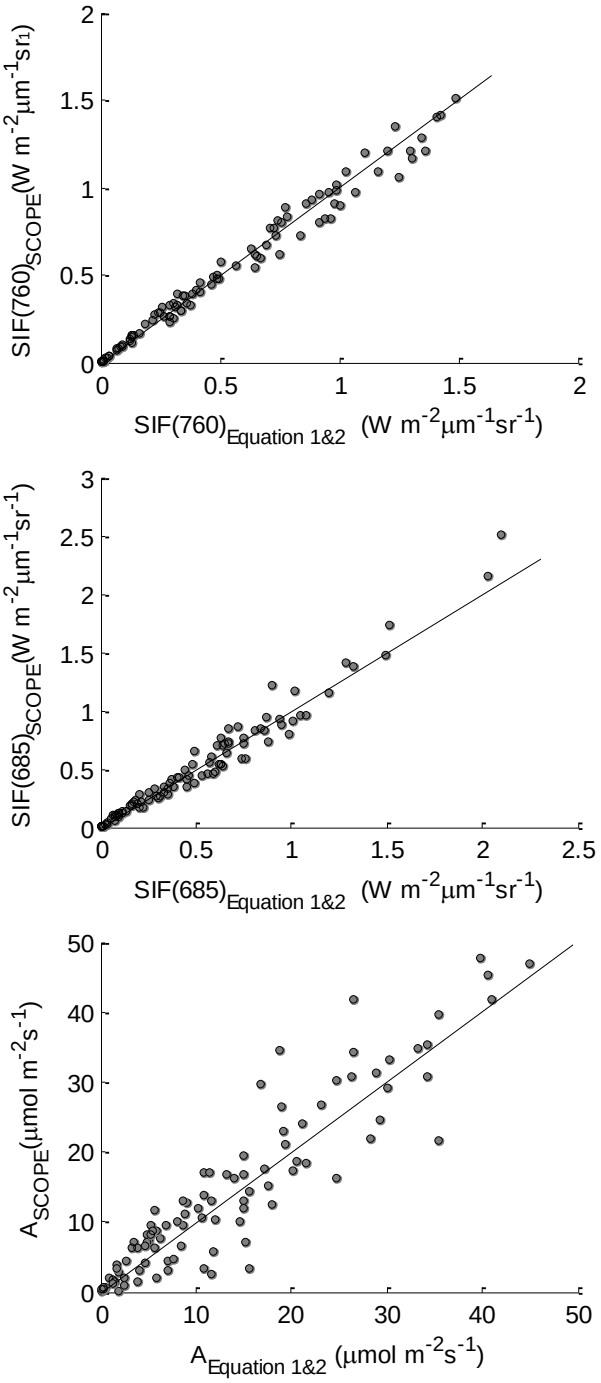

Figure 4.17. One hundred simulations of SIF at two wavelengths and *A* of the simple model versus simulations with SCOPE. The input for each simulation was randomly selected from uniform distributions of R_{in}, V_{cmo}, C_{ab}, L and q_s.

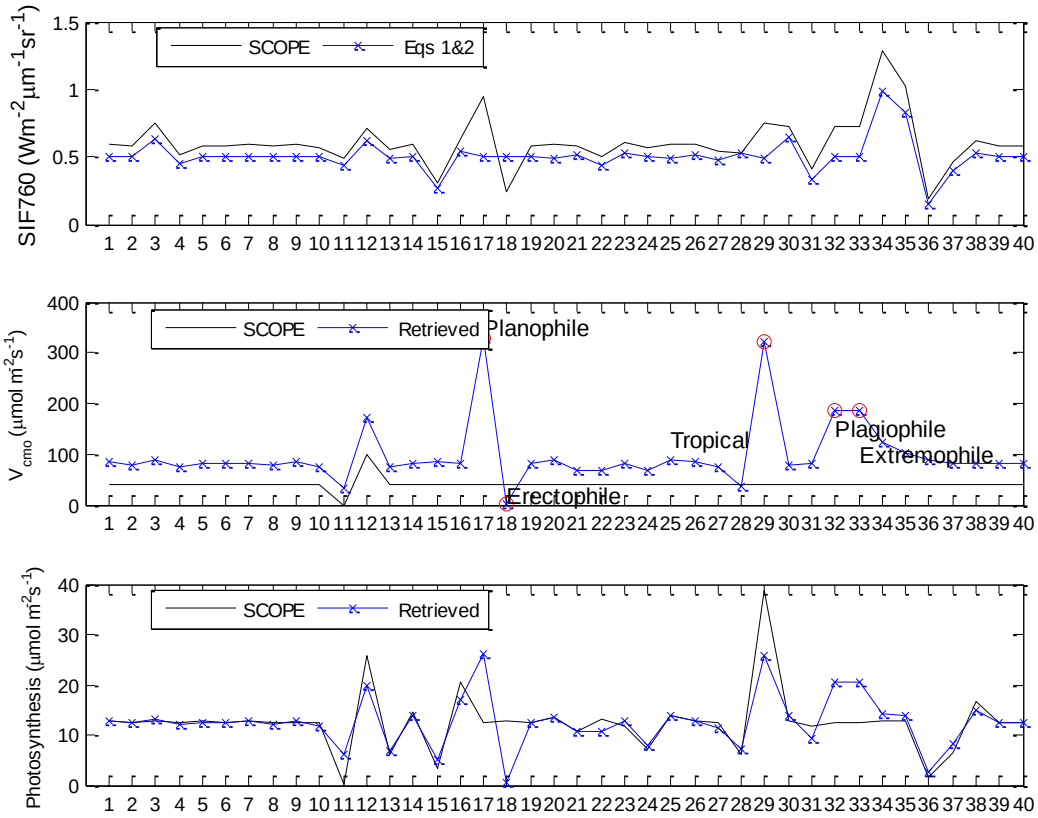

Figure 4.18. Top: simulations of SIF with SCOPE (line) and with the simple model (symbols) for 40 cases. In the 40 cases, SCOPE parameters were changed one by one in a systematic way. Middle: values of V_{cmo} as input to the SCOPE model (line) and corresponding values as retrieved from SCOPE-simulated SIF by the simple model (symbols). Bottom: *A* as simulated SCOPE (line) and *A* calculated with the simple model using the retrieved V_{cmo} as input.

In summary, a simple model for red and far-red fluorescence and photosynthesis has been formulated based on the model output of SCOPE. The simple model was approximately six orders of magnitude faster than SCOPE and performed well in comparisons to the full SCOPE model. (See also Section 4.5.2 on the SCOPE Emulator toolbox.)

4.5 Model applications

The major element here involved development and implementation of vegetation traits in a scene generator module of the FLEX End-to-End Mission Performance Simulator (FLEX-E). Additional activities involved (i) preliminary consideration of the effects of canopy geometry with SCOPE and alternative RT schemes, and development of a strategy for use of SIF in DGVMs via data assimilation; (ii) development of a SCOPE "Emulator toolbox" that serves to streamline and greatly speed up model computations, and which is included here as a complementary supplement to the FB Study; and (iii) assimilation of data from the *HyPlant* airborne system into modelling of the fluorescence-photosynthesis relationship.

4.5.1 Implementation of vegetation traits in scene generator module of FLEX simulator

An 'Automated Scene Generator Module' (A-SGM) was developed here with the main objective being to generate scenes driven by plant functional types (PFTs) and to generate time series scenes based on temporal profiles of PFTs.

The A-SGM toolbox:

- generates simulated scenes based on SCOPE or an emulated model;
- defines multiple land cover classes (e.g., plant functional types (PFTs)) and configures them with SCOPE/emulator input variables;
- generates time series of the simulated scenes based on temporal patterns of the (PFT-related) input variables; and
- stores and visualises input and output maps and generates animations of temporal profiles, in both the spectral and spatial domains.

The A-SGM is a simplified version of the SGM from the FLEX-E, but with the benefit that it is an independent platform with flexibility to incorporate new utilities. The core of the A-SGM is the radiative transfer model (RTM) SCOPE, a key RTM in support of sun-induced chlorophyll fluorescence research.

An overview of ARTMO's architecture is shown in Figure 4.19. Within this framework the A-SGM toolbox can be added as a new Module.

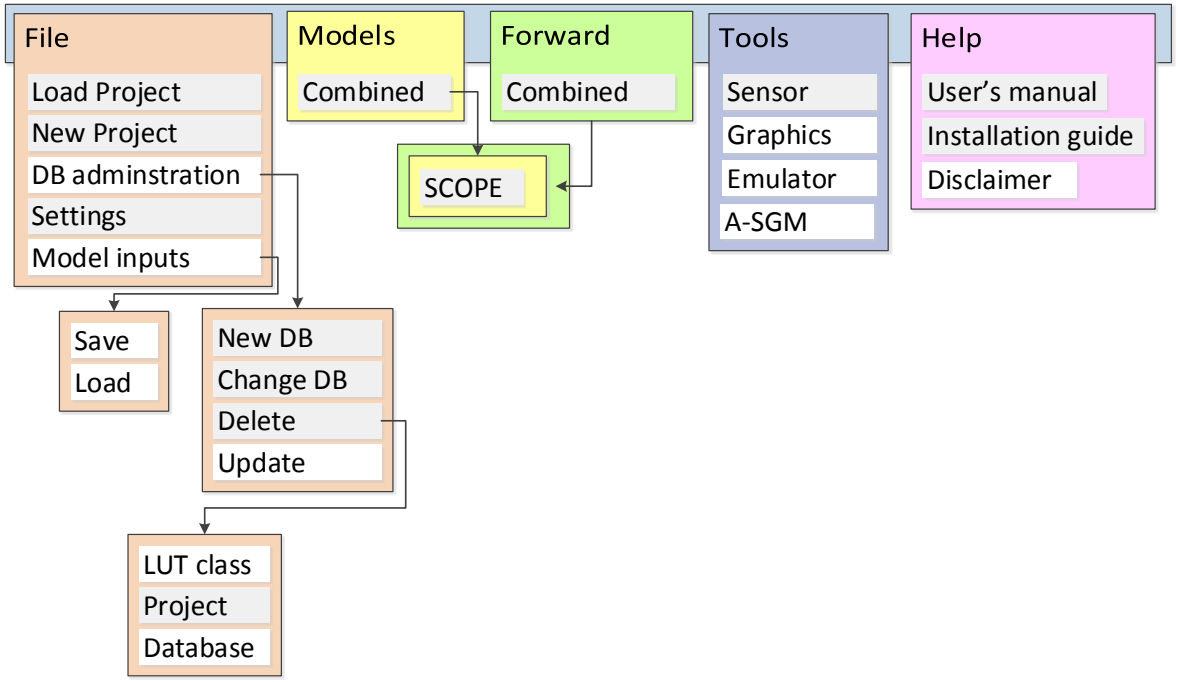

Figure 4.19. Hierarchical design as configured for A-SCOPE including A-SGM and Emulator.

The A-SGM toolbox is organised in a modular format, with all modules accessible from the A-SGM main drop-down menu (Figure 4.20).

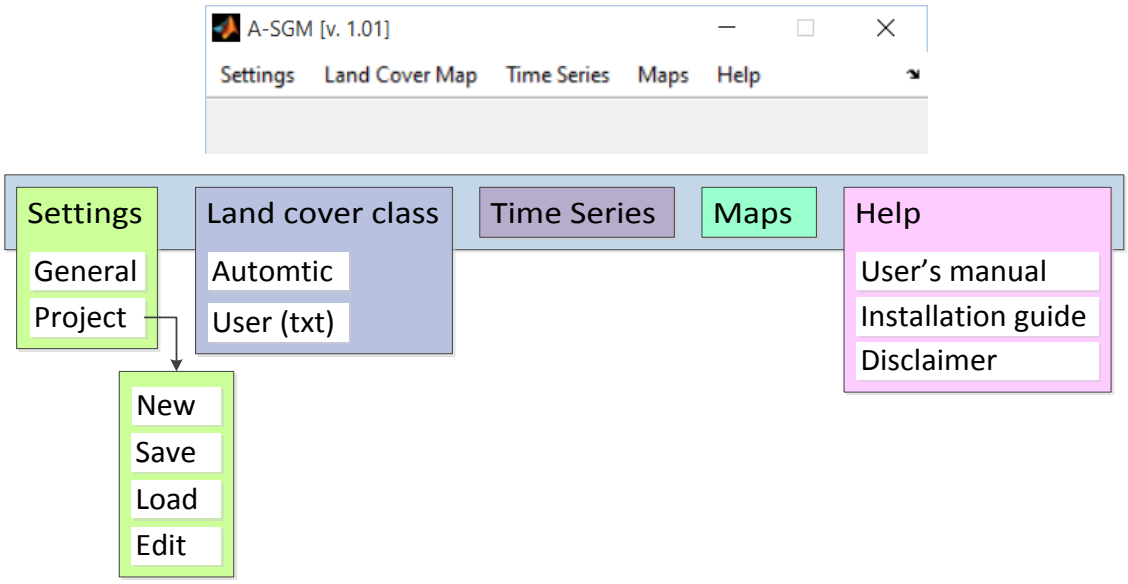

Figure 4.20. ARTMO's A-SGM architecture.

The functioning of the toolbox consists of four main steps:

1. **Settings:** Configures input data of the vegetation classes and temporal profiles.
2. **Land cover class:** Loads a land cover map.
3. **Time series:** Links vegetation classes to land cover classes and enables configuration of the time series.
4. **Maps:** Enables visualisation and storage of generated input and output maps.

More information about the A-SGM can be found in the User Manual. Here, we aim to apply the A-SGM for scene generation with multiple classes according to inputs from PFTs. The purpose of this exercise is to demonstrate the utility of the A-SGM for PFT-based scene generation.

To enable generation of realistic PFT-based simulations, a literature review was conducted to collect SCOPE input variables summarised at the scale of PFT. While PFTs are widely used in DGVMs such as ORCHIDEE, the scientific literature contained only limited recordings of biophysical parameter values at the global PFT scale. It appeared that only very few SCOPE variables have been summarised at the PFT scale, and usually they do not cover all PFTs and do not have temporal profiles.

With respect to SCOPE variables at the PFT scale, most published recordings focus on leaf area index. This is due to the availability of LAI maps at the global scale as delivered by operational

satellites (e.g., MODIS, MERIS). But for other SCOPE input variables the reporting of values at the PFT scale is almost non-existent, because currently no global satellite products exist for these aspects. For instance, for the commonly retrieved chlorophyll content variable, only PFT-related data was found at a local scale coming from experimental data. Even fewer recordings were found in the temporal domain.

Consequently, this activity demonstrates only the use of the developed A-SGM software to insert SCOPE input variables according to PFT classes. And since realistic values at the PFT scale have been found only for LAI, rendered scenes here are necessarily a simplification of how the spectral response of PFTs in reality would look like. The other SCOPE input variables have been kept fixed to their default values.

4.5.1.1 Results

The main purpose of the A-SGM is to generate simulated scenes according to a predefined sensor for different land cover classes and for given dates.

The functioning of the A-SGM was demonstrated with the generation of scenes based on RTM input data corresponding to PFTs. Based on LAI data, a synthetic image was simulated according to Sentinel-3 OLCI bands, based on LAI ranges for 15 PFTs. Also, for 6 latitudinal zones, monthly scenes based on temporal profiles of LAI profiles were simulated.

The 12 output images for Sentinel-3 OLCI are shown in Figure 4.21 for the far-red (740 nm) spectral band.

Given that SCOPE is able to provide multiple types of outputs, fluorescence profiles also can be created. Figure 4.22 shows temporal profiles of hemispherically integrated fluorescence plotted for 3 latitudinal classes. Temporal profiles of fluorescence per vegetation class can also be simulated.

The A-SGM is still a work in progress, and the following improvements are envisaged in a future version: (i) the possibility to load real land cover maps; and (ii) the upscaling towards top-of-atmosphere (TOA) radiance through coupling with an atmospheric model (i.e., MODTRAN). More PFT-related RTM input data will be collected so that (eventually) more realistic scenes will be simulated. These simulations will facilitate the development of retrieval algorithms with capabilities to better interpret S3-OLCI and FLEX-FLORIS data in space and time.

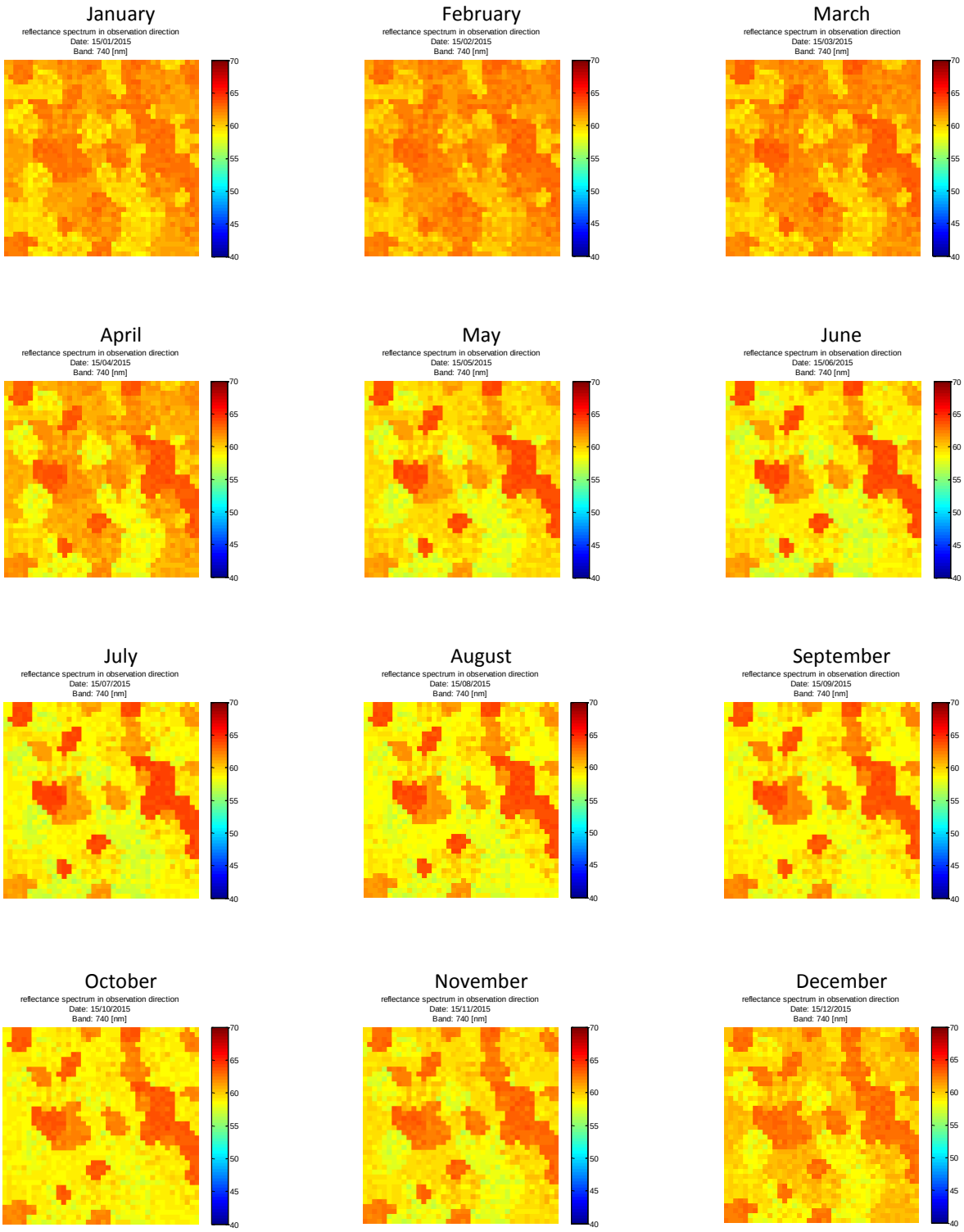

Figure 4.21. Simulated spectral output maps for Sentinel-3 OLCI based on monthly LAI temporal variation for six latitudinal zones.

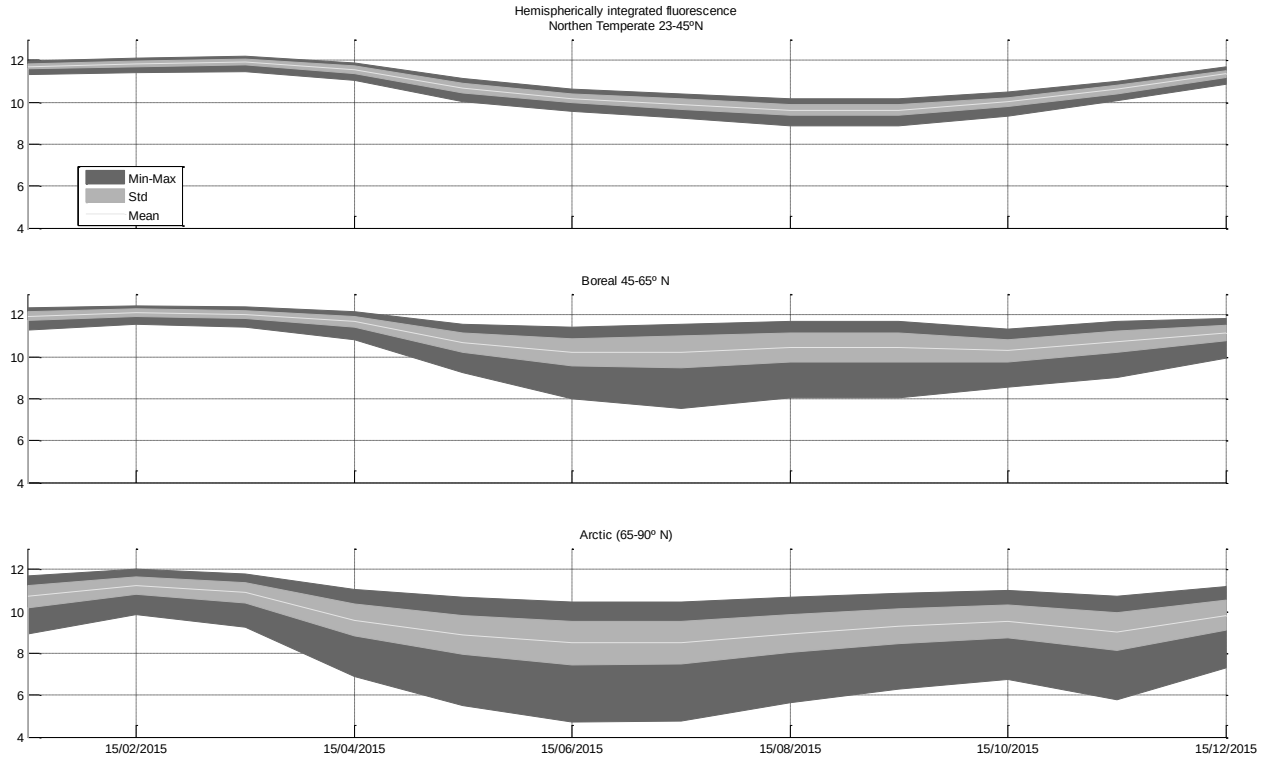

Figure 4.22. Temporal profiles of hemispherically integrated fluorescence for three latitudinal classes.

4.5.2 SCOPE Emulator toolbox

Since SCOPE or any advanced RTM can take a long computational time which makes them unfeasible in many applications, it has been proposed to substitute RTMs through so-called emulators. These are statistical models that approximate the functioning of a physically-based RTM. Emulators are advantageous in real practice because of the computational efficiency and excellent accuracy and flexibility for extrapolation, thereby opening up many new research and operational remote sensing opportunities.

In an activity complementary to the FB Study, a SCOPE emulator toolbox was created to facilitate the use of emulators (Rivera *et al.* 2015). A brief summary is included here.

The Emulator toolbox (Figure 4.23) enables analysis of multi-output machine learning regression algorithms (MO-MLRAs) based on their ability to approximate an RTM with little user interaction. The toolbox contains both linear and non-linear MO-MLRAs, including partial least squares regression (PLSR), kernel ridge regression (KRR) and neural networks (NN). The latest version (1.03) includes options for random forests and Gaussian processes regression (GPR). Although these MLRAs are not truly delivering multi-output, when trained in combination with principal component analysis (PCA) the full spectrum can be emulated with great accuracy. Particularly GPR shows accurate performances.

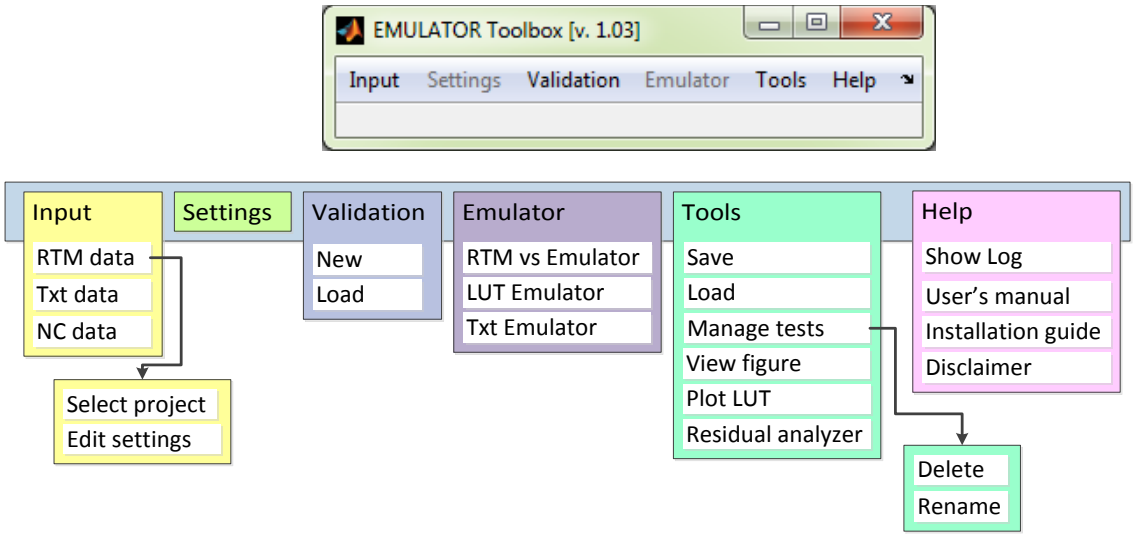

Figure 4.23. Emulator's main window (top) and its general architecture (bottom).

The modules must be used in a logical order, according to:

The toolbox enables users to train the MO-MLRA models with data from RTMs that are available within ARTMO. Various options are provided to optimise the training phase, e.g., PCA pre-processing step, ranging training/validation distributions or through cross-validation sub-sampling procedures. Goodness-of-fit performance and processing speed of the MO-MLRAs are then calculated. A successfully-validated MO-MLRA can then function as an emulator.

As a proof of concept, an analysis was conducted on the ability of the implemented MO-MLRAs to substitute for SCOPE in the generation of fluorescence outputs. Although PLSR could be considered as an accurate emulator, NN and KRR emulated fluorescence profiles with great precision (relative errors below 0.5% when trained with 500 or more samples), and this with a gain in processing speed from about 50 (NN) up to about 800 (KRR) times faster than SCOPE v1.60. It is foreseen that the Emulator toolbox will open up a diverse range of new applications using advanced RTMs, such as improved inversion strategies, global sensitivity analysis studies and rendering of simulated scenes in preparation for new satellite missions.

For more information about the functioning of the Emulator toolbox, we refer to Rivera *et al*. (2015) and the user manual (e.g., accessible at http://ipl.uv.es/artmo/).

4.5.3 Evaluation of canopy geometry effect with SCOPE and alternative RT schemes

Currently, there is no model that can incorporate the influence of horizontal inhomogeneity of vegetation clumping on canopy level fluorescence. Our aim here was to consider effects of 3D vegetation structure on TOC fluorescence, and to introduce models that might correct for the

effects of structure when estimating leaf level fluorescence and photosynthesis. Three different approaches were considered here to describe structural impact on SIF.

The first approach was to apply the principles of p-theory to the case of leaf level emission of fluorescence (Disney & Lewis 2007; Lewis & Disney 2007; Panferov *et al.* 2001). The spectral invariant or p-theory approach is based on the assumption that all spectral invariant quantities such as LAI, leaf normal angle distribution, canopy and leaf dimensions, canopy, leaf and intermediate level clumping, can all be encapsulated into one parameter named *p*, which is the average recollision probability of a photon after several orders of scattering. So far, p-theory has been used only to describe the relationship between leaf level single scattering albedo and canopy level albedo. We have reformulated the fundamental Newmann series type equation to incorporate the leaf level emission signal.

The second approach was to use a measure of vegetation clumping as an estimate of the ratio of sunlit leaf area to total leaf index (Oker-Blom *et al.* 1991; Nilson 1971). Assuming a known relationship between the rate of photosynthesis of sunlit and shaded leaves, estimates of GPP may be derived for sunlit leaves only. There is much more of a singular relationship for all vegetation types between the sunlit leaf GPP and SIF than between total GPP and SIF. For the clumping index (CI), we used the dataset of He *et al.* (2012). The index is based on the ratio of effective to true LAI. Clumping indicates how much leaf area is obstructed by other leaves. The lower the CI the greater the proportion of leaves in the canopy that are not visible from above, and the higher the CI the greater the proportion that are visible. CI ranges between 0 and 1, where values close to zero correspond to increased clumping and close to 1, reduced clumping.

The third is to derive DASF (directional area scattering factor) values over the red-edge and in the process retrieve estimates of the recollision probability (p) (Knyazikhin *et al.* 2013b). DASF can be thought of as the bidirectional reflectance factor for a canopy where all leaves have a leaf single scattering albedo of '1'. In this case there is no absorption and all incident photons will exit the canopy (Knyazikhim *et al.* 2013a,b). The retrieved recollision probability can be used within our first approach to estimate leaf level SIF values.

These approaches do not replace what is being done with the more detailed modelling efforts with SCOPE, but should lead to a better understanding of these structural impacts and of methods for mitigation of such effects. Of particular importance is that we can provide an alternative route to interpretation of the (leaf level) SIF signal than solely from using SCOPE (which does not, for instance, currently treat canopy structure in detail). Further application of these approaches is relatively straightforward (low computational cost), which also means that we can test the approaches using SIF estimates from current atmospheric instruments (e.g., GOME-2). This potentially provides a bridge between the interpretation of such coarse resolution, noisy data and the more detailed approach being used in FLEX. Preliminary application has been done here using GOME-2 data. The MPI-BGC GPP dataset from Jung *et al.* (2011) was compared to the SIF dataset by Joiner *et al.* (2013). Several authors have made similar comparisons and have found a linear correlation between GPP and SIF, albeit depending on plant functional type (PFT) (Joiner *et al.* 2014; Guanter *et al.* 2012; Frankenberg *et al.* 2011b). It is known that photosynthetic rates of shaded leaves are two to three times lower

than in sunlit leaves (He *et al.* 2012; Lichtenthaler *et al.* 2007). Most of the TOC SIF may be from sunlit leaves, thus there should be a closer correlation between what is, in effect, the GPP from sunlit leaves and total canopy GPP. If we can partition the GPP based on the CI and what we assume to be the ratio between sunlit and shaded leaf GPP, we can compare this to SIF to test if there is a closer to single relationship for all PFTs. Knowing that total GPP is the sum of GPP_{sun} and GPP_{shade}, we derived a factor which represents the fraction of total GPP which originates from sunlit leaves per unit ground area.

In addition, we use ground level spectrometer data to do a statistical analysis of the effects of vegetation structure on the SIF signal (Kato *et al.* 2014; Nichol 2014). For this we have a 3D digital canopy surface model which could be used. The idea is to model the TOC SIF signal from SCOPE by a surface roughness term which is derived from the canopy surface model. This would simulate the clumping and other structural effects not included in SCOPE.

4.5.3.1 Results

In simulating canopy level SIF ratios from leaf level SIF ratios, a comparison of results from p-theory versus those from SCOPE indicated that our truncated version of the canopy level SIF equation agreed closest with SCOPE (Figure 4.24). The simulation was for a canopy with LAI of 9.0, and planophile leaf normal angle distribution. The influence of reabsorption and re-emission needs to be further investigated.

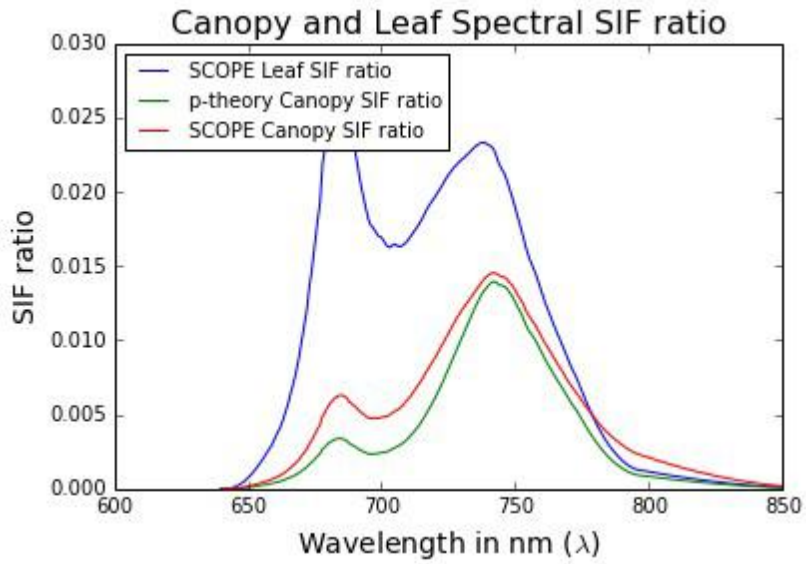

Figure 4.24. Comparison between SCOPE and p-theory canopy SIF ratio.

The study of relationships between SIF and total GPP per PFT revealed that, when structural differences were disentangled using clumping as an indicator of amount of GPP originating from sunlit leaves, a new relationship between SIF and sunlit GPP (GPP_{sun}) appeared to emerge owing to the collapsing of slopes of individual relationships toward a singular relationship among PFTs. Now, a solution is needed whereby the clumping index together with SIF might be used in a predictive manner to estimate GPP based on a single relationship between all PFT SIF

and GPP. The selection of areas to be included in the analyses had to be stringent enough to provide high levels of PFT purity. This was to avoid the influence of mixed vegetation in our analyses. The downside to this approach was that many PFTs which are not found in large uninterrupted areas on the globe have been undersampled.

DASF was calculated assuming a Lambertian reflecting surface. The anisotropic influence of vegetation including the 'hot-spot' was not included. This assumption will lead to a deviation between retrieved and true surface reflectance. A BRDF model could improve retrievals but this would need additional information regarding the surface properties. This is something that could be attempted in the future.

In conclusion, although the results are encouraging much work is still needed to address the effect of vegetation structure on the TOC SIF signal. The aim of providing a solution which can be incorporated into an operational model is still a work in progress.

4.5.4 Development of a strategy for use of SIF in DGVM via data assimilation

The objective here was to initiate investigation into whether data assimilation (DA) of SIF might be used to provide a (thus-far missing) constraint on carbon uptake as simulated by the ORCHIDEE Land Surface Model, and thus improve predictions of the net terrestrial carbon flux. Global SIF estimates from GOME-2 were used, and for the purpose of this exercise a simple linear relationship between GPP and SIF was assumed and its parameters optimised.

Two GOME-2 datasets of far-red fluorescence (O_2-A band) – identified here as the BERLIN SIF product (Köhler *et al*. 2015) and the NASA SIF product (Joiner *et al.* 2013) – were used, as they are readily available and convenient for this first assessment. We analysed the assumed GPP model parameters as a precursor to performing the DA. The DGVM ORCHIDEE was the main target of the DA, so a comparison was made between ORCHIDEE estimates of GPP and the SIF datasets.

If we are correct about the impact of structure on the signal (see Section 4.5.3), then such effects may complicate interpretation, so that 'structure-corrected' data would need to be used eventually.

4.5.4.1 Results

Initial indications pointed to the potential importance of SIF observations in several key areas of the globe, including South Amazonia, North America, Central Australia, Central Africa, and India. Such data seem likely to affect the seasonal cycle of (ORCHIDEE) GPP, including the duration of the growing season.

In general, there was a much higher correlation between the ORCHIDEE GPP and the BERLIN SIF product (Figure 4.25) than the NASA SIF product (Figure 4.26). The two SIF products have a different profile in most regions of the globe — in general the mean magnitude and amplitude/seasonality is greater in the BERLIN SIF product. Reasons for the differences between the BERLIN and NASA SIF products, and the resultant differences in the slope and intercept parameter distributions, will be discussed more fully with the working group and with

the respective data providers. For now the first assimilation experiments focused on the BERLIN GOME-2 SIF product.

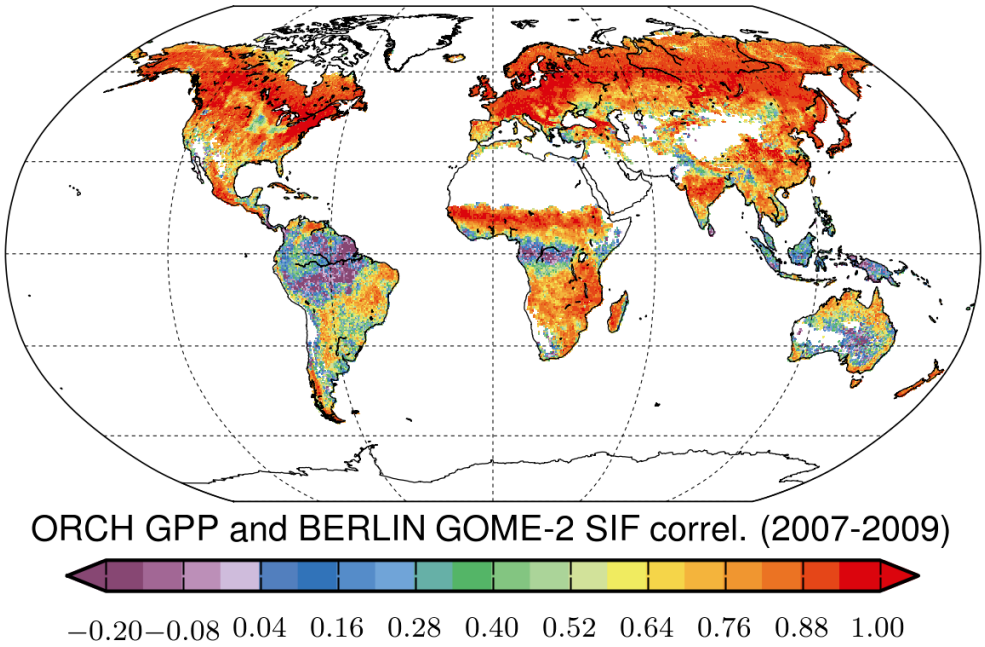

Figure 4.25. Correlation between the monthly BERLIN SIF product ($mWm^{-2}nm^{-1}sr^{-1}$) from GOME-2 and the monthly ORCHIDEE GPP ($gCm^{-2}m^{-1}$).

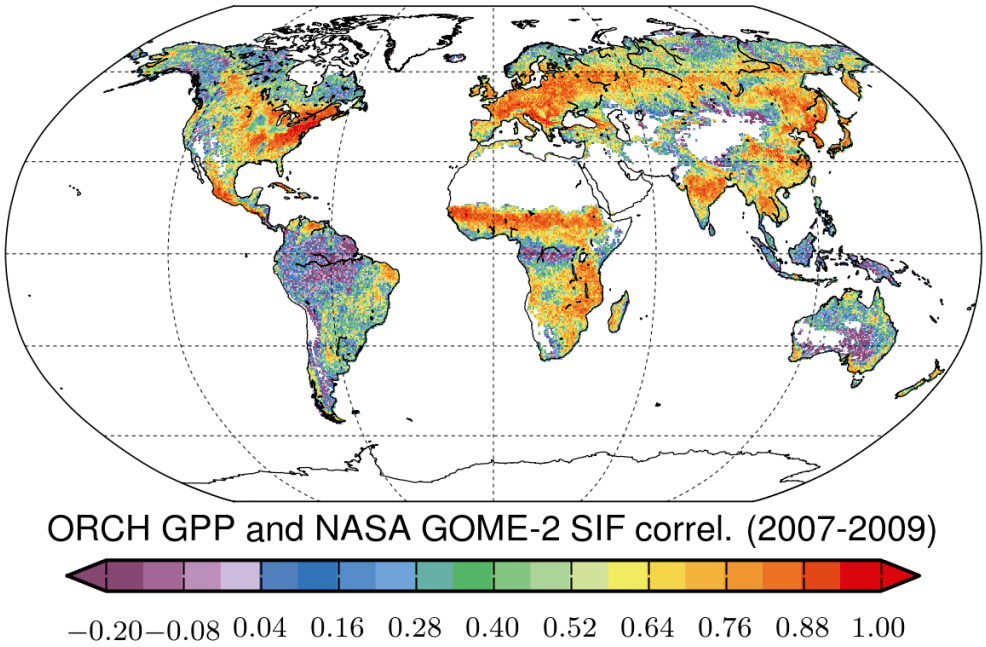

Figure 4.26. Correlation between the monthly NASA SIF product ($mWm^{-2}nm^{-1}sr^{-1}$) from GOME-2 and the monthly ORCHIDEE GPP ($gCm^{-2}m^{-1}$).

The results of the initial optimisation for one site is shown in Figure 4.27 for the Temperate Broadleaved Deciduous PFT in ORCHIDEE for both the simulated SIF and GPP. The corresponding changes in the SIF-GPP, photosynthesis and phenology-related parameter values were also analysed (data not shown).

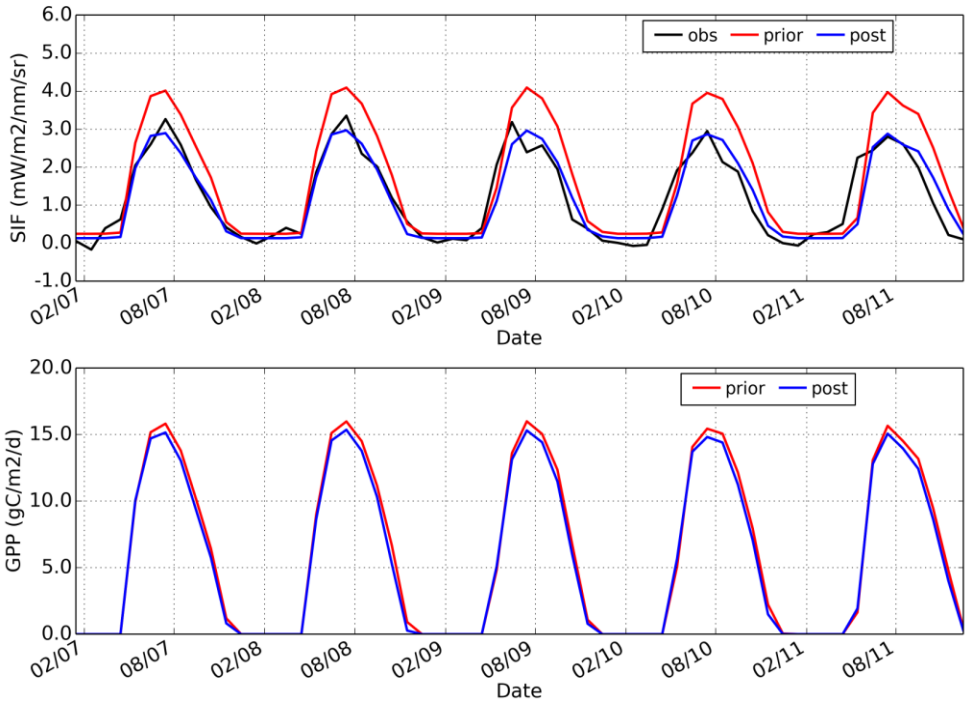

Figure 4.27. Daily time series for the Temperate Broadleaved Deciduous PFT at one site, showing the prior simulations of ORCHIDEE (red) compared to the posterior simulations (blue) after optimisation of the model parameters for SIF (top – compared to observations in black) and GPP (bottom).

DGVMs such as ORCHIDEE have various uncertainties, more so for some PFTs/regions than others. For instance, ORCHIDEE is known to have a large positive bias in global annual GPP estimates, and to have too long a growing season in the northern hemisphere. The preliminary results here suggest that SIF data may be very useful in constraining the parameters of ORCHIDEE, and thus resulting in better predictions of seasonal vegetation dynamics and carbon uptake.

The next stages are to perform further DA experiments with ORCHIDEE and other models. It is also necessary to understand more fully the differences among the SIF datasets being used.

4.5.5 Assimilation of *HyPlant* data into fluorescence-photosynthesis relationship

In this section, a simulation of fluorescence and photosynthesis was conducted for a *HyPlant* scene. Fluorescence was simulated using inputs from reflectance data, then a comparison was done of modelled and measured results.

HyPlant consists of two spectrometers, one designed to obtain hyperspectral reflectance, and the other to retrieve fluorescence in the oxygen absorption bands. Estimates of leaf chlorophyll

content and leaf area index were obtained from the hyperspectral reflectance by inverting PROSAIL with the ARTMO software (Figure 4.28, left two panels). We used these maps, together with the irradiance and relative humidity at the time of overpass, as input for the simplified SCOPE model of Section 4.4.3. Here, we used the simplified model instead of the full SCOPE model to reduce computation time. The time to reproduce a *HyPlant* scene on a PC with the simple model was about 0.4 s (compared to several *months* for the full SCOPE model). As a final step, we assimilated F_{760} as retrieved from *HyPlant* into the simplified SCOPE model using a Bayesian rule:

$$P_{posterior} = \frac{P_{a-priori} / \sigma_P^2 + f^{-1}(F_{760,HyPlant}) / \sigma_M^2}{1/\sigma_P^2 + 1/\sigma_M^2} \quad (4.5)$$

where P are the model parameters of the simplified SCOPE model, σ_M is the uncertainty of the measured fluorescence (provided as output of the retrieval algorithm), f denotes the simplified SCOPE model (and f^{-1} the inversion of the model, i.e., the parameters retrieved from the model with fluorescence as input), and σ_P is the uncertainty of the parameters. Here we assumed all parameters were known exactly, except for LAI. For LAI we used the uncertainty as estimated with the ARTMO software. The equation above gives the weighted mean of LAI obtained from reflectance, and the LAI as obtained from fluorescence. The weights are the reciprocals of the respective uncertainties. The data assimilation step brings the simulated fluorescence closer to the measurements by modifying the LAI.

4.5.5.1 Results

Retrieved C_{ab} and LAI, and the simulated F_{760} and A are shown in Figure 4.28, along with *HyPlant* measured F_{760}. There were some similarities between simulated and modelled fluorescence. The range of values was similar in the simulations and the modelled outputs, and fields with high and low fluorescence were clearly distinguishable. Within-field variations were different between *HyPlant* fluorescence and simulated fluorescence.

Figure 4.29 shows the simulated A and the simulated F_{760} along with the measurements, but now also the posterior estimates of F_{760} and photosynthesis. The posterior F_{760} was always in the range between the simulated and the measured values, and the difference between the measured and modelled F_{760} was positively related with the accuracy of the LAI estimate, and negatively related with the F_{760} measurements.

Within-field variability of the posterior F_{760} was larger than the *a priori* variability, while in some cases, the between-field variability was smaller. For example, the rectangles in Figure 4.29 show two fields, a potato field above a sugar beet field, with clearly different retrieved LAI and chlorophyll content and thus also different modelled *a priori* F_{760}. However, the *HyPlant* F_{760} was much less different between the two fields. As a result, the posterior modelled F_{760} modelled was also less different, and likewise, the posterior A is also less different between the sugar beet and the potato fields than the *a priori A*.

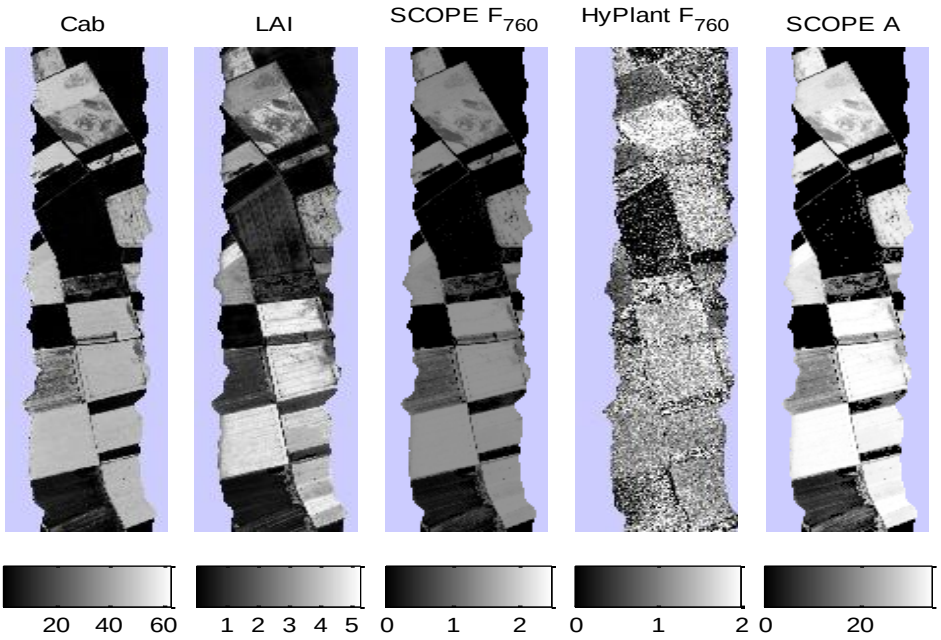

Figure 4.28. From left to right: Chlorophyll and LAI as retrieved from *HyPlant* data (Selhausen, Germany, 23 August 2012 13:50) with ARTMO; Fluorescence as simulated with the simplified SCOPE model of Section 4.4.3; *HyPlant* retrieved fluorescence at 760 nm in W m^{-1}µm sr^{-1}; and SCOPE simulated photosynthesis in µmol CO_2 $m^{-2}s^{-1}$ with the simplified model of Section 4.4.3.

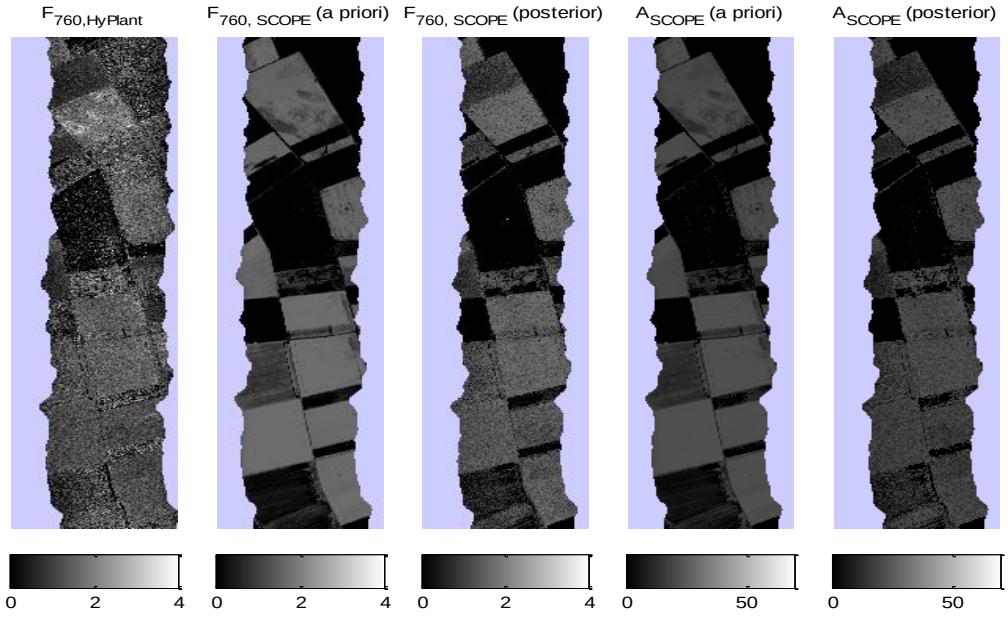

Figure 4.29. From left to right: F_{760} retrieved from *HyPlant* data; simulated F_{760} from LAI and Cab of *HyPlant* ('*a priori*'); posterior F_{760} after assimilation of *HyPlant* F_{760}; and *a priori* and posterior canopy photosynthesis. The unit of F_{760} is W m^{-1}µm sr^{-1}, and the unit of A is µmol CO_2 $m^{-2}s^{-1}$. The blue rectangle in the right two graphs shows a potato field above a sugar beet field.

4.6 Conclusions

Both **SCOPE and A-SCOPE have been updated** and three versions have been released – versions 1.54, 1.60, and 1.61 – with improved computation speed and accuracy of fluorescence output.

Effects of **Xanthophyll pigment changes** have been included in Fluspect, producing the Fluspect_B_CX model. Magnitude of the modelled PRI effect agreed with observations, but some differences in spectral shape were observed which are not yet explained. The xanthophyll effect has been empirically linked to NPQ, such that the biochemical routine and the Fluspect models can be coupled. This is an important step, as specific stress effects on fluorescence can be simulated together with PRI. This coupling has not yet been implemented in SCOPE.

Further progress was made for stress applications, with a novel technique proposed here for the quantitative assessment of **energy partitioning** among photosystems, and the development of a novel model for the prediction of changes in energy partitioning (as a result of spillover or state transition) in response to internal and external factors.

Also, the possibility was investigated to estimate **sustained NPQ** from changes in leaf PRI, and hence to derive a critical parameter in the MD12 fluorescence model from parallel measurements of leaf reflectance, thereby strongly reducing model uncertainty.

We evaluated the **Fluspect model**, a computationally fast radiative transfer algorithm that calculates leaf reflectance, transmittance, and fluorescence emission spectra between 640 nm and 850 nm. The model reproduced both the magnitude of the fluorescence and the effects of pigment composition on the shape and magnitude of fluorescence spectra in the forward and backward direction. Model inversion allowed retrieval of parameter values from measured leaf reflectance and transmittance spectra, and the parameter values were realistic and agreed with destructive measurements of chlorophyll and carotenoid concentrations. Fluspect provided realistic chlorophyll fluorescence simulations, with most of the fluorescence variability explicable from the PROSPECT parameters. However, the spectral distribution of the excitation light affected the shape of the chlorophyll fluorescence spectrum in a way that the Fluspect model could not fully reproduce. Ideally, measurements carried out under natural light conditions should be used to complete a full validation of the Fluspect model.

The **SCOPE model has also been compared to field data** of far-red fluorescence from *HyPlant*. SCOPE was able to reproduce the magnitude and seasonal cycle of fluorescence. In unstressed conditions, the effects of canopy structure and leaf composition dominated variations in the fluorescence signal, with a smaller contribution of photosynthetic regulation due to photochemical and non-photochemical quenching.

A **simple model** for red and near infrared fluorescence and photosynthesis has been formulated based on the model output of SCOPE, which is approximately six orders of magnitude faster than SCOPE. Also, an **Emulator toolbox**, developed as a complementary activity to the FB Study, is useful for evaluating various model emulators.

As a first attempt, **data assimilation has been applied to a *HyPlant* scene**, producing a map of canopy photosynthesis from the reflectance and retrieved fluorescence of *HyPlant*. Initial study of data assimilation using SIF to constrain the DVGM **ORCHIDEE** also yielded promising results.

An '**Automated Scene Generator Module' (A-SGM) software package** for the generation of simulated scenes according to **plant functional types (PFTs)** has been developed. The A-SGM is independent of the FLEX-E scene generator module in order to avoid compatibility problems, and with the purpose to introduce new utilities. It has several advantages including:

- a user-friendly GUI format in the ARTMO framework, with simplified RTM data input for PFTs, rapid generation of simulated scenes, and scene generation for any optical sensor as defined within ARTMO;
- capacity to render multiple time series scenes, with output options enabling visualisation of temporal profiles both of input maps and outputs;
- accommodation of simulated data from either an RTM (e.g., SCOPE) or RTM emulator, the latter greatly increasing processing speed (but with some reduction in accuracy).

5. Development of a calibration/validation strategy for FLEX products

5.1 Introduction

Within this task a thorough strategy for the calibration and validation of the FLORIS sensor and selected FLEX products was developed. Validation strategies were defined for fluorescence at the top of the canopy and for downstream products, e.g., photosynthetic efficiency and GPP. A thorough calibration/validation plan is essential in order to ensure a timely development and deployment of *in situ* observations representing relevant space and time scales. Product validation is an essential part of future algorithm development, fine-tuning, and eventually mission performance evaluation.

The main objectives were to:

- determine validation error metrics and product accuracies;
- define a Cal/Val strategy for basic fluorescence products;
- define FLEX Level-2/3 products and their validation plan; and
- define common protocols and state-of-the-art instruments to be used in estimation of fluorescence in the context of calibration/validation activities.

5.2 Validation error metrics and product accuracies

For the FLEX mission calibration and validation phase (Cal/Val), it is necessary to have quantitative estimates of the precision achieved by the Level-2 retrieval algorithms for each product delivered. Otherwise, measurements retrieved from FLEX data cannot be validated nor compared to perform time-series analysis or comparative analysis between different targets. Hence, a set of error metrics must be defined for application during the mission's Cal/Val phase.

Two main components were addressed:

- definition of error metrics for each product of the FLEX mission, so that the precision achieved by the mission and its retrieval algorithms may be estimated; and
- development of a product validation strategy that allows proofing that accuracies and mission objectives as defined in the FLEX Mission Requirements Document (MRD) (ESA 2015b) are met by each output product.

For error metrics definition, the products to be evaluated are:

- Fluorescence radiance at peaks: Red fluorescence (RF), Far-red fluorescence (FRF).
- Centre wavelength of peaks: λ_{RF}, λ_{FRF}.
- Total integrated fluorescence radiance: F_{tot}.
- Photochemical Reflectance Index (PRI)
- Photosynthetically Active Radiation (PAR)
- Apparent reflectance spectrum: ρ_{app}.

Other intermediate and secondary products will be considered in Section 5.4.

5.2.1 Error metrics for validation

Validation of FLEX products is based on the comparison between the so-called *ground truth* measurements and retrieved FLEX products. The error metrics will quantify this comparison and take into account the statistical distribution and spatial characteristics of the measurements taken at ground and satellite level.

5.2.1.1 Statistical and spatial characteristics of ground and satellite data

Both FLORIS products and ground truth measurements will have inherently associated uncertainties and variances from sources such as:

- intrinsic instrument accuracy caused by random and systematic noises;
- natural variability of target optical properties at different spatial scales;
- environmental variations in illumination during ground truth measurements; and
- error propagation in retrieval algorithms or radiative transfer simulations.

Metrics formulation should include the uncertainty of both ground truth and retrieved parameters. The case differs if both values present similar characteristics in their measurement; or, as with the FLEX End-to-End Mission Performance Simulator (FLEX-E), when the true values are available with absolute precision in order to evaluate the performance of the different modules and algorithms (Vicent *et al*. 2015a,b).

Another aspect is different spatial scale and sampling of the ground and satellite measurements. FLEX will deliver its products at a moderate resolution of 300 m/pixel in the best case. Routine validation likely will entail upscaling of sparse collected data from instruments with a smaller footprint, and error metrics must represent this situation. Details on how this validation can be achieved are provided in Section 5.3, based on earlier work from the FLUSS project (Lindstrot *et al.* 2013).

5.2.1.2 Suggested error metrics for validation

FLEX products to be validated can be either scalar (e.g., FRF, F_{tot} or PRI) or vectors (e.g., ρ_{app} and solar irradiance). Each type of parameter therefore requires a different metric. For scalar parameters we propose to use Welch's test, t (Welch 1974), since it is capable of comparing sets of ground truth measurements and retrieved satellite data, of unequal sample sizes and unequal variances. For vector parameters, the suggested metric is SIDTAN Spectral Similarity (Du *et al*. 2004), which combines properties of both Spectral Information Divergence and Spectral Angle Mapper.

5.2.1.3 Determination of the intrinsic variance of the test target and FLEX products

The variance of a parameter from a given target (Figure 5.1) can be due to several sources:

- instrumental performance, e.g., noise, stability;

- environmental conditions at the time of acquisition;
- natural variability, which is also modulated by the sampling strategy; and
- error propagation in indirect measurements in estimations.

Repeated measurements and sampling are needed to quantify the associated variance of the validation target.

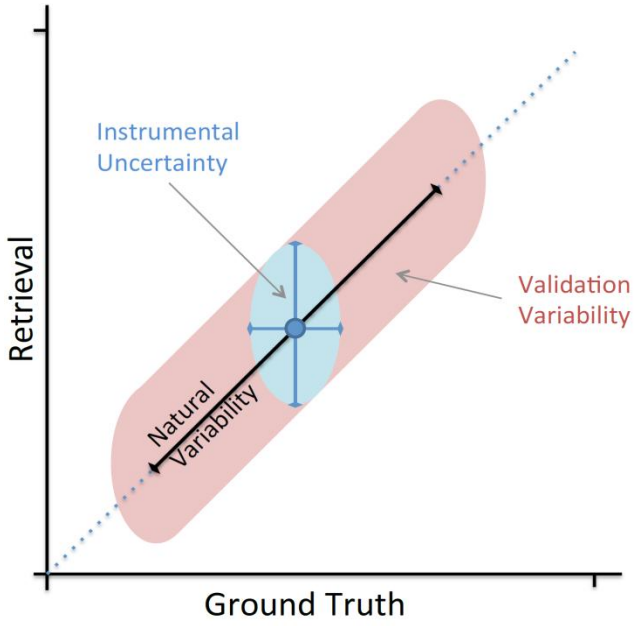

Figure 5.1. Sources of variance in ground and satellite data over a validation site.

Instrumental uncertainty can be determined under laboratory conditions, although characteristics may change under operational conditions. Performance also degrades with time, necessitating routine checks. Spaceborne instruments will need a vicarious calibration over established calibration/validation test sites. Field instruments require repeated measurements of dark current (no incident illumination) and a white reference.

Variability in environmental conditions (e.g., from disturbance in illumination) can increase variability of ground measurements. Environmental stability may be determined by measuring global irradiance in a stable setup, free of disturbances from surrounding objects for the duration of the target measurements, with an extra margin of several minutes before and after.

Inevitably, natural variability in optical characteristics will appear at the different spatial scales. Statistical analysis of spatially distributed ground measurements should be done, grouped by class in partially heterogeneous areas to avoid injecting variability of one class into others.

Ground truth fluorescence will be measured at canopy level by proximal sensing, implying that it is necessary to use retrieval algorithms. Evaluation of the algorithm accuracy and uncertainty can be tested by direct fluorescence measurements at leaf level, and followed by applying the retrieval algorithm to be evaluated.

The last contributor to variance in the reference validation signal is the upscaling to map level using RTMs, which need individual calibration and validation for all vegetation classes at each site. This requires measurement of the leaf and canopy parameters required by the models. Then fluorescence is measured directly at leaf level and retrieved from canopy level using field spectroradiometers. Given the inputs and outputs, it is possible to fine-tune the model to get the best fit for each Cal/Val site.

For FLEX data, the radiometric stability and atmospheric correction accuracy will determine the variance of the retrieved products. This variance can be derived from already established standard Cal/Val sites. In particular, radiance accuracy and variance can be derived by ground truth spectral radiance measurement of stable and homogeneous targets, such as desert plains. Atmospheric correction is determined by ground truth surface reflectance that is evaluated against the retrieved reflectance, and/or solar irradiance measured *in situ* with instruments of equal or higher performance than the FLEX sensors will compare to the one derived by the atmospheric correction algorithm.

To assess the accuracy of the RTM results (both for upscaling and for atmospheric correction) it is possible to perform a local or global sensitivity analysis through One Factor at a Time (OAT) or Variance Based Methods (Saltelli & Annoni 2010), which will allow propagation of uncertainties of the input parameters to the retrieved ones.

5.2.2 Product validation strategy

It is proposed to validate the FLEX retrieved products through comparison against the ground truth with three different validation scenarios. These scenarios range from the use of ground measurements to airborne measurements or cross-validation based on Radiative Transfer Models (RTMs). **Single spot** measurements (tower-based) may be used to monitor homogeneous targets. **Multiple spot** measurements (e.g., from UAVs or other roboticised or motorised instruments) would be useful for acquisition of sparse measurements over homogeneous or heterogeneous targets. **Mapping** measurements (from airborne platforms) can cover relatively large areas; or alternatively, RTMs may be used to build reference data over whole targets by utilising a tool such as the scene generator (SGM) developed for the FLEX-E (Rivera *et al*. 2014).

Global validation of the FLEX retrieved products is based on cross-comparison against ground truth measurements acquired over a set of Cal/Val sites (CVS) defined as physical sites around the globe and/or a set of temporal measurements in one or more CVS. Overall accuracy of the retrieved FLEX products will be measured applying the proposed error metrics and taking into account the intrinsic variance of the ground/satellite measurements over each site. The accuracy will be driven for those CVS where the variance is lower (e.g., homogeneity of the ground target, accuracy of the retrieval, lower instrument noises). In addition, the global validation might be affected by sites suffering systematic deviations, and analysis of the longer temporal trend will help to determine the source of the deviation.

Photosynthesis is another important aspect to be considered, given its dynamic adjustments to environmental changes. Adaptation mechanisms can be fast (in the order of seconds) or slow

(taking hours or days). For validation purposes, it is necessary to record, for instance, the illumination history of the test target to gauge transitional effects (e.g., sudden illumination changes). Changing conditions result in an increased variance in the true signal that will translate to the retrieved signal, and should not be interpreted as retrieval errors.

5.3 Definition of a Cal/Val strategy for basic fluorescence products

As defined by CEOS Working Group on Calibration and Validation (WGCV), ISO 9000 and the National Institute of Standards and Technology, validation is "the process of assessing, by independent means, the quality of the data products as derived from the system outputs". Validation can be carried out over several aspects of the sensor and the data provided by it, including sensor model, data processing, or a derived product. This section focuses on this last aspect, in particular the validation of the SIF product as provided by FLEX.

A global validation plan is introduced for FLEX SIF products, based on recommendations by CEOS (Morisette *et al*. 2006). It follows a "bottom-up" strategy whereby SIF measurements at TOC are up-scaled using aerial or satellite imagery to FLEX moderate resolution scale. Two options are proposed depending on availability of the *in situ* data: direct validation, i.e., when canopy level SIF is measured; and indirect validation, i.e., through numerical RTMs where availability of SIF monitoring is limited (such as in complex environments). Recommendations and requirements are presented for the exploitation of existing networks of measuring sites. Also, instrumentation requirements are outlined to properly measure SIF at different scales (leaf, canopy, local and regional).

The "bottom-up" approach is generally considered as an effective validation strategy. This approach, as developed for LAI in the framework of the Land Product Validation (LPV) Subgroup of the CEOS/WGCV (ESA 2015b), has been adapted here for validation of SIF products. The approach is considered as "bottom-up" because it suggests that methods should start with local field-level data and move towards global validation using satellite data. The LPV subgroup created a validation framework that, if followed, would ensure that different LAI products (but easily extended to other vegetation-related parameters) could be compared. The framework contains four stages, which will be followed in this plan and are summarised in Table 5.1.

Table 5.1. CEOS LAI validation framework.

Validation Stage	Description
Stage 1	Product accuracy is assessed from a small (approx. <30) set of locations and time periods by comparison with *in situ* or other suitable reference data.
Stage 2	Product accuracy is assessed from a significant set of locations and time periods. Spatial and temporal consistency of the product and with similar products has been evaluated over globally representative locations and time periods.
Stage 3	Uncertainties in the product and its associated structure are well quantified. Uncertainties characterised statistically over multiple locations and time periods representing global conditions.
Stage 4	Stage 3 results are systematically updated as the time-series expands when new product versions are released.

Guillevic *et al*. (2014) proposed four approaches (or categories) for validation of remotely sensed land surface temperature (LST) (extendable to any other parameters) and they were not mutually exclusive:

Category A: Comparison of satellite with *in situ* measurements: This is the traditional and most straightforward approach to validating any given parameter. It involves a direct comparison of satellite-derived value with collocated and simultaneously acquired measurement from ground-based instruments.

Category B: Radiance-based validation: This technique uses top-of-atmosphere (TOA) in conjunction with a radiative transfer model to simulate ground LST using data of surface emissivity and atmospheric profiles of air temperature and water vapour content.

Category C: Inter-comparison with similar products: A wide variety of airborne and spaceborne instruments collect similar data and many provide operational products. Inter-comparison of products from different satellite instruments can be valuable for determining the accuracy of a parameter, given that all the systems use the same (or compatible) retrieval algorithms.

Category D: Time series analysis: Analysing time series of satellite data over a temporally stable target site allows for identification of potential calibration drift or other issues of the instrument that manifest themselves over time. Furthermore, problems associated with cloud contamination for example may be identified from artefacts evident in the time series. Care must be taken in distinguishing between instrument-related issues such as calibration drift and real geophysical changes of the target site or the atmosphere.

All these approaches can be applied for FLEX products, and in fact all but one had been proposed in preparatory works for the validation plan during FLUSS. Category C (inter-comparison with similar products) was not considered since the main fluorescence products from FLEX do not have a similar product to compare against.

5.3.1 Parameters to be validated

5.3.1.1 Fluorescence products

Fluorescence at O_2-A and O_2-B

Fluorescence in FLEX is estimated by using the O_2 absorptions and their surrounding bands. Therefore, the estimation of SIF on those bands can be considered the most reliable, whereas SIF in other spectral bands might have larger uncertainty due to signal noise (e.g., at water absorption bands). The same happens to ground-based instruments using proximal sensing, since they follow the same retrieval spectral fitting (SFM) algorithm. However, at some support validation sites where instrumentation is not optimal for SFM, it might be necessary to use other retrieval methods that restrict their output to just to the O_2 absorptions. In those cases it will be necessary to count on algorithms exclusively based on O_2 absorptions.

Total fluorescence emission

Total fluorescence emission is the integral in the spectral domain of the SIF emission spectrum. It accounts for the total energy emitted as SIF by the vegetation's photosynthesis and it is necessary to close the energy budget. Since SFM retrieval provides the SIF spectrum, the total emission is just its integral. However, where the SIF measurements are limited to the O_2 bands, it is possible to use an empirical relationship between both retrievals and the total emission.

Emission peaks characterisation

Fluorescence emission is a dynamical process influenced by biophysical parameters of the vegetation, environmental conditions and the different stresses that the vegetation might sustain. Thus the emission intensity might be different at the red and far-red fluorescence peaks, and also at the spectral locations of the maxima. Peak maximum radiance and centre wavelength are directly measured from the retrieved SIF spectrum by the SFM. In the case of having only SIF at the O_2 bands available, determining the centre wavelength is not possible, but the RF peak emission can be approximated by the O_2-B SIF measurement, while the far-red peak emission can be linearly related to the O_2-A SIF measurement.

Photochemical reflectance index (PRI)

The PRI, while actually not a fluorescence product, is closely related to vegetation energy dissipation and photoprotection. PRI is originally defined as a normalised index between two bands in the green region, therefore, any spectrometer covering that region with a spectral resolution of 3 nm or less could provide this measurement. But for maximum accuracy, spectra should be collected with high sampling and radiometric resolution to distinguish the small differences due to changes in pigments. It is recommended here to use separate spectroradiometers for the full range (VNIR and/or SWIR) devoted to measuring PRI and other biophysical parameters, and for measuring fluorescence in the 650-850 nm range that requires higher spectral resolution in a smaller spectral range.

Temperature

Temperature is also an indicator of photosynthesis energy dissipation. Vegetation surface temperatures are related to energy fluxes within the canopy such as evapotranspiration. To decouple quenching processes from environmental changes also requires monitoring of air temperature. All approaches to determine land surface temperature from remotely sensed thermal infrared (TIR) data require accurate estimates of the emissivity of the surface of interest. A widely used approach for multi-spectral TIR data is the temperature-emissivity separation (TES) algorithm that has been developed originally for thermal ASTER images (Ullah *et al*. 2012).

5.3.1.2 Additional parameters to be measured

Other biophysical parameters necessary for proper interpretation and application of the fluorescence signal are leaf chlorophyll content, leaf area index, fAPAR, water content, photosynthesis rate, or canopy structural parameters. Information is also required on weather

conditions during *in situ* measurements. Aerosol optical thickness (AOT), ozone and water vapour in the atmosphere can affect radiance measurements taken at the sensor. Atmospheric conditions will affect airborne and satellite acquisitions. Collection of meteorological data are thus necessary to validate the atmospheric correction applied to satellite and airborne data, and to allow *in situ* measurements to be upscaled to at-sensor values. Details of requirements for these additional parameters are provided below in Section 5.4.

5.3.1.3 Ancillary data and metadata

These types of data include:

- geographic location, which allows comparison of *in situ* measurements to airborne/satellite imagery, and is obtainable through GPS geolocation;
- time stamp in UTC;
- detailed land use map of CVS;
- digital terrain model (DTM), to allow incorporation of topographic effects on incidence of solar illumination, surface pressure and optical path to the sensor (affecting the depth of the oxygen absorptions); and
- digital surface model (DSM), which is informative on canopy height.

5.3.2 FLEX bottom-up validation

The "bottom-up" validation approach is summarised in Figure 5.2. It consists of an integrated framework comprising measurements at the leaf, canopy, and landscape scale; strategies for sampling and comparison of *in situ* SIF maps with FLEX SIF products; data management; and staging of validation activities.

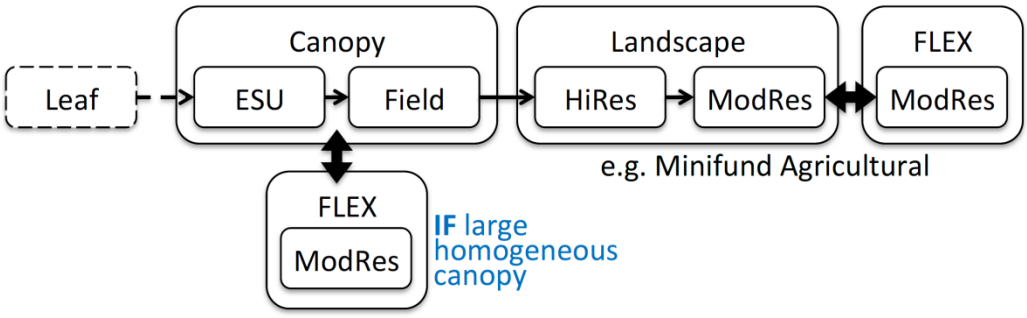

Figure 5.2. Scheme of a bottom-up validation approach, extended from CEOS.

Since fluorescence retrieval is done at canopy level, the bottom-up approach starts from canopy level measurements with point or local coverage, then extends to moderate resolution landscape level by means of an intermediate high-resolution data source. Optionally, leaf level SIF measurements might be performed in order to validate and/or constrain TOC measurements and retrieval methods. Intermediate high-res data can originate either from an airborne hyperspectral imager capable of SIF detection, or from high-res satellite data.

5.3.2.1 Canopy level measurements

Canopy measurements form the core of SIF validation for FLEX. Instruments on towers or masts should permanently monitor a portion of the vegetation below. Ideally, measurements will be of high spectral resolution for both the target and a white reference (or incoming irradiance). If the white reference (or irradiance sensor) is not located at the same distance as the top of canopy, a compensation for the differences in optical path must be applied since the O_2 absorption increases with optical path from the very first meters. The diurnal course should be measured, in order to reduce uncertainty in the SIF retrieval while providing additional information on physiological and photosynthetic state of the vegetation. Instrument placement must be such that the target area is not covered by any extraneous shadows (e.g., self-shading, neighbouring taller elements, etc.), and to avoid any possible canopy inhomogeneity in the surroundings of the tower's base. Pointing should be as close to nadir as possible. The minimum spot size covered by the detector must be at least as large as the smallest characteristic pattern of the target and will depend on canopy structure (MacArthur *et al*. 2013). This is especially critical in forest sites or structured crops (e.g., corn).

5.3.2.2 Field level sampling

Single spot continuous monitoring, however, does not necessarily represent the spatial variability of the field area, especially for less homogeneous or large fields (e.g., forests). An effective strategy is to define several scattered smaller areas or Elementary Sampling Units (ESUs) within each field, the number ESUs per field dependent on the extension of the field and degree of large-scale spatial variability within the field (Fitzpatrick-Lins 1981; Justice & Townshend 1981). Sampling pattern within each ESU will depend on the degree of heterogeneity of the vegetation. Multiple fixed instruments working in a network – or one instrument mounted on a movable platform – will be needed.

5.3.2.3 Landscape level measurements

A landscape can cover not only different vegetation types but also non-vegetated surfaces. Airborne high spatial resolution data can function as an intermediate link between field measurements and FLEX products.

Two approaches may be pursued:

- Derivation of SIF **directly** from proximal RS data: A high spectral resolution sensor is required. Fortunately current hardware and optical developments (ground and airborne) are yielding improved availability and cost for such instruments.
- Derivation of SIF **indirectly** from RS data: A spectrometer with limited spectral resolution prevents direct SIF retrievals. In this case a canopy fluorescence model would be used, and fed with inputs from moderate spectral resolution sensors (e.g., LAI, chlorophyll content, etc.) and environmental parameters from a flux tower.

SIF derived directly from airborne data

A spectral fitting method may be applied to the data. Accurate SIF retrievals from an airborne sensor are possible if certain conditions are met, including accurate atmospheric characterisation, availability of a detailed DEM, consideration of observation geometry and ground-sensor distance of each pixel, high sensor SNR in both O_2 bands, characterisation of sensor PSF and stray light, and consideration of angular effects due to differences in field of view between airborne and satellite systems. As a quality check, retrievals over bare soils must result in near zero SIF estimation.

It is anticipated that ongoing developments in miniaturised hyperspectral imagers – which may be mounted on low-altitude platforms such as unmanned aerial vehicles (UAVs), either multi-copters, airships, or motorised zip-lines – may allow such instruments to be used to build an extensive SIF map for numerous validation sites, instead of the current prospect of just a few aircraft-based ones.

SIF modelled from combined remote sensing and field data

A combined remote sensing and field data approach could be used to produce a high-resolution regional map of SIF when extensive TOC SIF measurements are not available. This approach would involve area mapping from high spatial resolution imagery, derivation of spatially distributed biophysical and structural parameters (including identification of vegetation and bare soil areas) via some standard classifier or a land-use map, and merging of that data with the corresponding *in situ* leaf fluorescence measurements. A canopy model can be inverted appropriately to yield photosynthesis/biochemical estimations of parameters. With sufficient sampling, a statistical regression could help extrapolate to other points away from the ESUs; otherwise, the average value of the estimated photosynthesis/biochemical parameters could be assumed for the whole field. If leaf level SIF measurements are not available for all points or vegetation types, a physiological leaf model coupled to the RT canopy model could be used to estimate SIF emission, albeit with a decrease in accuracy of the validation. Remote sensing data can come from airborne sensors or from high spatial resolution satellites with the necessary capabilities (e.g., Sentinel-2 or NASA's Landsat Data Continuity Mission, LDCM).

Reliability of this method is lower due to uncertainties of the measured biophysical parameters and the assumptions and applicability of the models. For instance, stress might or might not be included in the modelling of photosynthesis processes; complex canopies (e.g., forests, row-planted crops) might or might not be well represented by RT models.

5.3.2.4 Comparing in situ *SIF map with FLEX SIF product*

The resulting SIF map must be convolved to the spatial resolution of FLEX using the available geometry of acquisition and the sensor's PSF to project each pixel's field of view onto the SIF map overlaid to the DEM (Amorós-López *et al.* 2011). Importantly, non-fluorescent targets and bare soils in particular must be checked to ensure that FLEX provides a near zero value for these targets; if it does not, the atmospheric correction must be recalibrated in the absorption bands and/or the retrieval algorithm. An additional check should include analysis of seasonal and

yearly trends in retrieved SIF evolution over selected targets and comparison with *in situ* measurements. For proper validation, the area being tested must be sufficiently large as to provide at least one pure pixel in FLORIS. Sites should be spatially homogeneous and with a single vegetation type, so that single point TOC SIF measurement from towers can be well correlated with FLEX SIF retrievals. Reflectance and chlorophyll content should be characterised to discriminate temporal evolution of SIF from other evolving parameters.

5.3.2.5 Leaf level measurements

Leaf level measurements are useful in validation of canopy level retrievals. For support sites (not core sites), data might come from external published research where available, and not necessarily from a dedicated experiment within the FLEX mission. In any case, several issues must be considered, since linking leaf level fluorescence emission with canopy-leaving fluorescence is not a trivial task.

Multiple scattering within the canopy favours reabsorption of the red fluorescence and re-emission of far-red fluorescence, which complicates the comparison. **Canopy RTMs** include fluorescence excitation and emission (from both sides) to incorporate effects of canopy structure. Currently, only a few canopy models incorporate fluorescence – e.g., SCOPE (Van der Tol *et al.* 2009, Magnani *et al.* 2009), FluorSAIL2 (Miller *et al.* 2005, Pedrós *et al.* 2010), Fluspect (Verhoef 2011) – and they deal only with 1-D canopy structure. Also, 3D canopy models – such as FLiES (Kobayashi 2014), FLIGHT (Alton *et al.* 2007), DART (Gastellu *et al.* 2004; Malenovský personal communication) and Maier's[2] – might be sufficiently developed for future use with FLEX. Alternatively, validation could focus on homogeneous canopies, characterised by high fractional vegetation cover (FVC) and low structural effects (e.g., dense grass), in which fluorescence emission is mainly from the uppermost leaf layer.

Whenever simultaneous leaf and canopy fluorescence measurements are collected, a validation of the leaf-to-canopy upscaling should be performed, preferably over as many vegetation types as possible throughout the biomes. These would be carried out mostly during dedicated field campaigns, especially at core sites. Only a limited amount (in frequency and space) of such leaf-canopy validation might be feasible during the mission lifetime, but new developments in autonomous instrumentation (OPTIMISE COST-Action[3]) could change that.

5.3.2.6 Sampling strategies

Sampling within ESUs should take into account several considerations (Fitzpatrick-Lins 1981), including the spatial distribution of ESUs within a study area; the number of ESUs required within a study area; the required size of the individual ESU; and the number of ESUs required within one field or sample site. A standard procedure should be followed for sampling. Specific guidelines taking into account the density and homogeneity of vegetation cover are available in the literature (e.g., Vuolo *et al.* 2010).

[2] http://riel.cdu.edu.au/research/opportunity/2015/development-canopy-radiative-transfer-model-including-chlorophyll
[3] http://optimise.dcs.aber.ac.uk/

5.3.2.7 Incorporation of data into a common database

Datasets must be harmonised to facilitate production of compatible and consistent results from all validation sites. To achieve this, it is necessary to have: a common data format; format conversion algorithms to adapt data coming from already running external databases and instruments; a centralised database server; and automatic download and processing of data collected by the different systems.

5.3.2.8 Validation timeline

A timeline for validation activities is shown in Figure 5.3. Prior characterisation of selected calibration/validation sites is needed to determine the most adequate sampling strategy (i.e., instrument type) in each case. Posterior re-characterisation might be needed, especially at CVS sites that present strong seasonal evolution or odd behaviours with respect to expected seasonal or long term trends.

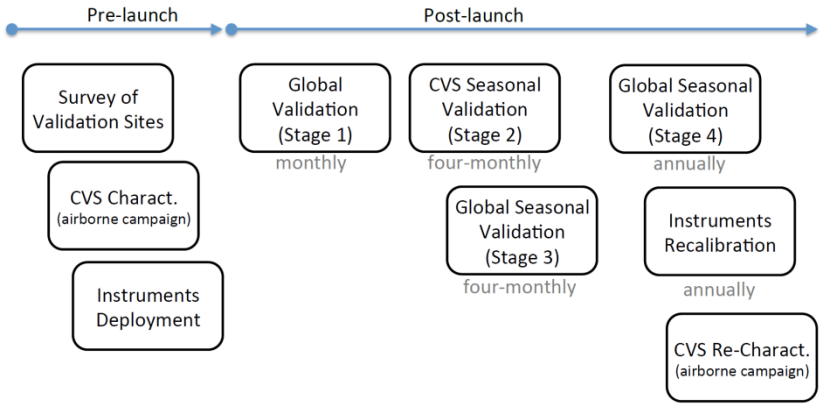

Figure 5.3. Time line of validation activities.

5.3.3 Validation sites

5.3.3.1 Spatial coverage of validation

The major drivers modulating the SIF emission at canopy level are vegetation type (structure, leaf type, spacing) and PAR. To ensure a global validity of a FLEX SIF product and to assess its confidence level, a balanced representation of global vegetation types is required. Vegetation types can be associated to biomes or ecosystems, that is, regions with similar climatic conditions with more or less the same kind of abiotic and biotic factors spread over a large area, creating a typical ecosystem over that area [Figure 5.4]. Incoming radiation depends on the season of the year, time of the day, and latitude. It is necessary to distribute permanent validation sites throughout all latitudes, so a relatively extensive network of validation sites is indicated.

The different sites will be classified as Core, Support and Auxiliary sites, depending on the completeness of their available instrumentation, and thus the degree of precision achieved for the validation process (Table 5.2). **Core sites** are established research sites explicitly dedicated

to continuous monitoring of solar-induced SIF, with sound financial support to assure their availability during the mission operative lifetime. **Support sites** can be from an existing network where most of the required infrastructure and ancillary data are already available; then it is only necessary to deploy and install instruments for SIF measurements. **Auxiliary sites** are additional networks that would help to determine baseline error and offset in the retrieval algorithm to make estimations over non-vegetated regions.

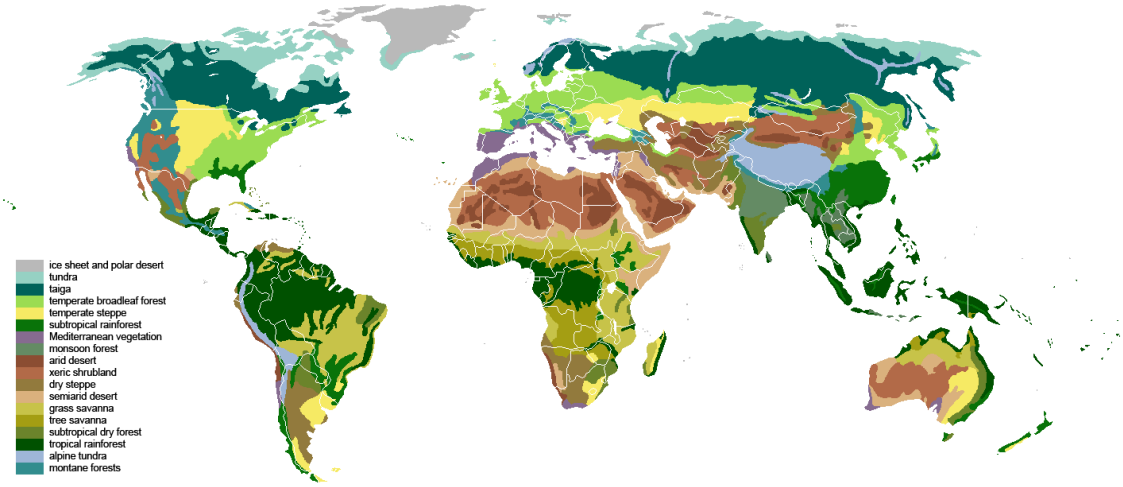

Figure 5.4. Global distribution of biomes.

Table 5.2. Classification of validation sites according to their purpose.

CVS Type	Purpose
Core	• Must include all ancillary measurements needed • Stage 1 validation only • Highest accuracy, best error budget
Support	• Use of already existing network, e.g., FLUXNET • Need to install SIF-specific instrumentation • Stage 2 to Stage 4 validation
Auxiliary	• Radiometric cal/val sites, e.g., CEOS cal/val network • Desert locations • Devoted to determine baseline and offset error (zero fluorescence) • FLORIS performance characterisation and recalibration

A validation scheme for **core sites** is presented in Figure 5.5.

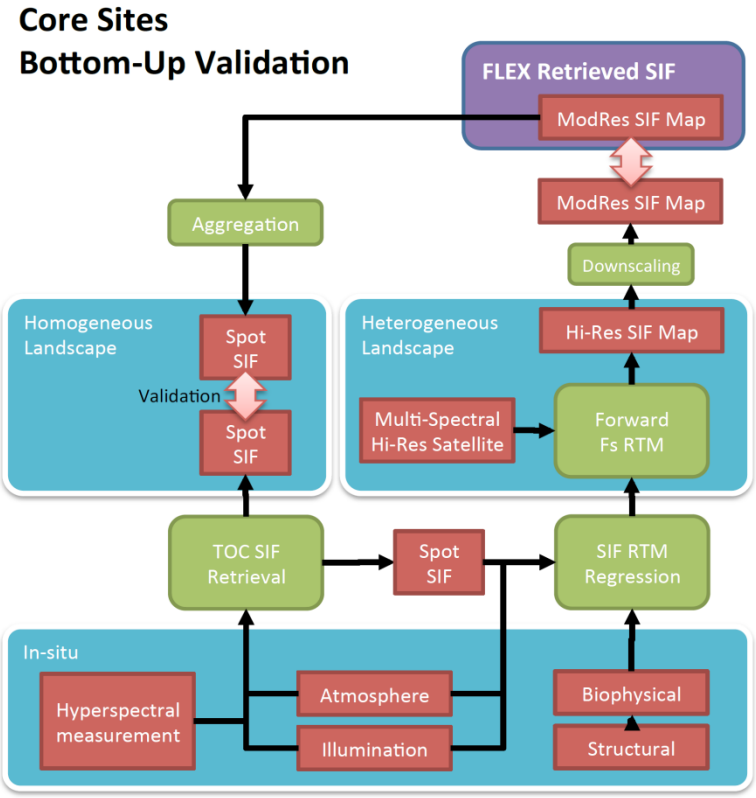

Figure 5.5. Validation scheme for core sites.

At this time, we are aware of only a few sites that perform continuous monitoring of canopy-level SIF, so further effort to identify more sites is needed. Known sites include (i) Avignon-Montfavet, a site maintained by the CNRS Laboratoire de Météorologie Dynamique (LMD) (France) at INRA's research area in Avignon; (ii) the Transregional Collaborative Research Centre 32 (TR32), Jülich (FZJ) (Germany); and (iii) the Bílý Kříž (Bily Kriz) site, maintained by CzechGlobe (Czech Republic).

For **support sites**, a promising network is FLUXNET (Figure 5.6 and Figure 5.7). This system of regional networks measures the exchanges of carbon dioxide (CO_2), water vapour, and energy between terrestrial ecosystems and the atmosphere. Over 500 tower sites are operated on a long-term and continuous basis, with distribution ranging from 70 degrees north to 30 degrees south.

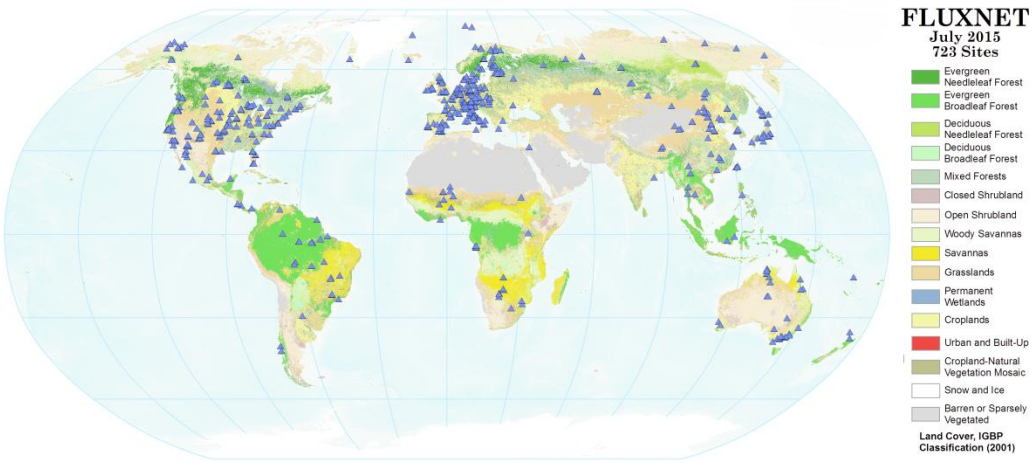

Figure 5.6. Global distribution of FLUXNET measuring stations.

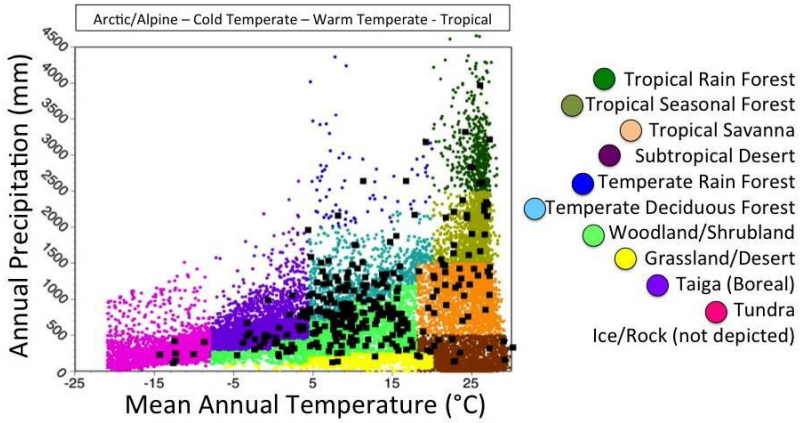

Figure 5.7. Diagram depicting FLUXNET coverage of biomes.

For **auxiliary sites**, the CEOS Cal/Val network could be suitable, since it covers most regions of the planet, and follows a strict standardisation of the measurement protocols.

5.3.3.2 Dedicated validation campaigns

Despite having an extensive network of validation sites available, in the best case only a few complete datasets of fluorescence, photosynthesis, fluxes and biophysical parameters spatially distributed over several vegetation types or biomes may be available. Airborne FLEX simulators could be used to extend validation over large regions, providing the highest validation accuracy. Alternatively, airborne hyperspectral sensors capable of resolving the O_2 absorptions could be used at the cost of reduced accuracy. Extensive ground truthing with these activities should measure every parameter relevant to the retrieval and interpretation of the SIF signal. These will be used to test all aspects of the process applied at permanent validation sites.

Dedicated field campaigns, due to their complexity and costs, will take place sporadically and be limited to a few selected sites. Such campaigns are foreseen to take place mostly during commissioning and the early operational phases of the mission. A validation scheme for dedicated field campaigns is shown in Figure 5.8.

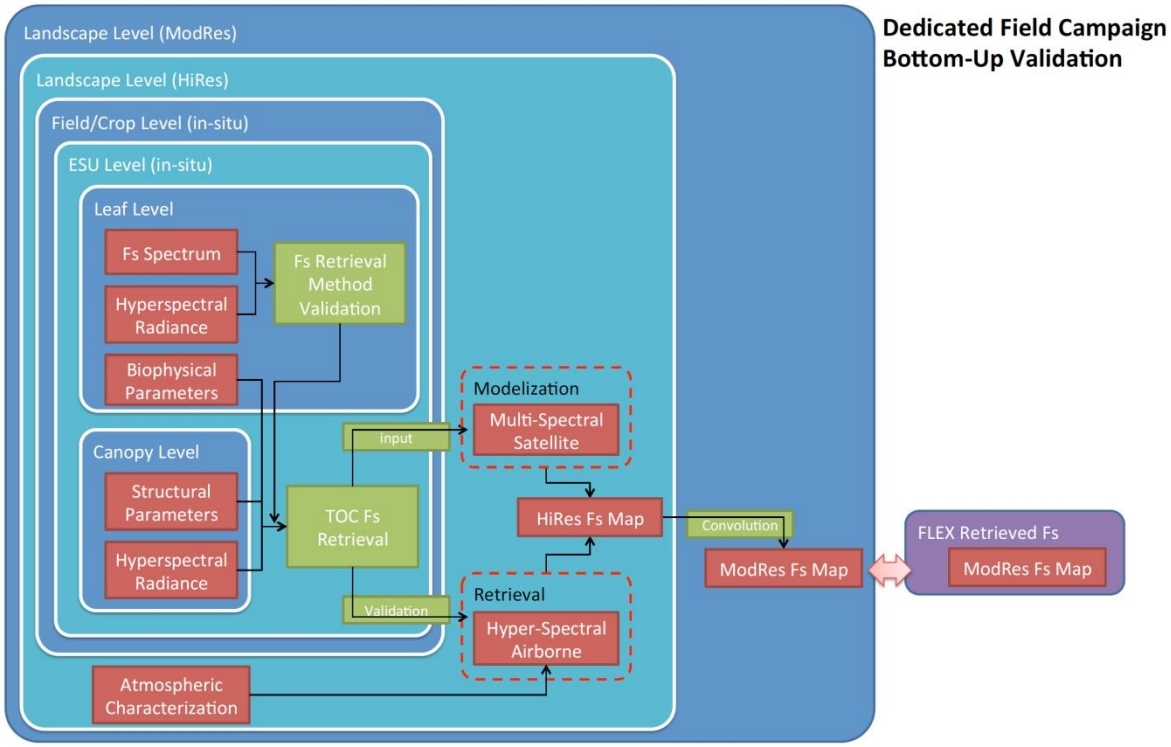

Figure 5.8. Validation scheme for dedicated field campaigns.

5.3.4 Instrumentation requirements

Requirements described here refer only to instruments necessary for SIF measurement. Other ancillary measurements already have established protocols and common instrumentation, so thus will not be specified here.

5.3.4.1 Canopy level spectrometers

Spectrometers used for canopy measurements will need to spectrally resolve O_2-A and O_2-B absorptions, with high SNR. They do not need to provide the same spectral bandwidth and resolution as FLORIS since the spectral calibration can easily be performed at the laboratory, but they should have a maximum Full Width at Half Maximum (FWHM) of 1.5 nm for the main absorption at O_2-A and 0.7 nm for the O_2-B in order to resolve SIF with the highest accuracy (Alonso & Moreno 2012). Instrumental setups for field and landscape measurements are depicted in Figure 5.9.

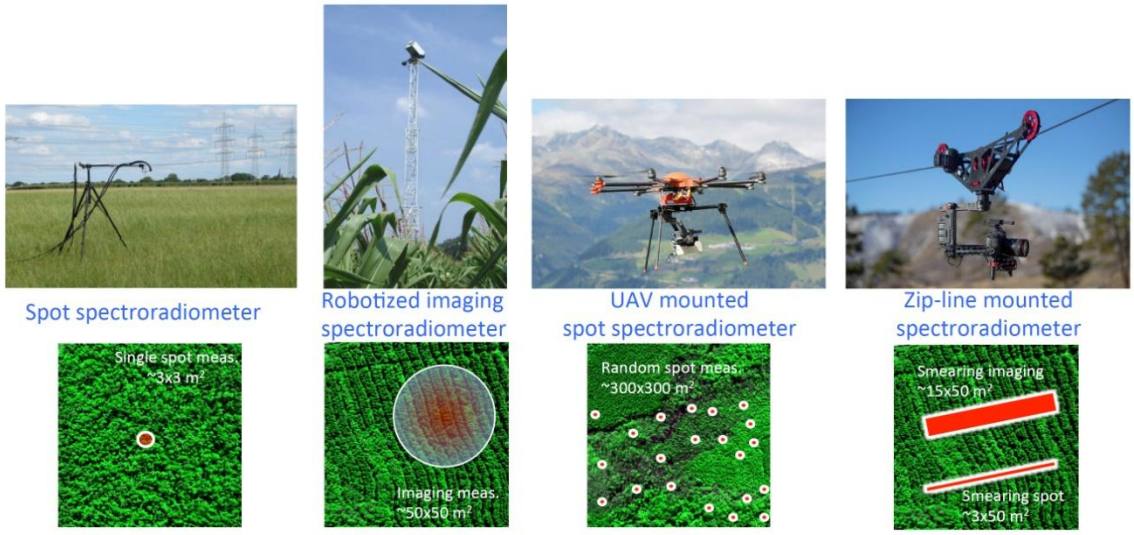

Figure 5.9. Instrumental setups to achieve field and landscape characterisation using various sampling strategies.

Instruments placed at core and support validation sites should perform permanent and continuous measurement (diurnal cycle) on a selected spot to allow obtaining of measurements simultaneous to FLEX acquisitions and to reduce retrieval error by fitting noisy data to smooth trend curves. Systems performing these measurements will need to be properly protected for weather and include a system to autonomously measure both white reference and target. Some of the systems already operating include:

- S-FLUOR Box (Jülich Research Centre, FZJ, Germany);
- Multiplexer Radiometer Irradiometer (MRI) (University of Milano-Bicocca, Italy);
- FUSION (NASA Goddard Space Flight Centre, USA); and
- AMSPEC-II (University of British Columbia, Canada).

Additionally, developments have been underway to mount spectrometers on autonomous UAVs (Burkart *et al.* 2014; Zarco-Tejada *et al.* 2012). Also, there are computer-controlled motorised zip-line dolly systems (e.g., flyline cable cam[4]), which deploy a zip-line between two towers or poles running high over the canopy, with a cradle that holds an automated spectroradiometer. Promising efforts on developing these systems are being coordinated by A. MacArthur at NERC (COST/OPTIMISE)[5], including the instrument characterisation requirements to obtain the highest accuracy in SIF retrievals.

5.3.4.2 Leaf level SIF fluorometers

The proposed leaf level instrumentation is a customised hand-held leaf clip (FluoWat) attached to a calibrated spectroradiometer using an optical fibre (Van Wittenberghe *et al*. 2013; Alonso & Moreno 2010). This leaf clip is a portable device that allows measuring real leaf reflectance,

[4] http://www.photoshipone.com/flyline-cable-cam-system/flyline-features/
[5] http://optimise.dcs.aber.ac.uk/

transmittance and fluorescence emission under natural conditions, whereby the fluorescence signal is measured by placing a short-pass filter that blocks incident light in the spectral range of SIF emission (>650 nm), thus permitting only the SIF signal to reach the sensor. Incoming radiance is measured as the sun-reflected radiance of a white standard panel placed in the clip, before and after each single measurement, with and without filter, and from which PAR can be integrated. Light absorbance by the leaf in the PAR region (fAPAR) can be derived from the leaf reflectance and transmittance measurements, permitting calculation of the light that is actually absorbed and usable for photosynthesis (APAR).

The spectroradiometer does not need to have high spectral resolution because the full emission spectrum is being measured. However, the fluorescence intensity is low compared to reflected radiance, thus a good SNR (>300) is required.

At present, we are not aware of other comparable systems capable of directly measuring red and far-red SIF (or the full emission) *in-vivo* under natural conditions.

5.3.4.3 Airborne spectrometers

Ideally, the airborne sensor for dedicated campaigns should be able to provide FLEX-like data. At this time, the only such instrument is *HyPlant* (Rascher *et al.* 2015). Alternatively, other hyperspectral sensors with coarser spectral resolution might be used, provided they are able to detect a SIF signal (Damm *et al.* 2015a; Panigada *et al.* 2014), e.g., the CASI-1500, AISA-Eagle, or APEX.

HyPlant is a hyperspectral imaging system for airborne and ground-based use developed by Forschungszentrum Jülich (Germany) and manufactured by SPECIM Spectral Imaging Ltd. (Finland). The system measures from 370 to 2500 nm and consists of five components: a dual channel VNIR & SWIR imager; a fluorescence imager; a data acquisition and power unit; a position and attitude sensor; and an adjustable mount. The fluorescence imager produces data at high spectral resolution (0.25 nm bandwidth and 0.1 sampling) in the spectral region of the two oxygen absorption bands.

The Compact Airborne Spectrographic Imager (**CASI**) (Itres, Canada) is a hyperspectral pushbroom sensor in the VNIR range (370 to 1051 nm). CASI can be set to a Spectral Mode that provides 288 bands with the highest spectral resolution in order to be able to resolve at least the O_2-A absorption band.

The **AISA Eagle** (SPECIM) is a hyperspectral sensor that covers the VNIR range (400-970 nm). It has 488 spectral channels, and a maximum spectral resolution of 2.9 nm, which restricts its use to the O_2-A band at best.

APEX is an airborne imaging spectrometer developed by a Swiss-Belgian consortium on behalf of ESA. It is intended as a simulator and a calibration/validation device for future spaceborne hyperspectral imagers. It records hyperspectral data in approximately 300 bands in the wavelength range between 400 nm and 2500 nm and at a spatial ground resolution of 2 m to

5 m, providing a spectral sampling interval of 0.55 to 8 nm, and spectral resolution of 0.6 to 6.3 nm, depending on the binning selected.

5.3.4.4 Satellite sensors

Satellite sensors preferably must provide a spatial resolution of at least one-tenth of the FLEX footprint, that is 30 m/pixel (although coarser resolutions might be also useful) in order to provide sub-pixel information for upscaling heterogeneous contributions with the proper proportionality. They must also provide a band setting that allows retrieval of necessary biophysical parameters in order to feed into the fluorescence models. Favoured missions are ESA's GMES Sentinel-2 and NASA's LDCM since they provide an extensive set of bands and they benefit from legacy retrieval algorithms. Other suitable sensors should also be considered to increase the chance to have a supporting image close to the FLEX acquisition date.

Sentinel-2 will carry an optical payload with visible, near infrared and shortwave infrared sensors capturing 13 spectral bands: 4 bands at 10 m, 6 at 20 m and 3 at 60 m spatial resolution (the latter dedicated to atmospheric corrections and cloud screening), with a swath width of 290 km. The 13 spectral bands guarantee consistent time series, indication of variability in land surface conditions, and minimisation of artefacts from atmospheric variability.[6]

The **Landsat Data Continuity Mission (LDCM)** is the future of Landsat satellites. It will continue to obtain valuable data and imagery to be used in agriculture, business, science, and government. The Landsat Program provides repetitive acquisition of high-resolution multispectral data of the Earth's surface on a global basis. Data from Landsat spacecraft constitutes the longest record of the Earth's continental surfaces as seen from space.[7]

5.4 Definition of FLEX Level-2/3 products and their validation plan

There are Level-2 products to be derived exclusively from FLEX (those related to photosynthesis), and other auxiliary products to be derived from S3/FLEX synergy. In this section, the Level-2 and Level-3 products proposed for the FLEX mission and their validation plan are described. They consist primarily of photosynthesis-related parameters that help to determine vegetation functioning and health status (Table 5.3).

Photosynthesis-related parameters require the highest retrieval accuracy. Those parameters include fAPAR, LAI and chlorophyll content, which are already offered by Sentinel-3. But since FLEX will provide higher resolution and sampling in the spectral regions sensitive to those parameters, this will allow their estimation with improved precision and accuracy.

Common biophysical parameters, such as Chl, LAI, fractional vegetation cover (FVC), or LST will be estimated using synergy of S3/FLEX, so these products also need to be validated. (They will be kept for internal use to avoid interfering with S3 official products).

[6] http://www.esa.int/esaLP/SEMTST4KXMF_LPgmes_0.html
[7] http://ldcm.nasa.gov

The validation process will be based on correlation estimation between satellite-derived values and *in situ* measurements, and requires upscaling of the *in situ* localised measurements to the satellite pixel size of 300x300 m^2/pixel. Some parameters are measurable only at the leaf level, in which cases two options could fill the intermediate step of canopy level estimation: (i) upscaling by means of RTM; and (ii) estimating the parameter from TOC spectroradiometer data using algorithms similar to those applied to FLEX data. Existing networks of measuring stations that support Global Earth Observation products can help fulfil these requirements.

Table 5.3. FLEX Products with their *in situ* measurement method and expected availability with respect to validation site type

	Product	Measurement Method	Val Sites
Level-2 Photosynthesis	PS-I PS-II contributions	Leaf: passive SIF Canopy: RTM upscaling	Core
	Fluorescence quantum efficiency	Leaf: active/passive SIF Canopy: RTM upscaling	Core
	Photosynthesis rate	Leaf: active F / gas exchange Canopy: gas exchange	Core
	Vegetation stress	Leaf: active/passive SIF Canopy: Monitoring of biophysical parameters	Core
	GPP	Canopy: gas exchange Landscape: flux tower	Core
	fAPAR	Leaf: clip spectroscopy Canopy: ceptometer network	Core & support
Level-2 Biophysical	LAI	Canopy: DHP[1] / LAI-meters	Core & support
	Chlorophyll	Leaf: RTM inversion Canopy: RTM inversion	Core C & S
	FVC	Canopy: DHP	Core & support

[1]Digital hemispherical photography

5.4.1 Biophysical parameters

The strategy for FLEX validation of biophysical parameters is to follow the S3 validation plan and CEOS protocol for similar products (Morisette *et al.* 2006) to implant these protocols at the selected core validation sites. There is also an increasing number of fAPAR and LAI validation sites that support a global network for validation of Global Climate Observation Systems (WMO-GCOS) (World Meterological Organization 2011).

5.4.1.1 Fraction of absorbed PAR (fAPAR)

The fAPAR refers to the fraction of PAR (400-700 nm) that is absorbed by a vegetation canopy. Since fAPAR is difficult to measure directly, it is inferred from models describing the transfer of

solar radiation in plant canopies, using remote sensing observations as constraints. Ground-based estimates of fAPAR require the simultaneous measurement of PAR above and below the canopy as well as architecture information to account for any non-foliar absorption. The fAPAR assessments are retrieved from space remote sensing platforms by numerically inverting physically-based models. Most of the derived products represent only the fraction absorbed by the live green part of the leaf canopy (Gobron & Verstraete 2009). While there is a range of methodologies for measuring fAPAR, the use of PAR meters located above and below the canopy is well-accepted. Integration of the individual measurements may be done using the approach of e.g., Eklund *et al*. (2011). In some environments, it might be advisable to deploy a network of sensors and wireless autonomous loggers (Rankine *et al*. 2014).

5.4.1.2 Leaf area index (LAI)

LAI is the fraction of leaf area over a given ground area. It is an indicator of the amount of green vegetation in a given location. Thus here green LAI is considered – and not total LAI – since it is the one used in most canopy models. A criterion for selection of core sites is that they should provide LAI monitoring based on methodology that takes into consideration gap fraction and leaf/wood separation, particularly following recommendations by Woodgate *et al*. (2015). Examples of suitable instruments include TRAC (Leblanc *et al*. 2002), PASTIS-57 (Simic *et al*. 2012), and VEGNET instruments (Portillo-Quintero *et al*. 2014), while appropriate methods include DHP (Leblanc & Fournier 2014), LAI-2200 (Leblanc & Chen 2001), and TLS LAI/PAI inversion methods (Jupp *et al*. 2009).

5.4.1.3 Chlorophyll content

Leaf chlorophyll concentration is the amount of chlorophyll present in the leaf, measured on a mass per leaf area basis. Since fluorescence is emitted from these pigments, the concentration is directly related to the potential fluorescence emission. Canopy chlorophyll content denotes the total amount of chlorophyll per unit area of the ground. Despite that leaf chlorophyll content has a vertical distribution within the canopy, in first approximation it might be estimated by multiplying the leaf area index and the chlorophyll concentration of the leaves (Dash *et al*. 2010).

Chlorophyll content validation is a particular case, since the retrieval proposed within FLEX estimates leaf chlorophyll content from RTM inversion. In this sense, the estimation would correspond to an effective value, and not necessarily to a mean one. Therefore, the proper way to validate this product should apply the same RTM inversion to the TOC radiometric measurements, besides measuring at leaf level which will be routinely done at core sites.

5.4.1.4 Fractional vegetation cover (FVC)

Fractional vegetation cover is the percentage of a unit surface area covered by vegetation from a nadir view. It is an estimate of clumping or discontinuity in the canopy. For some applications it is important to distinguish between total FVC – which includes leaves, stems, branches and the rest of the plant elements – and green FVC which only accounts for the green parts (mainly leaves) since these are the tissues performing photosynthesis.

5.4.1.5 Water content

Water content is the proportion of water stored in the leaves with respect to the total amount of material. Typical measurement methods are destructive sampling, spectral indices based on water absorption features, and numerical model inversion (Panigada *et al*. 2014).

5.4.1.6 Land surface temperature (LST)

Validation with ground-based measurements involves a comparison of satellite-derived LST with collocated and simultaneously acquired LST retrievals from *in situ* radiometers. The primary uncertainties in ground-based LST retrieval are associated with the accuracy of surface emissivity and down-welling radiance (Hook *et al*. 2007). Generally, neither spectral nor directional measurement of downwelling thermal radiation from the atmosphere is routinely sampled in the field. When derived from models or directional measurements, estimates of atmospheric radiation can have significant uncertainties, especially for warm and humid atmospheres. To represent the spatial variability within a satellite pixel, it is assumed that the sub-pixel temperature variability is mainly due to land cover heterogeneity and to variability in surface biophysical parameters, such as vegetation density, emissivity or albedo. The method estimates the temperature of each land cover class inside a mixed pixel using a land surface model driven by the measured atmospheric forcing and observed surface biophysical properties from a nearby tower/site. The atmospheric forcing is assumed to be uniform over the satellite footprint (Guillevic *et al*. 2014).

5.4.1.7 Canopy structural parameters

Other structural canopy parameters allow determination of geometrical structure and spatial distribution of the canopy. They will depend on the nature of the vegetation, and on the input requirements of the numerical models. Examples are Leaf Angle Distribution (LAD), canopy height, stand density, row distance and orientation, trunk diameter at chest height, height of first stem, etc. Recent advances in terrestrial and airborne LIDAR allow reconstruction of the 3D structure of the canopy with sufficient accuracy to derive most of the structural parameters (Jupp & Lovell 2007) – or even to use it as input in 3D RTMs (Schneider *et al*. 2014).

5.4.2 Photosynthesis related parameters

Photosynthesis is the process by which plants absorb CO_2 from the atmosphere (Gross Primary Productivity, GPP) and water and nutrients from the ground in order to produce biomass (Net Primary Productivity, NPP), releasing O_2 and part of the absorbed CO_2 in return. GPP is also related to the global water cycle, due to the strong coupling between photosynthetic rates and canopy transpiration.

Photosynthesis, CO_2 and water exchange can be measured *in situ* at leaf level using gas exchange chambers (some of them also measure fluorescence, e.g., LiCor LI-6400XT or Walz GFS-3000), but scaling up to the canopy level is not always easy due to non-linearities. Measuring photosynthesis exchanges at canopy level requires use of eddy-covariance towers (Baldocchi 2003), and these will be available at core and support validation sites.

5.4.2.1 PSI - PSII contributions

Photosynthesis utilises light energy to reduce carbon dioxide to sugar. The energy of light quanta is gained for photosynthesis through light absorption by the pigments in the photosynthetic pigment–protein complexes. In higher plants, these are the PSI and PSII complexes, and the pigments involved are the carotenoids and chlorophyll *a* and *b*. The dynamic portion of fluorescence emission has been associated to PSII, whereas PSI contribution to fluorescence emission is considered to be more stable. The contribution of PSI is mainly at the far-red emission band, while PSII contributes to both emission bands around 685 nm and 740 nm (Palombi *et al*. 2011).

PSII is the main target of mechanisms responsible for the photochemical and non-photochemical quenching, whereas PSI seems to be much less sensitive to photochemistry (Krause & Weis 1991) and more resistant than PSII to strong light stress (Havaux & Eyletters 1991). Therefore, the possibility to separate both contributions would result in very valuable information about the photosynthesis status.

Leaf level passive measurement of spectrally-resolved SIF would provide reliable estimates of PSI and PSII contributions to emitted fluorescence. This can be achieved by the analysis of the slow fluorescence dynamic of the Kautsky effect (Palombi *et al*. 2011). Also, it is possible to estimate PSI by using a 708nm monochromatic excitation light (Franck *et al*. 2002), by means of spectral separability assuming a fixed shape for the PSI contributions. Once the leaf level contributions have been established, this information – together with leaf reflectance, transmittance, canopy structural parameters and illumination conditions – can be fed into the canopy fluorescence RTM that will provide TOC PSI and PSII contributions, while taking into account all the reabsorptions and multiple scatterings that affect the total fluorescence emission.

5.4.2.2 Fluorescence quantum efficiency

This parameter corresponds to the ratio between energy emitted as fluorescence versus actual chlorophyll specific absorbed energy. Active systems (e.g., Moni-PAM) provide quantum efficiency at leaf level. A sufficient number of samples should be measured continuously around the overpass time in order to estimate the variability. Additionally, spatial sampling should take place representing all the illumination conditions within the canopy (Porcar-Castell *et al*. 2008, 2011). The FluoWat leaf clip may be used to measure both parameters: total SIF emitted energy and absorbed energy. At canopy level, measurement with the monitoring spectroradiometers and estimation of APAR from the PAR sensors distributed around the area will allow estimation of canopy level quantum efficiency.

5.4.2.3 Photosynthesis rate

InfraRed Gas Analyser (IRGA) systems measure gas exchange and photosynthesis rate at leaf, shoot or small-canopy level. Also at the leaf level, a PAM system may be used if illumination on the leaf is kept stable for a sufficient period before the measurement (Kolari *et al*. 2007).

5.4.2.4 Vegetation stress

There are many stresses that can inflict a cascade of structural, functional, and performance effects in vegetation (see Section 3). The CVS sites should incorporate, if not already available, the necessary instrumentation to monitor vegetation stress. For example, in the case of water stress, soil moisture probes should be available together with the standard flux tower measurements in order to provide evapotranspiration. Continuous measurement of PAR allows determination of cases where light stress can occur, e.g., on the first sunny days after winter in high latitudes. Similarly, leaf and air temperature probes are needed to determine temperature stress. Active fluorescence systems such as IRGA and MoniPAM are capable of determining if the actual photosynthesis rate is smaller than potential rate, indicating a possible stress regime.

5.4.2.5 Activation/deactivation of photosynthetic machinery

This parameter determines actual length of the growing season. It may be derived by data assimilation with a dynamical vegetation model accounting for temporal changes. Since the repeat cycle of FLEX overpass is a little less than once a month at equatorial sites, determination of the activation/deactivation date must be achieved by fitting a vegetation dynamical functional model to acquired data. It might also be necessary to refine estimates by reanalysing the time series as new observations are incorporated. At the higher latitudes the repeat cycle is shorter and the first estimations will probably be quite accurate already. Continuous monitoring with active and passive fluorescence systems will help to indicate when the vegetation shifts from a photorespiratory state to a photosynthetically active one.

5.4.2.6 Gross primary productivity (GPP)

GPP is derived by data assimilation with usage of external inputs (meteorological data, land-cover maps). Since all core validation sites will belong to a CO_2 flux monitoring network, the availability of high quality estimation of GPP (Reichstein *et al*. 2005) at different temporal scales is assured (Yang *et al*. 2015).

5.4.3 Atmospheric/illumination parameters

Information is required on weather conditions during *in situ* measurements. Aerosol optical thickness, ozone and water vapour in the atmosphere can affect radiance measurements taken at the sensor. While these atmospheric conditions are unlikely to have an impact on *in situ* measurements from field spectrometers, they will affect airborne and satellite acquisitions. Collection of meteorological data can be used to validate the atmospheric correction applied to satellite and airborne data, and to help upscale *in situ* measurements to at-sensor values.

5.4.3.1 Aerosols

Aerosols are the most critical atmospheric constituent affecting the retrieval of SIF, since they produce an infilling effect of absorption bands in a similar way as does fluorescence. However, the spectral shape of this additive term is quite different than the shape of fluorescence, allowing the separation of both contributions. The degree of interaction of aerosols with light

depends on aerosol load and nature (composition, size, shape). While under/over-estimation of aerosol optical properties could lead to over/under-estimation of the surface apparent reflectance, respectively, its spectral behaviour will be smooth. Consequently, it affects the shorter wavelengths but does not present any abrupt absorption spectral areas.

5.4.3.2 Surface pressure

O_2 spectral absorption bands, in which fluorescence is mainly estimated, present a strong dependency on surface pressure. This parameter should be measured at least at surface level. Variations in atmospheric surface pressure could modify the shape of the O_2 absorption band, creating an artificial infilling that could be misinterpreted as fluorescence.

5.4.3.3 Water vapour

Water vapour is easily quantified since location of its spectral absorption band regions are well known. However, changes in relative humidity (water vapour content) also produce changes in aerosol scattering. A challenge with water vapour is that it presents a strong spatial variation that is difficult to characterise. Therefore, *in situ* measurements should allow determination of a value around which the atmospheric correction will be evaluated.

5.4.3.4 Air temperature

Top-of-canopy air temperature, which is a standard product of flux and eddy towers, is necessary to evaluate the difference of leaf/air temperatures, which is an indication of how strong the thermal dissipation mechanism is with respect to the other quenching mechanisms. In this way, it is possible to identify stress situations from regular evapotranspiration.

5.4.3.5 Direct and global solar irradiance

By measuring global and direct solar irradiance at surface level, it is possible to determine aerosol type and load and water vapour presence, and to validate proposed atmospheric retrieval strategies. Typically, these parameters are provided as integrated values in the full solar spectrum. For the FLEX mission, additional measurements of the PAR contribution will be necessary. Also, it is advisable to install instrumentation to provide spectrally-resolved direct and global components of the solar irradiance, ideally with resolution similar to FLORIS.

5.4.3.6 Cloud cover

Areas located in the vicinity of bright clouds – or even directly covered by thin clouds – can be affected by an extra light contribution that can also produce artificial infilling of O_2 absorption bands, thus disturbing the fluorescence retrieval process. Scattered clouds could also affect the distribution of the diffuse component, which might be relevant for sites with strong 3D structural characteristics (e.g., preferential direction on row-planted crops).

5.4.3.7 Daily total PAR irradiance

Daily total PAR irradiance is usually provided by flux towers, and although not necessary for retrieving the SIF signal itself, the total is necessary to relate fluorescence, photosynthesis and GPP. Since FLORIS SIF is an instantaneous measurement, it does not relate directly to daily GPP, but it can constrain the integrated estimate when total PAR is taken into account.

5.4.4 Considerations

Most photosynthesis parameters need to be measured by active systems (PAM) and passive systems (FluoWat) at leaf level. FluoWat needs to be further developed in order to allow automatic continuous monitoring.

In order to characterise illumination and functional situations of the vegetation, it will be necessary to deploy networks of sensors. Guidelines are needed on how to distribute the network to capture the variability of the canopy (e.g., random distribution vs. patterns).

Periodic instrumental calibration (Jin & Eklundh 2015; MacArthur *et al*. 2013), including non-linearity (Pacheco-Labrador & Martin 2013), will be needed in order to avoid bias in retrievals. Also intercomparison of instruments (Anderson *et al*. 2013) might be desirable.

5.5 Definition of a common protocol and state-of-the-art instruments for calibration/validation of fluorescence

The FLEX/Sentinel-3 Tandem Mission study PARCS (Moreno *et al.* 2014) indicated that the use of datasets with different spectral and radiometric resolution and/or covering different spectral ranges can have an impact on the estimated fluorescence values (at both oxygen A and oxygen B absorption bands). Thus the identification of suitable instruments and protocols for fluorescence retrieval is mandatory to be able to define an appropriate calibration/validation plan for the FLEX mission.

Despite the fact that several research groups are now proposing field prototypes based on different spectroradiometer models to monitor top-of-canopy sun-induced fluorescence (Meroni *et al*. 2011, Cogliati *et al*. 2015a, Daumard *et al*. 2010), there is very little published work demonstrating whether data show good reproducibility. This is particularly true for the new generation of lightweight, miniaturised spectroradiometers that are sufficiently compact for easy deployment in the field in a cost-effective manner. In the context of calibration/validation activities, the identification of the most suitable, cost-effective and precise instrument for reliable fluorescence estimates is needed. This will allow the implementation of a network of stable sensors that follow the same measurement standards and calibration protocols across sites (Porcar-Castell *et al*. 2015).

Before systems can be recommended for continuous fluorescence measurements in the field, information is needed on their relative performances. To the best of our knowledge, only one study (Damm *et al*. 2011) quantified the expected impacts of sensor characteristics – such as spectral resolution (SR), spectral sampling interval (SSI), stability, and signal to noise ratio – on

the accuracy of fluorescence retrieval. But that study examined only the potential retrieval of the far-red (O_2-A band) region and was based exclusively on modelled data. Limited consideration was given to comparability of spectral measurement protocols and systems in the field, where instrument performance and quantification of measurement uncertainty under natural illumination are crucial to produce accurate data (Anderson *et al*. 2011).

5.5.1 Review of literature and documentation

A review of proximal sensing measurements regularly performed in Europe has been conducted in the framework of the COST action EUROSPEC ES0930 (Balzarolo *et al*. 2011) and updated in 2014 within the COST action OPTIMISE ES1309[8], which focuses on proximal sensing of sun-induced chlorophyll fluorescence. Although not exhaustive, it provided an overview of the current status of instruments and protocols used to estimate the sun-induced fluorescence from passive remote measurements. Overall, it portrayed the lack of consensus among researchers on what are the most suitable proximal sensing systems and protocols to obtain reliable fluorescence estimates.

Several hyperspectral systems have been developed and proposed in recent years for continuous proximal sensing of sun-induced fluorescence. Some have already provided the first long-term time series of reflectance and fluorescence on different ecosystems while others are still in a testing phase. Instruments dedicated to fluorescence estimation that have been operated for medium to long time periods (from weeks up to a year) are:

- the HyperSpectral Irradiometer (HSI) (Meroni *et al*. 2011);
- the Multiplexer Radiometer Irradiometer (MRI) and its compact version S-FLUOR box (Cogliati *et al*. 2015a);
- the UNIEDI system (Drolet *et al*. 2014);
- the TriFLEX (Daumard *et al*. 2010);
- NASA/GSFC's FUSION (Corp *et al*. 2010);
- the FluoSpec (Yang *et al*. 2015).

All these systems are prototypes, designed by assembling commercially available spectrometers. The spectrometers used are different models of Ocean Optics (Florida, USA) (HR2000+, HR4000, USB2000+) due to their relatively low cost and the possibility of configuring the spectral range and resolution. Their main differences are in the measurement setup and the calibration and acquisition protocol.

Recently, the SIF-Sys (Burkart *et al*. 2015) was developed by the Forschungszentrum Jülich GmbH (Germany) in an effort to address some of the limitations of the other systems. SIF-Sys has been tested in dedicated field experiments and will be installed at flux towers for long term and unattended data collection in the near future.

[8] http://optimise.dcs.aber.ac.uk/

5.5.2 Quality indicators for instrument performances under natural illumination

Characterisation of instrument performance and quantification of measurement uncertainty under natural illumination is crucial to produce accurate data (Anderson *et al*. 2011, Castro-Esau *et al*. 2006). Laboratory measurements can allow the characterisation of some sources of uncertainty (e.g., SNR, linearity) but optimally all uncertainties in field spectroscopy should be evaluated under conditions that typify the measurement scenario (Anderson *et al*. 2011). Such protocols are not yet available, but their development will be essential for evaluation of instrument performances under natural illumination.

A preliminary study by Julitta *et al*. (2015) provided a first quantitative assessment of the reproducibility of fluorescence retrieval at both oxygen bands using actual radiance spectra measured in the field. Using four spectroradiometers (three miniaturised systems from Ocean Optics – two HR4000 and one QE Pro and one ASD Fieldspec Pro), the study analysed the impact of the different device characteristics (e.g., SR, SSI, SNR) on SIF estimates. It found that an ultrafine resolution (less than 0.5 nm) is mandatory to achieve accurate estimates of the red fluorescence, whereas 1 nm is sufficient for the far-red fluorescence. SNR>1000 was recommended for accurate fluorescence estimation, at least under the specific conditions of the study.

Characterisation and calibration of instruments is essential to ensure direct comparison of results. Balzarolo *et al*. (2011) suggested that calibration of the optical sensors should be done at least annually against a common standard in a central laboratory prior to field deployment. However, it should be preferable to have tools to periodically check the stability of the sensor calibration during sensor operation. This can be done in the fields with different methods. Spectral calibration, for example, can be assessed regularly using field-measured irradiance data and the SpecCal algorithm (Busetto *et al.* 2011; Meroni *et al*. 2010).

To support calibration/validation activities, valuable assets would be the availability of a common calibration facility and a field calibration/validation process that ensures consistent data quality and comparability of optical measurements across a wide geographical range of sites in different countries. Portable calibration/verification standards could be provided that meet international standards, with regular re-calibration conducted in the common calibration facility and replacement of components as necessary.

Use of a trusted reference for calibration is described, for example, by Burkart *et al*. (2015) for the SIF-Sys measurement system. In addition, we investigated an approach here using the FluoWat leaf clip as the fluorescence reference standard to evaluate the performance of an OceanOptics QEPro spectroradiometer covering the 651-803 nm spectral range, and the results of fluorescence retrievals using spectral fitting methods (Cogliati *et al.* 2015b; Meroni *et al.* 2010). We found that the approach could be a valuable procedure to assess instrument performances under natural illumination and to quantify and compare the accuracy associated with fluorescence retrieval with different instruments and retrieval methods.

5.5.3 Optimum strategy for spectral measurements

Conducting *in situ* long-term spectral measurements in the field requires instrumentation specially designed for the task. The COST action EUROSPEC ES0930 has been working (from 2010-2014) to promote development of common measurement protocols and new instrumentation for establishing best practices and standardisation of *in situ* spectral measurements. This network remains active under a new action (OPTIMISE ES1309) initiated in 2014; it will assist the establishment of a network of scientists and industry representatives interested in optical data acquisition at high spectral, temporal and spatial resolutions in order to better understand linkages between light use, plant physiology and ecosystem functioning. This network will also endeavour to expand the work of EUROSPEC to include UAVs and "smart" spectral data storage systems, and it will explore in-depth the measurement and interpretation of multiscale chlorophyll fluorescence data.

Recently, Porcar-Castell *et al*. (2015) provided an exhaustive overview of the main results of EUROSPEC Cost Action. These results can be considered as a starting point for the definition of an optimum strategy for spectral measurements that could be adopted for the calibration and validation of fluorescence products. General requirements for field optical sensors include:

- waterproofing (should withstand direct rain)
- robust design (external parts withstanding tension)
- avoidance of holes and cavities (to prevent damage from birds, insect nests, etc.)
- attachments for easy field installation
- minimum payload (threshold depending on application)
- minimum size (threshold depending on application)
- low power consumption (threshold depending on site infrastructure)
- maximised long-term stability of optical parts to minimise recalibration frequency
- operating temperature range -50 to 50 °C (thermal distribution of terrestrial plants)
- low temperature-sensitivity
- linear sensor response
- high signal-to-noise ratio
- ideal cosine directional response function
- logical user interface and easy-to-program systems
- remote access to data and system control

Besides these general requirements, *in situ* spectral measurements can be conducted with variable setup and approaches. The optimal solution generally depends on the purpose, characteristics of the site, and amount of resources available.

5.6 Conclusions

Validation plan

A "bottom-up" validation strategy has been presented that complies with recommendations by the CEOS Working Group on Calibration and Validation for land products from moderate resolution sensors. Validation should be performed locally at dedicated (core) fluorescence

research sites, and globally at supporting sites in collaboration with the already existing monitoring FLUXNET network. These sites should be upgraded with the required instrumentation for continuous measurement of SIF, and would share data of additional parameters, in particular from carbon fluxes.

Validation should be based on trusted TOC SIF measurements over large homogeneous sites from towers or masts, upscaled to moderate resolution via a combination of high resolution mapping with RT models. A methodology has been proposed to include the intrinsic uncertainties of *in situ* and remote measurements into the validation process.

The possibility exists to extend to several vegetation types (or even for inhomogeneous canopies of a single type) using two approaches: using *in-situ* imaging spectrometers, or deploying miniature spectrometers on board autonomous UAVs (currently under development), in both cases in combination with RTMs and/or high-resolution mapping.

Dedicated field campaigns with airborne FLEX simulators and extensive field measurements deployed at selected sites will provide high accuracy validation of upscaling processes, radiative transfer fluorescence models, and TOC SIF measurements.

Validation should extend globally over relevant biomes and latitudes, continuously over seasonal changes, and it should contemplate the accuracy and precision of the SIF signal as well as coherence in evolution trends of other related parameters. Data from the different validation sites should be compiled in a homogenised database for easy and consistent processing.

Finally, we have detailed required instrumentation with corresponding characteristics, including existing systems that might be readily adopted.

Required developments

Instrumentation for SIF measurement described in this document corresponds to the current state of the art. To keep abreast of new developments, an initiative such as the COST action OPTIMISE ES1309 is helpful, as it involves over a hundred scientists in diverse fields who share a common interest in fluorescence spectroscopy under natural conditions. A dedicated effort will be necessary to focus on the particularities involved in validation activities.

Further developments on SIF proximal and remote sensing systems are needed in certain areas:

- **improved performances**—lower noise; higher SNR, radiometric resolution, and stability;
- **effective imaging capabilities**—for heterogeneous landscapes it will be necessary to improve existing systems to provide them with SIF retrieval capabilities;
- **autonomous mounts**—automated sampling; improved performance of pan/tilt platforms on towers, UAV systems and (still untried) zip-line systems; such systems have demonstrated capabilities but require direct human intervention, hindering routine long-term use; automatic recharge of autonomous untethered systems such as UAVs is needed;

- **automatic processing & archiving**—large continuous volumes of data need to be logged, processed, archived and distributed; there is a consolidated experience in flux tower networks which should be extended and adapted to cover fluorescence data streams (a non-trivial task, as those systems have been optimised for very specific types of data other than from hyperspectral sensors).

Depending on the particularities of each validation site, it might be necessary to adapt existing systems, or build structural parts, adaptors, support frames or insulation. This places a requirement on the identification of institutions, groups, and companies capable of such developments and manufacturing.

New developments are also needed in radiative transfer modelling of 3D canopies that incorporate fluorescence, either by building a monolithic leaf-canopy model or by allowing inputs of leaf properties from existing leaf fluorescence-photosynthesis RTMs. Various modelling teams are now initiating these activities. Since fluorescence RTMs are a key tool in upscaling, it is recommended to follow the development status of those models and to collaborate closely with them to validate their outputs and incorporate the best ones into the FLEX validation process.

Evaluation of instrument performance

A review of proximal sensing measurements indicated an increased demand for long-term spectral data during the last decade. However, there is a lack of consensus on what are the most suitable proximal sensing systems and protocols to obtain reliable fluorescence estimates.

Here we proposed procedures that can be adopted for evaluation of instrument performances under natural illumination, so as to identify the most suitable, cost-effective and precise instruments for deployment. These procedures include:

- comparison between measured and modeled data (e.g., to assess spectral stability);
- use of portable calibration/verification standards rotated periodically around sites or directly incorporated into instrument design;
- assessment of instrument performances in both fluorescence bands, using as truth the fluorescence values extracted with the FluoWat leaf clip;
- periodical measurement of a diurnal course of fluorescence;
- measurement of the Kautsky effect (spectrally and over time); and
- measurement of a non-fluorescent target throughout the day.

Finally, we suggest establishing or engaging a common calibration facility and developing a field calibration/validation process to ensure consistent data quality and comparability of optical measurements across a geographically wide range of sites internationally. Portable calibration/verification standards should be provided for validation activities across space and time and to help monitor change or degradation of instrument performances.

6. Overall Conclusions & Recommendations

The FLEX Bridge Study presents a composite of scientific activities designed to support the full exploitation of SIF information from the FLEX mission.

Study goals were to:

1. optimise approaches for SIF retrievals and applications in assessment of photosynthesis and stress status in terrestrial vegetation; and
2. develop a calibration/validation strategy for FLEX products.

Broad achievements included:

- advances in the fluorescence retrieval algorithm;
- improvements in the SCOPE model and affiliated sub-models;
- consolidation of retrieval strategies for Level-2 data products;
- advances in applications based on Level-2 data products; and
- development of strategies for calibration/validation of mission outputs.

Solar induced fluorescence retrieval optimisation and analysis

Capabilities were enhanced for the retrieval and analysis of sun-induced fluorescence from FLEX. These included provision of new simulation datasets, consolidation of algorithms for atmospheric correction of FLEX signals, improvements for SIF retrieval, formalisation of fluorescence-derived indices, and development of biophysical products.

In **data generation**, the existing FLEX/S3 spectral radiance databases were expanded with new simulations that allow for generation of either single pixels or synthetic composite imagery. Some of the new datasets were generated with the FLEX End-to-End Mission Performance Simulator (FLEX-E). The new databases afford versatility in simulating ideal or realistic scenarios and are valuable inputs for algorithm development.

The **atmospheric correction algorithm** was developed to a Level-2 processing chain, while also improving the coupling of atmospheric correction and fluorescence retrieval.

Fluorescence retrievals were improved for retrieval of the full SIF spectrum, and analyses conducted here demonstrated the feasibility of decoupling the PSI and PSII spectra from total canopy fluorescence.

Strategies were evaluated for better **estimates of APAR**, important for the calculation of yields. Further, insights were gained into potential causes of retrieval issues. **Normalisation strategies** of the SIF signal were evaluated for their capacity to minimise the impact of environmental conditions and vegetation structural parameters, and the importance of APAR and fAPAR for normalisation was substantiated.

Progress was made toward development of higher-level products for retrieval of **biophysical parameters** (or canopy state variables). For complex imagery, a retrieval strategy was

developed to extract LAI estimates. A complementary approach for cases of relatively homogenous pixels showed that a simplified version of SCOPE was able to simultaneously retrieve surface reflectance, fluorescence, and most biophysical paramaters of the model.

Development of vegetation stress indicators and applications

Opportunities and protocols for stress detection were expanded and refined using published and new datasets, testing of indicator prototypes, and evaluation of strategies to assess non-photochemical quenching and minimise sources of variability and error.

SIF can be used to study a wide variety of **abiotic and biotic stresses** across many species. In addition to water stress, temperature stresses, and nitrogen deficit studied during the PS Study, the influence of air pollution, insecticides, senescence, biotic stress, combined stresses, heavy metals, herbicide, ozone, UV radiation, salt and micro- and macronutrients deficiency were evaluated. Stress indices introduced in the PS Study were tested, and the results reiterated the importance of having ancillary measures for interpretation of SIF and to distinguish among stresses. Application of SIF for stress detection requires a good understanding of vegetation ecophysiology, suitable sampling methods, techniques for merging of data from various domains, and sound mechanistic models. The spectral and spatial resolution of FLORIS and the complementarity of the tandem mission position FLEX advantageously for applications.

The value of the **photochemical reflectance index** for interpretation of fluorescence is well known. Here, we have considered how best to incorporate PRI for canopy-level assessments and have proposed avenues by which PRI could be strengthened as a measure of non-photochemical quenching through compensating for the impacts of confounding factors, especially structural effects, illumination effects, and pigment pool sizes.

Finally, field datasets were utilised from stress experiments with the ***HyPlant*** airborne sensor which helped to quantitatively link vegetation stress and SIF. The far-red fluorescence was used here, for which the potential interplay of canopy characteristics with stress responses and fluorescence emission was indicated. An informative point was the apparent strong correlation of F_{760} to EVI (hence LAI), at least under heat stress. In the near future, as the extraction of the red fluorescence data from *HyPlant* campaigns is completed, this will more fully advance our understanding of stress responses in the field.

Photosynthesis model optimisation, updates, and applications

The SCOPE model and A-SCOPE graphic user interface were improved with new functionality for accommodating plant functional types, and SCOPE now has improved computation speed and greater accuracy of the fluorescence output. Further improvements will be facilitated with the creation here of a new leaf RT model that incorporates xanthophyll effects. Several types of applications were investigated.

Several modelling developments were relevant to applications of SIF for photosynthetic and stress evaluation. First, a new model, Fluspect_B_CX, was introduced to represent **xanthophyll pigment changes** related to NPQ and PRI. Second, a new model of **energy partitioning** between

the two photosystems was proposed to provide preliminary estimation of PSI and PSII fluorescence radiance. Third, the possibility was investigated to estimate **sustained NPQ** from changes in leaf PRI, thereby strongly reducing model uncertainty.

Testing and evaluation of recent versions of the models were done. The **Fluspect model** provided realistic chlorophyll fluorescence simulations, with most of the fluorescence variability explicable from the PROSPECT parameters. However, the spectral distribution of the excitation light affected the shape of the chlorophyll fluorescence spectrum in a way that the Fluspect model could not fully reproduce. Ideally, measurements carried out under natural light conditions should be used to complete a full validation of the Fluspect model. The **SCOPE model** was compared to field data of far-red fluorescence from *HyPlant*. The model reproduced the magnitude and seasonal cycle of fluorescence. In unstressed conditions, the effects of canopy structure and leaf composition dominated fluorescence variations in the far-red band, with a smaller contribution of photosynthetic regulation due to photochemical and non-photochemical quenching.

To facilitate applications and user convenience, a **simple model** for red and far-red fluorescence and photosynthesis has been formulated based on SCOPE. The simple model runs approximately six orders of magnitude faster than the full SCOPE model. Also, an **Emulator toolbox**, developed as a complementary activity to the FB Study, is useful to evaluate various model emulators.

Data assimilation of fluorescence products will be key to applications. As a first attempt, data assimilation has been applied to a *HyPlant* scene, producing a map of canopy photosynthesis from the reflectance and retrieved fluorescence of *HyPlant*. Additional activity explored SIF datasets of coarse spatial resolution that could inform FLEX activities at the more detailed scale. Initial study of data assimilation using SIF to constrain the DVGM **ORCHIDEE** yielded promising results. Considering that canopy 3D geometry influences SIF values, there is merit to having 'structure-corrected' data for future use.

A further product was the '**Automated Scene Generator Module' (A-SGM)** for the generation of simulated scenes according to plant functional types. This module is available in a user-friendly GUI format in the ARTMO framework, and it can rapidly generate simulated scenes for any optical sensor specified within ARTMO. The A-SGM accommodates data from either an RTM or an RTM emulator.

Development of a calibration/validation strategy

The FB Study has formulated a comprehensive cal/val strategy for FLEX mission products. The strategy covers methods to determine validation error metrics and product accuracies, cal/val for basic fluorescence products, validation of FLEX Level-2/3 products, and definition of common protocols and state-of-the-art instruments for use in the strategy.

A **"bottom-up" validation** strategy was proposed, with validation based on trusted TOC SIF measurements over large relatively homogeneous sites from towers or masts, upscaled to moderate resolution via a combination of high resolution mapping with RT models.

The possibility exists to extend to several vegetation types (or even for inhomogeneous canopies of a single type) using *in-situ* imaging spectrometers and/or UAV-based miniature spectrometers, in combination with RTMs and/or high-resolution mapping. Dedicated field campaigns with airborne FLEX simulators and extensive field measurements deployed at selected sites will provide high accuracy validation of upscaling processes, radiative transfer fluorescence models and TOC SIF measurements. Validation should extend globally over relevant biomes and latitudes, and continuously over seasonal changes, with data from the different validation sites compiled in a homogenised database. We have further proposed procedures for evaluation of instrument performances under natural illumination so as to identify the most suitable, cost-effective and precise instruments for deployment.

Significance for the FLEX mission

The FB Study supports the development of best practices for the retrieval, interpretation, and application of fluorescence measurements from space. These aspects are crucial in order to realise the full potential of space-based SIF technology in helping to meet the land challenges identified in ESA's Living Planet Programme (ESA 2015a). The completion of the FB Study also coincides with the conclusion of ESA's selection process for Earth Explorer 8 and the Agency's official announcement in mid-November 2015 that FLEX has been selected. Thus, the Study serves as a 'bridge' to future science activities.

Outputs of FLEX Bridge that are of key relevance to the FLEX/Sentinel-3 mission:

- **fluorescence retrieval & quantification** – extension of FLEX/S3 spectral radiance databases to support algorithm development; improvement in atmospheric correction and development to a Level-2 processing chain; improvement in retrieval of the full SIF spectrum; decoupling of PSI and PSII spectra; normalisation strategies for estimation of APAR; progress in retrieval of biophysical parameters; definition of calibration/validation approaches.
- **fluorescence interpretation** – strategies to incorporate PRI through compensating for confounding factors; evaluation of *HyPlant* campaign data on stress responses; strategies for quantifying and modelling NPQ and its components; formulation of a new leaf RT model incorporating xanthophylls; prototype model for energy partitioning between PSI and PSII; preliminary strategies to incorporate canopy 3D geometry effects; calibration/validation approaches.
- **fluorescence applications** – identification of SIF indicators for a wide variety of abiotic and biotic stresses; development of a prototype simplified model based on SCOPE; development of an Automated Scene Generator Module to incorporate plant functional types; creation of an emulator toolbox; testing of updated versions of SCOPE and Fluspect with simulated and field data; data assimilation of SIF to constrain a DVGM.

Recommendations

To build upon the findings of this study, we offer several recommendations.

First, additional developments are needed on optimisation of **signal retrieval and analysis**. Algorithms for decoupling PSI/PSII contributions should be tested under realistic scenarios. Similarly, estimation of biophysical parameters should be studied in more detail under such scenarios. Further work is required on quantification and incorporation of canopy structural effects on the SIF signal and for the individual PAR terms (especially APAR), notably in complex vegetation canopies; and a strategy for normalisation of SIF in the red region to compensate for vegetation structure must be formulated, especially considering reabsorption of the red band fluorescence. In general, methodologies need to be tested with more 'real world' datasets.

Second, a concerted effort is required on **data assimilation** techniques amenable to a broad range of applications, including global ecology, climate- and carbon modelling. Preliminary activity here utilised GOME-2 data to inform the more detailed acquisitions that will be possible with FLEX, but future activity will need to focus on finer-resolution captures and on both red and far-red fluorescence, for which the *HyPlant* airborne sensor will be a valuable platform.

Third, the new and enhanced **models** developed here require fuller validation and testing with more datasets on a wider variety of vegetation types. The new leaf-level models of physiology or RT will need to be implemented into SCOPE once final testing and validation are completed. It should also be noted that a few very challenging areas of science were tackled here related to estimation of non-photochemical quenching. That story is not yet complete and further refinement or correction of these analytical models likely will be needed. Efforts should also continue on formulation and testing of simplified models or emulators for use at canopy level, and usage of the new emulator toolbox will expedite such investigation.

Fourth, pre-implementation of the **cal/val strategy** that was pioneered here needs to start soon so that the necessary infrastructure can be put in place. Developments on SIF proximal and remote sensing systems are needed to improve performances, accommodate heterogeneous landscapes, handle automatic sampling, and conduct automatic processing & archiving. Additionally, there would be benefits to establishing or engaging a common calibration facility and having portable cal/val standards. A helpful step will be to identify institutions, groups, and companies capable of such developments and manufacturing. To keep abreast of new developments, future activities will benefit from interaction with other initiatives (e.g., COST action OPTIMISE ES1309) involving diverse teams of scientists sharing a common interest in fluorescence spectroscopy under natural conditions.

Finally, a priority should be placed on advancement of SIF **applications** and supporting the **users** of FLEX. There is a need for studies on stress applications of SIF in a wide variety of vegetation systems, along with investigation into PSI/PSII behaviour and implications for SIF retrievals and quantification. The user network will need to be consolidated and supported with necessary expertise and other resources. A communications plan should be developed and implemented to keep the FLEX user community informed and ready to adopt new developments. This activity should occur contemporaneously with work on the cal/val pre-implementation, as these users will also be involved in refinement of site selection and methodologies for the different application areas.

7. References

Ač A, Malenovský Z, Olejníčková J, Gallé A, Rascher U, Mohammed G. 2015. Meta-analysis assessing potential of steady-state chlorophyll fluorescence for remote sensing detection of plant water, temperature and nitrogen stress. *Remote Sensing of Environment* **168** 420-436.

Ač A, Malenovský Z, Urban O, Hanus J, Zitova M, Navratil M, Vrablova M, Olejníčková J, Spunda V, Marek M. 2012. Relation of chlorophyll fluorescence sensitive reflectance ratios to carbon flux measurements of Montanne grassland and Norway spruce forest ecosystems in the temperate zone. *Scientific World Journal 2012*, Article ID 705872, 13 pages, doi: 10.1100/2012/705872.

Adams III WW, Zarter CR, Ebbert V, Demmig-Adams B. 2004. Photoprotective strategies of overwintering evergreens. *BioScience* **54** 41-49.

Adams WW, Hoehn A, Demmig-Adams B. 1995. Chilling temperatures and the xanthophyll cycle. A comparison of warm-grown and overwintering spinach. *Australian Journal of Plant Physiology* **22** 75-85.

Agati G, Brunetti C, Di Ferdinando M, Ferrini F, Pollastri S, Tattini M. 2013. Functional roles of flavonoids in photoprotection: New evidence, lessons from the past. *Plant Physiology and Biochemistry* **72** 35-45.

Agati G, Azzarello E, Pollastri S, Tattini M. 2012. Flavonoids as antioxidants in plants: Location and functional significance. Plant Science **196** 67-76.

Agati G, Fusi F, Mazzinghi P, di Paola ML. 1993. A simple approach to the evaluation of the reabsorption of chlorophyll fluorescence spectra in intact leaves. *Journal of Photochemistry and Photobiology B: Biology* **17** 163-171.

Alonso L, Moreno J. 2012. Tech Note on the determination of optimal SR and SNR for FLORIS. ESA FLUSS Project.

Alonso L, Moreno J. 2010. A novel portable device to measure leaf reflectance, transmittance and fluorescence emission under natural conditions. Proceedings of the 4th Intl Workshop on Remote Sensing of Vegetation Fluorescence, 15-17 November 2010, Valencia, Spain.

Alton PB, Ellis R, Los SO, North PR. 2007. Improved global simulations of gross primary product based on a separate and explicit treatment of diffuse and direct sunlight, *Journal of Geophysical Research* **112** D07203.

Amorós-López J, Gomez-Chova L, Guanter L, Alonso L, Moreno J, Camps-Valls G. 2011. Multitemporal fusion of Landsat and MERIS images. Proceedings of the 6th International Workshop on the Analysis of Multi-Temporal Remote Sensing Images, 12-14 July 2011, Trento, Italy.

Anderson K, Dungan JL, MacArthur A. 2011. On the reproducibility of field-measured reflectance factors in the context of vegetation studies. *Remote Sensing of Environment* **115** 1893-1905.

Anderson K, Rossini M, Pacheco-Labrador J, Balzarolo M, MacArthur A, Fava F, Julitta T, Vescovo L. 2013. Inter-comparison of hemispherical conical reflectance factors (HCRF) measured with four fibre-based spectrometers. *Optics Express* **21** 605-617.

Avital S, Brumfeld V, Malkin S. 2006. A micellar model system for the role of zeaxanthin in the non-photochemical quenching process of photosynthesis-chlorophyll fluorescence quenching by the xanthophylls. *Biochimica et Biophysica Acta* **1757** 798-810.

Baldocchi DD. 2003. Assessing the eddy covariance technique for evaluating carbon dioxide exchange rates of ecosystems: past, present and future. *Global Change Biology* **9** 479-492.

Balzarolo M, Anderson K, Nichol C, Rossini M, Vescova L, *et al*. 2011. Ground-based optical measurements at european flux sites: A review of methods, instruments and current controversies. *Sensors* **11** 7954-7981.

Barber J, Malkin S, Telfer A. 1989. The origin of chlorophyll fluorescence in vivo and its quenching by the photosystem II reaction centre. *Philosophical Transactions of the Royal Society of London, Series B* **323** 227-239.

Barton CVM, North PRJ. 2001. Remote sensing of canopy light use efficiency using the photochemical reflectance index - Model and sensitivity analysis. *Remote Sensing of Environment* **78** 264-273.

Bernacchi CJ, Pimentel C, Long SP. 2003. In vivo temperature response functions of parameters required to model RuBP-limited photosynthesis. *Plant Cell and Environment* **26** 1419-1430.

Brugnoli E, Bjorkman O. 1992. Chloroplast movement in leaves: influence on chlorophyll fluorescence and measurements of light-induced absorbance changes related to ΔpH and zeaxanthin formation. *Photosynthesis Research* **32** 23-35.

Burkart A, Cogliati S, Schickling A, Rascher U. 2014. A novel UAV-based ultra-light weight spectrometer for field spectroscopy. *Sensors Journal* **14** 62-67.

Burkart A, Schickling A, Mateo MPC, Wrobel TJ, Rossini M, Cogliati S, Julitta T, Rascher U. 2015. A method for uncertainty assessment of passive sun-induced chlorophyll fluorescence retrieval using an infrared reference light. *Sensors Journal* **15** 4603-4611.

Busetto L, Meroni M, Crosta GF, Guanter L, Colombo R. 2011. Speccal: Novel software for in-field spectral characterization of high-resolution spectrometers. *Computer Geoscience* **37** 1685-1691.

Bussotti F, Agati F, Desotgiu R, Matteini P, Tani C. 2005. Ozone foliar symptoms in woody plant species assessed with ultrastructural and fluorescence analysis. *New Phytologist* **166** 941-955.

Bussotti F, Nali C, Lorenzini G. 2011. Chlorophyll fluorescence: From theory to (good) practice. An introduction. *Environmental and Experimental Botany* **73** 1-2.

Calderon R, Navas-Cortes JA, Lucena C, Zarco-Tejada PJ. 2013. High-resolution airborne hyperspectral and thermal imagery for early, detection of Verticillium wilt of olive using fluorescence, temperature and narrow-band spectral indices. *Remote Sensing of Environment* **139** 231-245.

Campbell PKE, Middleton EM, Corp L, van der Tol C, Huemmrich F. 2014. Diurnal dynamics and phenological changes in vegetation fluorescence, reflectance, and temperature indicative of vegetation photosynthetic properties and function. 5th International Workshop on Remote Sensing of Vegetation Fluorescence, 22-24 April 2014, Paris, France.

Camps-Valls G, Gomez-Chova L, Vila-Francés J, Amorós-López J, Muñoz-Marí J, Calpe-Maravilla J. 2006. Retrieval of oceanic chlorophyll concentration with relevance vector machines. *Remote Sensing of Environment* **105** 23-33.

Castro-Esau KL, Sanchez-Azofeifa GA, Rivard B. 2006. Comparison of spectral indices obtained using multiple spectroradiometers. *Remote Sensing of Environment* **103** 276-288.

Cazzaniga S, Dall'Osto L, Kong SG, Wada M, Bassi R. 2013. Interaction between avoidance of photon absorption, excess energy dissipation and zeaxanthin synthesis against photooxidative stress in *Arabidopsis*. *Plant Journal* **76** 568-579.

Cendrero-Mateo MP. 2013. Chlorophyll fluorescence response to water and nitrogen deficit. PhD Dissertation, University of Arizona, 125 pp.

Cerovic ZG, Samson G, Morales F, Tremblay N, Moya I. 1999. Ultraviolet-induced fluorescence for plant monitoring: Present state and prospects. *Agronomie* **19** 543-578.

Chappelle EW, Wood FM, McMurtrey JE, Newcomb WW. 1984. Laser-induced fluorescence of green plants 1. A technique for the remote detection of plant stress and species differentiation. *Applied Optics* **23** 134-138.

Chappelle EW, Williams DL. 1987. Laser-induced fluorescence (LIF) from plant foliage. *IEEE Transactions on Geoscience and Remote Sensing* **25** 726-736.

Cifre J, Bota J, Escalona JM, Medrano H, Flexas J. 2005. Physiological tools for irrigation scheduling in grapevine (*Vitis vinifera* L.): An open gate to improve water-use efficiency? *Agriculture, Ecosystems & Environment* **106** 159-170.

Cogliati S, Rossini M, Julitta T, Meroni M, Schickling A, Burkart A, Pinto F, Rascher U, Colombo R. 2015a. Continuous and long-term measurements of reflectance and sun-induced chlorophyll fluorescence by using novel automated field spectroscopy systems. *Remote Sensing of Environment* **164** 270-281.

Cogliati S, Verhoef W, Kraft S, Sabater N, Alonso L, Vicent J, Moreno J, Drusch M, Colombo R. 2015b. Retrieval of sun-induced fluorescence using advanced spectral fitting methods. *Remote Sensing of Environment* **169** 344-357.

Corp L, Middleton EM, Cheng Y-B, Huemmrich KF, Campbell PKE. 2010. Fusion: A fully ultraportable system for imaging objects in nature. Proceedings of the IEEE Geoscience and Remote Sensing Symposium (IGARSS), 25-30 July 2010, Honolulu HI.

Curran PJ, Windham WR, Gholz HL. 1995. Exploring the relationship between reflectance red edge and chlorophyll concentration in slash pine leaves. *Tree Physiology* **15** 203-206.

Damm A, Coops NC, Morsdorf F, Schaepman ME. Combining image spectroscopy and LiDAR to derive canopy Photochemical Reflectance Index (PRI) of a mixed forest. *Remote Sensing of Environment* (in preparation).

Damm A, Elbers J, Erler A, Gioli B, Hamdi K, Hutjes R, Kosvancova M, Meroni M, Miglietta F, Moersch A, Moreno J, Schickling A, Sonnenschein R, Udelhoven T, van der Linden S, Hostert P, Rascher U. 2010. Remote sensing of sun-induced fluorescence to improve modeling of diurnal courses of gross primary production (GPP). *Global Change Biology* **16** 171-186.

Damm A, Erler A, Hillen W, Meroni M, Schaepman ME, Verhoef W, Rascher U. 2011. Modeling the impact of spectral sensor configurations on the fld retrieval accuracy of sun-induced chlorophyll fluorescence. *Remote Sensing of Environment* **115** 1882-1892.

Damm A, Guanter L, Paul-Limoges E, Van der Tol C, Hueni A, Buchmann N, Eugster W, Ammann C, Schaepman ME. 2015a. Far-red sun-induced chlorophyll fluorescence shows ecosystem-specific relationships to gross primary production: An assessment based on observational and modeling approaches. *Remote Sensing of Environment* **166** 91-105.

Damm A, Guanter L, Verhoef W, Schläpfer D, Garbari S, Schaepman ME. 2015b. Impact of varying irradiance on vegetation indices and chlorophyll fluorescence derived from spectroscopy data. *Remote Sensing of Environment* **156** 202-215.

Dash J, Curran PJ, Tallis MJ, Llewellyn GM, Taylor G, Snoeij P. 2010. Validating the MERIS Terrestrial Chlorophyll Index (MTCI) with ground chlorophyll content data at MERIS spatial resolution. *Journal of Remote Sensing* **31** 5513-5532.

Daumard F, Champagne S, Fournier A, Goulas Y, Ounis A, Hanocq JF, Moya I. 2010. A field platform for continuous measurement of canopy fluorescence. *IEEE Transactions in Geoscience and Remote Sensing* **48** 3358-3368.

Demmig-Adams B. 1998. Survey of thermal energy dissipation and pigment composition in sun and shade leaves. *Plant and Cell Physiology* **39** 474-482.

Disney M, Lewis P. 2007. Spectral invariant behaviour of a complex 3D forest canopy. Proceedings of the ISPRS Working Group VII/1 Workshop, 12-14 March 2007, Davos, Switzerland.

D'Odorico P, Gonsamo A, Pinty B, Gobron N, Coops N, Mendez E, Schaepman ME. 2014. Intercomparison of fraction of absorbed photosynthetically active radiation products derived from satellite data over Europe. *Remote Sensing of Environment* **142** 141-154.

Donohue RJ, Roderick ML, McVicar TR. 2008. Deriving consistent long-term vegetation information from AVHRR reflectance data using a cover-triangle-based framework. *Remote Sensing of Environment* **112** 2938-2949.

Drolet G, Wade T, Nichol CJ, MacLellan C, Levula J, Porcar-Castell A, Nikinmaa E, Vesala T. 2014. A temperature-controlled spectrometer system for continuous and unattended measurements of canopy spectral radiance and reflectance. *International Journal of Remote Sensing* **35** 1769-1785.

Du Y, Chang C-I, Ren H, Chang C-C, Jensen JO, A'Amico FM. 2004. New hyperspectral discrimination measure for spectral characterization. *Optical Engineering* **43** 1777-1786.

Eklundh L, Jin H, Schubert P, Guzinski R, Heliasz M. 2011. An optical sensor network for vegetation phenology monitoring and satellite data calibration. *Sensors* **11** 7678-7709.

ESA. 2015a. ESA's Living Planet Programme: Scientific Achievements and Future Challenges – Scientific Context of the Earth Observation Science Strategy for ESA, ESA SP-1329/2 (2 volumes), European Space Agency, Noordwijk, The Netherlands.

ESA. 2015b. Report for Mission Selection: FLEX, ESA SP-1330/2 (2 volume series), European Space Agency, Noordwijk, The Netherlands.

Féret J-B, Francois C, Asner GP, Gitelson AA, Martin RE, Bidel LPR, Ustin SL, Le Maire G, Jacquemoud S. 2008. PROSPECT-4 and 5: Advances in the leaf optical properties model separating photosynthetic pigments. *Remote Sensing of Environment* **112** 3030-3043.

Fernandez-Jaramillo AA, Duarte-Galvan C, Contreras-Medina LM, Torres-Pacheco I, Romero-Troncoso RJ, Guevara-Gonzalez RG, Millan-Almaraz JR. 2012. Instrumentation in developing chlorophyll fluorescence biosensing: A review. *Sensors* **12** 11853-11869.

Fitzpatrick-Lins K. 1981. Comparison of sampling procedures and data analysis for a land use and land cover map. *Photogrammetric Engineering and Remote Sensing* **47** 343-351.

Franck F, Juneau P, Popovic R. 2002. Resolution of the photosystem I and photosystem II contributions to chlorophyll fluorescence of intact leaves at room temperature. *Biochimica et Biophysica Acta (BBA)-Bioenergetics* **1556** 239-246.

Frankenberg C, Butz A, Toon GC. 2011a. Disentangling chlorophyll fluorescence from atmospheric scattering effects in O_2 A-band spectra of reflected sun-light. *Geophysical Research Letters* **38** L03801, doi:10.1029/2010GL045896, 2011.

Frankenberg C, Fisher JB, Worden J, Badgley G, Saatchi SS, Lee J-E, Toon GC, Butz A, Jung M, Kuze A, Yokota T. 2011b. New global observations of the terrestrial carbon cycle from GOSAT: Patterns of plant fluorescence with gross primary productivity. *Geophysical Research Letters* **38** L17706, doi:10.1029/2011GL048738.

Gamon JA. 2015. Reviews and Syntheses: optical sampling of the flux tower footprint. *Biogeosciences* **12** 4509-4523.

Gamon JA, Berry JA. 2012. Facultative and constitutive pigment effects on the Photochemical Reflectance Index (PRI) in sun and shade conifer needles. *Israel Journal of Plant Sciences* **60** 85-95.

Gamon JA, Penuelas J, Field CB. 1992. A narrow-waveband spectral index that tracks diurnal changes in photosynthetic efficiency. *Remote Sensing of Environment* **41** 35-44.

Gamon JA, Serrano L, Surfus JS. 1997. The photochemical reflectance index: an optical indicator of photosynthetic radiation use efficiency across species, functional types, and nutrient levels. *Oecologia* **112** 492-501.

Garbulsky MF, Penuelas J, Gamon J, Inoue Y, Filella I. 2011. The photochemical reflectance index (PRI) and the remote sensing of leaf, canopy and ecosystem radiation use efficiencies A review and meta-analysis. *Remote Sensing of Environment* **115** 281-297.

Gastellu-Etchegorry JP, Martin E, Gascon F. 2004. DART: a 3D model for simulating satellite images and studying surface radiation budget. *International Journal of Remote Sensing* **25** 73-96.

Gitelson AA, Buschmann C, Lichtenthaler HK. 1998. Leaf chlorophyll fluorescence corrected for re-absorption by means of absorption and reflectance measurements. *Journal of Plant Physiology* **152** 283-296.

Gitelson AA, Gamon JA. 2015. The need for a common basis for defining light-use efficiency: Implications for productivity estimation. *Remote Sensing of Environment* **156** 196-201.

Gitelson A, Merzlyak MN. 1997. Remote estimation of chlorophyll content in higher plant leaves. *International Journal of Remote Sensing* **18** 2691-2697.

Gitelson AA, Peng Y, Arkebauer TJ, Suyker AE. 2015. Productivity, absorbed photosynthetically active radiation, and light use efficiency in crops: Implications for remote sensing of crop primary production. *Journal of Plant Physiology* 177, 100-109.

Gobron N, Pinty B, Taberner M, Melin F, Verstraete MM, Widlowski JL. 2006. Monitoring the photosynthetic activity of vegetation from remote sensing data. *Advances in Space Research* **38** 2196-2202.

Gobron N, Verstraete MM. 2009. Assessment of the Status of the Development of the Standards for the Terrestrial Essential Climate Variables T10: fAPAR. Global Terrestrial Observing System (GTOS), FAO, Rome.

Goss R, Lepetit B. 2015. Biodiversity of NPQ. *Journal of Plant Physiology* **172** 13-32.

Gouveia-Neto AS, Da Silva-Jr EA, Cunha PC, Oliveira-Filho RA, Silva LMH, Da Costa EB, Camara TJR, Willadino LG. 2011. Abiotic stress diagnosis via laser induced chlorophyll fluorescence analysis in plants for biofuel. In: Dos Santos Bernardes MA (ed.) *Biofuel Production – Recent Developments and Prospects,* pp. 3-22. InTech.

Grace J, Nichol C, Disney M, Lewis P, Quaife T, Bowyer P. 2007. Can we measure terrestrial photosynthesis from space directly, using spectral reflectance and fluorescence? *Global Change Biology* **13** 1484-1497.

Guanter L. 2006. New algorithms for atmospheric correction and retrieval of biophysical parameters in Earth Observation: Application to ENVISAT/MERIS data. Doctoral Thesis, University of Valencia, Spain.

Guanter L, Frankenberg C, Dudhia A, Lewis PE, Gomez-Dans J, Kuze A, Suto H, Grainger RG. 2012. Retrieval and global assessment of terrestrial chlorophyll fluorescence from GOSAT space measurements. *Remote Sensing of Environment* **121** 236-251.

Guillevic PC, Biard JC, Hulley GC, Privette JL, Hook SJ, Olioso A, Göttsche FM, Radocinski R, Román O, Yu Y, Csiszar I. 2014. Validation of land surface temperature products derived from the Visible Infrared Imaging Radiometer Suite (VIIRS) using ground-based and heritage satellite measurements. *Remote Sensing of the Environment* **154** 19-37.

Haboudane D, Miller JR, Pattey E, Zarco-Tejada PJ, Strachan IB. 2004. Hyperspectral vegetation indices and novel algorithms for predicting green LAI of crop canopies: Modeling and validation in the context of precision agriculture. *Remote Sensing of Environment* **90** 337-352.

Havaux M, Eyletters M. 1991. Is the in vivo Photosystem I function resistant to photoinhibition? An answer from photoacoustic and far-red absorbance measurements in intact leaves. *Zeitschrift für Naturforschung C* **46** 1038-1044.

Hay JE, McKay DC. 1985. Estimating solar irradiance on inclined surfaces: A review and assessment of methodologies. *International Journal of Solar Energy* **3** 203-240.

He L, Chen JM, Pisek J, Schaaf CB, Strahler AH. 2012. Global clumping index map derived from the MODIS BRDF product. *Remote Sensing of Environment* **119** 118-130.

Henry C. 2015. Improved leaf biochemical constituent retrieval using the theory of spectral invariants to correct hyperspectral remote sensing data for canopy structural effects. Master thesis, Remote Sensing Laboratories, University of Zurich, Switzerland.

Hernandez-Clemente R, Navarro-Cerrillo RM, Suárez L, Morales F, Zarco-Tejada PJ. 2011. Assessing structural effects on PRI for stress detection in conifer forests. *Remote Sensing of Environment* **115** 2360-2375.

Hihara Y, Sonoike K. 2001. Regulation, inhibition and protection of photosystem I. In: Aro E-M, Andersson B (eds.) *Regulation of Photosynthesis*, pp. 507-531. Kluwer Academic Publishers.

Hmimina G, Merlier E, Dufrene E, Soudani K. 2015. Deconvolution of pigment and physiologically related photochemical reflectance index variability at the canopy scale over an entire growing season. *Plant Cell and Environment* **38** 1578-1590.

Hogewoning SW, Douwstra P, Trouwborst G, van Leperen W, Harbinson J. 2010. An artificial solar spectrum substantially alters plant development compared with usual climate room irradiance spectra. *Journal of Experimental Botany* **61** 1267-1276.

Hook SJ, Vaughan RG, Tonooka H, Schladow SG. 2007. Absolute radiometric in-flight validation of mid infrared and thermal infrared data from ASTER and MODIS on the Terra spacecraft using the Lake Tahoe, CA/NV, USA, automated validation site. *IEEE Transactions on Geoscience and Remote Sensing* **45** 1798-1807.

Huang D, Knyazikhin Y, Dickinson RE, Rautiainen M, Stenberg P, Disney M, Lewis P, Cescatti A, Tian YH, Verhoef W, Martonchik JV, Myneni RB. 2007. Canopy spectral invariants for remote sensing and model applications. Remote Sensing of Environment **106** 106-122.

Inoue Y, Shibata K. 1973. Light-induced chloroplast rearrangements and their action spectra as measured by absorption spectrophotometry. *Planta* **114** 311-358.

Jacquemoud S, Ustin SL, Verdebout J, Schmuck G, Andreoli G, Hosgood B. 1996. Estimating leaf biochemistry using the PROSPECT leaf optical properties model. *Remote Sensing of Environment* **56** 194-202.

Jiang C, Fang H. 2012. Modeling soil reflectance using a global spectral library. AGU Fall Conference, 3-7 December 2012, San Francisco, CA.

Jin H, Eklundh L. 2015. In situ calibration of light sensors for long-term monitoring of vegetation. *IEEE Transactions on Geoscience and Remote Sensing* **53** 3405-3416.

Johnson GN. 2005. Cyclic electron transport in C3 plants: fact or artefact? *Journal of Experimental Botany* **56** 407-416.

Joiner J, Guanter L, Lindstrot R, Voigt M, Vasilkov AP, Middleton EM, Huemmrich KF, Yoshida Y, Frankenberg C. 2013. Global monitoring of terrestrial chlorophyll fluorescence from moderate spectral resolution near-infrared satellite measurements: methodology, simulations, and application to GOME-2. *Atmospheric Measurement Techniques* **6** 2803-2823.

Joiner J, Yoshida Y, Vasilkov AP, Middleton EM, Campbell PKE, Yoshida Y, Kuze A, Corp LA. 2012. Filling-in of near-infrared solar lines by terrestrial fluorescence and other geophysical effects: simulations and space-based observations from SCIAMACHY and GOSAT. *Atmospheric Measurement Techniques* **5** 809-829.

Joiner J, Yoshida Y, Vasilkov A, Schaefer K, Jung M, *et al.* 2014. The seasonal cycle of satellite chlorophyll fluorescence observations and its relationship to vegetation phenology and ecosystem atmosphere carbon exchange. *Remote Sensing of Environment* **152** 375-391.

Joiner J, Yoshida Y, Vasilkov AP, Yoshida Y, Corp LA, Middleton EM. 2011. First observations of global and seasonal terrestrial chlorophyll fluorescence from space. *Biogeosciences* **8** 637-651.

Joliot P, Johnson GN. 2011. Regulation of cyclic and linear electron flow in higher plants. *Proceedings of the National Academy of Sciences of the USA* **108** 13317-13322.

Julitta T, Corp L, Rossini M, Burkart A, Cogliati S, Davies N, Hom M, MacArthur A, Middleton E, Rascher U, *et al*. 2015. Comparison of sun-induced chlorophyll fluorescence estimates obtained from four portable field spectroradiometers. *Remote Sensing* (submitted).

Jung M, Reichstein M, Margolis HA, Cescatti A, Richardson AD, *et al.* 2011. Global patterns of land-atmosphere fluxes of carbon dioxide, latent heat, and sensible heat derived from eddy covariance, satellite, and meteorological observations. *Journal of Geophysical Research – Biogeosciences* **116** G00J07.

Jupp DL, Culvenor DS, Lovell JL, Newnham GJ, Strahler AH, Woodcock CE. 2009. Estimating forest LAI profiles and structural parameters using a ground-based laser called 'Echidna®. *Tree Physiology* **29** 171-181.

Jupp DL, Lovell JL. 2007. Airborne and ground-based lidar systems for forest measurement: background and principles. CSIRO Marine and Atmospheric Research Papers, No. 117.

Justice CO, Townshend JRG. 1981. Integrating ground data with remote sensing. In: Townshend J.R.G. (ed.) *Terrain Analysis and Remote Sensing*, pp. 38-58. George Allen and Unwin.

Kato T, Maignan F, MacBean N, Peylin P, Vuichard N, *et al.* 2014. Relationship of the model-simulated productivity with the in-situ fluorescence measurement at two flux sites. 5th International Workshop on Remote Sensing of Vegetation Fluorescence, 22-24 April 2014, Paris, France.

Knyazikhin Y, Lewis P, Disney MI, Stenberg P, Möttus M, *et al.* 2013a. Reply to Townsend *et al.*: Decoupling contributions from canopy structure and leaf optics is critical for remote sensing leaf biochemistry. *Proceedings of the National Academy of Sciences of the United States of America* **110** E1075.

Knyazikhin Y, Schull MA, Stenberg P, Möttus M, Rautiainen M, *et al*. 2013b. Hyperspectral remote sensing of foliar nitrogen content. *Proceedings of the National Academy of Sciences of the United States of America* **110** E185-E192.

Knyazikhin Y, Schull MA, Xu L, Myneni RB, Samanta A. 2011. Canopy spectral invariants. Part 1: A new concept in remote sensing of vegetation. *Journal of Quantitative Spectroscopy and Radiative Transfer* **112** 727-735.

Kobayashi H. 2014. Angular and canopy structure dependency of canopy scale chlorophyll fluorescence simulated by the newly developed three dimensional plant canopy fluorescence model. 5th International Workshop on Remote Sensing of Vegetation Fluorescence, 22-24 April 2014, Paris, France.

Köhler PL, Guanter L, Joiner J. 2015. A linear method for the retrieval of sun-induced chlorophyll fluorescence from GOME-2 and SCIAMACHY data. *Atmospheric Measurement Techniques* **8** 2589-2608.

Kolari P, Lappalainen HK, Hänninen H, Hari P. 2007. Relationship between temperature and the seasonal course of photosynthesis in Scots pine at northern timberline and in southern boreal zone. *Tellus B* **59** 542–552.

Konanz S, Kocsányi L, Buschmann C. 2014. Advanced multi-color fluorescence imaging system for detection of biotic and abiotic stresses in leaves. *Agriculture* **4** 79-95.

Kou J, Takahashi S, Oguchi R, Fan DY, Badger MR, Chow WS. 2013. Estimation of the steady-state cyclic electron flux around PSI in spinach leaf discs in white light, CO2-enriched air and other varied conditions. *Functional Plant Biology* **40** 1018-1028.

Kovac D, Malenovský Z, Urban O, Spunda V, Kalina J, Ac A, Kaplan V, Hanus J. 2013. Response of green reflectance continuum removal index to the xanthophyll de-epoxidation cycle in Norway spruce needles. *Journal of Experimental Botany* **64** 1817-1827.

Kramer DM, Avenson TJ, Edwards GE. 2004. Dynamic flexibility in the light reactions of photosynthesis governed by both electron and proton transfer reactions. *Trends in Plant Science* **9** 349-357.

Kramer DM, Evans JR. 2011. The importance of energy balance in improving photosynthetic productivity. *Plant Physiology* **155** 70-78.

Krause GH, Weis E. 1991. Chlorophyll fluorescence and photosynthesis: the basics. *Annual Review of Plant Physiology and Plant Molecular Biology* **42** 313-349.

Kuckenberg J, Tartachnyk I, Noga G. 2009. Detection and differentiation of nitrogen-deficiency, powdery mildew and leaf rust at wheat leaf and canopy level by laser-induced chlorophyll fluorescence. *Biosystems Engineering* **103** 121-128.

Lang M, Lichtenthaler HK, Sowinska M, Heisel JA, Miehé JA. 1995. Demonstrating water and temperature stress in the photosynthetic apparatus by fluorescence imaging. In Guyot G. (ed.) EARSeL Proceed. Internat. Colloq. Photosynthesis and Remote Sensing (pp. 29-35). Montpellier, Paris.

Laurent VCE, Schaepman ME, Verhoef W, Weyermann J, Chavez RO. 2014. Bayesian object-based estimation of LAI and chlorophyll from a simulated Sentinel-2 top-of-atmosphere radiance image. *Remote Sensing of Environment* **140** 318-329.

Laurent VCE, Verhoef W, Clevers JGPW, Schaepman ME. 2011a. Estimating forest variables from top-of-atmosphere radiance satellite measurements using coupled radiative transfer models. *Remote Sensing of Environment* **115** 1043-1052.

Laurent VCE, Verhoef W, Clevers JGPW, Schaepman ME. 2011b. Inversion of a coupled canopy-atmosphere model using multi-angular top-of-atmosphere radiance data: A forest case study. *Remote Sensing of Environment* **115** 2603-2612.

Laurent VCE, Verhoef W, Damm A, Schaepman ME, Clevers JGPW. 2013. A Bayesian object-based approach for estimating vegetation biophysical and biochemical variables from APEX at-sensor radiance data. *Remote Sensing of Environment* **139** 6-17.

Leblanc SG, Fournier RA. 2014. Hemispherical photography simulations with an architectural model to assess retrieval of leaf area index. *Agricultural and Forest Meteorology* **194** 64-76.

Leblanc SG, Chen JM. 2001. A practical scheme for correcting multiple scattering effects on optical LAI measurements. *Agricultural and Forest Meteorology* **110** 125-139.

Leblanc SG, Chen JM, Kwong M. 2002. Tracing radiation and architecture of canopies. TRAC Manual. Version, 2.3.

Lee J-E, Frankenberg C, Van der Tol C, Berry JA, Guanter L, Boyce CK, Fisher JB, Morrow E, Worden JR, Asefi S, Badgley G, Saatchi S. 2013. Forest productivity and water stress in Amazonia: Observations from GOSAT chlorophyll fluorescence. *Proceedings of the Royal Society B-Biological Sciences* **280** doi: 10.1098/rspb.2013.0171

Leufen G, Noga G, Hunsche M. 2014. Fluorescence indices for the proximal sensing of powdery mildew, nitrogen supply and water deficit in sugar beet leaves. *Agriculture* **4** 58-78.

Leufen G, Noga G, Hunsche M. 2013. Physiological response of sugar beet (*Beta vulgaris*) genotypes to a temporary water deficit, as evaluated with a multiparameter fluorescence sensor. *Acta Physiologiae Plantarum* **35** 1763-1774.

Levitt J. 1980. *Responses of Plants to Environmental Stresses. Vol.II. Water, Radiation, Salt and Other Stresses*. Academic Press.

Lewis P, Disney M. 2007. Spectral invariants and scattering across multiple scales from within-leaf to canopy. *Remote Sensing of Environment* **109** 196-206.

Lichtenthaler HK, Ač A, Marek MV, Kalina J, Urban O. 2007. Differences in pigment composition, photosynthetic rates and chlorophyll fluorescence images of sun and shade leaves of four tree species. *Plant Physiology and Biochemistry* **45** 577-588.

Lichtenthaler HK, Babani F. 2004. Light adaptation and senescence of the photosynthetic apparatus. Changes in pigment composition, chlorophyll fluorescence parameters and photosynthetic activity. In: Papageorgiou GC, Govindjee (eds.) *Chlorophyll a Fluorescence: A Signature of Photosynthesis,* pp. 713-736. Dordrect: Springer.

Lichtenthaler HK, Babani F. 2000. Detection of photosynthetic activity and water stress by imaging the red chlorophyll fluorescence. *Plant Physiology and Biochemistry* **38** 889-895.

Lichtenthaler HK, Buschmann C. 2001. Chlorophylls and carotenoids : Measurement and characterization by UV-VIS. *Current Protocols in Food Analytical Chemistry* ***F4.3.1-F4.3.8*** **(Supplement 1)** 1–8.

Lichtenthaler HK, Rinderle U. 1988. The role of chlorophyll fluorescence in the detection of stress conditions in plants. *CRC Critical Reviews in Analytical Chemistry* **19** 29-85.

Lindstrot R, Guanter L, Hollstein A, Filipitsch F, Kritten L, Fischer J, Verrelst J, Gómez-Chova L, Alonso L, Moreno J. 2013. FLUSS – Atmospheric corrections for fluorescence signal and surface pressure retrieval over land. ESA ESTEC Contract 4000102733, Final Report.

Liu X, Liu L, Zhang S, Zhou X. 2015. New spectral fitting method for full-spectrum solar-induced chlorophyll fluorescence retrieval based on principal components analysis. *Remote Sensing* **7** 10626-10645.

Liu LY, Zhao JJ, Guan LL. 2013. Tracking photosynthetic injury of Paraquat-treated crop using chlorophyll fluorescence from hyperspectral data. *European Journal of Remote Sensing* **46** 459-473.

MacArthur A, Alonso L, Malthus TJ, Moreno JF. 2013. Field spectroscopy sampling strategies for improved measurement of Earth surface reflectance. AGU Fall Meeting, 9-13 December 2013, San Francisco, CA.

Magnani F, Bensada A, Cinnirella S, Ripullone F, Borghetti M. 2008. Hydraulic limitations and water-use efficiency in *Pinus pinaster* along a chronosequence. *Canadian Journal of Forest Research* **38** 73-81.

Magnani F, Olioso A, Demarty J, Germain V, Verhoef W, Moya I, Goulas Y, Cecchi G, Agati G, Zarco-Tejada P, Mohammed G, Van der Tol C. 2009. Assessment of Vegetation Photosynthesis Through Observation of Solar Induced Fluorescence from Space. ESTEC Contract No. 20678/07/NL/HE, Final Report.

Maxwell K, Johnson GN. 2000. Chlorophyll fluorescence - a practical guide. *Journal of Experimental Botany* **51** 659-668.

McMurtrey JE, Chappelle EW, Kim MS, Meisinger JJ, Corp LA. 1994. Distinguishing nitrogen fertilization levels in field corn (*Zea mays* L.) with actively induced fluorescence and passive reflectance measurements. *Remote Sensing of Environment* **47** 36-44.

Meroni M, Barducci A, Cogliati S, Castagnoli F, Rossini M, Busetto L, Migliavacca M, Cremonese E, Galvagno M, Colombo R, di Cella UM. 2011. The hyperspectral irradiometer, a new instrument for long-term and unattended field spectroscopy measurements. *Review of Scientific Instrum*ents **82** 043106 (9pp).

Meroni M, Busetto L, Colombo R, Guanter L, Moreno J, Verhoef W. 2010. Performance of spectral fitting methods for vegetation fluorescence quantification. *Remote Sensing of Environment* **114** 363-374.

Meroni M, Rossini M, Guanter L, Alonso L, Rascher U, Colombo R, Moreno J. 2009. Remote sensing of solar-induced chlorophyll fluorescence: Review of methods and applications. *Remote Sensing of Environment* **113** 2037-2051.

Meroni M, Rossini M, Picchi V, Panigada C, Cogliati S, Nali C, Colombo R. 2008. Assessing steady-state fluorescence and PRI from hyperspectral proximal sensing as early indicators of plant stress: The case of ozone exposure. *Sensors* **8** 1740-1754.

Miller J, Berger M, Goulas, Y, Jacquemoud S, Louis J, Mohammed G, Moise N, Moreno J, Moya I, Pedrós R, Verhoef W, Zarco-Tejada P. 2005. Development of a Vegetation Fluorescence Canopy Model. European Space Agency ESTEC Contract No. 16365/02/NL/FF, Final Report.

Mohammed GH, Goulas Y, Magnani F, Moreno J, Olejníčková J, Rascher U, Van der Tol C, Verhoef W, Ač A, Daumard F, Gallé A, Malenovský Z, Pernokis D, Rivera JP, Verrelst J, Drusch M. 2014. 2012 FLEX/Sentinel-3 Tandem Mission Photosynthesis Study. ESA Contract No. 4000106396/12/NL/AF, Final report.

Monteith JL. 1972. Solar-radiation and productivity in tropical ecosystems. *Journal of Applied Ecology* **9** 747-766.

Moreno J, Rascher U, Goulas Y, Colombo R, Verhoef W, Damm A, Alonso L, Cogliati S, Daumard F, Rivera JP, Sabater N, Schickling A, Tenjo C, Timmermans J, Verrelst J, Drusch M. 2014. FLEX/S3 Tandem Mission Performance Analysis and Requirements Consolidation Study (PARCS), ESA Contract No. 4000105078/11/NL/AF, Final report.

Morisette JT, Baret F, Privette JL, Myneni RB, Nickeson JE, *et al*. 2006. Validation of global moderate-resolution LAI Products: a framework proposed within the CEOS Land Product Validation subgroup. *IEEE Transactions on Geoscience and Remote Sensing* **44** 1804-1817.

Mottus M, Takala TLH, Stenberg P, Knyazikhin Y, Yang B, Nilson T. 2015. Diffuse sky radiation influences the relationship between canopy PRI and shadow fraction. *ISPRS Journal of Photogrammetry and Remote Sensing* **105** 54-60.

Müller P, Li XP, Niyogi KK. 2001. Non-photochemical quenching. A response to excess light energy. *Plant Physiology* **125** 1558-1566.

Mullineaux CW, Emlyn-Jones D. 2005. State transitions: an example of acclimation to low-light stress. *Journal of Experimental Botany* **56** 389-393.

Munekage Y, Hashimoto M, Miyake C, Tomizawa KI, Endo T, Tasaka M, Shikanai T. 2004. Cyclic electron flow around photosystem I is essential for photosynthesis. *Nature* **429** 579-582.

Myneni RB, Hoffman S, Knyazikhin Y, Privette JL, Glassy J, Tian Y, Wang Y, Song X, Zhang Y, Smith GR, Lotsch A, Friedl M, Morisette JT, Votava P, Nemani RR, Running SW. 2002. Global products of vegetation leaf area and fraction absorbed PAR from year one of MODIS data. *Remote Sensing of Environment* **83** 214-231.

Nedbal L, Koblížek M. 2006. Chlorophyll fluorescence as a reporter on in vivo electron transport and regulation in plants. In: Grimm B, Porra R, Ruediger W, Scheer H. (eds.) *Biochemistry and Biophysics of Chlorophylls,* pp. 507-519. Kluwer Academic Press.

Nichol CJ. 2014. Seasonal and diurnal changes in boreal forest solar induced fluorescence (Fs) retrieved from a continuously operating spectrometer system for the estimation of light use efficiency. 5th International Workshop on Remote Sensing of Vegetation Fluorescence, 22-24 April 2014, Paris, France.

Niinemets U, Kollist H, Garcia-Plazaola JI, Hernandez A, Becerril JM. 2003. Do the capacity and kinetics for modification of xanthophyll cycle pool size depend on growth irradiance in temperate trees? *Plant Cell and Environment* **26** 1787-1801.

Nilson T. 1971. A theoretical analysis of the frequency of gaps in plant stands. *Agricultural Meteorology* **8** 25-38.

Nobel PS, Forseth IN, Long SP. 1993. Canopy structure and light interception. In: Hall DO *et al. Photosynthesis and Production in a Changing Environment*, pp. 79-90. Springer.

Oker-Blom P, Lappi J, Smolander H. 1991. Radiation regime and photosynthesis of coniferous stands. In: *Photon-Vegetation Interactions*, pp. 469-499. Springer.

Öquist G, Huner NPA. 2003. Photosynthesis of overwintering evergreen plants. *Annual Review of Plant Biology* **54** 329-355.

Pacheco-Labrador J, Martin MP. 2013. Nonlinear response in a field portable spectroradiometer: Characterization and effects on output reflectance. *IEEE Transactions on Geoscience and Remote Sensing* **52** 920-928.

Palombi L, Cecchi G, Lognoli D, Raimondi V, Toci G, Agati G. 2011. A retrieval algorithm to evaluate the Photosystem I and Photosystem II spectral contributions to leaf chlorophyll fluorescence at physiological temperatures. *Photosynthesis Research* **108** 225-239.

Panferov O, Knyazikhin Y, Myneni RB, Szarzynski J, Engwald S, Schnitzler KG, Gravenhorst G. 2001. The role of canopy structure in the spectral variation of transmission and absorption of solar radiation in vegetation canopies. *IEEE Transactions on Geoscience and Remote Sensing* **39** 241-253.

Panigada C, Rossini M, Meroni M, Cilia C, Busetto L, Amaducci S, Boschetti M, Cogliati S, Picchi V, Pinto F, Marchesi A, Colombo. 2014. Fluorescence, PRI and canopy temperature for water stress detection in cereal crops. *International Journal of Applied Earth Observation and Geoinformation* **30** 167-178.

Pedrós R, Goulas Y, Jacquemoud S, Louis J, Moya I. 2010. FluorMODleaf: A new leaf fluorescence emission model based on the PROSPECT model. *Remote Sensing of Environment* **114** 155-167.

Pfundel E. 1998. Estimating the contribution of Photosystem I to total leaf chlorophyll fluorescence. *Photosynthesis Research* **56** 185-195.

Pickett-Heaps CA, Canadell JG, Briggs PR, Gobron N, Haverd V, Paget MJ, Pinty B, Raupach MR. 2014. Evaluation of six satellite-derived Fraction of Absorbed Photosynthetic Active Radiation (FAPAR) products across the Australian continent. *Remote Sensing of Environment* **140** 241-256.

Plascyk JA. 1975. The MK II Fraunhofer line discriminator (FLD-II) for airborne and orbital remote sensing of solar-stimulated luminescence. *Optical Engineering* 14 339-346.

Porcar-Castell A, MacArthur A, Rossini M, Eklundh L, Pacheco-Labrador J, *et al*. 2015. Eurospec: At the interface between remote sensing and ecosystem CO_2 flux measurements in Europe. *Biogeosciences Discussions* **12** 13069-13121.

Porcar-Castell A. 2011. A high-resolution portrait of the annual dynamics of photochemical and non-photochemical quenching in needles of *Pinus sylvestris*. *Physiologia Plantarum* **143** 139-153.

Porcar-Castell A, Pfündel E, Korhonen JFJ, Juurola E. 2008. A new monitoring PAM fluorometer (MONI-PAM) to study the short-and long-term acclimation of photosystem II in field conditions. *Photosynthesis Research* **96** 173-179.

Porcar-Castell A, Tyystjärvi E, Atherton J, Van der Tol C, Flexas J, Pfündel EE, Moreno J, Frankenberg C, Berry JA. 2014. Linking chlorophyll *a* fluorescence to photosynthesis for remote sensing applications: mechanisms and challenges. *Journal of Experimental Botany* **65** 4065-4095.

Portillo-Quintero C, Sanchez-Azofeifa A, Culvenor D. 2014. Using VEGNET in-situ monitoring LiDAR (IML) to capture dynamics of plant area index, structure and phenology in aspen parkland forests in Alberta, Canada. *Forests* **5** 1053-1068.

Rankine C, Sanchez-Azofeifa GA, MacGregor MH, Musilek P. 2014. The use of synchronized wireless sensor networks for explicit in-situ FAPAR monitoring. 1st Workshop CEOS LPV FAPAR Sub-Group, European Commission's Joint Research Center, Ispra, Italy.

Rascher U, Alonso L, Burkart A, Cilia C, Cogliati S, Colombo R, Damm A, Drusch M, Guanter L, Hanus J, Hyvärinen T, Julitta T, Jussila J, Kataja K, Kokkalis P, Kraft S, Kraska T, Matveeva M, Moreno J, Muller O, Panigada C, Pikl M, Pinto F, Prey L, Pude R, Rossini M, Schickling A, Schurr U, Schüttemeyer D, Verrelst J, Zemek F. 2015. Sun-induced fluorescence – a new probe of photosynthesis: First maps from the imaging spectrometer *HyPlant*. *Global Change Biology* DOI: 10.1111/gcb.13017.

Rascher U, Agati G, Alonso L, Cecchi G, Champagne S, Colombo R, Damm A, Daumard F, de Miguel E, Fernandez G, Franch B, Franke J, Gerbig C, Gioli B, Gomez JA, Goulas Y, Guanter L, Gutierrez-de-la-Camara O, Hamdi K, Hostert P, Jimenez M, Kosvancova M, Lognoli D, Meroni M, Miglietta F, Moersch A, Moreno J, Moya I, Neininger B, Okujeni A, Ounis A, Palombi L, Raimondi V, Schickling A, Sobrino JA, Stellmes M, Toci G, Toscano P, Udelhoven T, van der Linden S, Zaldei A. 2009. CEFLES2: the remote sensing component to quantify photosynthetic efficiency from the leaf to the region by measuring sun-induced fluorescence in the oxygen absorption bands. *Biogeosciences* **6** 1181-1198.

Reichstein M, Falge E, Baldocchi D, Papale D, Aubinet M, *et al*. 2005. On the separation of net ecosystem exchange into assimilation and ecosystem respiration: Review and improved algorithm. *Global Change Biology* **11** 1424-1439.

Rivera J, Sabater N, Tenjo C, Vicent J, Moreno J. 2014. Synthetic scene simulator for hyperspectral spaceborne passive optical sensors. application to ESA's FLEX/Sentinel-3 tandem mission. Proc. 6th Workshop on Hyperspectral Image and Signal Processing: Evolution in Remote Sensing (WHISPERS), 25-27 June 2014, Lausanne, Switzerland.

Rivera J, Verrelst J, Gómez-Dans J, Muñoz-Marí J, Moreno J, Camps-Valls G. 2015. An emulator toolbox to approximate radiative transfer models with statistical learning. *Remote Sensing* **7** 9347-9370.

Rohacek K, Soukupova J, Bartak M. 2008. Chlorophyll fluorescence: A wonderful tool to study plant physiology and plant stress. In: Schoefs B (ed.) *Plant Cell Compartments – Selected Topics*, pp. 41-104. Kerala, India: Research Signpost.

Rodriguez JM, Ustin SL, Riano D. 2011. Contributions of imaging spectroscopy to improve estimates of evapotranspiration. *Hydrological Processes* **25** 4069-4081.

Rossini M, Meroni M, Migliavacca M, Manca G, Cogliati S, Busetto L, Picchi V, Cescatti A, Seufert G, Colombo R. 2010. High resolution field spectroscopy measurements for estimating gross ecosystem production in a rice field. *Agricultural and Forest Meteorology* **150** 1283-1296.

Rossini M, Nedbal L, Guanter L, Ač A, Alonso L, Burkart A, Cogliati S, Colombo R, Damm A, Drusch M, Hanus J, Janoutova R, Julitta T, Kokkalis P, Moreno J, Novotny J, Panigada C, Pinto F, Schickling A, Schüttemeyer D, Zemek F, Rascher U. 2015. Red and far red sun-induced chlorophyll fluorescence as a measure of plant photosynthesis. *Geophysical Research Letters* **42** 1632-1639.

Sabater N, Vicent J, Alonso L, Verrelst J, Moreno J. 2015. An atmospheric correction algorithm for the Fluorescence Explorer/Sentinel-3 tandem space mission. *Journal of Geographical Research - Atmospheres* (submitted).

Saltelli A, Annoni P. 2010. How to avoid a perfunctory sensitivity analysis. *Environmental Modeling and Software* **25** 1508-1517.

Schneider FD, Leiterer R, Morsdorf F, Gastellu-Etchegorry J.P, Lauret N, Pfeifer N, Schaepman ME. 2014. Simulating imaging spectrometer data: 3D forest modeling based on LiDAR and in situ data. *Remote Sensing of Environment* **152** 235-250.

Schreiber U, Bilger W, Neubauer C. 1994. Chlorophyll fluorescence as a non intrusive indicator for rapid assessment of in vivo photosynthesis. *Ecological Studies* **100** 49-70.

Simic A, Baret F, Weiss M, Lecerf R, Alessandrini A, Hanocq J-F, Marloie O. 2012. Production of the high resolution maps of biophysical variables based on SPOT imagery and in-situ measurements generated by PASTIS 57 for Hyytiala, Finland. Proceedings of 2012 IEEE International Geoscience and Remote Sensing Symposium (IGARSS), 22-27 July 2012, Munich, Germany.

Stewart DW, Costa C, Dwyer LM, Smith DL, Hamilton RI, Ma BL. 2003. Canopy structure, light interception, and photosynthesis in maize. *Agronomy Journal* **95** 1465-1474.

Suárez L, Berni JAJ. 2012. Spectral responses of citrus and their application to nutrient and water constraints diagnosis. In: Srivastava AK (ed.) *Advances in Citrus Nutrition*, pp.125-141. Springer.

Suárez L, Zarco-Tejada PJ, Sepulcre-Canto G, Perez-Priego O, Miller JR, Jimenez-Munoz JC, Sobrino J. 2008. Assessing canopy PRI for water stress detection with diurnal airborne imagery. *Remote Sensing of Environment* **112** 560-575.

Tao X, Liang S, Wang D. 2015. Assessment of five global satellite products of fraction of absorbed photosynthetically active radiation: Intercomparison and direct validation against ground-based data. *Remote Sensing of Environment* **163** 270-285.

Tartachnyk II, Radenmacher I, Kuhbauch W. 2006. Distinguishing nitrogen deficiency and fungal infection of winter wheat by laser-induced fluorescence. *Precision Agriculture* **7** 281-293.

Theisen AF. 2002. Detecting chlorophyll fluorescence from orbit: The Fraunhofer Line Depth Model. In: Muttiah RS (ed.) *From Laboratory Spectroscopy to Remotely Sensed Spectra of Terrestrial Ecosystems*, pp. 203-232. Netherlands: Kluwer Academic.

Tikkanen M, Grieco M, Aro EM. 2011. Novel insights into plant light-harvesting complex II phosphorylation and 'state transitions'. *Trends in Plant Science* **16** 126-131.

Tremblay N, Wang Z, Cerovic ZG. 2012. Sensing crop nitrogen status with fluorescence indicators: A review. *Agronomy for Sustainable Development* **32** 451-464.

Ullah S, Schlerf M, Skidmore AK, Hecker C. 2012. Identifying plant species using mid-wave infrared (2.5-6µm) and thermal infrared (8-14µm) emissivity spectra. *Remote Sensing of Environment* **118** 95-102.

Van der Tol C, Berry JA, Campbell PKE, Rascher U. 2014. Models of fluorescence and photosynthesis for interpreting measurements of solar-induced chlorophyll fluorescence. *Journal of Geophysical Research: Biogeosciences* **119** 2312-2327.

Van der Tol C, Verhoef W, Timmermans J, Verhoef A, Su Z. 2009. An integrated model of soil-canopy spectral radiances, photosynthesis, fluorescence, temperature and energy balance. *Biogeosciences* **6** 3109-3129.

Van Wittenberghe S, Alonso L, Verrelst J, Hermans I, Delegido J, *et al*. 2013. Upward and downward solar-induced chlorophyll fluorescence yield indices of four tree species as indicators of traffic pollution in Valencia. *Environmental Pollution* **173** 29-37.

Van Wittenberghe S, Alonso L, Verrelst J, Hermans I, Valcke R, Veroustraete F, Moreno J, Samson R. 2014. A field study on solar-induced chlorophyll fluorescence and pigment parameters along a vertical canopy gradient of four tree species in an urban environment. *Science of the Total Environment* **466-487** 185-194.

Van Wittenberghe S, Alonso L, Verrelst J, Moreno J, Samson R. 2015. Bidirectional sun-induced chlorophyll fluorescence emission is influenced by leaf structure and light scattering properties – A bottom-up approach. *Remote Sensing of Environment* **158** 169-179.

Van Wittenberghe S, Verrelst J, Rivera JP, Alonso L, Moreno J, Samson R. 2014. Gaussian processes retrieval of leaf parameters from a multi-species reflectance, absorbance and fluorescence dataset. *Journal of Photochemistry and Photobiology. B, Biology* **134** 37-48.

Verhoef W. 2011. Modelling vegetation fluorescence observations 7th EARSEL Workshop of the Special Interest Group in imaging spectroscopy, 11-13 April 2011, Edinburgh, UK, pp. 41-42.

Verhoef W, Bach H. 2003a. Remote sensing data assimilation using coupled radiative transfer models. *Physics and Chemistry of the Earth* **28** 3-13.

Verhoef W, Bach H. 2003b. Simulation of hyperspectral and directional radiance images using coupled biophysical and atmospheric radiative transfer models. *Remote Sensing of Environment* **87** 23-41.

Verrelst J, Alonso L, Camps-Valls G, Delegido J, Moreno J. 2012a. Retrieval of vegetation biophysical parameters using Gaussian process techniques. *IEEE Transactions on Geoscience and Remote Sensing* **50** 1832-1843.

Verrelst J, Muñoz J, Alonso L, Delegido J, Rivera J, Camps-Valls G, Moreno J. 2012b. Machine learning regression algorithms for biophysical parameter retrieval: opportunities for Sentinel-2 and -3. *Remote Sensing of Environment* **118** 127-139.

Verrelst J, Rivera Caicedo JP, Gomez-Dans J, Camps-Valls G, Moreno J. 2015a. Replacing radiative transfer models by surrogate approximations through machine learning. IEEE-IGARSS, 26-31 July 2015, MIlan, Italy.

Verrelst J, Rivera JP, Van der Tol C, Magnani F, Mohammed G, Moreno J. 2015b. Global sensitivity analysis of the SCOPE model: what drives simulated canopy-leaving sun-induced fluorescence? *Remote Sensing of Environment* **166** 8-21.

Verrelst J, Rivera JP, Van der Tol C, Magnani F, Mohammed G, Moreno J. 2014. A-SCOPE: Automating fluorescence modeling in support of FLEX. 5th International Workshop on Remote Sensing of Vegetation Fluorescence, 22-24 April 2014.

Vicent J, Sabater N, Tenjo C, Acarreta JR, Manzano M, Rivera JP, Jurado P, Franco R, Alonso L, Verrelst J, Moreno J. 2015a. Design of a satellite end-to-end mission performance simulator for imaging spectrometers and its application to the ESA's FLEX/Sentinel-3 tandem mission. Proc. of SPIE Optics+Photonics 2015, San Diego.

Vicent J, Sabater N, Tenjo C, Acarreta JR, Manzano M, Rivera JP, Jurado P, Franco R, Alonso L, Verrelst J, Moreno J. 2015b. FLEX End-to-End Mission Performance Simulator. *IEEE Transactions on Geoscience and Remote Sensing* (submitted).

Vuolo F, Atzberger C, Richter K, D'Urso G, Dash J. 2010. Retrieval of biophysical vegetation products from RapidEye Imagery. ISPRS Proceedings XXXVIII, 5-7 July 2010, Vienna, Austria.

Welch BL. 1974. The generalization of 'Student's' problem when several different population variances are involved. *Biometrika* **34** 28-35.

Widlowski JL. 2010. On the bias of instantaneous FAPAR estimates in open-canopy forests. *Agricultural and Forest Meteorology* **150** 1501-1522.

Wong CYS, Gamon JA. 2015. Three causes of variation in the photochemical reflectance index (PRI) in evergreen conifers. *New Phytologist* **206** 187-195.

Woodgate W, Disney M, Armston JD, Jones SD, Suarez L, *et al*. 2015. An improved theoretical model of canopy gap probability for Leaf Area Index estimation in woody ecosystems. *Forest Ecology and Management* **358** 303-320.

World Meteorological Organization. 2011. Supplemental details to the satellite-based component of the "Implementation Plan for the Global Observing System for Climate in Support of the UNFCCC (2010 Update)", GCOS-154.

Wu C, Huang W, Yang Q, Xie Q. 2015. Improved estimation of light use efficiency by removal of canopy structural effect from the photochemical reflectance index (PRI). *Agriculture Ecosystems & Environment* **199** 333-338.

Wu C, Niu Z, Tang Q, Huang W. 2010. Revised photochemical reflectance index (PRI) for predicting light use efficiency of wheat in a growth cycle: validation and comparison. *International Journal of Remote Sensing* **31** 2911-2924.

Yang X, Tang J, Mustard JF, Lee J-E, Rossini M, *et al*. 2015. Solar-induced chlorophyll fluorescence that correlates with canopy photosynthesis on diurnal and seasonal scales in a temperate deciduous forest. *Geophysical Research Letters* **42** 2977-2987.

Zarco-Tejada PJ, González-Dug V, Berni JA. 2012. Fluorescence, temperature and narrow-band indices acquired from a UAV platform for water stress detection using a micro-hyperspectral imager and a thermal camera. *Remote Sensing of Environment* **117** 322-337.

Zhang Y, Guanter L, Berry JA, Joiner J, Van der Tol, C, *et al*. 2014. Estimation of vegetation photosynthetic capacity from space-based measurements of chlorophyll fluorescence for terrestrial biosphere models. *Global Change Biology* **20** 3727-3742.

Zhao F, Guo Y, Verhoef W, Gu X, Liu L, Yang G. 2014. A method to reconstruct the solar-induced canopy fluorescence spectrum from hyperspectral measurements. *Remote Sensing* **6** 10171-10192.

8. Acronynms & Abbreviations

A	net canopy photosynthesis (assimilation)
AOT	aerosol optical thickness
APAR	absorbed photosynthetically active radiation
$APAR_{green}$	PAR absorbed by green leaves
APEX	Airborne Prism Experiment
ARTMO	Automated RTMs Operator
A-SCOPE	Automated SCOPE
A-SGM	Automated Scene Generator Module
ATBD	Algorithm Theoretical Baseline Document
ATP	adenosine triphosphate
AVHRR	Advanced Very High Resolution Radiometer
BFDF	bi-directional fluorescence distribution function
BHR	bi-hemispherical reflectance
C_{ab}	chlorophyll a&b content
Cal/Val	calibration/validation
C_{ca}	carotenoid concentration
C_{dm}	dry matter content
CEFLES-2	CarboEurope, FLEX and Sentinel-2
CEOS	Committee on Earth Observation Satellites
CI	clumping index
CO_2	carbon dioxide
cPRI	canopy PRI
CV	coefficient of variation
CVS	Cal/Val sites
C_w	leaf water
DA	data assimilation
DART	Discrete Anisotropic Radiative Transfer
DASF	directional area scattering factor
DCMU	(3-(3,4-dichlorophenyl)-1,1-dimethylurea)
DEM	digital elevation model
DGVM	Dynamic Global Vegetation Model
DHP	digital hemispherical photography
DOM	digital object model
DOY	day of year
DSM	digital surface model
DTM	digital terrain model
EC	eddy covariance
E_{dif}	diffuse irradiance
E_{dir}	direct irradiance
ESA	European Space Agency
ESU	Elementary Sampling Unit
ETR	electron transport rate
EVI	Enhanced Vegetation Index
f (or f^{-1})	simplified SCOPE (or inverted)
F	chlorophyll fluorescence
fAPAR	fraction of absorbed PAR
FB	FLEX Bridge
FLD	Fraunhofer Line Discrimination
FLEX	Fluorescence Explorer
FLEX-E	FLEX End-to-End Mission Performance Simulator
FLEX/S3	Fluorescence Explorer/Sentinel-3
FLORIS	Fluorescence Imaging Spectrometer
FLUSS	Atmospheric Corrections for Fluorescence Signal Retrieval Study
F_m	dark-adapted maximal fluorescence
F_o	dark-acclimated minimal fluorescence
FRF, FFR	far-red fluorescence
F_t	fluorescence at time *t* (from active sensors)
F_{tot}	total integrated fluorescence radiance
f_{vzz}	linear scaling coefficient in Fluspect model quantifying magnitude of PRI effect on NPQ
FVC	fractional vegetation cover
F_v/F_m	variable to maximal fluorescence (dark-adapted)
GCOS	Global Climate Observation Systems
GOME	Global Ozone Monitoring Experiment
GPP	gross primary productivity (or production)
GPR	Gaussian processes regression
GSA	global sensitivity analysis
GUI	graphic user interface
h	relative humidity
HCRF	hemispheric-conical reflectance factors
HSI	HyperSpectral Irradiometer
iPRI	PRI normalised for illumination effects
IRGA	InfraRed Gas Analyser
ISRF	instrument spectral response function
J	Jacobian
J_{max}	maximum electron transport rate
JRC-MGVI	Joint Research Centre MERIS Global Vegetation Index
JRC-TIP	Joint Research Centre Two-stream Inversion Package
kNPQs	rate constant of sustained thermal dissipation (non-photochemical quenching)
KRR	kernel ridge regression
LAD	leaf angle distribution
LAI (or L)	leaf area index
LAI_{green}	green leaf area index
LAI_{tot}	total leaf area index
LCC	leaf chlorophyll content
LDCM	Landsat Data Continuity Mission
LIDF	leaf inclination parameter (LIDFa or LIDFb)
LOS	line of sight
LPV	Land Product Validation
LST	land surface temperature
LUE	light use efficiency
LUE_p	photosynthetic light use efficiency
LUT	lookup table

m	Ball-Berry stomatal conductance parameter
MCMC	Monte Carlo Markov Chain
MD12	Magnani-Dayyoub 2012 model
MERIS	Medium Resolution Imaging Spectrometer
ML	machine learning
MLRA	machine learning regression algorithms
MODIS	Moderate Resolution Imaging Spectroradiometer
MO-MLRA	multi-output MLRA
MPI-BGC	Max Planck Institute for Biogeochemistry
MRI	Multiplexer Radiometer Irradiometer
NADPH	nicotinamide adenine dinucleotide phosphate
NBS	narrow band spectrometer
NDVI	Normalised Difference Vegetation Index
$NDVI_m$	modified NDVI
NIR	near infrared
NN	neural network
NO	numerical optimisation
NPP	net primary productivity (or production)
NPQ	non-photochemical quenching
NPQ_S	sustained NPQ
NSFI	Nitrogen Stress Fluorescence Index
OAT	One Factor at a Time (sensitivity analysis)
O_2-A(B)	oxygen A (or B) band
OLCI	Ocean and Land Colour Imager
OS	orbit state
p	recollision probability (p-theory)
P	model parameters of simplified SCOPE
PAM	pulse-amplitude modulated
ρ_{app}	apparent reflectance spectrum
PAR	photosynthetically active radiation
PARCS	Performance Analysis and Requirement Consolidation Study
PAR_{inc}	incoming PAR
PAR_{out}	reflected PAR
PAR_{soi}	PAR_{trans} reflected by soil background
PAR_{trans}	PAR transmitted through canopy
PCA	principal component analysis
PCs	principal component spectra
PFT	plant functional type
PLSR	partial least squares regression
PQ	photochemical quenching
PRI	Photochemical Reflectance Index
PS Study	Photosynthesis Study
PSF	point-spread function (sensor)
PSI (PSII)	photosystem I (II)
PSIII-EM	PSI and PSII source spectral functions
qL_S	fraction of functional reaction centres
q_S	solar zenith angle (sine)
R	reflectance
R^2	coefficient of determination
REIP	red-edge index position (or red-edge inflection point)
RF	red fluorescence
R_{in}	incident shortwave radiation
RMSE	root mean square error
RS	remote sensing
R_{si}	spectrally integrated shortwave irradiance
RT	radiative transfer
RTM	radiative transfer model
RTMo	radiative transfer module for incident solar and sky radiation
Rubisco	ribulose-1,5-bisphosphate carboxylase/oxygenase
S3	Sentinel-3
S/C	stress to control ratio
SCOPE	Soil Canopy Observation of Photochemistry and Energy fluxes (model)
SD	standard deviation
SeaWiFS	Sea-viewing Wide Field-of-view Sensor
SFM	spectral fitting method (algorithm)
SIF	solar- or sun-induced fluorescence
SLC	soil-leaf-canopy (RT model)
SLSTR	Sea and Land Surface Temperature Radiometer
SNR	signal-to-noise ratio
SpecFit	Spectrum Fitting (algorithm)
SR	spectral resolution
SSI	spectral sampling interval
SVD	singular vector decomposition
SWIR	short-wave infrared spectrum
T	transmittance
TES	temperature-emissivity separation algorithm
TIR	thermal infrared
TOA	top of atmosphere
TOC	top of canopy
TSFI	Temperature Stress Fluorescence Index
UAV	unmanned aerial vehicle
UTC	Coordinated Universal Time
V	violaxanthin
V2Z	input parameter in Fluspect to represent leaf xanthophyll de-epoxidation status
Vcmo	maximum carboxylation capacity at optimum temperature (also V_{cmax})
VIS	visible spectrum
VNIR	visible to near infrared spectrum
WBS	wide band spectrometer
WGCV	CEOS Working Group on Calibration and Validation
WMO	World Meteorological Organization
WP	workpackage
WSFI	Water Stress Fluorescence Index
Z	zeaxanthin

9. Appendices

9.1 Team involvements

Activity	Lead Scientist / Institutions
Management & coordination of activities	**Lead: G. Mohammed**
Overall study management & coordination	P & M Technologies
Study activity website and services; contract administration	P & M Technologies
Solar induced fluorescence (SIF) retrieval optimisation and analysis	**Lead: R. Colombo**
Data generation: Extension of FLEX/S3 spectral radiance database	University of Twente
Data generation: Generation of a synthetic Level-1b products dataset using FLEX End-to-End Mission Performance Simulator	University of Valencia
Towards Level-2a products: Optimisation of atmospheric correction algorithm using S3/FLEX	University of Valencia
Towards Level-2a products: Optimisation of retrievals of full SIF spectrum and contributions from Photosystem I & II features using the measured frequency spectrum	University of Milano-Bicocca
Towards Level-2b products: Evaluation of strategies to retrieve APAR	University of Zurich
Towards Level-2b products: Definition and derivation of additional SIF-derived indices from databases available	University of Milano-Bicocca
Towards Level-2c products: Development of biophysical parameter retrieval algorithms for advanced exploitation of FLEX data products	University of Valencia
Towards Level-2c products: Simultaneous retrieval of canopy state variables by model inversion of integrated tandem mission data	University of Twente
Development of vegetation stress indicators and applications	**Lead: U. Rascher**
Linking *HyPlant* data to vegetation stress	Forschungszentrum Jülich
Strategies to measure non-photochemical protection	University of Zurich
Stress indicators and applications	Global Change Research Ctr
Sources of variability and error in stress detection	P & M Technologies
Photosynthesis model optimisation, updates, and applications	**Lead: C. van der Tol**
Archiving, documentation, implementation of SCOPE model updates	University of Twente
Archiving, documentation, implementation of A-SCOPE model updates	University of Valencia
Model code for spectral changes (PSI-PSII spillover) due to stress factors	University of Bologna
Dataset of sustained (long-term) quenching parameters for different species under drought	University of Bologna
Incorporation of dynamic xanthophylls reflectance in SCOPE	University of Twente
Model performance assessment	University of Twente
Implementation of vegetation traits in scene generator module of FLEX simulator	University of Valencia
Evaluation of the effect of canopy geometry with SCOPE and alternative radiative transfer schemes	University College London
Development of a strategy for use of SIF in DGVMs via data assimilation	University College London
Development of a calibration/validation strategy	**Lead: J. Moreno**
Validation error metrics and product accuracies	University of Valencia
Definition of a calibration/validation strategy for basic fluorescence products	University of Valencia
Definition of FLEX Level-2/3 products and their validation plan	University of Valencia
Definition of common protocol and state-of-the-art instruments for use in estimation of fluorescence in the context of calibration/validation activities	University of Milano-Bicocca
Final deliverables	**Lead: G. Mohammed**
Final report and recommendations; Technical Data Package	P & M Technologies / All

9.2 Study meeting dates

Meeting name	Acronym	Location	Date
Kick-Off Meeting	KO	Telecon	03 October 2014
Telecon	- -	Telecon	03 December 2014
Progress Meeting 1	PM1	ESTEC	19 February 2015
Final Review	FR	ESTEC	08 December 2015

9.3 Journal publications

This compilation includes papers from the various FLEX activities – the PS Study, PARCS, FLEX Bridge, and the HyPlant campaigns – which were produced during the period of the FLEX Bridge Study (01 October 2014 – 30 September 2015).

Ač A, Malenovský Z, Olejníčková J, Gallé A, Rascher U, Mohammed G. 2015. Meta-analysis assessing potential of steady-state chlorophyll fluorescence for remote sensing detection of plant water, temperature and nitrogen stress. *Remote Sensing of Environment* 168: 420-436.

Cogliati S, Rossini M, Julitta T, Meroni M, Schickling A, Burkart A, Pinto F, Rascher U, Colombo R. 2015. Continuous and long-term measurements of reflectance and sun-induced chlorophyll fluorescence by using novel automated field spectroscopy systems. *Remote Sensing of Environment* 164: 270-281.

Cogliati S, Verhoef W, Kraft S, Sabater N, Alonso L, Vicent J, Moreno J, Drusch M, Colombo R. 2015. Retrieval of sun-induced fluorescence using advanced spectral fitting methods. *Remote Sensing of Environment* 169: 344-357.

Damm A, Guanter L, Paul-Limoges E, Van der Tol C, Hueni A, Buchmann N, Eugster W, Ammann C, Schaepman ME. 2015. Far-red sun-induced chlorophyll fluorescence shows ecosystem-specific relationships to gross primary production: An assessment based on observational and modeling approaches. *Remote Sensing of Environment* 166: 91-105.

Rascher U, Alonso L, Burkart A, Cilia C, Cogliati S, Colombo R, Damm A, Drusch M, Guanter L, Hanus J, Hyvärinen T, Julitta T, Jussila J, Kataja K, Kokkalis P, Kraft S, Kraska T, Matveeva M, Moreno J, Muller O, Panigada C, Pikl M, Pinto F, Prey L, Pude R, Rossini M, Schickling A, Schurr U, Schüttemeyer D, Verrelst J, Zemek F. 2015. Sun-induced fluorescence: A new probe of photosynthesis: First maps from the imaging spectrometer *HyPlant*. *Global Change Biology* DOI: 10.1111/gcb.13017.

Rivera JP, Verrelst J, Gómez-Dans J, Muñoz-Marí J, Moreno J, Camps-Valls G. 2015. An emulator toolbox to approximate radiative transfer models with statistical learning. *Remote Sensing 7*: 9347-9370.

Rossini M, Nedbal L, Guanter L, Ač A, Alonso L, Burkart A, Cogliati S, Colombo R, Damm A, Drusch M, Hanus J, Janoutova R, Julitta T, Kokkalis P, Moreno J, Novotny J, Panigada C, Pinto F, Schickling A, Schüttemeyer D, Zemek F, Rascher U. 2015. Red and far-red sun-induced chlorophyll fluorescence as a measure of plant photosynthesis. *Geophysical Research Letters* 42: 1632-1639.

Sabater N, Vicent J, Alonso L, Verrelst J, Moreno J. 2015. An atmospheric correction algorithm for the Fluorescence Explorer/Sentinel-3 tandem space mission. *Journal of Geographical Research - Atmospheres* (submitted).

Van der Tol C, Rossini M, Cogliati S, Verhoef W, Colombo R, Rascher U, Mohammed G. 2015. A model and measurement comparison of diurnal cycles of sun induced chlorophyll fluorescence of crops. *Remote Sensing of Environment* (submitted).

Verrelst J, Rivera JP, Van der Tol C, Magnani F, Mohammed G, Moreno J. 2015. Global sensitivity analysis of the SCOPE model: What drives simulated canopy-leaving sun-induced fluorescence? *Remote Sensing of Environment* 166: 8-21.

Verrelst J, Van der Tol C, Magnani F, Sabater N, Rivera JP, Mohammed G, Moreno J. 2015. Evaluating the predictive power of sun-induced chlorophyll fluorescence to estimate net photosynthesis of vegetation canopies: A SCOPE modelling study. *Remote Sensing of Environment* (submitted).

In addition, team members contributed to the following report and to the preparations for the Earth Explorer 8 User Consultation Meeting, 15-16 September 2015, Krakow, Poland:

ESA. 2015b. Report for Mission Selection: FLEX, ESA SP-1330/2 (2 volume series), European Space Agency, Noordwijk, The Netherlands.

9.4 Errata

Corrections and revisions will be listed here if applicable.

To date, no pages have been corrected, changed, updated, or replaced.

www.FLEX-Bridge.ca